EXAMINING THE EFFECTS OF V3 INTERNEURONS AND ASTROCYTES ON EMBRYONIC STEM CELL-DERIVED MOTONEURON MATURATION *IN VITRO*.

Anna Hephzibah Hands

UCL Institute of Neurology

PhD Supervisors:

Professor Linda Greensmith

Professor Rob Brownstone

A Thesis submitted in partial fulfilment of the requirements for the degree of Doctor of Philosophy from University College London.

2020

Declaration

I, Anna Hephzibah Hands confirm that the work presented in this Thesis is my own. Where information has been derived from other sources, I confirm that this has been indicated in the Thesis.

Abstract

Motor function is fundamental to human survival and behaviour. Consequently, muscle impairment and paralysis can severely impact quality of life, as in patients with Amyotrophic Lateral Sclerosis (ALS) and spinal cord injury. Restoring muscle control following damage to motor circuits has proven an elusive goal. Strategies to artificially restore function to paralysed muscles are currently being investigated, and most methods rely on stimulation of host nerves. However, this is only effective in conditions where motoneurons and Neuromuscular Junctions (NMJs) remain intact, which is not the case in neurodegenerative disorders such as ALS.

A novel strategy to overcome muscle paralysis involves two emerging technologies; the use of stem cell replacement strategies and optogenetics. Embryonic Stem Cell (ESC)-derived cells can be genetically manipulated to express light-sensitive genes such as ChannelRhodopsin-2 (ChR2). When grafted into a peripheral nerve within embryoid bodies (EBs), ESC-derived, ChR2-expressing motoneurons can grow axons that form functional NMJs, enabling optical control of muscle contraction by light stimulation of the graft. Surprisingly, engraftment of purified motoneuron aggregates does not result in the formation of functional NMJs. This suggests that other, non-motoneuronal cells within EBs contribute to the ability of ESC-derived motoneurons to mature and functionally innervate host muscle. In this Thesis, I examine the possibility that spontaneous activity arising from intra-graft microcircuits is necessary for motoneuron maturation.

To investigate this possibility, I generated co-cultures *in vitro* with pure populations of ESC-derived motoneurons, astrocytes and V3 interneurons. Immunocytochemistry was used to assess the morphology and synapse formation of motoneurons when cultured alone or in combination with other cell types. The effect of co-culture on the electrophysiological properties and spontaneous activity of motoneurons was investigated by single cell patch-clamping and calcium imaging.

My results show that co-culture of motoneurons with astrocytes promotes motoneuron survival and morphological maturation, accelerates their electrophysiological development, increases the density of motoneuronal

cholinergic synapses, and enables the development of glutamatergic, motoneuronal spontaneous activity. Motoneurons in astrocyte-containing co-cultures also display spontaneous calcium activity, though calcium activity emerges a week later than spontaneous activity recorded by patch clamping and has different burst characteristics. In contrast to astrocytes, V3 interneurons alone have little, if any, effect on motoneuron maturation. However, together with astrocytes, V3 interneurons accelerate the emergence of spontaneous, glutamatergic activity, alter the density of glutamatergic and cholinergic synapses onto motoneurons, and lead to more mature patterns of spontaneous glutamatergic activity in the motoneuron co-cultures.

These results provide insight into the influence of other cell types on motoneuron maturation and suggest that astrocytes and V3 interneurons could be added to motoneurons to produce a more mature, spontaneously active graft for use in cell replacement strategies to overcome muscle paralysis.

Impact Statement

Amyotrophic lateral sclerosis (ALS) is an adult-onset, progressive neurodegenerative disease in which motoneurons degenerate, resulting in muscle atrophy and paralysis; in the final stages of the disease even muscles involved in swallowing or breathing are affected. Typically, ALS patients die of respiratory failure within 3-5 years of disease onset. Despite extensive research, there is currently no effective disease-modifying treatment for ALS.

Our laboratory has been developing a novel strategy for the treatment of ALS that aims to overcome the loss of muscle function. This strategy involves the use of embryonic stem cell (ESC)-derived motoneurons (within embryoid bodies) that have been genetically modified to express light-sensitive proteins. When engrafted into peripheral nerves, these motoneurons have been shown to survive and extend axons to innervate denervated muscles. Moreover, these engrafted motoneurons can be activated using light to induce muscle contraction in a highly controlled manner, thereby restoring muscle function.

To develop this approach into a safe and effective therapy, it is necessary to identify the optimal conditions for motoneuron maturation to maximize functional muscle innervation. To establish the optimal cellular composition of the grafts, in

this Thesis I explored the role of non-motoneuronal cells, specifically astrocytes and V3 interneurons, on ESC-motoneuron maturation *in vitro*.

The results presented in this Thesis demonstrate that astrocytes play a fundamental role in the maturation of ESC-derived motoneuron morphology, synaptic connectivity, electrophysiological properties, and spontaneous activity *in vitro*, and are a prerequisite to the effects of spinal neural cell types, such as V3 interneurons, on motoneuron maturation in co-culture. These findings contribute to the growing literature exhibiting the importance of astrocytes to the functioning of the central nervous system.

In the presence of astrocytes, spinal V3 interneurons influenced the complement of synapses formed by ESC-derived motoneurons *in vitro* and promoted more mature patterns of spontaneous activity; an interesting insight into how neighbouring spinal neurons can affect the formation and activity of motor circuits.

These results suggest that the inclusion of astrocytes in peripherally-transplanted stem cell-derived grafts could promote the maturation of motoneurons and therefore increase the likelihood of functional innervation of muscle. The inclusion of V3 interneurons could also promote successful muscle innervation by the graft.

Moreover, the spinal cord-specific co-culture platform used in this Thesis provides a tool for investigating the interaction between motoneurons and other spinal cell types. Such a tool could be used to model diseases with spinal cord pathology, such as ALS.

The main findings of this Thesis have been disseminated to both academic audiences, e.g. Society for Neuroscience 2019, and non-academic audiences, e.g. in the 3-Minute Thesis competition and as part of PPL PWR SCL CLB (a series of talks to virtually exchange knowledge during lockdown due to Covid-19 in Spring 2020). Aside from contributing knowledge and understanding of cell-cell interactions affecting motoneuron maturation, the stem cell culture techniques used in this Thesis can be viewed as a very simplified ‘spinal cord in a dish’, a concept that may inspire the next generation of young scientists.

‘Whatever you do, work at it with all your heart, as working for the Lord, not for human masters’

Colossians 3:23, *New International Version*

“Unfortunately, nature seems unaware of our intellectual need for convenience and unity, and very often takes delight in complication and diversity.”

(Santiago Ramón y Cajal, 1906)

Acknowledgements

This Thesis would not have been possible without the kind support of many people, to whom I would like to express my sincerest gratitude. I would firstly like to thank my primary and secondary supervisors, Professor Linda Greensmith and Professor Rob Brownstone for their advice and mentorship, and for the opportunity to complete my PhD in their labs. Even when experiments were difficult or frustrating, meetings with my supervisors always renewed my enthusiasm for science and my Thesis. My thanks must also go to Dr Barney Bryson for the fundamental role his work played in this Thesis and for his training and guidance, particularly regarding cell culture experiments.

I want to thank all the other members of the Greensmith and Brownstone labs, past and present, as well as the Schiavo lab, for sharing their skills, knowledge and time, and for making the last few years so enjoyable. In particular, these experiments would have been infinitely more difficult without the excellent training and support in patch clamping and calcium imaging techniques from Dr Calvin Smith and Dr Ayisha Shabbir, respectively. I am also grateful to Dr Charlotte Spicer and Dr Alex Kourgiantaki who kindly proofread chapters of this Thesis and to Rachel Bonnington with whom I have regularly shared much needed tea and sympathy.

I greatly appreciate the support of the Brownstone and Greensmith lab managers, Dr Nadine Simons-Weidenmaier and James Dick, and would like to thank them for their advice, technical assistance and moral support. Chatting to both while working at neighbouring desks never failed to brighten my day. I also want to extend my thanks to other members of the Sobell Department, particularly Kully, Debbie, Ligia, Coral and Chris.

This work was supported by Susan Brenner-Morton at Columbia University's Zuckerman Institute, who I would like to thank for her contribution of many of the antibodies used in this Thesis; by Professor Aharon Lev-Tov at the Hebrew University Medical School, who kindly donated the SpinalCore software; and by Professor Samuel Pfaff and his lab at the Salk Institute for Biological Studies, to whom I am indebted for the donation of the *Sim1::cre;Rosa-LSL-tdtomato* mouse embryonic stem cell line, which was used in every chapter of this Thesis.

This project could not have happened without the many training opportunities and, crucially, the funding provided by the Wellcome Trust and my course organiser, Professor David Attwell. I am especially grateful for their continued financial support during periods of illness and throughout the Covid-19 pandemic.

Finally, I would like to thank my family and friends for their unfailing support and patience. I would especially like to thank my husband, Micah King, and my parents, Dr Alison Cooke and Dr Tim Hands, for their love and encouragement during the undertaking that has been my PhD.

Table of Contents

List of figures

List of tables

List of abbreviations

5-FDU	5-fluoro-2′-deoxyuridine
5-HT	5-hydroxytryptamine
ACh	Acetylcholine
ACSF	Artificial Cerebrospinal Fluid
AD-MSC	Adipose-Derived Mesenchymal Stem Cells
AHP	Afterhyperpolarisation Potential
ALS	Amyotrophic Lateral Sclerosis
ALS-FRS	ALS Functional Rating Scale (non-revised, original)
ALS-FRS-R	ALS Functional Rating Scale Revised
AM	Acetoxymethyl esters
AMPA	α-amino-3-hydroxy-5-methyl-4-isoxazolepropionic acid
ANOVA	Analysis Of Variance
AP	Action Potential
as	Astrocytes
ATP	Adenosine Triphosphate
atr	Atropine
ATXN2	Ataxin-2
BM-MSC	Bone Marrow-derived Mesenchymal Stem Cells
BMP4	Bone Morphogenic Protein
BTIII	Beta tubulin 3
CAG	CMV early enhancer/chicken β actin
Cat. #	Catalogue number
CD14	Cluster of Differentiation 14
ChAT	Choline Acetyltransferase
ChR2	Channelrhodopsin-2
CMAP	Compound Muscle Action Potential
CNQX	Cyanquixaline
CNS	Central Nervous System
CoV	Coefficient of Variation
CSF	Cerebrospinal Fluid
D	Dorsal
DA	Dopamine
DMEM	Dulbecco’s Modified Eagle’s Medium
DIV	Days In Vitro from the end of differentiation
DMSO	Dimethyl Sulfoxide
DNA	Deoxyribonucleic Acid
DRP	Dipeptide Repeat Peptide
EAATs	Excitatory Amino Acid Transporters
EB	Embryoid Body
ECM	Extracellular Matrix
En1	Engrailed 1
EPHA4	Ephrin type-A receptor 4

EPSP	Excitatory Postsynaptic Potential
ER	Endoplasmic Reticulum
ESC	Embryonic Stem Cell
Evx1	Even-Skipped Homeobox 1
FA	Flail Arm
FACS	Fluorescently-Activated Cell Sorting
FES	Functional Electrical Stimulation
FGF	Fibroblast Growth Factors
FI slope	Steady state Firing Frequency-current slope
FL	Flail Leg
FOV	Field Of View
FTD	Frontotemporal Dementia
FUS	Fused in Sarcoma
FVC	Forced Vital Capacity
GABA	Gamma Aminobutyric Acid
GDNF	Glial-cell Derived Neurotrophic Factor
GFAP	Glial Fibrillary Acidic Protein
GFP	Green Fluorescent Protein
GLT-1	Glutamate Transporter 1
Hb9	Homeobox protein 9
HMC	Hypaxial Motor Column
I_A	Transient outward K+ current
IFF	Initial Firing Frequency
I_h	Hyperpolarisation-activated depolarising current
I_{Nap}	Non-inactivating Na+ current
iPSCs	induced Pluripotent Stem Cells
Isl1	Insulin gene enhancer protein
KIF5A	Kinesin heavy chain isoform 5A
Lhx1	LIM Homeobox 1
Lhx3	LIM Homeobox 3
LMC	Lateral Motor Column
LMN	Lower Motoneuron
MACS	Magnetically-Activated Cell Sorting
MAR	Missing At Random
MCAR	Missing Completely At Random
mec	Mecamylamine
micRNA	Micro RNA
MMC	Medial Motor Column
MMc	Mitomycin-C
MN	Motoneuron
mRNA	Messenger RNA
MSC	Mesenchymal Stem/stromal Cells
MU	Motor Unit
NeuN	Hexaribonucleotide Binding Protein-3
NIV	Non-Invasive Ventilation

Nkx2.2	NK2 Homeobox 2
NMDA	N-Methyl-D-aspartic Acid
NMJ	Neuromuscular junction
NPC	Neural Progenitor Cells
NSC	Neural Stem Cells
PC	Principle Component
PCA	Principle Component Analysis
PCD	Programmed Cell Death
PEG	Percutaneous Endoscopic Gastronomy
PGC	Preganglionic motor Column
PLO	Poly-L-Ornithine
PLS	Primary Lateral Sclerosis
PMA	Progressive Muscular Atrophy
PMC	Phrenic Motor Column
pMN	Motoneuron Progenitors
PMT	Photomultiplier
PNS	Peripheral Nervous System
RA	Retinoic Acid
RAP	Rebound Action Potential
RC	Renshaw Cell
ReaChR	Red-shifted variant of Channelrhodopsin
RGC	Retinal Ganglion Cells
RMP	Resting Membrane Potential
RNA	Ribonucleic Acid
ROI	Region Of Interest
S100β	S100 calcium-binding protein β
SAA	Spike Amplitude Adaptation
SAG	Smoothened agonist
SCI	Spinal Cord Injury
Sema3A	Semaphorin 3A
SFA	Spike Frequency Adaptation
SFF	Steady-state Firing Frequency
Shh	Sonic hedgehog
SK	Small conductance calcium-activated K+ channels
SOD1	Cu/Zn superoxide dismutase
SPARC	Secreted Protein Acidic and Rich in Cysteine
TBS	Tris-Buffered Saline
TDP-43	Transactive response DNA-binding protein-43
TGFβ	Transforming Growth Factor β
TNFα	Tumour Necrosis Factor
TrkA	Tropomyosin receptor kinase A
tRNA	Tranfer RNA
UBQLN2	Ubiquilin-2
UK	United Kingdom

UMN	Upper Motoneuron
UPR	Unfolded Protein Response
UPS	Ubiquitin/Proteasome System
V	Ventral
V3	V3 interneuron
vAChT	Vesicular Acetylcholine Transporter
VCP	Valosin-Containing Protein
vGAT	Vesicular GABA Transporter
vGluT1	Vesicular Glutamate Transporter 1
vGluT2	Vesicular Glutamate Transporter 2
YFP	Yellow Fluorescent Protein

1 Chapter 1: General Introduction

1.1. Paralysis

Movement is vital for all human experience of the world and underpins all our physical interactions. Never is this more apparent than when the ability to move is lost, which occurs following disease or traumatic injury. In addition to the obvious practical difficulties and socio-economic impact presented by paralysis (Larkindale et al., 2014), the inability to move is devastating for patients and their families. Patients paralysed as a result of Spinal Cord Injury (SCI) or progressive neurodegenerative disorders are at a significantly higher risk of psychological morbidity (Craig et al., 2009, 1994a; Hancock et al., 1993; Lulé et al., 2018; Post and van Leeuwen, 2012), due partly to feelings of lack of control (Craig et al., 1994b; Post and van Leeuwen, 2012). Restoration of key muscle functions, particularly those such as hand grasping, would allow patients to interact with and regain some control of their environment, dramatically increasing quality of life, improving the mental health of both patients and their families, and decreasing the cost to society (Anderson, 2004; Larkindale et al., 2014). Several strategies to aid natural regeneration and restore movement following paralysis have been investigated, including approaches involving Functional Electrical Stimulation (FES), which can result in some improvements. However, the success of such methods varies greatly, depending on the nature of the injury or disorder. For example, many of these strategies rely on some residual healthy motoneuronal function, which is not present in many cases, including complete spinal injuries and disorders such as Amyotrophic Lateral Sclerosis (ALS).

1.1 Amyotrophic lateral sclerosis (ALS)

ALS is a progressive neurodegenerative disease in which motoneurons degenerate, resulting in atrophy and paralysis of limb, respiratory and bulbar muscles. Consequently, ALS patients gradually become unable to move, talk, chew, swallow or breathe independently (Peters et al., 2015; Petrov et al., 2017). The typical age of ALS onset is between 50-60 years of age (Chiò et al., 2011) and death is usually caused by respiratory failure within 1-5 years of diagnosis (Oskarsson et al., 2018). Although approximately 10% of ALS cases are familial and have a genetic determinant, most cases are sporadic (Bruijn et al., 2004).

While the initial disease process is difficult to disentangle from compensatory and secondary disease pathomechanisms, common pathologies observed across different cases of ALS include protein aggregation in motoneurons and non-neuronal cells, abnormal levels of Ribonucleic Acid (RNA) and RNA-binding proteins, disruption to the cell cytoskeleton and/or function, and non-cell-autonomous effects from cells around motoneurons (Peters et al., 2015). ALS is the most common form of adult motoneuron disease with an incidence of 2 in 100000 and a prevalence of 5 in 100000 (Chiò et al., 2013; Peters et al., 2015). Several studies have shown that the prevalence and incidence of ALS is slightly higher in men than in women (McCombe and Henderson, 2010; Talman et al., 2016). Over the past 20-30 years, intensive research effort has significantly improved our understanding of the genetics of ALS and a multitude of disease pathomechanisms. Despite this, however, there is currently no cure or effective disease-modifying therapy for ALS.

1.1.1 ALS: Clinical phenotypes

ALS has heterogeneous clinical presentation, but cases can be categorised into different clinical phenotypes based on the symptoms of Lower and Upper Motoneuron degeneration (LMN and UMN, respectively) and site of symptom onset. ‘Lower motoneurons’ are motoneurons in the spinal cord and brainstem that connect directly to muscles, often called the ‘final common path’, through which the nervous system controls bodily movement (Burke, 2006; Sherrington, 1906). The term ‘upper motoneuron degeneration’ is a clinically useful term referring to motor deficits seen when lower motoneurons are denervated due to degeneration of axons that project to them from the cerebral cortex and brainstem. Approximately 30% of ALS cases have both UMN and LMN involvement at disease onset; this is described as typical or ‘classical’ ALS (Chiò et al., 2011). Typical ALS patients have a mean survival time of 3-4yrs (Grad et al., 2017; Oskarsson et al., 2018; Takeda et al., 2020). Symptoms begin in a discrete body region, usually the bulbar region, an arm or a leg, and progress to contralateral limbs and/or to other spinal and/or bulbar areas (Grad et al., 2017; Ravits et al., 2013; Takeda et al., 2020).

The remaining 70% of ALS patients are comprised of ALS variants. Despite the phenotypic differences compared to ‘Typical ALS’, these variants are commonly

placed on the ALS spectrum because the underlying molecular neuropathology and genetics overlap significantly (Ravits et al., 2013). One such variant is Bulbar-onset ALS, which comprises 34% of ALS cases (Chiò et al., 2011). Bulbar-onset ALS has predominantly LMN involvement and is characterised by dysarthria or dysphagia with atrophy of bulbar muscles. The mean survival of Bulbar-onset ALS is two years, shorter than for Typical ALS (Chiò et al., 2011; Takeda et al., 2020).

Progressive Muscular Atrophy (PMA) is another phenotypic variant of ALS with predominantly LMN involvement, though a proportion of diagnosed PMA patients later develop UMN signs as the disease progresses (Kim et al., 2009; Rowland, 2010; Visser et al., 2007). Approximately 5% ALS patients have PMA (Rowland, 2010; Wijesekera et al., 2009) and mean survival time is similar to Typical ALS (Wijesekera et al., 2009).

Of ALS patients with predominantly LMN involvement, a subset of patients display long-lasting deterioration of either the upper or lower limbs, while other systems remain relatively normal; these are Flail Arm (FA) and Flail Leg (FL) Syndrome, respectively. FA and FL syndrome account for 11% and 6% of ALS patients respectively and have a longer mean survival time than Typical ALS (approximately six years) (Chiò et al., 2011; Talman et al., 2009; Wijesekera et al., 2009). FA syndrome is four times more prevalent in men than women (Wijesekera et al., 2009).

Other variants of ALS are characterised by predominantly UMN involvement. For example, Primary Lateral Sclerosis (PLS) patients present with exclusively UMN involvement, though a proportion initially diagnosed with PLS develop LMN symptoms within four years of onset (Gordon et al., 2006). Indeed, patients are not considered to have pure PLS unless no LMN involvement is observed 3-4 years after diagnosis (Almeida et al., 2013b; Gordon et al., 2006; Pringle et al., 1992; Talman et al., 2009). PLS patients account for approximately 5% of ALS cases and those displaying exclusively upper motoneuron signs have dramatically longer survival times than patients with Typical ALS (Talman et al., 2009, 2016). A second variant of ALS with predominantly UMN involvement is hemiplegic ALS – also known as Mills' Syndromes – which manifests with unilateral symptoms. Hemiplegic ALS is a rare variant, accounting for

approximately 1% of ALS patients, with long survival times, often exceeding 10 years (Jaiser et al., 2019; Takeda et al., 2020).

In addition to motor symptoms, approximately 50% of ALS patients present with cognitive impairment (Raaphorst et al., 2010; Ringholz et al., 2005). Indeed, 10-20% of ALS patients are diagnosed with Frontotemporal Dementia (FTD) (Belzil et al., 2016; Gordon et al., 2011; Ringholz et al., 2005; Taylor et al., 2016) and it is likely that in many diagnosed ALS patients, symptoms of cognitive impairment may not become acute enough during the period of rapid disease progression to be diagnosed as FTD (Raaphorst et al., 2010). FTD is caused by the loss of cortical neurons in the frontal and temporal cortices, which impairs judgement and executive skills, often leading to unusual behaviours such as social withdrawal, confrontation seeking, and personality changes. Some less common language variants of FTD involve deterioration in language output, difficulty understanding the meaning of words, or hesitant and repetitive speech (Solomon et al., 2019). Unlike Alzheimer's Disease, FTD does not involve classical memory loss (Solomon et al., 2019; Taylor et al., 2016). Motor dysfunction is also a significant symptom of patients diagnosed with FTD, with approximately 50% of FTD patients displaying some form of motor dysfunction and 5-12% of FTD patients receiving a concomitant diagnosis for ALS (Burrell et al., 2011; Ferrari et al., 2011; Solomon et al., 2019). This link between ALS and FTD is now known to be the result of shared genetic and pathological mechanisms. The discovery that mutations in the *C9orf72* gene can cause both ALS and FTD resulted in a paradigm shift in our understanding of these two previously clinically unrelated disorders. ALS was thought to be purely a motor/movement disorder and FTD a cognitive, behavioural form of dementia. It is now clear that *C9orf72* mutations are the most common cause of familial ALS, FTD and ALS-FTD. The link between these two diseases is further strengthened by findings that show that mutations in several other genes can also cause both diseases. This has led to the suggestion that ALS and FTD form part of a continuum of a broader ALS-FTD spectrum disorder (Giordana et al., 2011; Taylor et al., 2016; Wilson et al., 2001).

1.1.2 The genetics of ALS

Approximately 10% of ALS cases are described as familial meaning that there is a family history of ALS (Brenner and Weishaupt, 2019; Bruijn et al., 2004; Taylor

et al., 2016). The remaining cases of ALS are described as sporadic, with no known prior family history of the disease. Familial ALS is frequently transmitted as dominant, high penetrance genetic traits, and a causative genetic mutation has been identified in about 60% of cases (of European kindreds, at least) (Smith et al., 2013). Though sporadic cases are traditionally thought of as having little or no genetic component, at least 10% of sporadic ALS components have mutations in the same genes implicated in familial ALS (Smith et al., 2013; Taylor et al., 2016). Rather than implying the absence of a disease-modifying genetic component, therefore, lacking a family history of ALS may reflect either incomplete penetrance of the genetic trait (Smith et al., 2013) or inconsistent methods of defining and gathering family histories (Al-Chalabi, 2017).

The first ALS gene was discovered in 1993 and encoded for cytosolic Cu/Zn superoxide dismutase (SOD1) (Rosen et al., 1993). Since then, at least 25 different genes have been implicated in familial ALS, sporadic ALS, or both, many of which are detailed in Table 1.1. The functions of ALS-linked genes have given insight into the pathomechanisms of ALS and the differences between clinical phenotypes. For example, the discovery of ALS-related mutations in TDP-43 and FUS highlighted the role of RNA dysregulation, discussed below (Section 1.1.3.2). Although TDP-43 and FUS mutations account for a relatively small proportion of ALS cases (Table 1.1), their discovery caused a significant change in thinking about ALS pathomechanisms as, prior to their discovery, research was focussed almost entirely on the pathological function of mutant SOD1.

Mutations in the *SOD1* gene account for approximately 20% of familial ALS cases and are associated with 2% of sporadic ALS cases (Table 1.1). The wild-type SOD1 protein is an antioxidant that neutralises free superoxide radicals (McCord and Fridovich, 1969). The mutant SOD1 protein was found in the protein inclusions characteristic of ALS pathology (Kato et al., 1996, 2001) and the molecular basis for mutant SOD1 toxicity is multifactorial. The function of wildtype SOD1 is to detoxify superoxide anions produced by aerobic respiration, so a likely effect of mutant SOD1 is to provoke oxidative stress and form toxic nitrotyrosines (Beckman et al., 1993; Peters et al., 2015). However, SOD1 knockout mice do not show significant motor abnormalities, indicating that a loss of SOD1 function is unlikely to account for SOD1-ALS (Turner and Talbot, 2008). The effects of mutant SOD1 are dose dependent, with disease severity increasing with load of

Table 1.1: ALS genetics: causative genes.

The Table summarises the key genes known to cause ALS and includes a brief description of their known function. The genes are ordered according to frequency with which they are observed in patients with familial ALS. For frequencies <1%, genes are ordered alphabetically. Not all genes whose mutations cause ALS are included, nor are genes that alter disease risk and/or modify disease progression; for a more complete list, see (Mejzini et al., 2019).

Locus	Gene	Protein	Functionality	Proportion of ALS		Reference
				Familial	Sporadic	
9p21-22	*C9ORF72*	C9ORF72	Transcription & pre-mRNA splicing regulation? Membrane trafficking via Rab GTPase family? Autophagy regulation?	25-50%	5-10%	DeJesus-Hernandez et al., 2011; Gijselinck et al., 2012; Renton et al., 2011; Smith et al., 2013
21q22.1	*SOD1*	Cu/Zn superoxide dismutase	Major cytosolic antioxidant	20%	2%	Rosen et al., 1993
q36	*TARDBP*	TDP-43	Transcription & pre-mRNA splicing regulation; micRNA biogenesis; RNA transport & stabilization; translational regulation of ApoE-II & CFTR	5%	<1%	Kabashi et al., 2008; Sreedharan et al., 2008
16p11.2	*FUS*	FUS/TLS	Transcription & pre-mRNA splicing regulation; micRNA processing; mRNA transport & stabilization; maintenance of genomic integrity; regulating protein	5%	<1%	Kwiatkowski et al., 2009; Vance et al., 2009

			synthesis at synapse			
10p15-p14	*OPTN*	Optineurin	Golgi maintenance; exocytosis; vesicular trafficking; regulator of NF-κB signaling pathway; autophagy process	4%	<1%	Maruyama et al., 2010
12q13.3	*KIF5A*	Kinesin Family Member 5A	Neuronal motor protein for anterograde transport of organelles	1-4%	<1%	Brenner et al., 2018; Nicolas et al., 2018
10q22.3	*ANXA11*	Annexin A11	Cell division, Ca^{2+} signalling, vesicle trafficking & apoptosis (Wang et al., 2014)	2%	?	Smith et al., 2017a
9p13.3	*VCP*	Valosin-containing protein	Protein degradation via the Ubiquitin/ Proteasome System (UPS), autophagy & ER; membrane fusion	1–2%	<1%	Johnson et al., 2010
2p13	*DCTN1*	Dynactin	ER-to-golgi transport; centripetal movement of lysosomes & endosomes; spindle formation, chromosome movement; nuclear positioning; axonogenesis	1%	<1%	Puls et al., 2003
14q11	*ANG*	-Angiogenin	RNA processing & tRNA modification;	<1%	<1%	Greenway et al., 2004, 2006

			vascularization ; RNase activity & stress granule assembly; neurite outgrowth & pathfinding			
22q11.23	*CHCHD10*	Coiled-coil-helix-coiled-coil-helix domain containing 10	Mitochondrial genome stability; cristae integrity & mitochondrial fusion	<1%	<1%	Bannwarth et al., 2014
3p21.1	*GLT8D1*	Glycosyltransferase 8 Domain Containing 1	?	<1%	<1%	Cooper-Knock et al., 2019
12q13.1	*HNRNPA1*	hnRNPA1	Packing & transport of mRNA; micRNA biogenesis	<1%	<1%	Kim et al., 2013; Liu et al., 2016
5q31.2	*MATR3*	Matrin 3	RNA processing; stabilizing mRNAs; gene silencing; chromatin organization	<1%	<1%	Johnson et al., 2014
17p13.2	*PFN1*	Profilin-1	Regulates ATP-mediated actin polymerization	<1%	<1%	Wu et al., 2012
5q35	*SQSTM1*	p62	Autophagy & UPS degradation; regulator of NF-κB signalling pathway; immune response	<1%	?	Fecto et al., 2011; Teyssou et al., 2013
2q36.1	*TUBA4A*	α-tubulin 4a	Microtubule subunit	<1%	<1%	Smith et al., 2014

Xp11.23 -Xp13.1	*UBQLN2*	Ubiquilin 2	Protein degradation via UPS	<1%	<1%	Deng et al., 2011
12q14.1	*TBK1*	TANK-binding kinase 1	Regulates autophagy & inflammation	?	?	Freischmidt et al., 2015

the mutant protein (Gill et al., 2019; Peters et al., 2015), suggesting that a toxic gain-of-function may account for the deleterious effects of mutant SOD1. Whatever the molecular basis for SOD1 cytotoxicity, mutant SOD1 pathology disrupts multiple cellular processes (Peters et al., 2015). Different *SOD1* mutations result in different clinical phenotypes. For example, the D90A mutation, the most common *SOD1* mutation globally, causes limb-onset ALS and progresses slowly, whereas A4V mutation causes sudden disease onset with rapid progression that involves respiratory muscles early in the disease (Pansarasa et al., 2018; Ravits et al., 2013).

A paradigm-shifting insight into the link between genetics and clinical phenotype was revealed in 2011, when the association between mutations in *C9orf72* and the comorbidity of ALS and FTD was first identified. *C9orf72* mutations are now known to cause 40-50% of familial ALS/FTD as well as 8-10% of sporadic cases (DeJesus-Hernandez et al., 2011; Gijselinck et al., 2012; Renton et al., 2011). The wild-type function of the gene is unknown, although its structure implicates a role in membrane cell trafficking (Peters et al., 2015) and more recent evidence suggests a role in autophagy (Leskelä et al., 2019). The mutation in the *C9orf72* gene is a G_4C_2 expansion repeat motif located within a normally non-coding intron within the *C9orf72* promoter. The expansion shows somatic instability, with different cells in the same individual expressing different length expansions (Sareen et al., 2013). Sense and antisense transcripts across the G_4C_2 expansion segment form RNA foci in the nucleus of motoneurons (Almeida et al., 2013a; DeJesus-Hernandez et al., 2011; Donnelly et al., 2013; Lagier-Tourenne et al., 2013; Sareen et al., 2013). It is thought that these RNA foci may compromise cellular viability by sequestering transcription factors (Sareen et al., 2013), altering transcript splicing, or generating short functional RNA fragments which act as siRNA or miRNA to silence gene expression (Peters et al., 2015). Noncanonical, repeat-associated non-ATG–mediated (RAN-mediated)

translation from all possible reading frames of the intronic hexanucleotide repeat produces a variety of atypical Dipeptide Repeat Peptides (DRPs), which aggregate in the cytoplasm (Ash et al., 2013; Gendron et al., 2013; Mori et al., 2013b, 2013a; Wen et al., 2014; Zu et al., 2011). Some of these atypical peptides have been shown to be neurotoxic in *Drosophila* (Mizielinska et al., 2014) and mammalian neurons *in vitro* (Wen et al., 2014). Moreover, antibodies which promote the clearance of these DRPs have been shown to improve neurodegenerative and behavioural phenotypes, and increase survival in a mouse model of *C9of72*-mediated ALS (Nguyen et al., 2019).

In addition to causative mutations, such as in *SOD1* and *C9orf72*, several genetic risk factors or susceptibility genes have been identified – i.e. mutations which modify the disease or enhance ALS susceptibility (Taylor et al., 2016). For example, ataxin-2 is a potent modifier of TDP-43 toxicity in animal and cellular ALS models and is mislocalised in spinal neurons of ALS patients (Elden et al., 2010). Furthermore, Elden et al. (2010) demonstrated that intermediate-length expansions in the ataxin-2 gene are significantly associated with ALS, establishing *ATXN2* as a relatively common ALS susceptibility gene. Other gene variants have been shown to modify the disease; loss-of-function KIF5A mutations was associated with increased survival of ALS patients compared to the rest of the ALS cohort (Nicolas et al., 2018). Other examples include genes that modulate the expression of EPHA4; in ALS patients, disease onset and survival is inversely correlated with EPHA4 expression and loss-of-function mutations in *EPHA4* are associated with long survival (Van Hoecke et al., 2012).

Thus, ALS genetics can provide insight in distinguishing between clinical ALS phenotypes. However, there is significant overlap in the clinical presentations of different ALS mutations, suggesting that multiple mechanisms can cause the same ALS phenotype. Conversely and remarkably, the same mutation in the same gene within the same family can cause different clinical ALS presentation, suggesting that the molecular cascade initiated by the mutation is not the only factor that affects clinical ALS phenotype (Ravits et al., 2013). Nonetheless, study of ALS genetics has led to the discovery of a variety of ALS pathomechanisms.

1.1.3 ALS: Pathomechanisms

The symptoms of ALS are predominantly caused by the progressive degeneration of the motor cortex and lower motoneurons. Other cell types show differing vulnerability to ALS toxicity. For example, non-neuronal cells are generally spared in ALS (Nagai et al., 2007). Different motoneuron subtypes also differ in their vulnerability to ALS. While lower somatic motoneurons innervating voluntary muscles degenerate, gamma motoneurons (Lalancette-Hebert et al., 2016) and certain lower motoneuron subgroups are relatively resistant to degeneration, including ocular motoneurons, which regulate eye movement, and motoneurons in the Onuf's nucleus that innervate the sphincters responsible for continence (Gizzi et al., 1992; Kaminski et al., 2002; Mannen, 2000; Schrøder and Reske-Nielsen). Additionally, there is a gradient of vulnerability among spinal alpha motoneurons, such that those innervating fast-twitch muscle are most severely affected and degenerate first, and motoneurons that innervate slow-twitch muscle are more resistant and die later in disease progression (Kanning et al., 2010).

Many pathomechanisms have been proposed to lead to the death of motoneurons in ALS. Moreover, secondary phenomena induced by the disease process can involve wildtype proteins and cellular pathways not directly affected by the mutant protein. Some of these secondary phenomena may be compensatory mechanisms that initially ameliorate the disease but eventually become pathological. Distinguishing primary, secondary and compensatory mechanisms is an important consideration when identifying targets for therapeutic intervention. Common pathomechanisms observed in ALS include deposition of ubiquitinated and cytoplasmic protein aggregates in motoneurons and non-neuronal cells, aberrant RNA metabolism, disruption to the cell cytoskeleton and dysfunctions in axon transport, mitochondrial dysfunction, neuroinflammation, and oxidative stress. In addition, there are non-cell-autonomous effects from cells around motoneurons (Bruijn et al., 2004; Peters et al., 2015; Yamanaka and Komine, 2018). While these mechanisms are most well characterised in genetic ALS models, autopsies (Peters et al., 2015) and studies using induced Pluripotent Stem Cells (iPSCs) from sporadic ALS patients (Israel et al., 2012) show that the pathological mechanisms of sporadic and familial ALS at least partly overlap.

1.1.3.1 Protein aggregation

Protein pathology was one of the earliest identified pathological markers of ALS (Peters et al., 2015). Protein inclusions containing ubiquitinated material were observed in spinal motoneurons in ALS patient post-mortem tissue as early as the 1980s (Leigh et al., 1988) and subsequently have been shown to contain many of the proteins implicated in ALS, including SOD1 (Kato et al., 1996, 2001), TDP-43 (Neumann et al., 2006), FUS (Vance et al., 2009) and atypical dipeptides from the G_4C_2 expansion repeat motif of *C9orf72* (Ash et al., 2013; Mori et al., 2013a). These inclusions are observed in both familial and sporadic ALS (Ramesh and Pandey, 2017). The prevalence of neuronal inclusions in ALS has led to the proposal that they may be responsible for ALS pathology. However, recent evidence suggests that this is not the case. For example, there is evidence from mouse models of mutant SOD1-mediated ALS that soluble oligomers of mutant SOD1 proteins are more toxic than larger SOD1 aggregates (Gill et al., 2019; Proctor et al., 2016; Zhu et al., 2018).

The superfluity of protein inclusions and/or misfolded proteins in ALS likely puts pressure on the protein handling and degradation systems of affected cells, inducing Endoplasmic Reticulum (ER) stress and the Unfolded Protein Response (UPR) (Peters et al., 2015). 'ER stress' is the accumulation of intralumenal misfolded proteins due to interference with the oxidative protein folding processes in the ER. ER stress triggers the UPR; cytosolic and nuclear signalling increases the capacity for protein folding or triggers apoptosis if the adaptation mechanisms are insufficient to handle the ER stress (Ron and Walter, 2007). Evidence of both ER stress (Ilieva et al., 2007; Kikuchi et al., 2006) and the UPR (Atkin et al., 2008; Hetz et al., 2009) have been observed in both ALS mouse models and patients. Furthermore, mutations in some ALS-causing genes such as *VCP* and *UBQLN2* (Table 1.1) impair protein degradation pathways. One mechanism modulated by the UPR is autophagy – i.e. the intracellular turnover of cellular components such as amino acids and lipids. Autophagy is impaired in various models of ALS, though the role of autophagy in the disease process seems to change as the disease progresses (Ramesh and Pandey, 2017). There is evidence that increasing macroautophagic protein degradation reduces the accumulation of aggregates in the spinal cords of mice with mutant SOD1 (Hetz et al., 2009) and TDP-43 proteinopathy (Wang et al., 2013), and can prolong survival of mutant

SOD1 mice (Hetz et al., 2009). Thus, disruption to protein metabolism, either directly by mutations in important component genes or indirectly by overwhelming the unfolded protein-handling capacity of the cell, is one fundamental pathomechanism in ALS.

1.1.3.2 Disrupted RNA processing

As shown in Table 1.1, many mutations implicated in ALS are involved in DNA/RNA interactions. In normal physiological conditions, these DNA/RNA-interacting proteins are predominantly nuclear. Frequently, mutant variants of these proteins are mislocated to the cytoplasm, depleting the nucleus of the affected protein. The most commonly implicated in ALS are TDP-43 and FUS; they are involved in DNA/RNA-binding, transcription, RNA splicing, miRNA biogenesis, mRNA transport, mRNA transcript stability, translation, autophagy, the stress response, and TDP-43 is particularly important for the degradation of abnormal mRNA (reviewed by Birsa et al., 2020 and Ederle and Dormann, 2017). TDP-43 (Neumann et al., 2006) and FUS (Kwiatkowski et al., 2009; Vance et al., 2009) have been identified as key components of ubiquitinated inclusions in the brains and spinal cords of ALS patients. It is unclear whether the associated toxicity of mutations in these proteins is due to the loss of functioning protein in the nucleus, acquired cytotoxic function or both. However, it is clear that the native function of these proteins is severely impaired; for example, expression of the Q331K human mutant TDP-43 variant causes alteration in the splicing of >1000 RNA transcripts (Arnold et al., 2013). Hence, therapies solely targeting neuronal inclusions may not be sufficient to restore physiological RNA-processing and alleviate ALS symptoms.

1.1.3.3 Cytoskeletal and axon transport deficits

The unusually long length of motor axons renders motoneurons particularly dependent on intracellular transport mechanisms. Disruptions in these pathways may contribute to the vulnerability of motoneurons in ALS. Many genes implicated in ALS do indeed affect the structure and maintenance of the cytoskeleton, including α-tubulin 4a and profilin-1, and intracellular transport, such as dynactin and KIF5A (Table 1.1). Axons of ALS patients (Hirano et al., 1984) and mutant SOD1 mice show evidence of neurofilament accumulation, which may be indicative of impaired anterograde transport (Pun et al., 2006). Moreover, *in vivo*

assays revealed impaired retrograde axon transport in motoneurons of early symptomatic mutant SOD1 mice (Bilsland et al., 2010; Gibbs et al., 2018). Therefore, therapies that target the deficits in axonal transport are being investigated as a potential therapeutic approach for treating ALS (Gibbs et al., 2018).

1.1.3.4 Mitochondrial dysfunction

Early studies of post-mortem tissues from ALS patients identified morphological abnormalities in the mitochondria of spinal motoneurons and the motor cortex (Gautam et al., 2019; Hirano et al., 1984; Sasaki and Iwata, 1999). These mitochondrial abnormalities may partly result from disruption to mitofission and mitophagy, which has been implicated in SOD1- (Xie et al., 2015), *C9orf72*- (Chai et al., 2020) and TDP-43- (Xu et al., 2010) mediated ALS pathology. In mouse models of SOD1-ALS, evidence of mitochondrial dysfunction include deficits in oxidative phosphorylation (Jung et al., 2002; Mattiazzi et al., 2002) and mitochondrial calcium buffering capacity (Damiano et al., 2006). Also, in mouse models, mitochondrial degeneration has been shown to occur at disease onset, concomitant with the onset of peripheral weakness and before motoneuronal death, suggesting that mitochondrial decline might be the trigger for functional decline in ALS (Kong and Xu, 1998).

1.1.3.5 Non-cell-autonomous pathomechanisms

Although motoneuronal toxicity is a determinant of disease initiation, the ALS disease process is modified by other cell types. This concept of a non-cell autonomous pathomechanism was initially and powerfully demonstrated when Clement et al (2003) showed that survival of chimeric mice was prolonged when mutant $SOD1^{G93A}$-expressing motoneurons were surrounded by wildtype non-neuronal cells (Clement et al., 2003). Selective diminishment of mutant $SOD1^{G93A}$ in the astrocytes (Yamanaka et al., 2008) or microglia (Boillee et al., 2006) in mutant mice substantially slowed disease progression late in the disease time course without affecting disease onset. Similarly, selective knockout of $SOD1^{G93A}$ in oligodendrocytes both delayed disease onset and prolonged survival (Kang et al., 2013). In contrast, a reduction in mutant SOD1 expression in Schwann cells accelerated disease progression (Lobsiger et al., 2009). These results *in vivo* have been supported by *in vitro* studies of both SOD1-mediated ALS (Nagai et

al., 2007) and other disease ALS etiologies; for example, astrocytes differentiated from iPSCs derived from mutant *C9orf72* ALS patients induce non-cell autonomous pathophysiology in wildtype motoneurons (Birger et al., 2019; Zhao et al., 2019). *In vitro* studies have shown that mutant astrocytes were not toxic to other neuronal subtypes, and mutant fibroblasts, microglia, cortical neurons and myocytes were not toxic to motoneurons (Nagai et al., 2007), suggesting motoneurons are selectively vulnerable to mutant astrocytes. Thus, non-neuronal cells have been shown to have a clear role in ALS progression.

Alterations in the excitability of motoneurons implicates other neuronal subtypes in the etiology of ALS. Electrophysiological studies in ALS models variously observe that motoneurons have unchanged, hyper- or hypo- excitability (reviewed in King et al., 2016). It has been suggested that this variation in electrophysiological findings is due to the heterogeneity of the motoneuron population (Felix and Zytnicki, 2015; Leroy et al., 2014) and/or changes in spinal circuitry that facilitate excitotoxicity as the disease progresses (Brownstone and Lancelin, 2018). One mechanism that leads to excitotoxicity results from accumulation of glutamate in the synaptic cleft; overstimulation of postsynaptic excitatory amino acid receptors increases intracellular Ca^{2+} concentrations, leading to the activation of Ca^{2+}-dependent enzymes and Ca^{2+}-induced oxidative stress by increasing the production of reactive oxygen species (ROS) (Almaas et al., 2002; Hill et al., 2016). This leads to mitochondrial dysfunction and eventually cell death (García and Massieu, 2003).

Though intracellular Ca^{2+} concentration may also be increased by other mechanisms, such as Ca^{2+} release from internal stores, glutamate excitotoxicity particularly is implicated in ALS. ALS patients have dysregulated glutamate signalling, transport, and metabolism (Couratier et al., 1993; Rothstein et al., 1990, 1992; Selvaraj et al., 2018). Moreover, motoneurons differentiated from iPSCs derived from *C9ORF72* mutation-carrying ALS patients showed altered glutamate receptor subunit expression and increased vulnerability to glutamate excitotoxicity *in vitro* (Selvaraj et al., 2018). Most compellingly, the only licenced pharmacological treatment for ALS in the United Kingdom (UK), Riluzole, is an inhibitor of glutamate neurotransmission and is neuroprotective both *in vitro*, *in vivo* (Doble, 1996) and in ALS patients, as discussed in the next Section.

Therefore, any changes in spinal circuitry that increase the amount or strength of excitatory input to motoneurons are likely to be deleterious in ALS.

Brownstone and Lancelin (2018) put forward a mechanistic theory suggesting that homeostatic compensation in spinal circuitry hastens motor degeneration in ALS and similar progressive motor disorders. According to this proposal, in response to an initial pathological reduction in motoneuron output, there is a homeostatic increase of excitatory input from Ia and descending afferents to motoneurons in order to maintain force output. The increase of excitatory, predominantly glutamatergic, input would then lead to or exacerbate glutamate excitotoxicity and accelerate motoneuron death. In support of this theory, functional elimination of Ia afferents was found to be protective in mutant SOD1 mice (Lalancette-Hebert et al., 2016). Therefore, it is important to take homeostatic compensation into account when designing therapeutic agents to target the pathomechanisms of ALS.

1.1.4 Treatment of ALS

Despite all that has been discovered about ALS pathomechanisms since the disease was first identified over 150 years ago, the treatment of ALS patients remains largely focused on symptom management rather than curing or modifying disease progression. Typical interventions include Percutaneous Endoscopic Gastronomy (PEG) to ameliorate weight loss caused by increased metabolic rate and dysphagia as neurons innervating muscles become affected (Dorst et al., 2015), as well as Non-Invasive Ventilation (NIV) to compensate for diaphragm weakness and to alleviate the symptoms of respiratory insufficiency (Dorst and Ludolph, 2019). These interventions can significantly extend the survival of ALS patients (Berlowitz et al., 2016; Bond et al., 2019; Bourke et al., 2006; Hirose et al., 2018; Kleopa et al., 1999; Sancho et al., 2018).

In addition to such physical interventions, the only licenced pharmacological treatment for ALS in the United Kingdom (UK) is Riluzole, although its beneficial effects are limited. Riluzole has been shown to improve the survival rate of ALS patients and slow the deterioration of muscle strength, with the largest improvement observed in ALS patients with bulbar onset (Bensimon et al., 1994; Lacomblez et al., 1996; Miller et al., 1996), who typically have a faster rate of

progression. However, the benefit is limited, equating to approximately 2-3 months of extended life (Bellingham, 2011; Miller et al., 2002).

Enormous effort has focused on identifying new pharmacological treatments for ALS. The antioxidant, Edaravone, initially developed for treatment of ischemic stroke (Takei et al., 2017), was approved for the treatment of ALS in Japan in 2015 followed by five other countries, including the US and China (Mitsubishi Tanabe Pharma, 2019; Rothstein, 2017). While Edaravone failed to show any significant improvement on patient's ALS Functional Rating Scale (ALS-FRS) score in the initial Phase III clinical trial (Abe et al., 2014), a subpopulation of ALS patients, defined by moderate baseline clinical characteristics, were found to be responsive to Edaravone (Edaravone (MCI-186) ALS 16 study group, 2017; Tanaka et al., 2016; Writing Group et al., 2017). To date, Edaravone has not been licenced in the EU.

It is disappointing that after 20 years of intensive research, Riluzole remains the only widely licensed treatment for ALS, and even this confers limited benefits. This is not due to a lack of endeavour; clinical trials of more than 21 other drugs targeting at least six different pathomechanisms have proved to be unsuccessful (Petrov et al., 2017). Furthermore, no pharmacological treatment discovered thus far can restore function already lost by the disease and there remains currently no cure or effective disease modifying treatment for ALS.

1.2 Traditional and experimental approaches to overcoming paralysis

The characteristic phenotype of ALS is progressive muscle paralysis. Muscle paralysis is also the defining characteristic of a number of other neurological disorders and occurs as a result of traumatic injuries such as brachial plexus injury and SCI. Various approaches have been explored to overcome paralysis.

1.2.1 Functional electrical stimulation

Electrical stimulation can be used to treat or supplement function lost in cases of neurological dysfunction (Peckham and Knutson, 2005). Therapeutic electrical stimulation of muscles, peripheral nerves, spinal cord and/or brain regions is frequently used during neurorehabilitation to improve tissue health or voluntary function (Angeli et al., 2014; Luo et al., 2020; Wagner et al., 2018), by, it is

thought, stimulation neuroplasticity and speeding up axon regeneration (Chan et al., 2016). In contrast to therapeutic electrical stimulation, FES is used to replace or assist the voluntary abilities of neurologically-impaired individuals (Peckham and Knutson, 2005). To restore/supplement motor function, the most common approach is to stimulate peripheral lower motoneuron axons innervating the target muscle. For example, the Walkaide footdrop stimulator sends electrical current to the common peroneal nerve at a certain point in the gait cycle to correct for footdrop during walking in individuals with neurological disorders (that spare the common peroneal nerve), increasing walk speed and decreasing effort (Dai et al., 1996). Similarly, stimulators have been developed to restore the hand grasp/release functions and supplement grip strength in tetraplegic individuals (Gan et al., 2011, 2012; Prochazka et al., 1997).

The limitation of peripheral FES is the requirement for surviving lower motor axons innervating target muscles. Some injuries such as brachial plexus injury involve extensive damage to lower motoneuron axons, meaning FES is ineffective. Furthermore, in disorders such as ALS, where lower motoneurons are progressively degenerating, electrical stimulation of the unhealthy motoneurons could cause further damage to the degenerating axons and exacerbate disease progression. Indeed, there is evidence that electrical stimulation is harmful in rodent models of ALS (Lepore et al., 2010), and, when electrical stimulation of the diaphragm (diaphragmatic pacing) was trialled in ALS patients for safety and efficacy, it was concluded that pacing reduced survival duration (DiPALS Writing Committee et al., 2015).

One option to bypass the need of lower motoneuron involvement is direct stimulation of muscle to elicit contraction. However, the stimulus magnitude required to cause contraction by direct muscle stimulation is higher than for nerve stimulation (Peckham and Knutson, 2005). Moreover, for muscle that is denervated, as in ALS, the stimulus magnitude required is ten-fold higher than for innervated muscle (Prochazka et al., 1997). As electrical stimulation is non-specific, high stimulus magnitudes could also activate non-motor axons. These include smaller diameter nociceptive axons and terminals that transmit pain (Peckham and Knutson, 2005) (Anna Hands at SfN 2019!) and do not seem to degenerate in ALS until much later in disease progression, if at all (Heads et al., 1991). Therefore, FES is not always effective at restoring or improving motor

Table 1.2: Limitations of different experimental approaches to overcoming paralysis

*Unless overcome by pharmacological intervention (Deshpande et al., 2006).

Challenges	Functional Electrical Stimulation	CNS stem cell replacement	Peripheral engraftment of stem cell-derived motoneurons	
			Electrical stimulation	Optical stimulation
Restores direct voluntary muscle control	✓ (sometimes)	✗	✗	✗
Specific to target motoneurons	✗	n/a	✗	✓
Does NOT cause muscle fatigue	✗	✓	✗	✓
Safe for patients with motor degeneration	✗	✓	✗	✓
Permissive environment for axon extension	n/a	✗*	✓	✓
feasible distance for axon to extend to reach muscle	n/a	✗	✓	✓
Enables exogenous control of muscle contraction	✓ (sometimes)	✗	✓	✓

function (Table 1.2).

1.2.2 CNS cell-based therapies

Another approach being explored to help recovery of voluntary movement in cases of paralysis is the transplantation of therapeutically useful cells into the Central Nervous System (CNS). These may be stem cells or stem cell-derived motoneurons. Transplanted stem cells being considered by current ALS research and investigated in clinical trials include autologous Bone Marrow-derived (BM) and Adipose-Derived (AD) Mesenchymal Stem Cells (MSCs), olfactory ensheathing cells, granulocyte colony-stimulating factor-stimulated peripheral blood stem cells, and human Neural Stem or Progenitor Cells (NSCs and NPCs, respectively) (Goutman et al., 2019). This Section will particularly focus on MSCs

and NPCs as the most well-explored stem cell therapies transplanted into the CNS to date.

1.2.2.1 Pre-clinical models show stem cells transplanted into the CNS may facilitate recovery in ALS by trophic mechanisms

Mesenchymal stem/stromal cells (MSCs) are oligopotent cells, which can be isolated by a relatively simple procedure from bone marrow, umbilical cord tissue, fat tissue (Forostyak and Sykova, 2017) and even menstrual blood (Wu et al., 2018), and used autologously (avoiding the need for immunosuppressants). MSCs differentiate into chondrocytes, osteocytes and apidocytes (Herzog et al., 2003) and there is evidence that they can be differentiated towards a neural fate (Mezey et al., 2000; Tropel et al., 2006). Various preclinical studies have demonstrated positive effects of MSCs on survival and motor activity in rodent models of ALS using various delivery methods, though primarily intrathecally (Forostyak et al., 2014; Garbuzova-Davis et al., 2008; Kim et al., 2010). It is thought that MSCs wield their benefits via growth factors that promote neuroprotection and neuroregeneration; indeed, MSCs transplanted intrathecally reduced the levels of apoptosis and inflammation, leading to improved motoneuron survival in the host tissue (Forostyak et al., 2014).

Preclinically, Neural Stem Cells (NSCs) also have beneficial effects. A meta-analysis carried out by Teng et al. (2012) of 11 studies by ALS investigators showed that transplanting mouse or human NSCs into the spinal cord can dramatically delay onset and slow disease progression in a mutant SOD1 ALS mouse model. NSCs primarily give rise to neurons, glia and oligodendrocytes, although the majority of NSCs remain as quiescent NPCs after transplantation *in vivo*. Surprisingly, non-neuronal NSC-derived cells appear to be more impactful than neuronal NSC-derived cells, most likely because they release or induce the release of beneficial trophic factors that promote the survival of host motoneurons (Teng et al., 2012). Thus, both MSCs and NSCs are attractive therapeutic targets for cell-based therapies for ALS, likely working by releasing trophic factors that are neuroprotective and promote regeneration.

Many Phase I and II clinical trials of stem cell-based therapies have been carried out on ALS patients and all have shown the treatments to be safe and well tolerated (Table 1.3). Though most clinical trials so far conducted were not

Table 1.3: Summary of clinical (mesenchymal and neural) stem cell trials in ALS.

The Table was adapted and updated from Goutman et al. 2019. Abbreviations: AD-MSC, adipose-derived mesenchymal stem cells; ALS-FRS, ALS Functional Rating Scale (non-revised, original); ALS-FRS-R, ALS Functional Rating Scale Revised; CMAP, compound muscle action potential; FVC, forced vital capacity; BM-MSC, bone marrow-derived mesenchymal stem cells; NPC, neural progenitor cell; NSC, neural stem cells.

Stem cell type	Clinical trial phase	Delivery method (target)	Patients (Controls)	Results	Reference
BM-MSC	Phase I/II	Intrathecal (10 patients) Intrathecal + Intravenous (9 patients)	19 (0)	No safety concerns.	Karussis et al., 2010
BM-MSC	Pilot	Intrathecal	10 (0)	'Trend towards disease stabilization' using ALS-FRS-R (individual patient characteristics are not reported such as disease duration, which could impact interpretation). No safety concerns	Prabhakar et al., 2012
BM-MSC	Phase I	Intrathecal (8 patients) Intravenous (6 patients)	14 (0)	1 lost to follow up per group and 1 subject death (due to respiratory insufficiency and infection). Despite this, authors conclude there are no safety concerns.	Nabavi et al., 2019
BM-MSC	Phase I/IIa	Intrathecal	26 (0)	No safety concerns. Significant reduction in rate of ALS-FRS-R decline compared to 6months pre-transplant for up to 6 months post-transplant; FVC stable of above 70% for	Syková et al., 2017

				9 months in 80% subjects; stable weakness scales at 3 months in 75% patients	
BM-MSC	Phase I	Intrathecal	12 (0)	No safety concerns. Decreased inflammatory proteins and microRNAs and increased pro-regenerative microRNAs in patient CSF and blood plasma. Beneficial effects on progression correlated with higher cell doses.	Sobuś et al., 2018
BM-MSC	Phase I	Intrathecal	7/8 completed treatment (0)	No acceleration in ALS-FRS-R decline rates. No safety concerns	Oh et al., 2015
BM-MSC	Phase II	Intrathecal	33 (31)	No safety concerns. Reduced ALS-FRS-R rate changes from baseline, reduced pro-inflammatory and increased anti-inflammatory cytokines in MSC-injected compared to control group. No survival difference	Oh et al., 2018
BM-MSC	Phase III	Intrathecal	100 estimated (100)	Study in progress, results not yet reported	Clinical Trial NCT03280056
BM-MSC	Phase II	Intramuscular, Intrathecal	48 participants in total	No safety concerns. 1-month post-transplantation (treated vs	Berry et al., 2019

				placebo): slowed rate of disease progression in rapid progressor subgroup, CSF neurotrophic factors increased, and CSF inflammatory biomarkers decreased.	
BM-MSC	Phase I/II, Phase IIa	Intramuscular or Intrathecal (Phase 1/2) Intramuscular + Intrathecal (Phase 2a)	26 (0) 6 patients: Intramuscular 6 patients: Intrathecal, 14 patients: Intramuscular + Intrathecal	No safety concerns. Reduced rate of decline in ALS-FRS-R and FVC .	Petrou et al., 2016
BM-MSC	Case report	Intraventricular	1 (0)	No safety concerns	Baek et al., 2012
BM-MSC	Phase I	Intraspinal	7 (0) (+ 2 patients under compassionate use)	4 patients showed a reduction in the ALS-FRS-R and FVC decline (statistics not reported/ performed). No safety concerns	Mazzini et al., 2006, 2008
BM-MSC	Phase I	Intraspinal	10 (0)	No change in the rate of decline of clinical measures. No safety concerns	Mazzini et al., 2010, 2012
BM-MSC	Phase I	Intraspinal	11 (0)	No severe safety concerns. No acceleration in rate of functional decline.	Blanquer et al., 2012
BM-MSC	Phase II	Intraspinal	13 (0)	No safety concerns. Authors report 9 of 13 patients improved post procedure (no clear criteria for assessment)	Deda et al., 2009

BM-MSC	Pilot	Intraarterial	7 (0) 5 completed full regimen	No safety concerns. Results not well reported, no apparent change in disease progression	Moviglia et al., 2012
BM-MSC	Phase I/II	Intramuscular	22 (0)	No safety concerns. Comparison of placebo- and BM-MSC-injected muscle showed significant improvement in only one measure of MU properties (D50 Index of CMAP scan).	Geijo-Barrientos et al., 2020
AD - MSC	Phase I	Intrathecal	27 (0)	Positive safety profile. Side effects related to increased protein and nucleated cell levels in CSF and thickened lumbosacral nerve roots. 4 subject deaths; autopsy revealed no tumors. Efficacy testing in progress (see NCT03268603)	Staff et al., 2016
AD - MSC	Phase II	Intrathecal	60 estimated (0)	Study in progress, results not yet reported	Clinical Trial NCT03268603
AD - MSC	Phase I	Intra-cerebroventricular	6 (0) (late-stage)	No treatment-related safety concerns. 'Unimpressive' results.	Duma et al., 2019
NSC	Phase I	Intraspinal	15 (0)	No safety concerns. Possible slowing of disease progression in patients without	Feldman et al., 2014; Glass et al., 2012; Riley et al., 2012, 2014;

				bulbar symptoms early in disease course, however, number of subjects fulfilling this criterion is small	Tadesse et al., 2014
NSC	Phase II	Intraspinal	15 (0)	No safety concerns. 1 post-op deterioration in neurological function, 1 central pain syndrome. No effect on progression rates versus historical controls after 9 months but improved functional and survival outcomes using ALS/SURV measure relative to historical controls after longer-term follow up (6 years).	Glass et al., 2016; Goutman et al., 2018
NSC	Phase I	Intraspinal	6 (0)	No safety concerns. No increase in disease progression rates through 18 months, despite some transitory improvements post-transplantation in 3 patients.	Mazzini et al., 2015
NSC	Phase I	Intraspinal (cervical/ lumbar)	Lumbar: 6 (0), Cervical: 12 (0)	No safety concerns after 60-month follow-up. Transitory decrease in ALS FRS-R	Mazzini et al., 2019

				progression up to 4 months post-transplantation.	
NPC	Phase I	Intraspinal	18 estimated (0)	Study in progress, results not yet reported	Clinical trial NCT02943850

designed or powered to effectively measure efficacy, some studies have shown beneficial effects resulting from stem cell-based treatments. For example, many clinical trials showed slowed functional decline following treatment with MSCs (Berry et al., 2019; Geijo-Barrientos et al., 2020; Mazzini et al., 2006, 2008; Oh et al., 2018; Petrou et al., 2016; Sobuś et al., 2018; Syková et al., 2017) and NPCs (Goutman et al., 2018; Mazzini et al., 2019). In some studies, the beneficial effect on functional decline was transitory, only observed in the months immediately after transplantation of MSCs (Berry et al., 2019; Syková et al., 2017) or NPCs (Mazzini et al., 2019). For bone marrow-derived MSCs, the beneficial effects of treatment have been associated with reduced inflammatory and increased anti-inflammatory and neurotrophic factors in the CSF, usually measured in the first few months after transplantation (Berry et al., 2019; Oh et al., 2018; Sobuś et al., 2018). This suggests that, at least for bone marrow-derived MSCs, the mechanism of action is similar in humans and preclinical animal models.

There are many elements of stem cell-based therapies that need further clarification to realise the benefits expected based on results in preclinical animal models. These include the type and dosage of transplanted stem cells, the optimal treatment window relative to disease onset, the effect of the microenvironment on the graft (particularly for ALS), and the therapeutic mechanism of action (Goutman et al., 2019). Despite the lack of consensus in the scientific community about the efficacy of current methods, the stem cell based therapy NeuroNata-R, based on autologous BM-MSC transplantation, has been approved as a clinical ALS treatment in South Korea (Corestem, 2019).

1.2.2.2 Challenges to stem cell-based therapies

An alternative to the transplantation of undifferentiated cell types is to replace lost, damaged or diseased motoneurons in the spinal cord with healthy, stem cell-

derived, differentiated motoneuron spinal grafts. Murine embryonic stem cell-derived motoneurons grafted into the chick embryonic spinal column have been shown to integrate into local spinal circuitry and extend axons out to muscle targets (Wichterle et al., 2002). However, unlike in the embryo, the environment of the adult spinal cord is not naturally permissive for axon growth. In the adult CNS, there are inhibitory molecules in the extracellular matrix, such as chondroitin sulphate proteoglycans and myelin-associated inhibitory proteins, and the astroglial scar, which inhibit axon growth. Following injury, invasion of the lesion site by inflammatory cells can upregulate the release of these molecules, further inhibiting axonal growth (van Niekerk et al., 2016). These limitations can be overcome experimentally. Deshpande et al (2006) found that three conditions were necessary to enable Embryonic Stem Cell (ESC)-derived motoneurons transplanted into the spinal cord of adult rats to reinnervate muscle targets and form functional Neuromuscular Junctions (NMJs): 1) the exposure of the engrafted cells to dibutyryl cyclic adenosine monophosphate to promote motoneuron survival and axon extension, 2) subcutaneous administration of rolipram, putatively to neutralise the effects of myelin-mediated axon repulsion, and 3) concurrent transplantation of Glial-cell Derived Neurotrophic Factor (GDNF)-expressing cells into the sciatic nerve, potentially to attract motor axons to distal targets.

While this result is promising, there are further barriers to achieving reinnervation of muscle targets by engrafted stem cell-derived motoneurons in human patients (Table 1.2), apart from the complications that arise from such a multi-facetted therapy. Firstly, ALS pathology of the host tissue may prevent this result being replicated. Indeed, the survival of transplanted mouse stem cell-derived motoneurons in the lumbar spinal cords of a rodent model of ALS carrying the mutant form of human SOD1 was significantly reduced compared to transplanted wildtype controls, suggesting the diseased host environment is detrimental to long-term graft survival (López-González et al., 2009). Secondly, in humans, the distances over which an axon must travel to reach target muscles are much greater than in chick and rodent models. With axon growth estimated to occur at approximately 1-3mm/day (Chan et al., 2016), it would take a human motor axon well over 6 months to extend the length of, for example, an adult arm; even 6 months is too long, especially considering the short survival times of diagnosed

ALS patients. Finally, even if extending axons were able to eventually reach target muscles, the target muscles may atrophy, particularly during long periods of inactivity, and become refractory to innervation in the denervation period. Thus, achieving reinnervation of denervated muscle targets by transplanting cells grafted into the spinal cord is at the very least challenging.

1.3 Peripheral engraftment and stimulation of stem cells: an alternative approach to overcoming paralysis

The peripheral nervous system (PNS) represents a more suitable engraftment site than the CNS because the environment of the PNS has far greater capacity to support axon regeneration. The inhibitors of axon growth present in the CNS are absent in the PNS, the clearance of debris is quicker, and PNS axons upregulate axon growth-promoting regeneration-associated genes following injury (Huebner and Strittmatter, 2009; van Niekerk et al., 2016). Moreover, cells can be grafted closer to the target muscle meaning extending axons have a shorter distance to travel and reinnervation takes less time. Therefore, the axons reach the muscle before extensive atrophy, while it is still receptive to innervation.

1.3.1 Electrical stimulation of engrafted stem cells

The permissive environment of the PNS has been shown to enable transplanted ESC-derived motoneurons to survive and functionally innervate the muscle. Yohn et al. (2008) engrafted embryoid bodies (EBs) containing ESC-derived motoneurons – which expressed Green Fluorescent Protein (GFP) under the Hb9 promoter – into transected tibial nerves of adult mice. They found that transplanted motoneurons survived and formed functional NMJs with the denervated host muscle 60-90 days after surgery. By lesioning the tibial nerve above the transplantation site, the contribution of engrafted motoneurons to the tetanic force of the muscle could be determined; when electrically stimulated, the graft was able to produce average tetanic forces that were 44% of that in non-lesioned controls. Evaluation of ESC-derived motor units revealed mean force values and ranges similar to control muscles. There was a larger number of type I fibres and the fatigue resistance of the motor units was increased suggesting that the reinnervated muscle had a larger proportion of slow, fatigue-resistant motor units. The ESC graft also significantly attenuated signs of denervation-associated muscle atrophy. Thus, peripheral engraftment of ESC-derived

motoneurons within an EB overcomes many of the limitations of spinal transplantation and lessens atrophy of the denervated muscle.

The position of the graft outside the CNS means that central control of the denervated muscle via the graft is not possible and artificial stimulation of the graft is required. Yohn et al. (2008) electrically stimulated engrafted ESC-derived motoneurons to successfully elicit graft-mediated muscle contraction. However, as mentioned in Section 1.2.1 and Table 1.2, there are limitations to electrical stimulation in a therapeutic context. Firstly, electrical stimulation is non-specific, stimulating surviving host neurons, which may include ascending nociceptive axons, and this could be uncomfortable. In addition, electrical stimulation recruits motor units in a non-physiological order; fast fatigable before slow fatigue-resistant motor units. This makes it difficult to modulate muscle force, reducing feasibility and therapeutic usefulness (Bryson et al., 2014; Llewellyn et al., 2010). Finally, as mentioned above, there is evidence that electrical stimulation is not safe in ALS (DiPALS Writing Committee et al., 2015; Lepore et al., 2010). Therefore, to take peripheral engraftment of ESC-derived motoneurons forward as a therapy for ALS, an alternative way of stimulating the graft is required.

1.3.2 Optical stimulation of engrafted stem cells

The dawn of optogenetics in the last two decades has presented an alternative approach to stimulate neurons: optical stimulation. Optogenetics refers to the introduction of the genes for light-sensitive ion-conducting microbial opsins into neurons and other cell types, enabling their activity to be monitored and controlled optically (Boyden et al., 2005; Zemelman et al., 2002). There are three branches of naturally occurring light-sensitive microbial opsins: bacteriorhodopsins, halorhodopsins and channelrhodopsins (Zhang et al., 2011). Bacteriorhodopsins and halorhodopsins (Han and Boyden, 2007; Oesterhelt and Stoeckenius, 1971; Okuno et al., 1999; Zhang et al., 2007) are typically inhibitory in neural systems, the former pumping protons out of the cell and the latter pumping chloride ions into the cell. Channelrhodopsins, in contrast, are ion channels that allow cations to flow through the opsin pore and therefore tend to cause depolarisation (Boyden et al., 2005; Nagel et al., 2003). Since their initial discovery, many more light-sensitive ion-conducting opsins have been discovered and designed such that opsins with a variety of properties (e.g. wavelength sensitivity and latency to

channel opening/closing) are now available (Deisseroth, 2015). For example, spectral variants, such as ReaChR (Lin et al., 2013), have been developed with red-shifted excitation spectra, improving the depth of light penetration compared to the blue-green light that activates conventional opsins (Hu et al., 2020). Optogenetic channel expression can be achieved by breeding transgenic animals or introducing viral vectors. Specific cell types can be targeted by controlling expression of these optogenetic channels with cell type-specific promoters, either directly (Arenkiel et al., 2007) or through cre-recombinase-dependent systems (Atasoy et al., 2008). In this way, optogenetics can be used to probe the function of certain neuron types in circuits and in awake and behaving animals.

The demonstration of optogenetic techniques in primates was of particular significance because it opened up the possibility of using optogenetics therapeutically (Han et al., 2009). Optogenetic therapies are being investigated for treatment of hearing and vision loss (Kleinlogel et al., 2020), epilepsy (Walker and Kullmann, 2019), mood disorders (Albert, 2014), cardiac disorders (Richter and Bruegmann, 2019), some neurodegenerative diseases (Vann and Xiong, 2016), and peripheral nerve regeneration (Xu et al., 2020). The most well developed optogenetic therapy is for the treatment of vision loss due to retinitis pigmentosa (Kleinlogel et al., 2020). Two ongoing clinical trials are testing the ability of first-in-class gene therapy application of optogenetics to confer new light sensitivity to the retina of patients, with (NCT03326336) and without (NCT02556736; RetroSense-Therapeutics, 2016) concurrent use of a wearable optoelectronic visual stimulation device. With the first safety review of the ongoing PIONEER Phase I/II clinical trial concluding that the treatment was well-tolerated (GenSight Biologics, 2019; Martel et al., 2020), these trials are laying the groundwork for the translation of optogenetic techniques from bench to bedside.

Our lab made use of channelrhodopsin-2 (ChR2) to enable optical stimulation of peripheral ESC-derived motoneuron grafts to restore muscle function (Bryson et al., 2014). In this study, a transgenic murine ESC line was generated that expressed ChR2 under the ubiquitously expressed CAG promoter. These ESCs were differentiated *in vitro* to produce EBs containing motoneurons. The differentiated EBs were engrafted into partially-denervated branches of the sciatic nerve of adult mice. They reinnervated the muscle such that, after 35 days, optical stimulation of the engrafted EBs caused contraction of lower hind limb muscles.

The contribution of ESC-derived motoneurons to the force of contraction was only 12% of that elicited by electrical stimulation, even though grafted ChR2-expressing motoneurons accounted for ~50% of all motor units. The authors suggest that the reduced force output of muscle fibres controlled by ChR2-expressing motoneurons reflects a lack of NMJ maturity due to the 35-day period of inactivity preceding optical stimulation (Bryson et al., 2014). In contrast to electrical stimulation, optical stimulation specifically activates neurons from the graft with no unwanted effects on host neurons. It recruits motor units in a physiological order (Llewellyn et al., 2010) and does not result in rapid muscle fatigue (Bryson et al., 2014; Llewellyn et al., 2010). Theoretical modelling suggests that shorter internodal distance in the smaller diameter axons of motor neurons innervating slow motor units is an important determinant of orderly recruitment of motor units by optogenetic axon stimulation; the shorter internodal distance means more nodes are illuminated and threshold irradiance is lower in small diameter compared to large diameter axons (Arlow et al., 2013).

Bryson et al. (2014)'s proof-of-concept demonstrated the ability to overcome paralysis in disorders and injuries involving a loss of motoneurons, such as occurs in ALS, and to reinnervate specific muscle targets, as well as providing a means of artificially controlling muscle function in a highly specific manner. Future work aims to improve the force output elicited by optical stimulation of the graft by, for example, chronic optical stimulation of ChR2-expressing motoneurons in the graft, which has recently been shown to enhance NMJ formation in *in vitro* models (Machado et al., 2019).

1.3.3 Cellular composition of stem cell-derived grafts: no motoneuron is an island.

'No man is an island, entire of itself; every man is a piece of the continent, a part of the main'

[Meditation XVII, Devotions upon Emergent Occasions by John Donne, 1624]

The cellular composition of ESC-derived grafts has a fundamental impact on the therapeutic potential of using ESCs to restore muscle function. Magown et al (2016) found that roughly half of ESC-derived grafts transplanted into the denervated peripheral nerves developed teratocarcinomas by 1 month after implantation. These likely arose from a small percentage of dividing cells that remained in the EB graft after stem cell differentiation (Magown et al., 2016).

Indeed, one of the defining characteristics of an EB is its ability to form a teratoma upon transplantation *in vivo* (Martin and Evans, 1975). A therapeutically safer and more useful graft will require a purely post-mitotic and well-characterised cellular composition.

The Greensmith and Bryson labs have shown that, while grafts of purified motoneurons survive and extend axons into the muscle, they do not functionally innervate muscles with the same success as motoneurons within EBs. NMJs innervated by motoneurons from purified grafts also exhibited morphological signs of immaturity and inactivity such as terminal axonal sprouting, suggesting that the motoneurons are inactive and immature (Bryson, unpublished observations). Other groups have experienced similar problems using purified motoneuron aggregates to restore muscle function (Magown et al., 2017).

It is perhaps unsurprising that purified motoneuron grafts do not perform as well as motoneurons surrounded by other cell types. After all, in the spinal cord, the identity and maturation of a motoneuron is not determined cell-autonomously, it is guided by motoneuron position in relation to gradients of signalling molecules along the spinal cord and by its interactions with surrounding developing cells, such as a spinal interneurons, astrocytes and target muscle. Consistent with John Donne's sentiment that no man can fully exist or develop in isolation (Donne, 1624), so too no motoneuron is an island.

1.4 Motoneuron development

The birth of motoneurons and other neurons in the spinal cord is orchestrated by the influence of external factors on transcription factor and gene expression. Spinal neuron identity is initially determined by the anatomical position of progenitor cells in relation to gradients of certain signalling molecules in the spinal cord. Sonic hedgehog (Shh) released ventrally from the floor plate and Bone Morphogenic Protein (BMP4) released dorsally from the ectoderm and roof plate (Bond et al., 2012; Chiang et al., 1996) pattern the differentiation of spinal progenitors in the dorsoventral axis (Alaynick et al., 2011; Wilson and Maden, 2005). Caudal patterning factors include Retinoic Acid (RA) secreted from the mesoderm (Bayha et al., 2009; Niederreither et al., 1997) and Fibroblast Growth Factors (FGFs) secreted from the neuromesodermal progenitor region (Jose Sanz-Ezquerro et al., 2017). Wnts are also released caudally (Petros et al.,

2011). The gradients of these molecules are opposed by rostrally-secreted Wnt antagonists (Petros et al., 2011) and the interaction between the caudally- and rostrally- released patterning factors orchestrates developmental patterning in the rostrocaudal axis. Depending on the concentrations of dorsoventral and rostrocaudal patterning factors that a spinal progenitor is exposed to, it will express a certain combination of Hox and LIM homeodomain transcription factors (Liu et al., 2001; Wilson and Maden, 2005). Consequently, spinal progenitors can be divided into domains that give rise to different subtypes of neuron and glial cells. For example, the ventral half of the spinal cord can be divided into 5 neural progenitor domains in the dorsoventral axis: p0-p3 progenitor domains that initially give rise to various spinal interneuron subtypes, and pMN, a progenitor domain that gives rise to motoneurons (Alaynick et al., 2011). Later in embryonic development and continuing into the first month after birth, astrocytes and oligodendrocytes are generated from these progenitor domains (Bayraktar et al., 2014). As with spinal neurons, different progenitor domains produce different subtypes of astrocyte that can be distinguished by their expression of certain factors (Clarke et al., 2020; Hochstim et al., 2008).

By exploiting our understanding of spinal motoneuron differentiation during spinal cord development, it is possible to guide the differentiation of stem cells towards certain spinal cell fates *in vitro* (Section 3.1.2). These cells can then be used to model spinal circuitry *in vitro* and/or to develop therapies, such as those described in Sections 1.2.2 and 1.3.

1.4.1 Motoneuron subtypes

Motoneurons generated by the motoneuronal progenitor domain of the spinal cord can be further divided into 5 columns, each occupying a region in dorsoventral and rostrocaudal space (Davis-Dusenbery et al., 2014) and anatomically defined by the expression of certain Hox and LIM homeodomain transcription factors (Soundararajan et al., 2006; Tsuchida et al., 1994). These 5 columns are the phrenic motor column (PMC), the lateral motor column (LMC), the hypaxial motor column (HMC), the preganglionic motor column (PGC) and the medial motor column (MMC). Columnar identity is important because it correlates with certain motoneuronal functional properties such as which target a motoneuron innervates. For instance, LMC motoneurons innervate the limbs and

PMC motoneurons innervate the diaphragm (Davis-Dusenbery et al., 2014). Moreover, motoneurons in different motor pools display different development trajectories of their electrophysiological properties, developing at different rates or in different directions. For example, in electrophysiological experiments in rat, Carrascal et al. (2005) found that rheobase – that is, the minimum current required to elicit an Action Potential (AP) – increased in hypoglossal motoneurons but decreased in oculomotor motoneurons between P1 and P21.

Motoneurons can be further divided into alpha, beta and gamma motoneurons, which innervate exclusively extrafusal muscle fibres, both extra- and intra- fusal muscle fibres, or exclusively intrafusal muscle fibres in the muscle spindle, respectively (Stifani, 2014). Alpha motoneurons generally have larger cell somas than beta and gamma motoneurons and are important for spinal reflexes as they receive monosynaptic input from sensory neurons (Eccles et al., 1960; Stifani, 2014). Alpha motoneurons can be further subdivided into fast-fatigable, fast fatigue-resistant and slow fatigue-resistant, named after the types of muscle fibre that they innervate. There is also a size differential among alpha motoneuron subtypes such that fast-fatigable < fast fatigue-resistant < slow fatigue-resistant. Though there are no definitive genetic criteria to distinguish alpha motoneuron subtypes, there are trends in size (as described above), excitability and firing patterns (Stifani, 2014), which are explored below. Furthermore, as mentioned in Section 1.1.3, different subtypes of motoneuron also show different vulnerabilities to diseases such as ALS.

Different motoneuron subtypes have different input resistances. Input resistance is inversely correlated with neuron size, so alpha < beta and gamma, and of alpha motoneurons, fast fatiguable < slow fatigue-resistant (Bakels and Kernell, 1993; Leroy et al., 2014). This is because input resistance is also inversely correlated with the number of ion channels in the membrane and, assuming channel density is roughly similar in the neurons considered, a larger neuron has more ion channels in its membrane. Differences in passive membrane properties affects rheobase such that it is lower (Bakels and Kernell, 1993) in slow motoneurons than in fast motoneurons (Leroy et al., 2015). In consequence, during physiological activation of the muscle, small, slow alpha motoneurons are recruited before larger, fast motoneurons (Denny-Brown and Pennybacker, 1938; Henneman, 1957; Llewellyn et al., 2010; Peckham and Knutson, 2005). In mice,

orderly, physiological motoneuron recruitment (achieved by optical motoneuron stimulation) was found to reduce fatigue and enhance performance compared to disordered motoneuron recruitment (achieved by electrical stimulation; Llewellyn et al., 2010).

Slow and fast motoneurons also display different firing properties. Leroy et al. (2014 and 2015) distinguished two subtypes of motoneuron in the mouse lumbar spinal cord based on when they began firing during a long-lasting depolarising current pulse at rheobase; immediate-firing motoneurons began firing immediately at pulse onset and delayed-firing motoneurons displayed delayed firing onset. They identified the immediate-firing motoneurons as slow motoneurons and delayed-firing motoneurons as fast motoneurons by the expression of relevant markers and electrophysiological properties (Leroy et al., 2014). The two motoneuron subtypes differed not only in rheobase and input resistance but immediate-firing, slow motoneurons had increased Action Potential (AP) width and Afterhyperpolarisation Potential (AHP) duration compared to delayed-firing, fast motoneurons (Leroy et al., 2014, 2015). Furthermore, Spike Frequency Adaptation (SFA) – that is, a longer interspike interval between the last two spikes in a spike train than the first two – was evident in slow motoneurons at rheobase, whereas, far from showing SFA, fast motoneurons showed an acceleration of firing frequency throughout the depolarising current pulse (Leroy et al., 2015). Abolishing the I_A and slowly deactivating outward K^+ currents in delayed-firing fast motoneurons resulted in an immediate-firing, slow phenotype (Leroy et al., 2015).

The functional importance of differences in properties between fast and slow motoneurons is illustrated by Duch et al. (2000)'s study of an identified motoneuron, MN5, that changes from slow to fast during moth metamorphosis. Comparing MN5 pre- and post- metamorphosis, they found a reduction in input resistance, an increase in rheobase, and changes in the Ca^{2+} and K^+ currents, along with extensive remodelling of the dendritic arbour. These changes are important to enable a motoneuron that mediated slow larval crawling to produce the powerful, fast muscle contractions required for flight. Though mammals do not undergo changes so dramatic as larval metamorphosis, the electrophysiological properties of mammalian motoneurons do change in response to exercise. Moreover, different exercise regimes affect slow versus

fast motoneurons differently. For example, daily spontaneous running of rats in a wheel altered the properties of slow, but not fast motoneurons (Beaumont and Gardiner, 2002). Conversely, chronic muscle overload of rat medial gastrocnemius caused a shift of the properties of fast motoneurons to become more slow-like, presumably to enable more sustained, fatigue-resistant muscle output (Krutki et al., 2015). These changes in motoneuron properties are mirrored to some extent by changes in muscle fibres (Allen et al., 2001). Thus, motoneuronal properties are not fixed but can change dynamically throughout life in response to environmental demands.

Despite the dramatic differences in disease vulnerability, properties and function, historically many developmental studies of motoneurons have treated slow and fast motoneurons (and sometimes motoneurons from different motor pools) as a homogeneous population, likely distorting conclusions drawn about motoneuron development. Furthermore, in electrophysiological experiments, an inherent bias towards patching smaller neurons, because they survive, may have biased data sets towards slow motoneurons (Smith and Brownstone, 2020). It is important to bear in mind these limitations when considering results from such studies of motoneuron development.

1.5 Characteristics of motoneuronal maturation

The maturation of a motoneuron during development can be characterized by changes in motoneuron size, morphology, electrophysiological properties, and connectivity. These developmental changes have profound functional implications.

1.5.1 Changes in motoneuronal size and morphology during development

During *in vivo* development, soma size has been shown to increase as motoneurons mature (Allan and Greer, 1997; Brozanski et al., 1989; Cameron et al., 1989, 1990; Carrascal et al., 2005; Kanjhan et al., 2016; Núñez-Abades and Cameron, 1995; Ulfhake and Cullheim, 1988; Vinay et al., 2000a, 2000b; Williams et al., 2019). However, within the same species, different motoneuron subtypes reach adult soma size at different times, suggesting a different trajectory of soma size development. For example, cat genioglossal and phrenic motoneurons were found to reach their adult soma size by 8 and 12 postnatal weeks respectively, while the soma size of hindlimb motoneurons continued increasing past the

twelfth postnatal week (Cameron et al., 1989). The source of these discrepancies may be the different mature soma sizes of different motoneuron subtypes (e.g. fast > slow alpha motoneurons), or different developmental trajectories of motoneurons at different spinal levels; motoneuron size in the cervical spinal cord matures earlier than in the lumbar spinal cord (Smith and Brownstone, 2020). Thus, while there is a significant increase in motoneuronal soma size during development, there are subtype specific divergences in the trajectory of this increase and in the mature adult soma size reached.

Focusing on soma size as a measure of motoneuron size can be a bit of a red herring. In fact, in cat, dendrites constitute about 95% of the surface area and 75% of the volume of motoneurons (Ulfhake and Kellerth, 1981). The morphology of the dendritic arbour influences the number and type of synaptic input received by a neuron (Purves et al., 1981) and dendrites integrate the majority of synaptic inputs to a neuron. Dendrites are therefore crucial to the computational capability of a neuron and the CNS as a whole (London and Häusser, 2005). Many classes of motoneuron across multiple model organisms have been shown to increase the size (i.e. dendritic length, area and/or volume) and complexity (i.e. number of branch points) of the dendritic arbour during development (Allan and Greer, 1997; Brozanski et al., 1989; Carrascal et al., 2005; Kanjhan et al., 2016; Núñez-Abades and Cameron, 1995; Ulfhake and Cullheim, 1988).

Developmental changes in dendritic arborisation are often coincident with changes in motoneuronal function. For example, the onset of phrenic rhythmic respiratory discharge in E17 rat embryos is coincident with a radical reorganisation of phrenic motoneuronal dendritic morphology (Allan and Greer, 1997). Changes in dendritic morphology are not only related to developmental changes in motoneuronal function but to differences in function between mature motoneurons; motoneurons from different motor pools have different dendritic morphologies (Vrieseling and Arber, 2006). Indeed, in rat hypoglossal motoneurons, dendritic morphology varies depending on whether the motoneuron innervates a retractor or protruder tongue muscle (Altschuler et al., 1994). Thus, the morphology of the dendritic arbour develops in concert with the function of each neuron, though the mechanistic, causal relationship between dendritic morphology and function remains unclear.

1.5.2 Electrophysiological maturation of motoneurons.

Concurrently with, and often because of, changes in morphology, size and the complement of the ion channels and pumps expressed in the membrane, the electrophysiological properties of neurons change during development and significantly impact motoneuron function. Passive membrane properties determine whether a subthreshold dendritic synaptic potential will propagate far enough to reach the axon initial segment and exceed the local threshold for initiation of an AP (Koester and Siegelbaum, 2013). Active membrane properties determine, among other things, the shape of the AP, whether a motoneuron fires repetitively, and at which frequency. These properties are essential to motoneuron function. For example, in addition to motoneuron recruitment, muscle tension is regulated by the frequency of motoneuron firing (Enoka and Duchateau, 2017).

While functionally distinct neuronal subtypes can sometimes be distinguished by their different electrophysiological properties, many of the changes during development are stereotypical across different motoneuronal subtypes and between different model organisms and cell models (Table 1.4). For example, the input resistance and membrane time constant decrease while, where measured, whole cell capacitance increases (Table 1.4). These changes in passive membrane properties are related to increasing motoneuron size and increased ion channel density in the motoneuronal membrane during development (Koester and Siegelbaum, 2013). Rheobase tends to increase, indicating that motoneurons become less excitable as they mature (Table 1.4). However, this trend is not consistent: Carrascal et al., 2005 found lower rheobase in older rat oculomotor motoneurons than young.

Motoneurons are capable of firing APs very early on in development; for example, in *Xenopus laevis*, APs are first elicited at the time of closure of the neural tube (Spitzer and Lamborghini, 1976; Spitzer et al., 2000a). However, AP morphology changes somewhat stereotypically in motoneurons during development. AP amplitude in motoneurons generally increases, though no change in AP amplitude was observed by Smith and Brownstone between P2 and P23 in mouse lumbar motoneurons (Table 1.4; Smith and Brownstone, 2020). AP duration decreases (Table 1.4), due to the maturation of voltage-gated sodium channels and delayed rectifier channels responsible for the upstroke and

Table 1.4: Developmental changes in motoneuronal electrophysiology in different types of motoneuron

This table shows whether the property increases or decreases during the developmental window considered. ^ means and increase, ˅ means a decrease and ~ means no change. DIV = days in vitro from the end of the differentiation. RMP = Resting Membrane Potential.

Paper	Xie and Ziskind-Conhaim, 1995	Viana et al., 1994	Gao and Ziskind-Conhaim, 1998	Martin-Caraballo and Greer, 1999	Vinay et al., 2000b	Carrascal et al., 2005	Carrascal et al., 2005	Smith and Brownstone, 2020	Smith and Brownstone, 2020	Miles et al., 2004	Bryson et al., 2014	Machado et al., 2019	Toma et al., 2015	Takazawa et al., 2012
Motoneuron (MN) type	Rat lumbar	Rat hypoglossal	Rat lumbar	Rat phrenic	Rat lumbar	Rat hypoglossal	Rat oculomotor	Mouse cervical	Mouse lumbar	Mouse ESC-derived	Mouse ES-derived	Mouse ESC-derived	Mouse iPSC-derived	Human ESC-derived
Method	*In vitro* explant cultures	Slice preparation	Slice preparation	Slice preparation	Brainstem-spinal cord preparation	Slice preparation	Slice preparation	Slice preparation	Slice preparation	Un-purified MN cultures	Purified MNs on astrocytes	Purified MNs in 3D spheres with purified astrocytes	Un-purified MN cultures	Un-purified MN cultures
Time period	E15-P3	P0-P21	E15-P3	E16-P1	P0-P5	P1-P21	P1-P21	P2-21	P2-21	DIV1-4	DIV1-35	DIV1-21	DIV1-42	DIV1-13
RMP	˅	~		˅	~			~	~	˅			~	~
Input/membrane resistance	˅	˅	˅	˅	˅	˅	˅	˅	˅	˅	˅	˅	˅	˅
Capacitance								^	^	^	^	^	^	
Membrane time constant		˅		˅		˅	˅	˅	˅					

Rheobase		∧		∧	∧	∧	∨							~
Firing frequency				∧		∧	∧	∧	∧		∧		∧	∧
Action potential amplitude		∧	∧	∧	∧			∧	~			∧		
Action potential duration		∨	∨	∨		∨	∨	∨	∨		∨	∨	∨	∨
Proportion of neurons with AHP			∧			∨	∨						∧	
Frequency that repetitive firing was observed	∧										∧	∧	∧	∧
Proportion of neurons with post-inhibitory rebound action potentials						∧	∧							∧
Proportion of neurons with sag		∧				∧	∧							
Spike frequency adaptation ratio													∧	∧

downstroke of the AP, respectively (Rekling et al., 2000).

As development progresses, motoneurons become more capable of repetitive firing, sustained throughout a depolarising current pulse. Studies of mammalian phrenic (Martin-Caraballo and Greer, 1999; Su et al., 1997), oculomotor (Tsuzuki et al., 1995) and lumbar (Vinay et al., 2000a) motoneuron development found that, *in vivo,* developing motoneurons could be divided into two populations using a supra-rheobase current pulse: one that sustained repetitive firing throughout the pulse (tonic firing) and another that only fired one or two APs at the beginning (phasic firing). A similar observation was made in cultured ESC-derived (Bryson et al., 2014; Machado et al., 2019; McCreedy et al., 2014; Miles et al., 2004) and iPSC-derived (Toma et al., 2015) motoneurons. The proportion of phasic firing motoneurons reduced as development progressed, though subpopulations of phasic oculomotor and phrenic motoneurons persisted into adulthood and may have a physiological role in the adult animal (Su et al., 1997; Tsuzuki et al., 1995). The inability of immature motoneurons to fire in a tonic manner is likely because the depolarised membrane potential prevents the return of inactivated Na^+ channels to a closed state and so prolongs the refractory period (Vinay et al., 2000b). There are three ways in which this may be overcome during development. The first is an increase in the density of voltage-gated sodium channels. The second is the development of a persistent, non-inactivating Na^+ current (I_{Nap}) with subthreshold activation. This has been observed in facial, hypoglossal, trigeminal (Rekling et al., 2000) and lumbar (Miles et al., 2005) motoneurons and blocking I_{Nap} with Riluzole inhibits repetitive firing in lumbar motoneurons (Miles et al., 2005). The third way is the development of high conductance delayed rectifiers and transient outward (I_A) K^+ currents that underly the (fast) AHP, which repolarise the motoneuron, enabling repetitive firing.

The AHP is an essential determinant of firing rate, and so the regulation of muscle tension (Enoka and Duchateau, 2017). During both *in vivo* (Carrascal et al., 2005; Martin-Caraballo and Greer, 1999; Vinay et al., 2000a, 2000b) and *in vitro* (Takazawa et al., 2012; Toma et al., 2015) development, maximum motoneuronal firing rate increases (Table 1.4); this is likely due to a reduction in the duration and amplitude of the AHP, as has been shown to occur during the first two postnatal weeks in rat hypoglossal motoneurons (Viana et al., 1994). Indeed, blocking SK channels with apamin to artificially shorten the AHP increased firing

frequency in mouse lumbar motoneurons (Miles et al., 2005). The change in AHP amplitude and duration is likely due in part to a postnatal decrease in I_A (Vinay et al., 2000b) and the development of specialised cholinergic synapses (C-boutons) in the first two postnatal weeks (Wilson et al., 2004), which are thought to affect motoneuronal AHP and firing frequency by modulating SK channel activity (Deardorff et al., 2013, 2014).

During repetitive firing in response to a sustained suprathreshold depolarising input, motoneuron firing undergoes various types of adaptation. For example, during repetitive firing, AP duration lengthens and AP amplitude decreases, suggesting that the conductances shaping APs change during sustained firing (Rekling et al., 2000). As might be expected, capacity for this adaptation changes during development. For example, SFA is the increase in inter-spike interval during a sustained depolarising input. SFA is more prevalent and marked in more mature motoneurons, as observed both in slice recordings (Martin-Caraballo and Greer, 1999) and in cultured ESC-derived (Bryson et al., 2014; Takazawa et al., 2012) and iPSC-derived (Toma et al., 2015) motoneurons (Table 1.4). Although experimental evidence and modelling of P8-14 lumbar mouse motoneurons suggests that the main factor required for SFA is the slow inactivation of Na^+ channels (Miles et al., 2005), it is unclear how conductances are different in embryonic and neonatal animals such that SFA is less marked. To add to the complexity of the question, as discussed above, SFA also varies between slow and fast motoneurons.

Other aspects of motoneuron electrophysiological maturation occur due to the development of the hyperpolarisation-activated depolarising current (I_h). I_h opposes membrane hyperpolarisation (e.g. from an inhibitory input) and is predominantly underpinned by hyperpolarisation-activated cyclic nucleotide-gated ion channels. There is a ten-fold increase in I_h density during *in vivo* development in hypoglossal motoneurons (Bayliss et al., 1994; McLarnon, 1995; Viana et al., 1994) that causes changes in motoneuron properties. For example, the sag potential during sustained hyperpolarising inputs is more pronounced in adult rat hypoglossal (Carrascal et al., 2005; Viana et al., 1994) and oculomotor (Carrascal et al., 2005) than in neonatal motoneurons. The developmental increase in sag is often accompanied by an increase in the occurrence of Rebound Action Potentials (RAPs) following hyperpolarisation (Carrascal et al.,

2005; Viana et al., 1994; Table 1.4). While inwardly rectifying currents such as I_h may be the main cause of RAPs, it has been suggested that they require more rapidly-activating excitatory currents than I_h, which is self-limiting (Robinson and Siegelbaum, 2003). For example, adult turtle lumbar motoneurons express low voltage-activated Ca_V3 channels that also contribute to post-inhibitory rebound activity and can lead to RAPs (Canto-Bustos et al., 2014). The function of RAPs is unclear but they are thought to contribute to the rhythmic activity of motoneurons during locomotion (Bertrand and Cazalets, 1998; Martin-Caraballo and Greer, 1999). Thus, the emergence of RAPs along with other developmental changes in electrophysiological properties can be used as indicators of motoneuron functional maturation.

1.5.3 The types of synapses formed by motoneurons

While the electrophysiological properties of a motoneuron determine whether and how it will fire in response to a dendritic input, the connectivity of a motoneuron's axon determines the effect of that motoneuron's output. The most well-studied connection that motoneurons form is with the muscle end plates at the NMJ to enable muscle control. Motor axons release acetylcholine (ACh) onto the end plate causing an endplate potential that results in an influx of calcium across the sarcolemma and muscle fibre contraction. Apart from the role of glutamate in synaptic elimination during development (Personius et al., 2016), the activity of the NMJ is entirely cholinergic. The important role of motoneurons as the 'final common path' of neural information to muscles and the accessibility and convenience of the NMJ mean that it has been very well studied. However, anatomical studies have shown that motoneuronal axon collaterals also form synapses with neurons in the spinal cord (Cullheim et al., 1977). Indeed, ventral root stimulation of spinal cord slices *ex vivo* uncovers recurrent inhibition and recurrent excitation due to other motoneuronal synapses in the spinal cord (Bhumbra and Beato, 2018; Moore et al., 2015). These synapses are conserved between species and underpin important aspects of motor control.

Recurrent inhibition is the result of reciprocal connections between excitatory motor axons and inhibitory spinal interneurons called Renshaw cells (RCs; Bhumbra et al., 2014; Moore et al., 2015). Motoneurons project to local Renshaw cells (Renshaw, 1946) and, in turn, RCs inhibit the same motoneurons and

modulate the activity of synergists and antagonist motor pools (Alvarez and Fyffe, 2007; Bhumbra et al., 2014; Granit et al., 1957). While the exact function of RCs in motor control is not clear, their incorporation into motor circuits and the cholinergic and glutamatergic inputs they receive from motor axons (and proprioceptive afferents; Alvarez et al., 2005) are being characterised more fully. Though initially motoneuronal input to RCs was thought to be cholinergic (Eccles et al., 1954), both in early (Eccles et al., 1954) and more recent (Mentis et al., 2005) experiments some residual glutamatergic activity remained after blockade of cholinergic receptors (Mentis et al., 2005). Indeed, colloidal gold immunoelectron analysis found both glutamate in motoneuron axon terminals on RCs (Richards et al., 2014). Recently, it has been demonstrated by paired intracellular recordings that motoneuron-to-RC synapses have mixed neurotransmitter dependency; some are cholinergic and some are glutamatergic (Bhumbra and Beato, 2018; Lamotte d'Incamps et al., 2017). It is not yet known whether the different sorts of motoneuron-to-RC synapses (cholinergic or glutamatergic) have different functions.

Recurrent excitation results from synaptic motoneuronal excitation of other motoneurons both intra- and inter- segmentally (Bhumbra and Beato, 2018), and has been observed in many organisms, including rodents from juvenile ages (Ichinose and Miyata, 1998) up to P20 (Bhumbra and Beato, 2018). As fast motoneurons receive ten-fold more recurrent excitation than slow motoneurons, recurrent excitation of motoneurons in neighbouring spinal segments is thought to amplify the strength of motor output (Bhumbra and Beato, 2018). However, it is unclear exactly what function such amplification might have. One option is that feedback excitation between motoneurons may enable the motor system to produce a prolonged response to a brief stimulus (Li et al., 2006).

The neurotransmitter dependency of motoneuron-mediated recurrent excitation reported in the literature varies, partly due to earlier assumptions that these synapses would be cholinergic (Cullheim et al., 1977). Some functional studies of neonatal animals (P1-6 rats (Ichinose and Miyata, 1998) and P0-4 mice (Nishimaru et al., 2005)) have indeed shown a cholinergic component to the recurrent excitation. However, a recent electrophysiological study showed that recurrent excitation was purely glutamatergic in both juvenile (P7-14) and more mature mice (P10-20; Bhumbra and Beato, 2018), and Richards et al. (2014)

showed a similar density of glutamate in putative MN-MN synapses as are found in MN-RC synapses. It may be that some of the discrepancy is due to differences in the maturity of the animals studied.

1.6 Motoneuron activity affects maturation

Some elements of motoneuron maturation are observed in pure *in vitro* cultures and so seem to be intrinsic. For example, McCreedy et al., (2014) showed that pure motoneuron cultures developed repetitive firing in response to depolarising current pulses and spike frequency adaptation, along with a mature ion channel and neurotransmitter receptor complement (McCreedy et al., 2014). However, many aspects of motoneuron maturation are impacted by external factors such as spontaneous activity, inputs from surrounding neurons, target-derived signals and non-neuronal cells such as glia. One such factor is activity, which affects axon guidance, dendritic size and connectivity. Broadly, during embryonic development this activity predominantly comes from spontaneous activity in the spinal cord, and during postnatal development motoneuron maturation is impacted by activity from incoming descending spinal and supraspinal inputs.

1.6.1 Spontaneous network activity in the spinal cord has a significant role in motoneuron maturation

Once spinal neurons are born and begin to form networks in the embryonic spinal cord, spontaneous network activity begins to develop. In murine spinal motor networks, spontaneous activity, as recorded from the ventral roots, arises around embryonic day (E) 12. At this time point, hindlimb motoneuron axons have not yet reached their muscle targets (Jones, 1979) meaning that spontaneous activity is likely a target muscle-independent process (Hanson and Landmesser, 2003). Initially, spontaneous activity is synchronised across all levels of the spinal cord and exhibits regular short spike-episodes. At E14, this pattern of activity coexists with regular long-lasting episodes at a lower frequency (Yvert et al., 2004) and activity in the ventral spinal cord (but not the dorsal spinal cord) was correlated with muscle contraction when observed in organotypic cultures (Rosato-Siri et al., 2004). As the cord develops further, different activity patterns emerge at different levels as the network begins to segregate into more specialised sub-networks (Rosato-Siri et al., 2004; Yvert et al., 2004). Calcium influx is associated with spontaneous spinal network activity (Montague et al., 2017; O'donovan et

al., 1998), likely affecting the maturation of the functional properties of spinal neurons such as neuron migration and axonal outgrowth (Spitzer et al., 2000b). Spontaneous activity is also found to arise in other regions of the CNS, albeit with a different timeline to the ventral spinal cord (O'donovan et al., 1998), and has been observed in the spinal cords of various model organisms. This commonality suggests that spontaneous activity is a common feature of network development.

Spontaneous activity in the spinal cord arises and is modulated by both chemical neurotransmission via synapses and electrical neurotransmission via gap junctions. The neurotransmitter dependency of spontaneous activity in mice (and other model organisms) changes as the spinal cord develops (O'donovan et al., 1998). Between E12 and E15.5 (phase I; Hanson and Landmesser, 2003), the activity is dependent on cholinergic signalling and there is a switch to glutamatergic dependence from E15.5 onwards (phase II; Hanson and Landmesser, 2003; Rosato-Siri et al., 2004). GABA- and glycin- ergic signalling also play an important role in spontaneous spinal network activity. Initially, GABA and glycine positively modulate the activity and, after the onset of phase II, negatively modulate it, due to a developmental change in the chloride reversal potential for spinal neurons (Hanson and Landmesser, 2003; Myers et al., 2005). The importance of synaptic transmission to spontaneous activity is clear as complete blockage of synaptic transmission with low external calcium and high external magnesium concentrations eliminates spontaneous activity in a reversible manner (Hanson and Landmesser, 2003). As spontaneous activity is eliminated when synaptic transmission is blocked, gap junctional connectivity is certainly not sufficient to facilitate spontaneous activity. However, it has been suggested that gap junctions may generate more localised calcium waves that affect spinal axon outgrowth and pathfinding (Spitzer et al., 2000b). Moreover, in perinatal mice, gap junctions have been shown to synchronise activity between motoneurons of the same motor pool – i.e. motoneurons innervating the same muscle (Montague et al., 2017; Personius et al., 2001). One study found that interfering with gap junctional connectivity within motor pools during development by knocking out a key component of the developmental motoneuron gap junction, connexin-40, shortened the period of multiple innervation of the NMJ. The authors concluded that synchronous spontaneous activity of a motor pool delayed

synaptic elimination during postnatal neuromuscular development by reducing synaptic competition (Personius et al., 2007).

1.6.1.1 The role of spontaneous activity in axon guidance

Spontaneous activity in the spinal cord affects other aspects of motoneuronal axon outgrowth and NMJ formation in addition to refinement of innervation at the NMJ. For example, in chick, embryonic spontaneous activity affects the accuracy of guidance decisions during axon outgrowth towards target muscles. When such spontaneous activity was pharmacologically blocked, motoneurons made dorsoventral guidance errors during axon outgrowth in the limb and there was altered expression of guidance molecules. These effects were prevented by restoration of the activity with optical stimulation in embryos electroporated with a viral ChR2 DNA construct (Kastanenka and Landmesser, 2010). Frequency of firing was also important; artificially decreasing frequency of firing resulted in increased instances of inaccurate dorsoventral axon pathfinding decisions and artificially increasing firing reduced the accuracy of motor pool-specific axon targeting (Hanson et al., 2008). In addition to the developmental role of spontaneous activity in axon guidance, activity elicited electrically (Al-Majed et al., 2000; Brushart et al., 2002; Chan et al., 2016; Gordon, 2016; Liu et al., 2013), by optogenetic methods (Park et al., 2015; Ward et al., 2016; Xiao et al., 2015; Xu et al., 2020) or by exercise (Sabatier et al., 2008) has been shown to promote motor axon regeneration following nerve injury.

1.6.1.2 Spontaneous activity shapes spinal circuitry

Spontaneous activity also affects the formation of central spinal circuitry. Warp et al. (2012) found that if spontaneous activity in the spinal columns of zebrafish was inhibited using optogenetic techniques within a critical window, not only was there a reduction in correlated activity in ipsilateral neurons later in development, but many spinal neurons showed prolonged immature spontaneous transients. This suggests that spontaneous activity was essential for their recruitment into the neural circuitry (Warp et al., 2012). Montague et al. (2017) also demonstrated a role for spontaneous activity in the formation of spinal neural assemblies in chick embryos. They showed that cadherin expression and correlated spontaneous network activity regulate each other and both affect the correct formation of the facial and abducens motor nuclei.

1.6.1.3 Spontaneous activity affects spinal synaptic strength

The regulation of the strength of spinal circuitry may also be affected by spontaneous network activity. Reduction of spinal network activity in chick embryos by addition of lidocaine, resulted in a homeostatic increase in both glutamatergic and GABAergic synaptic strength. This suggests that, in addition to effects on axon guidance and motor circuit formation and refinement, spontaneous activity can be self-regulatory and is important for regulating of the balance of excitatory and inhibitory activity within the spinal cord (Gonzalez-Islas and Wenner, 2006).

1.6.2 The effect of activity on the dendritic morphology of motoneurons

The development of a functional nervous system requires the formation of highly detailed and stereotyped patterns of neuron connectivity (Goodman and Shatz, 1993). To achieve this connectivity, elements of dendritic arbour development are determined by chemical and trophic cues that guide extending growth cones and dendritic filopodia to their targets (Kalb and Hockfield, 1992). However, this initial set of synaptic connections is often exuberant and is refined by activity-dependent mechanisms. This activity may be spontaneous activity in the spinal cord, from inputs from surrounding spinal neurons, or descending spinal and supraspinal inputs, which are important for the correct formation of motor circuits (Smith et al., 2017b). These activity-dependent developmental processes largely take place during a ‘critical period’ of early postnatal life and have fundamental effects on neuronal morphology, electrophysiology and synaptic connectivity (Kalb and Hockfield, 1992).

Glutamatergic neurotransmission has been shown to be important for the activity-dependent development of the motoneuronal dendritic arbour (Inglis et al., 1998, 2002). Motoneurons express high levels of glutamate receptor subunits during the critical period of postnatal development (Kalb et al., 1992) and administering glutamate receptor antagonists in this period, but not during adulthood, prevents mature motoneuronal dendritic architecture from being established (Kalb and Hockfield, 1990a, 1990b). Reductions in the size of the dendritic arbour were observed when activity was reduced by knocking down the AMPA receptor subunit, GluA1, in cultures of mixed spinal neurons. *In vivo,* global and MN-specific GluA1 knockout mice also showed reductions in dendritic arbour size,

accompanied by a variety of defects in motor behaviour (Zhang et al., 2008a). Conversely, increasing motoneuronal activity (by disrupting glycinergic transmission) caused the dendritic arbour size of hypoglossal motoneurons to increase (Fogarty et al., 2016). Thus, a certain level of excitatory neurotransmission during the critical period of development is essential for physiologically-useful elaboration of the motoneuronal dendritic arbour.

However, the role of synaptic activity in dendritic arbour development may be more complex than 'more activity = more elaboration'. In larval zebrafish, older and less active dorsal motoneurons have larger and more dynamic dendritic arbours whereas younger and more active ventral motoneurons have smaller and less dynamic dendritic arbours. If activity is supressed by viral expression of the inwardly rectifying potassium channel, $K_{ir}2.1$, then the dendritic arbours of the ventral motoneurons become more dynamic, though no stable change in size was observed (Kishore and Fetcho, 2013). Therefore, activity may also have homeostatic effects on motoneuronal dendrite development.

Though activity-dependent changes to dendritic morphology are predominantly confined to a critical period of postnatal development, dendrites retain the capacity for dynamism during adulthood. The continuing importance of activity to the maintenance of the motoneuronal dendritic arbour is illustrated in animals with spinal cord injury. Following spinal cord injury and consequent deprivation of descending input to lumbar motoneurons in rats, the size and complexity of the motoneuronal dendritic arbour was reduced compared to uninjured animals. This reduction was not observed in injured rats that underwent an exercise paradigm, which presumably activated motoneurons via Ia afferents. These effects were not only relevant to injury models; uninjured animals that underwent the exercise paradigm showed modestly increased motoneuronal dendritic arbour size compared to uninjured animals that did not undergo the paradigm (Gazula et al., 2004). Thus, motoneuronal morphology is affected by activity both during development and in adulthood.

1.6.3 The effect of different spinal interneurons on motoneuronal activity *in vitro*

As activity, both spontaneous and from inputs, is modulated by various neurotransmitters, it naturally follows to ask whether different spinal interneuron subtypes exert different effects on motoneuron activity. This question was

investigated by Sternfeld et al. (2017) using *in vitro* co-cultures. To do this, they made use of differentiation protocols that have been developed in recent years to generate different spinal neural subtypes from ESCs. They found that motoneurons cultured on monolayers of cortical astrocytes developed spontaneous activity. Spontaneous bursts had reduced amplitude and were less synchronous when inhibitory V1 interneurons were added to the co-culture. These effects were eliminated by inhibitory antagonists. V1 interneurons also increased the complexity of the networks that formed. The addition of V3 interneurons to motoneuron-V1 interneuron-astrocyte co-cultures restored synchrony of spontaneous firing, suggesting that V3 interneurons provided a strong excitatory drive that dominates network output (Sternfeld et al., 2017). Although this is an *in vitro* model, it provides important insight into the role that different spinal interneuron subtypes can play in shaping spontaneous activity in spinal motoneuron networks.

1.6.4 Rhythmic spontaneous and evoked activity within embryoid bodies

The importance of spontaneous activity in the maturation of motoneurons and motor circuits *in vivo* prompts the question of whether motoneurons within EBs engrafted into the peripheral nerve are active. Magown et al. (2017) showed that, of seventeen transplanted mice that displayed graft-dependent muscle activity, nine demonstrated graft-dependent rhythmic contractions. Six of these nine showed rhythmic contractions spontaneously, in the absence of electrical stimulation of the engrafted EB, and rhythmic contractions were evoked in the remaining three either by a single electrical pulse or a short train of pulses delivered to the engrafted EB. The rhythmic muscle activity was dependent on glutamatergic transmission and modulated by muscarinic and GABAergic/glycinergic transmission within the engrafted EB. Moreover, transmitters that cause fictive locomotion in spinal cord (NMDA, 5-HT and DA) increased the duration of evoked activity and increased the force generated by spontaneous bursts. Magown et al. (2017) interpreted their data as evidence of microcircuit formation between interneurons and motoneurons within the EB and of its importance to the functional outcome of the graft.

1.6.5 Spinal V3 interneurons: a candidate cell type to drive motoneuron activity

The importance of spontaneous activity, its modulation by spinal interneurons, and the presence of active microcircuits within engrafted EBs (Magown et al., 2017) led to the hypotheses, firstly, that spinal interneurons within the EB were driving activity in the motoneurons to promote maturation and enable successful muscle reinnervation, and, secondly, that the absence of such spinal interneurons prevented purified motoneuron aggregates from having the same capacity. V3 interneurons were identified as a candidate spinal interneuron type to further investigate this hypothesis as they are generated in large numbers by the RA and Shh agonist (SAG) concentrations used to differentiate motoneuron-containing EBs (Sternfeld et al., 2017).

V3 interneurons are glutamatergic interneurons that project onto many spinal neuronal subtypes, including contralateral (Zhang et al., 2008b) and ipsilateral (Chopek et al., 2018) motoneurons, and other V3 interneurons. Initial experiments that attenuated synaptic transmission of, or acutely silenced, V3 interneurons indicated that V3 interneurons were involved in stabilising locomotor rhythm and balancing motor output between the two halves of the spinal cord (Zhang et al., 2008b). The involvement of V3 interneurons in locomotion is further supported by computational modelling studies exploring the circuits responsible for gait transitions (Danner et al., 2017). Moreover, as mentioned above, *in vitro* experiments showed that V3 interneurons are important drivers of rhythmic excitatory activity in mixed embryonic stem cell-derived cultures, as knockdown of V3 interneurons disrupted rhythmic calcium bursting (Sternfeld et al., 2017). However, V3 interneurons are a heterogeneous population and different subpopulations have different functions. Dorsal and ventral subpopulations of V3 interneurons can be distinguished by cell location, morphology, electrophysiological properties, postnatal maturation trajectory, and function (Borowska et al., 2013, 2015; Chopek et al., 2018; Zhang et al., 2008b). For example, analysis of c-FOS expression showed that the dorsal and ventral populations of V3 interneurons were differentially active during running and swimming tasks (Borowska et al., 2013). Electrophysiological investigations demonstrated that, based on soma size and functional connectivity, the ventral V3 population could be further subdivided into medial and lateral subpopulations, which could form a layered circuit putatively integrating central inputs and feeding

them to motoneurons (Chopek et al., 2018). Chopek et al., (2018) proposed that the ventral V3 interneuron circuitry could be one of the redundant but sufficient cell types providing rhythmic drive to motoneurons during repetitive behaviours such as locomotion. Due to their rhythmic, excitatory properties both *in vitro* and *in vivo*, the fact that they synapse directly onto motoneurons, and their presence in the EBs, V3 interneurons are a promising candidate spinal interneuron to be investigated for their influence on ESC-derived motoneuron maturation *in vitro*.

1.7 Target-derived signals affect the survival and maturation of motoneurons and their integration into spinal circuitry

While spontaneous activity has a fundamental effect on motoneuron maturation, the characteristics of motoneurons are also affected by target-derived signals. Motor pools arise at the time at which motor axons reach their peripheral muscle targets. As this coincident timing suggests, muscle-derived signals such as GDNF are important for the appropriate innervation of NMJs, with the muscle spindles being particularly affected if GDNF is absent (Gould et al., 2008). Exposure to muscle-derived GDNF initiates the expression of certain ETS transcription factors such as Pea3 and ER81. These transcription factors play an important role in the development of distinct functional properties by different motor pools. For example, Pea3 mutant mice showed dysregulated motoneuron migration and settling within the spinal cord at cervical levels and dysregulated patterns of muscle innervation (Haase et al., 2002; Livet et al., 2002). Mutant mice also demonstrated aberrant motoneuronal dendritic arborisation and sensory-motor connectivity (Vrieseling and Arber, 2006). Thus, muscles have an essential role in defining the morphology and connectivity of the motoneurons that innervate them, ensuring an integrated spinal system.

Muscle-derived signals are also important for motoneuron survival in the spinal cord. During development, there is a 40-50% reduction in the neuronal population as part of a highly stereotyped period of Programmed Cell Death (PCD; Sendtner et al., 2000). Specific ablation of skeletal muscle cells in transgenic mouse embryos by cre-dependent DNA recombination increased death in the motoneuronal, but not the spinal interneuron population, to 90% (Grieshammer et al., 1998). Conversely, treatment of avian embryos with GDNF during the natural period of motoneuron death (E6-9) rescued 25% of motoneurons from

PCD. In addition, in both chick and mouse, GDNF treatment prevented the 50% spinal motoneuron death and atrophy that is normally induced by peripheral axotomy (Oppenheim et al., 1995). Thus, through effects on motoneuron survival and on the transcription factor profile of motoneurons in different motor pools, muscle-derived factors promote and direct the maturation of motoneurons and motor circuits.

1.8 Glial cells in the spinal cord affect the survival and functional properties of motoneurons

In addition to other spinal neurons and muscle targets, a third major cell type that influences motoneuron maturation and survival are glial cells such as astrocytes. Until recently, glia were thought to have a predominantly structural role in the nervous system – indeed, their name is from the Greek meaning 'keep things together'. The fundamental importance of glia in the CNS made the subtleties of their influence difficult to study by conventional ablation methods; indeed, *in vivo* ablation of astrocytes in the adult mouse brain resulted in neuronal death (Cui et al., 2001; Delaney et al., 1996; Procko and Shaham, 2010). In recent years, advances in genomics and imaging techniques have enabled myriad functions of astrocytes and other glial cell types to be uncovered, including metabolic support of neurons, neurotransmitter uptake and recycling, protection against oxidative stress, synapse formation, gliotransmission, circuit function, and regeneration and repair (Hill et al., 2016). Far from being a purely structural cell type, in fact glia 'keep together' the functioning of the entire CNS.

1.8.1 The heterogeneity of astrocytes

Astrocytes are electrically inert cells derived from the same progenitors as neurons (McGann et al., 2012), although they are born later both *in vivo* (Hill et al., 2016) and *in vitro* (using the RA and SAG concentrations used to differentiate motoneuron-containing EBs; Bryson et al., 2014). There are more than nine types of astrocyte in the murine CNS, based on morphology and expression of astrocyte-enriched proteins (Haim and Rowitch, 2016), but broadly astrocytes come in two forms, protoplasmic and fibrous astrocytes, which can be distinguished by their morphology and location in the brain (grey and white matter, respectively; McGann et al., 2012). There are also specialised types of astrocyte, such as Bergmann glia in the cerebellum (Haim and Rowitch, 2016).

Morphologically similar astrocytes in different regions of the CNS express different proteins, introducing further heterogeneity. For example, astrocytes in the ventral horn of the spinal cord express a different profile of proteins to those in the dorsal horn (Oberheim et al., 2012; Olsen et al., 2007) with profound effects on sensory-motor connectivity (Molofsky et al., 2014) and neuronal properties (Kelley et al., 2018; Olsen et al., 2007). Human and primate astrocytes show even greater diversity, are larger and more complex than murine astrocytes (Oberheim et al., 2009), and more capable of promoting electrophysiological maturation of motoneurons *in vitro* (Taga et al., 2019). Furthermore, engraftment of human astrocytes into mouse brain early in development enhances the performance of these human glial chimeric mice in learning tasks (Han et al., 2013). Thus, not only do astrocytes vary in size and complexity within and between species, but the astrocyte diversity has fundamental consequences for behaviour.

1.8.2 Astrocytes modulate neuronal metabolism, synaptic transmission and survival

In the mature brain, protoplasmic astrocytes infiltrate the neuropil, parcelling out the gray matter in a non-overlapping manner and ensheathing synapses. A single mouse cortical astrocyte can contact over 100,000 synapses and this number is much larger in humans (Bushong et al., 2002). Astrocytes also have end feet in contact with the vasculature, meaning they have a ready supply of glucose and are well placed to support neurons metabolically.

The concentration of neurotransmitters such as glutamate in the synaptic cleft is in a large part controlled by astrocytes. Astrocytes express numerous active glutamate transporters such as Excitatory Amino Acid Transporters (EAATs) and Glutamate Transporter 1 (GLT-1; Hill et al., 2016). While neurons do express some transporters, the majority of free glutamate is removed from the synaptic cleft by glial transporters (80% at Schaeffer collateral–CA1 synapses in the hippocampus, for example; Tzingounis and Wadiche, 2007); this keeps the synaptic concentration in the nanomolar range when the synapse is inactive (Herman and Jahr, 2007) and prevents extracellular build-up of glutamate during prolonged periods of activity. Astrocytes break the glutamate down into glutamine and also synthesise glutamine *de novo* (Hertz and Chen, 2017). The glutamine is then shuttled back to the neuron for use in glutamate synthesis (Schousboe et al., 2014). In this way, astrocytes help neurons to maintain their stores of

glutamate, which facilitates prolonged firing. A proportion of glutamate is also metabolised to pyruvate, which is used in astrocytic glycolysis to generate Adenosine Triphosphate (ATP); this helps to offset the high cost of transporting glutamate. The product of this glycolysis is lactate, which is thought to be shuttled into the extracellular space where it can be taken up by neurons and converted to pyruvate for use in oxidative metabolism (Mason, 2017; Schousboe et al., 2014). Thus, astrocyte uptake of glutamate maintains efficient synaptic transmission and supports neuronal energy metabolism while preventing glutamate excitotoxicity (Hill et al., 2016; Tzingounis and Wadiche, 2007).

Given their role in protecting against excitotoxicity, it is unsurprising that ablation of astrocytes in adult mice causes neuronal death (Cui et al., 2001; Delaney et al., 1996) similar to that observed when glutamate transporters are depleted (Cui et al., 2001; Rothstein et al., 1996). The reliance of different neural subtypes on protection by astrocytes is not uniform; for example, when astrocytes were ablated in adult mice brain, while Purkinje cells had disordered morphologies, their numbers were not reduced whereas granule cells were depleted (Delaney et al., 1996). Astrocytes also secrete factors that affect neuronal survival; for example, Semaphorin 3A (Sema3A) is a factor secreted by astrocytes in the ventral horn of the spinal cord and has been shown to promote the survival of motoneurons *in vitro.* Moreover, knocking *Sema3A* out in astrocytes depleted spinal α-motoneurons *in vivo,* though γ-motoneurons are unaffected (Molofsky et al., 2014). Advances in genetic and physiological experimental tools are enabling more subtle investigation into the multifarious mechanisms by which astrocytes support neurons.

1.8.3 The maintenance of fast-type motoneuron characteristics by astrocytes

In addition to differentially affecting the survival of motoneuron subtypes, astrocytes affect the fundamental characteristics of motoneurons by modulating the extracellular ion concentrations. Ventral horn astrocytes surrounding fast motoneurons were found to express higher levels of the inwardly rectifying K^+ channel, Kir4.1, than dorsal horn astrocytes (Kelley et al., 2018). Kir4.1 has been shown to be important for astrocytic uptake of K^+ (Djukic et al., 2007) and the homeostatic modulation of extracellular K^+ concentrations in the ventral horn of the spinal cord (Olsen et al., 2007). Astrocytic Kir4.1 was found to be dispensable

for motoneuron survival but required for the maintenance of characteristic fast alpha motoneuron morphology; a conditional knockout of astrocyte-encoded Kir4.1 showed normal motoneuronal soma size at P14 but reduced soma area of fast alpha motoneurons, but not slow alpha or gamma motoneurons, at P30 and 6 months. Conversely, viral-mediated overexpression of Kir4.1 was sufficient to increase average motoneuronal soma size. The electrophysiological properties of fast alpha motoneurons were also affected by conditional knockout of Kir4.1 in astrocytes. Rheobase was decreased, input resistance increased and steady-state firing frequency decreased in the knockout mice; the fast alpha motoneurons seemed to have become more slow-like. The changes in fast alpha motoneuron properties had profound functional consequences. Fast-type muscle fibres were found to have reduced diameters suggesting they too had become more slow-like, and knockout mice had reduced peak grip strength, an altered gait and were quicker to fall in a rotarod task (Kelley et al., 2018). Thus, by modulation of K^+ uptake through Kir4.1, ventral horn astrocytes enable fast alpha motoneurons in the spinal cord to fire at the high frequencies necessary to produce strong contractions; this is an important example of non-cell-autonomous motoneuronal development.

1.8.4 The role of astrocytes in synapse formation and elimination

In the past 20 years, astrocytes in the CNS and Schwann cells in the PNS have been recognised as critical in the establishment of synaptic connectivity (Pfrieger and Barres, 1997; Ullian et al., 2001) and regulation of synaptic nanostructure (Broadhead et al., 2020). Indeed, a feeder-layer of astrocytes significantly increased synapse density and the frequency of spontaneous glutamatergic events in primary murine motoneuron cultures (Ullian et al., 2004a) and human iPSC-derived motoneurons (Taga et al., 2019). Astrocytes have been shown to regulate the formation of many types of synapse, including glutamatergic, GABAergic, glycinergic and cholinergic synapses (Allen and Eroglu, 2017).

Various secreted and contact-mediated astrocytic molecules involved in different aspects of synapse formation and circuit maturation have been identified, predominantly using *in vitro* assays. Astrocytes secrete molecules that positively regulate structural synapse formation. For example, thrombospondins (Christopherson et al., 2005) and hevin (Kucukdereli et al., 2011) mediate the

formation of presynaptically active but postsynaptically silent (due to a lack of AMPA receptors) glutamatergic synapses in primary cultures of rat Retinal Ganglion Cells (RGCs). Astrocytes release other synaptogenic molecules that modulate the formation of functional synapses by increasing the density of postsynaptic receptors. For example, glypicans 4 and 6 lead to the clustering of the GluA1 receptor subunit of the AMPA receptor at the developing postsynaptic density in primary cultures of rat RGCs (Allen et al., 2012). Astrocytes also release molecules that inhibit aspects of synapse formation. For example, SPARC both antagonises the activity of hevin and decreases the number of postsynaptic AMPA receptors (Kucukdereli et al., 2011). Similarly, though TNFα increases AMPA receptor levels at existing synapses in hippocampal pyramidal cells, it also decreases the $GABA_A$ receptors at inhibitory synapses (Stellwagen et al., 2005). The expression profile of these synaptogenic molecules differs between astrocytes from different brain regions, meaning that astrocytes from different regions have different synaptogenic potentials (Buosi et al., 2018).

There are also contact-mediated mechanisms by which astrocytes control synapse formation, though these are less well-studied. These contact-mediated mechanisms act in embryonic neurons and appear to be important permissive steps to synapse formation (Allen and Eroglu, 2017). For example, E17 rat retinal ganglion neurons are unable to respond to secreted synaptogenic signals until they have been physically contacted by an astrocyte (Barker et al., 2008). Thus, astrocytes regulate synapse formation both positively and negatively through both contact-mediated mechanisms and secreted signalling molecules.

Synapse elimination is also controlled by astrocytes via both secreted factors and contact-mediated mechanisms. Astrocytes phagocytose excess synapses in the brain through the action of phagocytic receptors on their surface (Chung et al., 2013) and secrete astrocytic TGFβ, which leads to the tagging of synapses for phagocytosis by microglia (Allen and Eroglu, 2017; Bialas and Stevens, 2013; Schafer et al., 2012). Thus, either by direct synapse engulfment or tagging of synapses for microglial engulfment, astrocytes have an important role in synapse elimination as well as in synapse formation.

1.8.5 Astrocytes are important for the formation of motor circuits

In addition to a general role in synapse formation and elimination, astrocytes have region-specific roles in circuit formation. Domain-specific deletion of astrocytes in the spinal motoneuronal progenitor domain resulted in a decrease and increase of motoneuron innervation by proprioceptive afferents and inhibitory inputs respectively, although cholinergic innervation of motoneurons was unaffected. Notably, the deficits were not rescued by immigration of astrocytes from adjoining regions (Tsai et al., 2012). This is likely because, as mentioned above, astrocytes in different regions have different synaptogenic potentials *in vitro* (Buosi et al., 2018). Indeed, a similar effect on the balance of proprioceptive and inhibitory inputs to motoneurons can be achieved by astrocyte-specific deletion of Sema3A, a molecule expressed in ventral (but not dorsal) spinal astrocytes; motoneurons in Sema3A knockout mice had fewer vGluT1 (likely proprioceptive) somatic synapses and more vGAT (inhibitory) somatic synapses. Furthermore, the dorsoventral positioning of TrkA-positive afferents was dysregulated in Sema3A knockout mice such that they aberrantly terminated in the medial spinal cord (as opposed to the dorsal spinal cord; Molofsky et al., 2014). Thus, region-specific expression of synaptogenic molecules in astrocytes has a fundamental effect on motor circuitry and the balance of excitation and inhibition in the spinal cord.

1.8.6 Participation of astrocytes in motor circuit function

In addition to their role in circuit formation, astrocytes also have a striking role in the functioning of circuits. In zebrafish, astrocytes control futility-induced passivity by integrating sensory information from various sources and controlling the activity of a downstream population of GABAergic neurons (Mu et al., 2019). A role for astrocytes in mammalian spinal circuit function has also been demonstrated. For example, Morquette et al. (2015) showed that, in rat trigeminal sensory-motor circuit for mastication, astrocytes responded to NMDA released by sensory afferents with a rise in internal calcium and secretion of a calcium chelator, S100β. The resulting reduction in external calcium concentration caused neurons in this nucleus to switch from tonic firing to rhythmic bursting. Stimulation of the main sensory trigeminal nucleus *in vivo* at certain frequencies elicits chewing (Lund and Dellow, 1971) and the frequency of bursting elicited by sensory afferent stimulation, NMDA or S100β corresponded to the chewing frequency observed *in vivo* in rats. Therefore, it was proposed that astrocytes in

this nucleus have an essential role in the sensory control of mastication (Morquette et al., 2015). In addition to mastication, astrocytes also play an active role in the function motor circuits controlling other behaviours, including respiration (Gourine et al., 2010) and locomotion (Acton and Miles, 2015; Acton et al., 2018; Broadhead and Miles, 2020).

1.8.7 Astrocytes were selected as a candidate cell type.

Due to the importance of astrocytes for the survival, metabolism, synapse formation of motoneurons as demonstrated both *in vivo* and *in vitro,* it was hypothesised, firstly, that astrocytes within the EB would promote motoneuron maturation and enable their successful reinnervation of the muscle, and secondly, that the absence of astrocytes prevented purified motoneuron aggregates from having the same capacity. Astrocytes were therefore selected, alongside V3 interneurons, as a candidate cell type to investigate this hypothesis and seek a graft composition that would promote functional muscle reinnervation.

1.9 Aims of this Thesis

Peripheral engraftment of ESC-derived motoneurons, genetically modified to respond to light, represents a novel approach to restore function to paralysed muscles in conditions such as ALS or following traumatic injury (Bryson et al., 2014). However, current data suggests that engraftment of motoneurons alone is insufficient and results in sub-optimal reinnervation of target muscles (Bryson, unpublished observation; Magown et al., 2017). Indeed, given the fundamental role of surrounding spinal neurons and astrocytes in the maturation and function of motoneurons both *in vitro* and *in vivo*, it is unsurprising that peripheral grafts comprising only of ESC-derived motoneurons were not able to functionally innervate target muscle. In this Thesis, I aim to test the hypothesis that other cell types that normally interact with motoneurons in the spinal cord, such as V3 interneurons and astrocytes, are required to enable peripherally engrafted ESC-motoneurons to mature and form functionally useful connections.

To explore this hypothesis, the specific aims of this Thesis are:

1. To identify the cell types present in engrafted embryoid bodies that may affect ESC-derived motoneuron maturation;

2. To assess the effect of co-culture with V3 interneurons and astrocytes on ESC-derived motoneuron maturation *in vitro*, by assessing:
    a. Motoneuron size and morphology,
    b. Cholinergic and glutamatergic synapse formation,
    c. Motoneuronal electrophysiological properties,
    d. Spontaneous activity on a single-cell and network level.

2 Chapter 2: Materials and Methods

2.1 ESC expansion

The transgenic cell lines used are described in Table 2.1 and the reagents and solutions used are described in Table 2.2. ESCs were stored in liquid nitrogen in freezing medium (see Table 2.2). During expansion, differentiation and culture, cells were maintained in a humidified incubator at 37°C in 5% carbon dioxide (CO_2).

ESC colonies were expanded in ESC medium on a feeder layer of mouse embryonic fibroblasts, except Vic_1244 ESCs, which were cultured in a feeder-free manner in feeder-free medium (Table 2.2).

2.2 ESC differentiation: 5-day RA/SAG differentiation protocol

ESC differentiation was performed as described by Magown et al. (2016). Undifferentiated ESC colonies were dissociated with 0.25% Trypsin (Invitrogen) and grown in suspension in uncoated, non-treated plastic dishes (Corning) to promote Embryoid Body (EB) formation. In the first two days, EBs were cultured in ADFNK medium (Table 2.2). For the subsequent three days, the EBs were cultured in ADFNK medium supplemented with 1μM retinoic acid (Sigma) and 0.5μM Smoothened Agonist (SAG; Merck). This differentiation protocol will herein be described as the 5-day RA/SAG differentiation protocol.

Table 2.1: Transgenic ESC lines used.

ESC line	Designation	Source	Transgene	Effect	Purpose
H14IG#13	H14IG#13	(Bryson et al., 2014)	*Hb9::CD14-IRES-GFP*	Tags Hb9-expressing cells (including motoneurons) with membranous CD14 and cytoplasmic GFP.	The CD14 and GFP can be used to purify Hb9-positive (mostly motoneurons) by MACS (Section 2.4.1) and FACS (Section 2.4.2), respectively
H14IG#13 /CCRY#1 A/CG#9G	C9G	(Bryson et al., 2014)	*Hb9::CD14-IRES-GFP*	Tags cells which express Hb9	The CD14 can be used to purify

				(including motoneurons) with membranous CD14 and cytoplasmic GFP.	motoneurons by MACS (Section 2.4.1).
			CAG::ChR2-YFP	*CAG* drives the expression of membranous Channelrhodopsin-2 (ChR2) linked to Yellow Fluorescent Protein (YFP) in all cells.	ChR2 is an opsin that enables the cells to be stimulated with blue light.
			CAG::Gdnf	*CAG* drives the expression of the Glial cell line-Derived Neurotrophic Factor (GDNF) in all cells.	GDNF improves long term motoneuron survival *in vitro*.
G14#H6	H6	(Bryson et al., 2014)	*GFAP::CD14*	Tags cells which express Glial Fibrillary Acidic Protein (GFAP; including astrocytes) with membranous CD14.	The CD14 can be used to purify GFAP-positive (mostly astrocytes) by MACS (Section 2.4.1).
#1244	Vic_1244	Kindly donated by the Pfaff lab, Salk Institute for Biological Studies (Sternfeld et al., 2017)	*Sim1::cre;Rosa-LSL-tdtomato*	Tags Sim1-expressing cells (V3 interneurons) with the red fluorescent protein, tdTomato.	The tdTomato can be used to sort Sim1-expressing cells (V3 interneurons) by FACS (Section 2.4.2).

Table 2.2: Reagents and solutions

Solution	Recipe
Freezing medium	80% ES-screened Foetal Bovine Serum (FBS; HyClone) and 20% dimethyl sulphoxide (Sigma-Aldrich)
ADFNK medium	Advanced-DMEM/F12 (Invitrogen) and Neurobasal medium (Invitrogen) mixed at 1:1 ratio supplemented with 2 mM Glutamax (Gibco), 0.1 mM 2-mercaptoethanol (Sigma-Aldrich), 10% knock-out serum replacement (Invitrogen), and 1X Penicillin/Streptomycin (Gibco)
ESC medium	Knockout-DMEM (Invitrogen), 15% ES-screened heat-inactivated FBS (HyClone), 1X non-essential amino acids (Invitrogen), 1X EmbryoMax ES cell qualified nucleosides (Millipore), 2mM Glutamax (Gibco), 1X Penicillin/Streptomycin (Gibco), 1ng/ml ESGRO Leukaemia Inhibitory Factor (LIF) medium supplement (Millipore), 50µg/ml plasmocin prophylactic (InvivoGen) and 0.1mM 2-mercaptoethanol (Sigma-Aldrich)
Feeder-free medium	Advanced-DMEM/F12 (Invitrogen) and Neurobasal medium (Invitrogen) mixed at 1:1 ratio supplemented with N2 supplement (100X; Gibco), B27 supplement (50X; Gibco), 1X Penicillin/Streptomycin (Gibco), 0.1 mM 2-mercaptoethanol (Sigma-Aldrich), 1ng/ml ESGRO LIF medium supplement (Millipore), 3µM CHIR99021 (Sigma-Aldrich) and 1µM PD0325901 (Sigma-Aldrich)
Wash buffer	10ng/ml Trypsin-free DNase 1 (Roche) in L15 medium (Gibco)
MACS buffer	5µg/ml Bovine Serum Albumin (BSA; Sigma-Aldrich) in sterile Dulbecco's Phosphate-Buffered Saline (PBS; Sigma). Sonicated for 10 minutes and then filtered using a 20µm filter (Falcon). 10ng/ml Trypsin-free DNase 1 (Roche) added after filtration.
FACS buffer	5µg/ml BSA (Sigma-Aldrich), 1.27mM Ethylenediaminetetraacetic Acid (EDTA; Sigma-Aldrich), 10mM HEPES buffer (Sigma-Aldrich) in sterile Dulbecco's PBS (Sigma). Sonicated for 10 minutes and then filtered using a 20µm filter (Falcon). 10ng/ml Trypsin-free DNase 1 (Roche) added after filtration.
Tris-buffered saline (TBS)	50mM Tris-base, 154mM NaCl in 18MΩ distilled water
Blocking solution	TBS supplemented with 5% donkey serum (Sigma-Aldrich) and 0.2% Triton-X 100 (Sigma-Aldrich)
Oxygenated artificial cerebrospinal fluid (ACSF)	127mM NaCl, 3 mM KCl, 2 mM $CaCl_2$, 10 mM d-glucose, 26 mM $NaHCO_3$, 1.2 mM NaH_2PO_4 and 1mM $MgCl_2.6H_2O$ in 18MΩ distilled water (made up to pH 7.35 with NaOH and bubbled through with oxygen for >20 minutes).
Intracellular fluid (ICF)	131mM potassium methane sulfonate, 6mM NaCl, 1.1mM EGTA-KOH, 10mM HEPES buffer, 0.3mM $MgCl_2.6H_2O$, 3mM adenosine triphosphate (ATP-Mg), 0.5mM guanosine triphosphate (GTP-Na), 2.5mM L-glutathione, 5mM phosphocreatine and 0.1mM in 18MΩ distilled water (made pH = 7.25 at 295-300mOsm).
Recording media	156mM NaCl, 10mM HEPES, 10mM D-glucose, 3mM KCl, 2mM $MgSO_4$, 2mM $CaCl_2$ and 1.25mM KH_2PO_4 in 18MΩ distilled water
Diluent	0.1M borate buffer, 0.2% Triton X-100 (Sigma-Aldrich), 0.003% H_2O_2, pH 8.5

2.3 Differentiation and purification methods for different cell types

Day 5 EBs generated using the RA/SAG differentiation protocol described in Section 2.2 were treated differently according to the desired cell population, as described below.

2.3.1 Motoneurons

Unless otherwise stated in the text, the C9G ESC line was used to generate pure motoneuronal populations (rather than the H14IG#13 ESC line). ESC-derived motoneurons were collected from day 5 EBs that had been treated with the antimitotic agent, mitomycin-C (2μM for 2 hours at 37°C). Motoneuron purification was achieved by Magnetically-Activated Cell Sorting (MACS) as described below (Section 2.4.1), using the CD14 tag expressed under the control of the *Hb9* promoter.

2.3.2 V3 interneurons

To differentiate V3 interneurons, Vic_1244 ESCs underwent the RA/SAG differentiation protocol as described in Section 2.2. On day 5, Vic_1244 EBs were resuspended in non-supplemented ADFNK medium to be collected on day 9. ADFNK medium was changed every other day. On day 9, V3 interneurons were treated with the antimitotic agent, mitomycin-C (2μM for 2 hours at 37°C), and purified by Fluorescently-Activated Cell Sorting (FACS) as described below (Section 2.4.2), according to their *Sim1* promoter-driven tdTomato expression.

2.3.3 Astrocytes

To generate pure populations of astrocytes, H6 ESCs underwent the RA/SAG protocol as described in Section 2.2. Day 5 EBs were plated on matrigel-coated T-75 flasks in non-supplemented ADFNK medium and cultured for a further 7 days, changing the media every other day. On day 12 of the differentiation, the astrocytes were purified by MACS as described below (Section 2.4.1), according to the CD14 tag expressed under the *gfap* promoter. The yield of astrocytes was 23 ± 12% (n = 5 differentiations). Aliquots of pure astrocytes were frozen and stored in liquid nitrogen. After purification, astrocytes were plated in ADFNK medium on poly-L-ornithine and murine-laminin coated glass coverslips (600 cells/mm^2) and the media was changed every other day. When the astrocytes had divided to create a monolayer, the coverslips (VWR, catalogue number (cat.

#): 631-0150) were treated with mitomycin-C (2μM, 2 hours, 37°C) to prevent further division. Note that, one treatment was often not enough to prevent division in the culture so multiple treatments were sometimes used. As soon as a monolayer had formed and been treated to prevent division, astrocytes were maintained by gently replacing half of the media (half-replace) every other day. Neuronal populations could then be plated onto the astrocyte monolayers.

2.4 Cell purification methods

Different cell populations were purified either by Magnetically-Activated Cell Sorting (MACS) or by Fluorescently-Activated Cell Sorting (FACS) according to the tags and fluorescent reporters expressed.

2.4.1 Magnetically-Activated Cell Sorting (MACS)

ESC-derived motoneurons and astrocytes were purified from dissociated day 5 and day 12 EBs, respectively, by anti-CD14 MACS enrichment as described by Bryson et al. (2014). EBs were washed in wash buffer (Table 2.2) and dissociated with Accumax (Sigma-Aldrich) for 15 minutes at 37°C. A cell suspension was achieved by gently pipetting and washing three times in wash buffer. In between washes, cells were centrifuged (1200rpm, 4 minutes) and the supernatant discarded. After the final wash, cells were resuspended in MACS buffer (Table 2.2) and passed through a 40μm cell strainer (Falcon, cat. #: 352340) to ensure a single cell suspension. The cells were centrifuged (1200 rpm, 4 minutes), re-suspended in 200μl of MACS buffer containing 2-5μg/ml mouse anti-human CD14 antibody (Biolegend, cat. #: 325602), and incubated for 15 minutes at room temperature. After washing in MACS buffer, the cells were re-suspended and incubated in 1:10 goat anti-mouse IgG MicroBeads (Miltenyi) for 15 minutes at room temperature. After the secondary antibody incubation, the cells were washed again, re-suspended in 600μl of MACS buffer and applied to a pre-washed MS magnetic column mounted in an OctoMACS magnet (Miltenyi). CD14-expressing cells tagged with MicroBeads were magnetically retained in the column while untagged cells flowed through. The column was washed three times with 500μl MACS buffer, and, following removal of the column from the magnet, the CD14-positive cell fraction eluted with 1ml MACS buffer, according to the manufacturer's instructions. In some experiments, the unsorted cells – the 'flowthrough' – were also collected for culture and analysis.

2.4.2 Fluorescently-Activated Cell Sorting (FACS)

Vic_1244 ESC-derived V3 interneurons were purified from dissociated day 9 EBs by anti-tdTomato FACS enrichment. In addition to purifying V3 interneurons, FACS was also used to investigate the effectiveness of the MACS purification protocol by sorting cell populations differentiated from the H14IG#13 line (Table 2.1) according to GFP expression (Chapter 3, section 3.3.2.1).

To prepare differentiated cells for FACS, EBs were washed in wash buffer and dissociated with Accumax (Sigma-Aldrich) for 15 minutes at 37°C. A cell suspension was achieved by gently pipetting and washing three times in wash buffer. In between washes, cells were centrifuged (1200rpm, 4 minutes) and the supernatant discarded. After the final wash, cells were resuspended in FACS buffer (Table 2.2) and passed through a 40µm cell strainer to ensure a single cell suspension. Finally, the dissociated cells were resuspended in FACS buffer to a concentration of 10-20million cells/ml and stored on ice until purification by FACS.

FACS was performed on the FACSAriaIII at the UCL Great Ormond Street Institute of Child Health Flow Cytometry Core Facility, supported by the Great Ormond Street Children's Charity, (grant reference U09822; October 2007), and UCL Capital Equipment Funding, School of Life and Medical Sciences (September 2012).

2.5 Neuron/astrocyte co-cultures

To determine the effects of co-culture with V3 interneurons (V3) and astrocytes (as) on motoneuron (MN) maturation, four co-culture conditions were used (Figure 2.1 A): MN alone (680 MNs/mm^2), MN+V3 (680 neurons/mm^2), MN+as (340-450 neurons/mm^2) and MN+V3+as (340-450 neurons/mm^2). The MN to V3 ratio was 1:2. Astrocytes were present as a monolayer beneath the neurons. Cells were plated in ADFNK medium supplemented with GDNF (10ng/ml) on poly-L-ornithine and murine-laminin coated glass coverslips or onto astrocyte monolayers depending on the condition. A time course of the co-culture protocol up to motoneuron plating can be seen in Figure 2.1 B, including the order in which cells were added to the co-cultures (which was kept consistent between experiments). After motoneurons were plated, co-cultures were maintained for up to 31 days *in vitro* with media being half-replaced every other day.

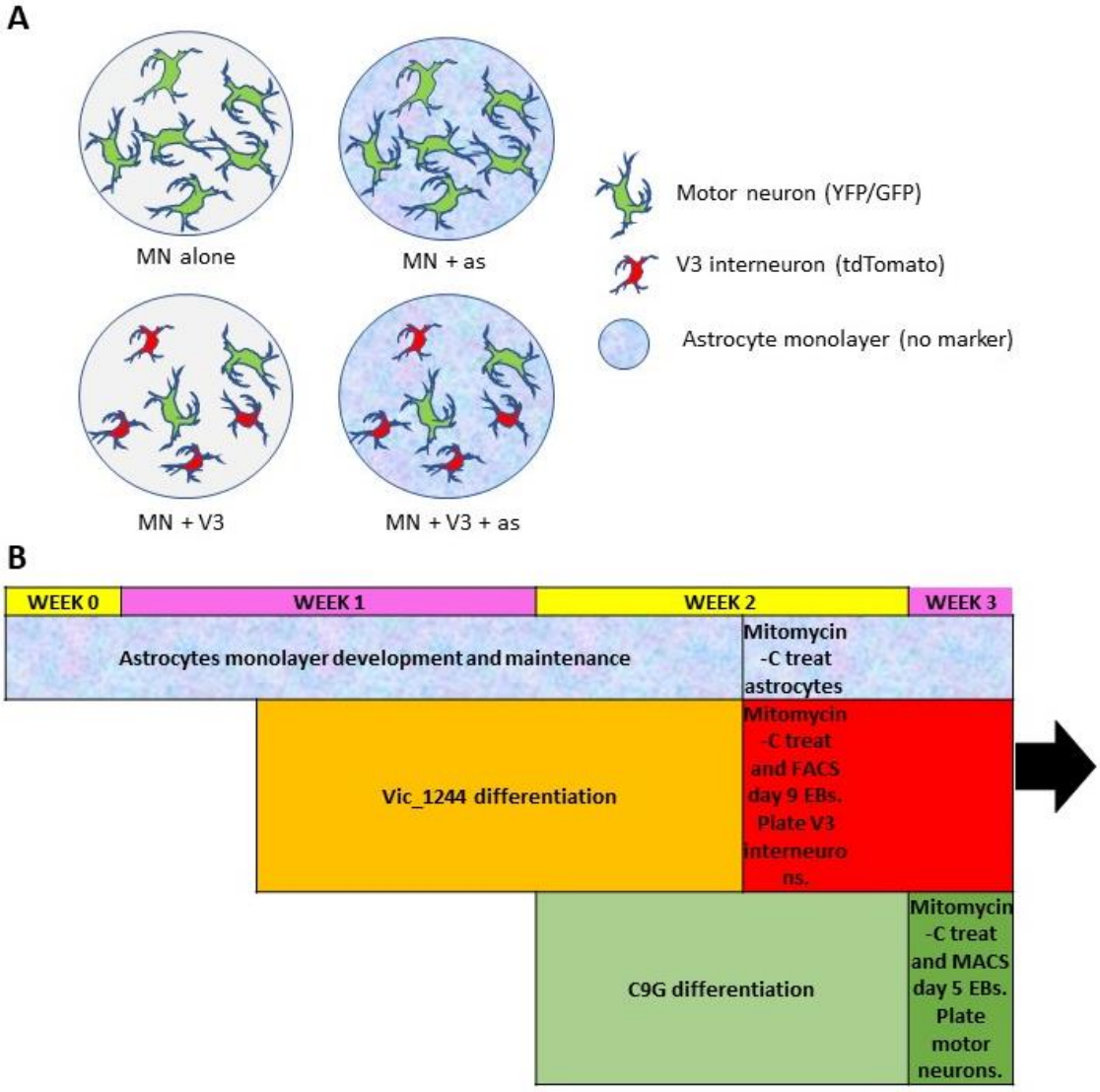

Figure 2.1: Co-culture of motoneurons with V3 interneurons and astrocytes.

A: Diagrammatic representation of the four co-culture conditions. Two V3 interneurons were plated for every motoneuron. Astrocytes were present as a monolayer. B: The time course of setting up the co-cultures. Note that the astrocyte monolayer was often established up to three weeks before motoneurons were plated and that V3 interneurons were plated two days before the motor neurons; during this time, the ADFNK media was supplemented with ciliary neurotrophic factor (10ng/ml), brain-derived neurotrophic factor (10ng/ml) and GDNF (10ng/ml). After motor neurons were plated, ADFNK media was supplemented only with GDNF (10ng/ml).

2.6 Live cell imaging

To investigate the effectiveness and sensitivity of the MACS protocol, cytoplasmic GFP expression (driven by the Hb9 promoter) of the MACS-purified cell population and the cell population not captured by the purification process (the flowthrough population) was compared (Chapter 3). MACS-purified motoneurons and flowthrough (derived from C9G ESCs; 3 x 10^4 cells per well)

were plated separately on poly-L-ornithine and murine laminin coated coverslips in ADFNK medium and supplemented with the antimitotic agent 5-fluoro-2′-deoxyuridine (5-FDU, 2µM; Sigma, cat. #: F0503) to prevent further cell division. Media was gently half-replaced every other day.

Live cells were imaged in either recording media or ACSF (Table 2.2) using a confocal LSM500 microscope (Zeiss). Figure 2.2 shows the filters used to distinguish cytoplasmic GFP and membrane-bound YFP.

2.7 Fixation of co-cultures

Co-cultures were fixed for labelling by incubation in 4% paraformaldehyde (Agar Scientific) in TBS (10 minutes, room temperature) followed by three washes in TBS (5 minutes, room temperature, Table 2.2). Co-cultures were protected from light and stored in TBS at 4°C prior to labelling.

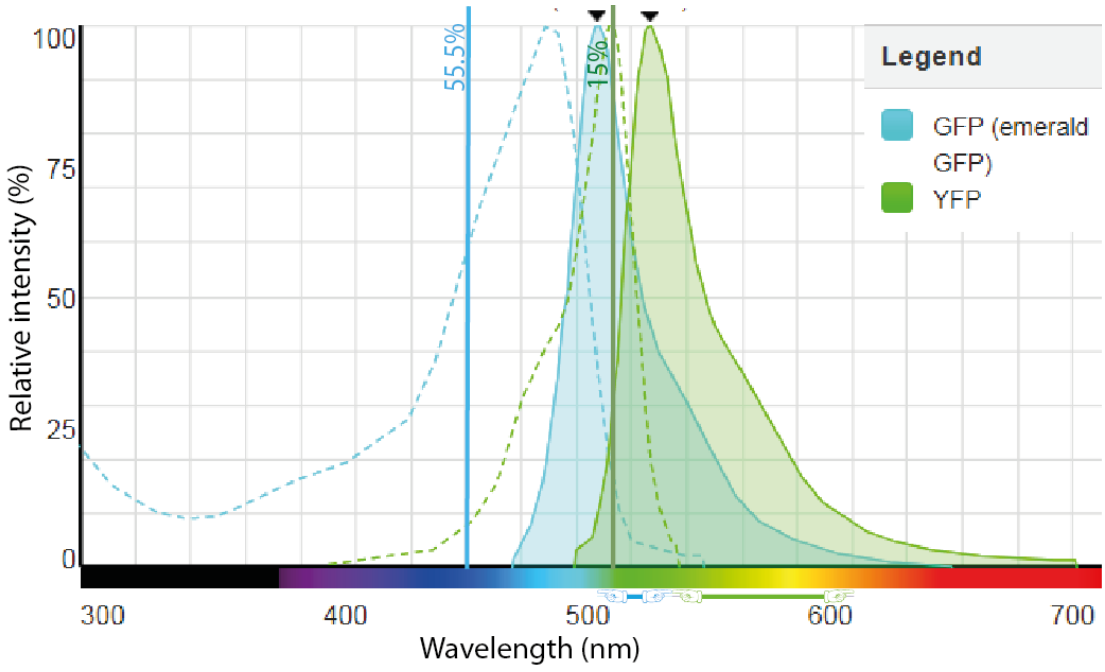

Figure 2.2: The spectra of GFP (blue) and YFP (green) using ThermoFisher's Fluorescence Spectraviewer

The dotted lines represent the excitation wavelengths and the solid shaded areas represent the emission wavelengths of the fluorescent reporters detailed in the legend. Vertical lines show the wavelength of excitation laser used with the % power applied. Horizontal lines tipped with hands beneath the x-axis show the wavelengths detected by the emission filters.

2.8 Immunofluorescent labelling of co-cultures

Cells were blocked and permeabilised with blocking solution (Table 2.2) for 45 minutes. Following this, cells were incubated with primary antibodies (Table 2.3) in blocking solution overnight at room temperature. Negative controls were performed that were not exposed to primary antibodies. After washing in TBS (3 times 5 minutes), cells were incubated with secondary antibodies (Table 2.4) in blocking solution for 2 hours at room temperature. After further washing in TBS (3 x 5 minutes), coverslips were then mounted on slides in Mowiol 40-88 (Sigma-Aldrich) for imaging with either a Zeiss LSM800 or LSM500 laser scanning microscope using Zen 3.0, blue edition software).

2.8.1 Tyramide signal amplification of choline acetyltransferase labelling

Because the Choline Acetyltransferase (ChAT) labelling using the method described above (Section 2.8) was faint, in Section 3.3.2.2, a Tyramide Signal Amplification (TSA) kit (TSA^{TM}-Plus Fluoroscein System, Perkin-Elmer LAS Inc.) was used for better visualisation of the signal. Fixed cells on coverslips were incubated in primary and secondary antibodies as described in Section 2.8. A biotinylated secondary antibody was used for ChAT protein amplification (Table 2.4). In tandem with the secondary incubation, ABC mix (1:100 reagent A and reagent B in TBS) was prepared and incubated for >30 minutes to allow horse radish peroxidase complexes to form. Cells were washed in TBS (3 x 5 minutes) and incubated with the ABC mix for 20 minutes. After further washing (3 times for 5 minutes), the cells were incubated for 90s with diluted Cy5-conjugated amplification reagent (1:200 amplification reagent in diluent) and immediately washed once more (3 x 5 minutes). The coverslips were then mounted on slides in Mowiol and left to dry overnight before imaging.

2.9 Testing antibodies for spinal neuron markers

Antibodies for spinal neuron markers used in Chapter 3 were validated in mouse spinal tissue.

2.9.1 Experimental animals

All procedures and experiments involving animals were carried out under License from the UK Home Office in accordance with the Animals (Scientific Procedures) Act 1986 (Amended Regulations 2012) and following ethical approval from UCL

Table 2.3: Primary antibodies used in immunocyto- and immunohisto- chemistry

Target	Host	Source	Catalogue number	Notes about target	Dilution
Chapter 3					
Beta-tubulin III (BTIII)	Rabbit, mouse	BioLegend	845502, 801202	Labels neuronal cytoskeleton	1:500
Chx10	Rabbit	Susan Morton, Zuckerman Institute, Columbia University		Transcription factor expressed in V2a interneurons	1:4000-8000
Dbx1	Rabbit	Susan Morton, Zuckerman Institute, Columbia University		Transcription factor expressed in V0 interneurons	1:2000-6000
En1	Guinea pig	Susan Morton, Zuckerman Institute, Columbia University		Transcription factor expressed in V1 interneurons	1:1000
Evx1	Mouse	Susan Morton, Zuckerman Institute, Columbia University		Transcription factor expressed in V0v, V0c, V0g interneurons	1:50
Hb9	Guinea pig	Susan Morton, Zuckerman Institute, Columbia University		Transcription factor expressed in Motoneurons and Hb9+ interneurons	1:8000
Isl1	Guinea pig	Susan Morton, Zuckerman Institute, Columbia University		Transcription factor expressed in dI3 interneurons and MMC, LMCm and PGC motoneurons	1:5000
NeuN	Mouse	BioLegend	834501	Labels neuronal nuclei	1:1000

Nkx2.2	Mouse	DSHB	74.5A5	Transcription factor expressed in V3 interneurons	1:50
Choline acetyltransferase (ChAT)	Goat	Chemicon	AB144P	Expressed in cholinergic neurons	1:40
Vesicular acetylcholine transporter (vAChT)	Goat	Millipore	ABN100	Expressed in cholinergic neurons, particularly at the synapse	2ug/ml
Chapter 4					
GFP	Rabbit	Invitrogen	A11122		1:1000
Vesicular glutamate transporter 2 (vGluT2)	Guinea pig	Millipore	AB2251-I	Presynaptic marker of glutamatergic synapses	1:1000
Vesicular acetylcholine transporter (vAChT)	Goat	Millipore	ABN100		2ug/ml
Homer1	Mouse	Synaptic Systems	160 011	Putatively glutamatergic postsynaptic marker	1:100
mCherry/tdTomato	Chicken	Abcam	ab205402		1:2500

Institute of Neurology. The following mice were used in the experiments below: E12-14 and P3/2 wild-type mice (C57BL/6J × SJL, Charles River Laboratories) for spinal cord dissection.

2.9.2 Tissue processing

Spinal cords were dissected from 12.5-13.5 day old wildtype mouse embryos by Dr Emma Wilson and Dr Ione Meyer based on the protocol outlined by Henderson et al. (1995). Pregnant females were euthanised with an intraperitoneal injection of pentobarbital sodium (200 mg/ml, Merial) and subsequent cervical dislocation (as confirmation of death) as outlined by Schedule 1 procedure in the Animals Scientific Procedures Act, 1986. A laparotomy was performed, and the uterus removed. Embryos were removed from the amniotic sacs and transferred to chilled Hanks' Balanced Salt Solution

Table 2.4: Secondary antibodies used in immunocyto- and immunohisto-chemistry

Marker	Host	Source	Catalogue number	Emission wavelength (nm)	Dilution
Chapter 3					
Goat IgG	Donkey	Life Technologies	A11057	568	1:500
Guinea pig	Donkey	Susan Morton, Zuckerman Institute, Columbia University		647	1:700
Guinea pig	Donkey	Susan Morton, Zuckerman Institute, Columbia University		555	1:500
Guinea pig- IgG	Goat	Abcam	Ab175714	568	1:500-1000
Mouse	Donkey	Invitrogen	A31571	647	1:1000
Mouse IgG	Donkey	Invitrogen	A10037	568	1:1000
Mouse IgG	Donkey	Life Technologies	A21202	488	1:1000
Rabbit IgG	Donkey	Life Technologies	A31573	647	1:1000
Rabbit IgG	Donkey	Life Technologies	A10042	568	1:1000
Rabbit IgG	Donkey	Invitrogen	A21206	488	1:1000
Mouse	Goat	Invitrogen	A21240	647	1:1000
Mouse IgG	Goat	Invitrogen	A11004	568	1:1000
Mouse IgG	Goat	Invitrogen	A21141	488	1:1000
Rabbit IgG	Goat	Invitrogen	A21245	647	1:1000
Rabbit IgG	Goat	Invitrogen	A11011	568	1:1000
Rabbit IgG	Goat	Invitrogen	A11008	488	1:1000
Goat IgG	Horse	Biotinylated	BA-2001	Biotinylated	Vector Laboratories
Chapter 4					
Guinea pig	Donkey	Millipore		647	1:700
Rabbit IgG	Donkey	Invitrogen	A21206	488	1:1000
Mouse IgG	Donkey	Abcam	ab175658	405	1:1000
Chicken IgY	Donkey	Jackson ImmunoResearch		564 (Cy3)	1:1000
Goat	Donkey	Life technologies	A11057	568	1:1000

(HBSS, Ca^{2+}- and Mg^{2+}- free) containing Penicillin/ Streptomycin (100 units/ml or 100 µg/ml). After removal of the head, the neural tube was separated from the rest of the embryo under a light dissection microscope, by the delicate removal of skin on the back of the embryo and teasing of the neural tube away from the body. Then the meninges were removed, and the neural tube collected.

P2/3 animals were euthanised by Dr Bilal Malik by decapitation and exsanguination as outlined by Schedule 1 procedures in the Animals Scientific Procedures Act, 1986. The spinal cord tissue was immediately collected under a light dissection microscope: skin on the back was removed and the spinal column separated from the rest of the pup. Then the muscle, vertebrae and meninges were cut away and the spinal cord gently removed.

Spinal cord/neural tube tissue was mounted on a silicon mounting block, using insect pins, and then fixed in 4% paraformaldehyde in TBS for 1 hour at room temperature, before transfer to 20% sucrose solution in TBS, for cryoprotection at 4°C overnight. Samples were then carefully mounted in O.C.T. medium (Tissue-Tek 4583), within flat-bottomed aluminium foil moulds. The moulds were then frozen on dry ice. Serial longitudinal or transverse frozen sections (20µm) were cut from the entire tissue block using a BrightTM cryostat and the sections were mounted onto poly-lysine coated slides (VWR, cat. #: 631-0107). After being air-dried (>1 hour at room temperature), sections were immunolabelled as described below.

2.9.3 Immunofluorescent labelling (spinal tissue and EB sections)

Sections were washed three times with TBS, blocked with blocking solution. Primary antibodies (Table 2.3) in blocking solution (Table 2.2) were then applied to the sections and incubated overnight at room temperature. Sections were next washed (3 x 5 minutes in TBS) and incubated in secondary antibodies (Table 2.4) in blocking solution (2 hour, room temperature). DAPI (Sigma D9542; used 1:1000) was usually mixed with secondary antibody solution. The sections were washed (3 x 5 minutes in TBS). Finally, the sections were covered with coverslips using Mowiol and allowed to dry.

2.10 Image processing

Images were taken using a confocal LSM800 microscope (Zeiss) using Zen 3.0, blue edition software. Either Imaris (version 9.5) or ImageJ was used for image processing.

2.10.1 EB characterisation: nuclei counts

To characterise the interneuron content of EBs in Chapter 3, EB sections were labelled for markers of various types of spinal neuron and tile scans taken using a Plan Apochromat 20x/0.8 M27 objective on a confocal LSM800 microscope (Zeiss). The pinhole was 37-43µm except for detection of DAPI, for which the pinhole was occasionally set to 31µm. The spots function of Imaris, version 9.5, was used to count the nuclei in each EB section labelled for each neuronal marker (estimated nuclear diameter = 5µm). No true nuclei were found to be less than 2µm by manual measurement, so DAPI spots less than 2µm in diameter were excluded as debris. The proportion of DAPI-positive nuclei labelled for each marker was determined for each EB section. Sections from multiple EBs from each differentiation were counted for each quantified marker.

2.10.2 Quantification of neuronal survival, soma size and morphology

For quantification of motoneuronal soma size and morphology in Chapter 4, tile scans of week 2 co-cultures were made using a Plan Apochromat 20x/0.8 M27 objective on a confocal LSM800 microscope (Zeiss) with a pinhole = 28-38µm. Analysis was performed using the measurement and surfaces function of the Imaris software. Motoneurons expressed GFP and the V3 interneurons expressed tdTomato; the signal was amplified with antibodies.

To calculate neuronal survival, the numbers of neurons (both motoneurons and V3 interneurons) in each tile scan were manually counted using ImageJ and neuron density calculated. A uniform neuron distribution was assumed, and the total area of the coverslip were used to calculate the number of total surviving neurons. By comparing this value to the number of neurons that had originally been plated, a value for percentage total neuron survival was obtained.

Neuronal morphology was analysed by looking at the somatic and proximal dendritic compartments of neurons. Motoneurons or V3 interneurons too close to other neurons were excluded as the edge of the soma could not be distinguished.

Soma diameter was manually measured using the measurement function in Imaris along the minor axis of the soma. The edge of the soma was traced manually, and the resultant cross-sectional area measured using the Surfaces function in Imaris.

Overlapping neurites from the different neurons in culture made characterising the complete morphology of individual neurons extremely difficult. Therefore, the number and diameter of primary neurites, which have both been shown to correlate with dendritic complexity *in vivo* (Ulfhake and Cullheim, 1988; Ulfhake and Kellerth, 1981), were used as indicators of morphological complexity. Primary neurite diameter was manually measured at the junction between the neurite and the soma using ImageJ and averaged to obtain a value for mean primary neurite diameter for each neuron. The number of primary neurites per neuron was manually counted. A primary neurite was defined as a neuronal process directly protruding from the cell soma. Sometimes there was a fork in the neurite near to the cell soma; whether these counted one or two primary neurites was difficult and relied on the judgement of the experimenter. Some error may have been introduced into the dataset in this way. Due to the overlap of neuronal processes in the co-cultures, more detailed analysis of neuronal morphology could not be performed reliably from these images.

2.10.3 Synapse counts

For quantification of synapse density in Chapter 4, confocal z-stacks of motoneuron cell bodies and proximal dendrites were taken using a Plan-Apochromat 63x/1.40 Oil DIC M27 objective lens. For glutamatergic synapses: pinhole = 34µm, scaling per pixel = 0.01 x 0.01 x 0.3µm. For cholinergic synapses: pinhole = 40-48µm, scaling per pixel = 0.01 x 0.01 x 0.4µm. Only one motoneuronal cell body was included in each z-stack, which had the effect of excluding motoneuronal cell bodies that were close to other motoneuronal cell bodies from the analysis. Coverslips were excluded from the analysis if there was tubular extracellular Homer1-positive debris present, as this was taken to indicate unhealthy cells and skewed the count of Homer1 puncta. Analysis was performed using Imaris software (version 9.5). Motoneuronal GFP labelling was used to mask the image to restrict analysis to the motoneuron. The spots function of Imaris software was used on the masked Homer1 puncta to determine the

number of putatively glutamatergic, postsynaptic densities on and in motoneuron cell bodies (estimated puncta diameter = 250nm). The unmasked labelling for the presynaptic marker (either vGluT2 for glutamatergic synapses or vAChT for cholinergic synapses) was used to create a 'surface'. A synapse was defined as GFP-masked Homer 1 spot less than 350nm from a particular presynaptic surface. A GFP-masked Homer1 punctum less than 350nm from both vGluT2 and vAChT surfaces was deemed to be a synapse of both cholinergic and glutamatergic character or a 'dual synapse'. The number of synapses was normalised to the total GFP surface area to determine the density of motoneuronal synapses.

Although V3 interneurons were labelled with tdTomato, due to the complexity and density of neuronal projections in the co-cultures at this time point, it was difficult to resolve the neuronal morphology of each synapse – i.e. the cell type the pre- and post- synaptic boutons belonged to.

2.11 Drugs

The effect of various drugs on spontaneous activity observed in electrophysiology (Section 2.12) and calcium imaging (Section 2.13) experiments was investigated in Chapters 4 and 5.

Perfusion of the preparation with drugs dissolved in ACSF was performed at a flowrate of between 2-3ml/min.

Cyanquixaline (CNQX; Abcam, ab120044) was used at a concentration of 30μM in accordance with similar experiments in the literature (Ullian et al., 2004a).

Mecamylamine (mec; Sigma, M9020) was used at a concentration of 50μM in accordance with *in vivo* electrophysiological experiments on motoneuron in the literature (Hoang et al., 2018; Lamotte d'Incamps et al., 2017); this concentration has been shown to inhibit >95% nicotinic acetylcholine receptors in guinea pig small intestinal myenteric neurons (Zhou et al., 2002).

There was difficulty in achieving a consistent atropine (atr; Sigma, A0132) concentration. Unlike the other two drugs used, the low solubility of atropine in water meant that a stock solution in water could not be made. Creating a stock solution of atropine in ethanol or DMSO was attempted but both vehicles were found to independently effect motoneuronal spontaneous burst frequency (data

not shown). Therefore, atropine powder was dissolved directly into ACSF solution. Difficulty weighing out the small quantities required (0.0003g for 10μM atropine) made reproducible atropine concentration difficult to achieve. Therefore, although ideally atropine would have been used at a concentration of 10μM as in similar experiments in the literature (Magown et al., 2017), in reality, the concentration of atropine varied between 25-100μM.

2.12 Electrophysiology

In Chapter 5, the effect of co-culture with astrocytes and/or V3 interneurons on the maturation of motoneuronal electrophysiological properties was investigated.

2.12.1 Single cell patch clamping

Single cell patch-clamp recording techniques were used to study the intrinsic properties of ESC-derived motoneurons in co-culture 1, 2, 3 and 4 weeks after plating. Experiments were performed in an open diamond bath imaging chamber for round coverslips (RC-25, Warner Instruments) perfused continuously with ACSF (Table 2.2; flowrate = approx. 1.5ml/minute). The temperature was kept between 26-30°C using an in-line solution heater (Warner Instruments) controlled by a dual control heat-controller (Warner Instruments). Cells were visualized with infrared differential interference contrast microscopy using a Leica DMLFSA upright microscope. Purified motoneuron cultures were used so motoneuron identity was assumed for all neurons. In the V3 interneuron-containing cultures, V3 interneurons were identified and avoided by their tdTomato expression. Patch electrodes (resistance 3-7 MΩ) were pulled on a Sutter P-97 puller (Sutter Instrument Company, Novato, CA) from 1.5mm outer diameter filamented boro-silicate glass (World Precision Instruments, Sarasota, FL) and filled with ICF (Table 2.2). Recordings were made by single cell patch-clamping using a MultiClamp 700A amplifier (Axon Instruments, Inc), low-pass filtered at 10kHz and digitized at 25kHz using a CED Power3 1401 and Signal software (Cambridge Electronic Design Ltd, Cambridge, UK).

All recordings were made in current clamp with an injection of a biased current to maintain a potential near -70mV unless otherwise stated. Electrophysiological properties were measured from the recordings as described in Table 2.5. In some astrocyte-containing cultures, CNQX had to be added to remove spontaneous activity so other electrophysiological properties could be recorded and measured.

The characteristics of motoneuronal spontaneous activity were measured from between three and six 30s recordings (with no current injection), using SpinalCoreN (a kind gift from Prof. A. LevTov). A spontaneous burst was defined as spontaneous depolarisations measured by single cell patch clamping containing at least one action potential that exceeded 0mV (not to be confused with calcium bursts measured using calcium imaging in Chapter 6). A small section of the trace containing no spontaneous bursts was manually defined as the baseline. The beginning of a burst was the point baseline was exceeded by six standard deviations, with a minimum burst length of 30ms. In the occasional traces containing Excitatory Post-Synaptic Potentials (EPSPs), the beginning of a burst was instead defined as the point at which the trace crossed a manually defined threshold above the largest EPSP (15-20mV above baseline). In this way, only spontaneous activity with action potentials was included. The event end was defined as the return to two standard deviations above baseline. From this information, SpinalcoreN measured the mean and standard deviation of **spontaneous burst duration** (ms) and **cycle time** (time from the beginning of one event to the start of the next; ms) for each motoneuron. **Rhythmicity** was then measured by calculating the Coefficient of Variation (CoV) of the cycle time (Equation 1; mean = μ, standard deviation = σ); the higher the CoV, the less rhythmic the spontaneous activity.

Equation 1: Coefficient of variation

$$\boldsymbol{CoV = \frac{\sigma}{\mu} \times 100}$$

Table 2.5: Methods used to measure motoneuronal electrophysiological properties.

Property	Method of measurement
Resting membrane potential (RMP) (mV)	RMP was determined by taking the baseline membrane potential recorded with no current injection. This was averaged for each cell across at least 3 traces.
Input resistance (MOhm)	Input resistance was measured by various using three different methods (see below) and a final value determined by averaging. If any one value of input resistance varied by more than 50% from the average of the other two measures then it was excluded. Input resistance was measured by three different methods:

	1) Signal software provided a measure of membrane resistance following a 500ms hyperpolarising pulse in current clamp. For method, see page 53 of the Signal Version 5 Manual (Cambridge Electronic Design Ltd, 1996). 2) An average of traces at a 500ms current injection of -20pA was taken and the voltage difference between the RMP and the membrane potential 50ms before the end of the pulse measured. Ohm's law was then used to determine input resistance. 3) The cell was challenged with a series of increasingly hyperpolarised, 500ms square pulses. An current-voltage (IV) graph was plotted using the potential 50ms before the end of a 500ms hyperpolarising pulses plotted against current injection. A linear trendline was fit to this curve in Excel and the slope or 'slope resistance' was used as a measure of input resistance. A curved IV graph can indicate the development of hyperpolarisation-activated current which complicate attempts to measure input resistance. Therefore, if an **R^2 value of the linear fit** was less than 0.96 then the value for input resistance determined from the IV graph was excluded.
Membrane time constant (µs) and **capacitance** (pF)	**Membrane time constant** and **capacitance** were automatically measured from traces of 500ms square pulses at 5mV, recorded in voltage clamp by Signal according to methods described on page 53 of the Signal Version 5 Manual (Cambridge Electronic Design Ltd, 1996). This method was validated by comparison with manually calculated values obtained for several motoneurons.
Lowest **Sag ratio** and **Sag-I slope**	The sag ratio was determined by measuring the trough in the first 200ms comparing it to the steady state potential 50ms before the end of a 500ms hyperpolarising pulse. The cell was challenged with a series of increasingly hyperpolarising 500ms square pulses. The sag ratio for each trace was then plotted against current injection. The lowest **sag ratio** (i.e. the point where sag was most pronounced) was recorded as was the slope of the sag ratio-current graph (**sag-I slope**).
Action potential half width (ms)	A single Action Potential (AP) was elicited by a 20ms square pulse and multiple recordings were averaged. The duration of the AP was measured at the voltage halfway between threshold and the AP peak to determine the **AP half width**.
Rheobase (pA)	Motoneurons were challenged with 500ms square pulses of increasing current injection. **Rheobase** was defined as the minimal current intensity at which the cell first fired an action potential. It was calculated by determining the difference between the current injected at baseline and the current injected at the point of action potential firing.

Action potential amplitude (mV)	**Action potential amplitude** was defined as the amplitude of the first AP elicited at rheobase, when the motoneuron was challenged with 500ms square pulse.
Depolarisation block (expressed as a multiple of rheobase)	Depolarisation block occurs when a neuron becomes desensitised following repeated firing due to the cumulative inactivation of Na^+ ion channels and can temporarily no longer fire action potentials. In more mature cells, the de-inactivation of the Na^+ ion channels (see Chapter 1: General Introduction, Section 1.5.2) allows repetitive firing. In the case of a 500ms square pulse, here **depolarisation block** (Db) was considered to have taken place at the current intensity that a neuron no longer fired APs in the last 150ms (Id) and was calculated according to Equation 2 (h = current injected at baseline, rheo = rheobase). Equation 2: Depolarisation block $$Db = \frac{Id - h}{rheo}$$ Note that, as discussed further in Section 2.12.2.2.2., not all motoneurons experienced depolarisation block. This may have been because some neurons were not challenged by large enough currents, since maximum current injection intensity was not standardised.
Spike Amplitude Adaptation (SAA) (mV)	**SAA** was determined by calculating the difference in amplitude between the first and last spikes in the spike train at 2 x rheobase. SAA was therefore used as an indicator of depolarisation block.
Initial firing frequency (IFF) (Hz)	The **IFF** was the reciprocal of the initial interspike interval between the first two peaks elicited by a 500ms square pulse at 2 x rheobase.
Steady-state firing frequency (SFF) (Hz)	Steady-state firing interval was the interspike interval between the last two peaks of a trace at 2 x rheobase, at which point firing was considered to have reached steady-state. The **SFF** was the reciprocal of the steady-state firing interval. Note that traces where no spikes occurred in the last 150ms of the 500ms square pulse were excluded, as these motoneurons were considered to have undergone depolarisation block.
FI slope (SFF) (Hz/pA)	Frequency-current slope (**FI slope**) was determined from a plot of SFF against the current injection fit with a linear trendline. If the data had more than one linear component, the slope of the primary phase was measured. In the Principle Component Analysis, a second measure of FI slope, calculated from the plot of IFF against current injection, was used alongside FI slope (SFF).

Spike Frequency Adaptation (SFA) ratio	The Spike Frequency Adaptation (SFA) ratio was determined by dividing SFF by IFF at each increment of current injection. The lowest **SFA ratio** for each motoneuron was used as this was the point at which SFA was most pronounced.
Spontaneous burst frequency (bursts/min)	A spontaneous burst was defined as spontaneous activity with peaks that exceeded 0mV. **Spontaneous burst frequency** was measured from three to six 30s recordings with no current injected.
Spontaneous EPSP frequency (EPSPs/min)	Putative spontaneous Excitatory Postsynaptic Potentials (EPSPs) were defined as depolarisations from the RMP without peaks exceeding 0mV. **Spontaneous EPSP frequency** was measured from between three and six 30s recordings with no current injected. In some recordings, the RMP was not stable enough to distinguish EPSPs and so values for these motoneurons were excluded.
Time the motoneuron had spent in the recording chamber (binned into hours)	The **time the motoneuron had spent in the recording chamber** was noted and binned by the hour.

2.12.2 Analysis of electrophysiological data

Analysis of electrophysiological data was performed using R, version 3.5.2.

2.12.2.1 Statistical analysis of individual electrophysiological properties

For comparisons between conditions and time points for each electrophysiological property (including the principle components), the normality of each dataset was first checked using a Shapiro-Wilk test. Where necessary, the validity of the assumption of homogeneous variance was checked using Levene's test. Significance between conditions was determined with a Welch's Two Sample t test if the assumption of normality and homogeneous variance were upheld, or a non-parametric Mann Whitney U test if it was not.

Where multiple comparisons were concerned, an ANOVA was performed with a post hoc Tukey HSD Multiple Comparison test, if the assumption of normality was upheld. If the assumption of normality was found to be invalid, a non-parametric Kruskal Wallis test was performed with a post hoc Dunn's Multiple Comparison tests.

The data in the tables in Chapter 5 are given as the mean ± standard deviation (n). Different symbols were used to represent different comparisons:

- ∞ denote a comparison between weeks 1 and 2; p<0.05 = ∞, p<0.01 = ∞∞, p<0.001 = ∞∞∞.
- * denote a significant difference with the MN alone culture condition within that time point. Note that comparisons were only made for weeks 1 and 2. p<0.05 = *, p<0.01 = **, p<0.001 = ***.
- ¥ denotes a significant difference compared to MN+as condition for that time point; p<0.05 = ¥, p<0.01 = ¥¥, p<0.001 = ¥¥¥.

2.12.2.2 Principle Component Analysis of electrophysiological data

Principle component analysis (PCA) was used to generate a database of principle components. The dataset contained 18 variables:

- Resting Membrane Potential, RMP (mV)
- Input resistance (MOhm)
- Capacitance (pF)
- Membrane time constant (μs)
- Sag ratio
- Sag-I slope
- Time the motoneuron had been in the recording chamber (binned into hours)
- Rheobase
- Action potential amplitude at rheobase (mV),
- Spike Amplitude Adaptation
- Initial Firing Frequency at 2 x rheobase, IFF (Hz)
- FI slope (IFF)
- FI slope (steady-state firing frequency)
- Spike Frequency Adaptation (SFA) ratio
- Depolarisation block (expressed as a multiple of rheobase)
- R^2 value of the linear fit of the IV graph
- Spontaneous burst frequency (bursts/minute)
- Spontaneous EPSP frequency (bursts/minute)

Note that SFF at 2 x rheobase was not included in the PCA analysis because in the MN+V3 culture condition depolarisation block had almost always occurred by 2 x rheobase, so SFF at 2 x rheobase could not be determined and therefor was missing.

The dataset containing many missing values that needed to be imputed to enable a PCA to be carried out. There are three kinds of missing data: data Missing

Completely At Random (MCAR), data Missing At Random (MAR) (i.e. if the missing data can be explained by another variable in the dataset) or data missing not at random (i.e. due to a property inherent to the individual motoneuron that could not be explained by any other variable in the dataset) (Koutoumanou et al., 2018). MCAR and MAR missing data were observed in the electrophysiological dataset and were dealt with as follows:

2.12.2.2.1 Data missing completely at random

To reduce the amount of missing data, cases where a large amount of data were missing completely at random, such as when the electrode was knocked and the patch was lost before many recordings could be taken, were excluded from the analysis. This is casewise deletion; it does not bias results though it may reduce precision (Koutoumanou et al., 2018). Where only one or two items of data were missing completely at random, the value was imputed with the mean. This produces unbiased results for this kind of missing data but falsely increases the precision of the results (Koutoumanou et al., 2018).

2.12.2.2.2 Data Missing At Random

Most of the remaining missing data occurred in either:

1) in every co-culture condition because the measurement of depolarisation block was missing, or
2) in the astrocyte-free co-culture conditions.

This data can be described as Missing At Random (MAR) – missing data that can be explained/predicted in terms of other recorded measurements. Below is a discussion of why data was missing and how it was imputed in each case.

1. There were two possible reasons that the measurement of depolarisation block was missing and therefore two alternative methods of imputation were used:
    a) If the motoneuron did not display sustained repetitive firing then depolarisation block as defined above could not be measured. For these neurons, it could be argued that depolarisation block had already occurred at rheobase, resulting in the lack of sustained, repetitive firing. In these

cases, depolarisation block was assumed to occur at a single multiple of rheobase, and was imputed with a value of 1.

b) If depolarisation block was not observed in the intensity range of current injected then a measure for that motoneuron could not be taken. For these cases, it was assumed that depolarisation block would occur with higher current injection and the missing values were imputed with the maximum possible value for depolarisation block observed plus the depolarisation block range. However, this is an imperfect solution; an alternative explanation could be that the motoneuron may never display depolarisation block, in which case this imputation would be inappropriate.

2. As mentioned above, the rest of the MAR data were exclusively from motoneurons in astrocyte-free conditions. These motoneurons frequently did not display firing and therefore many measurements of firing properties were not applicable and therefore missing. Due to the clear dependence on the presence of astrocytes, these missing values were imputed with means from the astrocyte-free conditions (astrocyte mean-imputation method). Any form of mean imputation is an imperfect solution because it may give a biased estimate for this type of missing data (Koutoumanou et al., 2018) but imputation was necessary to enable the analysis to be performed. The astrocyte-mean model was used for the analysis in Section 5.3.5.

   To investigate the robustness of my conclusions to the imputation method used, the PCA analysis was also performed on two test datasets where this astrocyte-dependent MAR data (described in 2 above) had been imputed either with a population mean (population mean-imputation method) or with 0 (0-imputation method). The graphs generated by each analysis are compared in Figure 5.11 in Chapter 5. Therefore, in general, conclusions drawn from PCA analysis of the dataset were robust to different methods of imputation for astrocyte-dependent MAR data. However, there was evidence that some comparisons involving PC2 were affected by imputation method.

2.13 Calcium imaging of motoneuron cultures

In Chapter 6, the effect of co-culture with V3 interneurons on the spontaneous calcium bursting in motoneurons cultured with astrocytes was investigated. To

ensure that coverslips containing the co-cultures were compatible with snug insertion into the open diamond bath imaging chamber (RC-25, Warner Instruments), glass coverslips (Fisher, cat. #: 10476784) were manually reduced to approximately 5mm in diameter using a diamond knife, prior to cell plating.

2.13.1 Calcium dye loading

For calcium imaging experiments, co-cultures were loaded with green fluorescent calcium indicator Fluo-8 AM (Abcam, ab142773). The stock solution of 1mM Fluo-8 AM was prepared by dissolving it in 20% Pluronic acid (PF-127) in 100% DMSO (Hamad et al., 2015; Wilson et al., 2007). Stock solution was diluted in ADFNK to a final Fluo-8 AM loading concentration of 5µM. Co-cultures were incubated with Fluo-8 AM loading solution for 20 minutes at 37ºC in a humidified incubator with 5% CO_2. Before imaging, the cells were washed in ACSF (3 x 5 minutes at room temperature) to remove excess dye followed by 10 minutes incubation at room temperature for cells to stabilise and complete de-esterification of the calcium dye. The coverslip was then transferred to the recording chamber for recording, perfused with temperature controlled (between 26-30°C), carbogenated ACSF, using an in-line solution heater (Warner Instruments) controlled by a dual control heat-controller (Warner Instruments).

2.13.2 Two-photon calcium imaging

Dye-loaded cells were imaged by raster scanning on an upright (Olympus BX51WI) two-Photon microscope (Bruker Corporation) equipped with an ultrafast tuning (>50nm/s full range, 680nm to 1300nm) laser (InSight™ DeepSee™, Spectra-Physics; <120fs pulse width, 80MHz repetition rate) through a 20X water immersion objective (numerical aperture = 1; Olympus, model: XLUMPLFLN20XW, cat. #: N2699600). Recordings were performed in darkness and further protection from light was provided by a black-out curtain.

Fluo-8 AM dye was excited at 860 nm with fluorescence collected through a green emission filter (ET525/70). Note that endogenous GFP/YFP of C9G ESC-derived motoneurons was not detected by the settings used, so the green fluorescence observed was predominantly due to the Fluo-8 AM dye. The V3 interneurons were distinguished by their tdTomato expression using 1100nm excitation wavelength and the red fluorescence was collected by a red emission filter (ET595/50). A Dodt gradient contrast image of the cells was obtained using

720nm excitation wavelength. PrairieView software (Brüker) was used to acquire time series of fluorescent images with the following parameters: 29 frames/s, dwell time = 0.4µs/px, 512x512 pixel images with 1.16µm/px, frame period = 0.034s, scan line period = 63.1µs, mean green laser power ± standard deviation = 7.2 ± 1.9%, range of green laser power = 6-10%, mean green PMT detector gain ± standard deviation = 57 ± 7.2%, range of green PMT detector gain = 45-67%.

Excitation laser power was always kept below 10% because it was observed that laser powers >10% elicited calcium waves in the astrocyte monolayer that spread throughout the syncytium. To further prevent damage to the astrocyte monolayer, neuron cell bodies were imaged such that the astrocyte monolayer was out of plane.

A Field Of View (FOV) was defined as one region on a coverslip containing multiple neurons. Except for ensuring the presence of neuronal cells, FOVs were selected at random and were non-overlapping. Cell bodies were identified as Regions Of Interest (ROIs) using the Dodt detector images. Vic_1244 ESC-derived V3 interneurons and C9G ESC-derived motoneurons were distinguished by the presence and absence of red fluorescence, respectively.

One limitation observed during these experiments was that the coverslip was sometimes not quite level, such that the plane of view cut through the cells and the coverslip at a slight angle; background regions on opposite sides of the FOV consistently showed different levels of activity. Because of this, amplitude of the calcium signal could not necessarily be compared between each cell in the same FOV, as the measure would depend on where the cell sat in the plane of view.

Calcium imaging data from coverslips with evidence of neuronal death, such as extensive neurite blebbing, or astrocyte division were excluded from the analysis.

2.13.3 Data processing and analysis

Raw data was processed to find df/f0 (where f0 = signal at baseline) using code written in R, version 3.5.2 (see Chapter 9: Appendix, Section 9.1). df/f0 data was used for the analysis described below. Some ROIs/neurons displayed a steady decrease of calcium signal intensity over time. This was interpreted as bleaching of the Fluo-8 AM calcium dye. If present in every neuron in an FOV, the bleaching

signal was removed by subtracting the signal of a silent neuron in the FOV from the other neurons. If present in only one or a subset of neurons in the FOV, bleaching neurons were excluded from further analysis. Similarly, if a neuron showed a steady increase in calcium signal over time, this was interpreted as an increasingly unhealthy neuron and the neuron was excluded from further analysis (Chapter 9: Appendix, Section 9.1). Neurons with calcium events were referred to as bursting neurons.

2.13.3.1 Correlation analysis

Correlation of calcium activity between pairs of bursting neurons in the same FOV was determined by calculating the Pearson correlation coefficient using the cor() function in R, version 3.5.2. If all bursting neuron pairs had correlation coefficients >0.6, then the activity was considered correlated. If all bursting neuron pairs had correlation coefficients >0.3, then the activity was considered mostly correlated.

2.13.3.2 Event characteristics

Prior to event detection, the traces were offset making baseline signal approximately 0. Events were detected and analysed using SpinalCoreN. The baseline signal was manually defined as a section of trace >0.5s long (>14 data points) that contained no events, and the mean and standard deviation of the signal during this period determined. The threshold for the start and end of calcium events was defined as two standard deviations above baseline. To prevent event detection being contaminated with high frequency noise, a minimum event duration of 500ms was applied. ‘Short’ events were defined as events between 500-3000ms and ‘long’ events were defined as events >3000ms.

For each event, the start and end times, peak position, peak amplitude, event duration and event cycle time were measured by SpinalCoreN. Events interrupted by the beginning or end of a recording were excluded from the analysis. The mean and standard deviation of peak amplitude, event duration and event cycle time were calculated for each neuron. The CoV of each characteristic was calculated (Equation 1). Note that CoV of event cycle time is the inverse of event rhythmicity – i.e. low CoV of event cycle time indicates events were more rhythmic.

2.13.3.3 Quantifying event onset and bursting order

Quantifying event onset and examining the variability of the bursting order was predominantly performed in Microsoft Excel. Calcium event start times were exported from SpinalCoreN and the start times of events in different neurons in the same FOVs were matched up. For each calcium event, the earliest bursting neuron had start time (T_0) and the latency of event start time (Λ) for each neuron in an FOV was calculated by subtracting T_0 for each calcium event from the start time of that neuron (t_n):

Equation 3: Latency of calcium event start time for each neuron in an FOV

$$\Lambda = t_n - T_0$$

Neuron bursting order was found by ranking the neurons according to their start time for each calcium event. To determine the bursting order variability for each neuron across different calcium events, the bursting order variance for each neuron was calculated using the VAR.P() command. To determine whether the variability in bursting order was different from random, a similarly structured dataset with random rankings was randomly generated using R. The bursting order variance of the real and randomly generated datasets were then compared in R.

The extent of bursting order randomness (r) for each FOV was the mean bursting order variance of the real dataset (var(x)) divided by the mean bursting order variance of the randomly generated dataset (var(rand)) multiplied by 100:

Equation 4: Extent of bursting order randomness.

$$r = \frac{var(x)}{var(rand)} \times 100$$

2.14 Statistical analysis

This section describes the statistical analysis methods used throughout this work (unless otherwise stated in the text). Statistics were performed using R, version 3.5.2. Values are given as mean ± standard deviation (n) unless otherwise stated. The bold horizontal line in the boxplots represents the median. Unless otherwise stated, statistical tests were conducted according to the flowchart in Figure 2.3. A Shapiro-Wilk test was used to test the assumption of normality. Where necessary, a Levene's test was used to validate homogeneity of variance. * = $p<0.05$, ** = $p<0.01$, *** = $p<0.001$, and **** = $p<0.0001$.

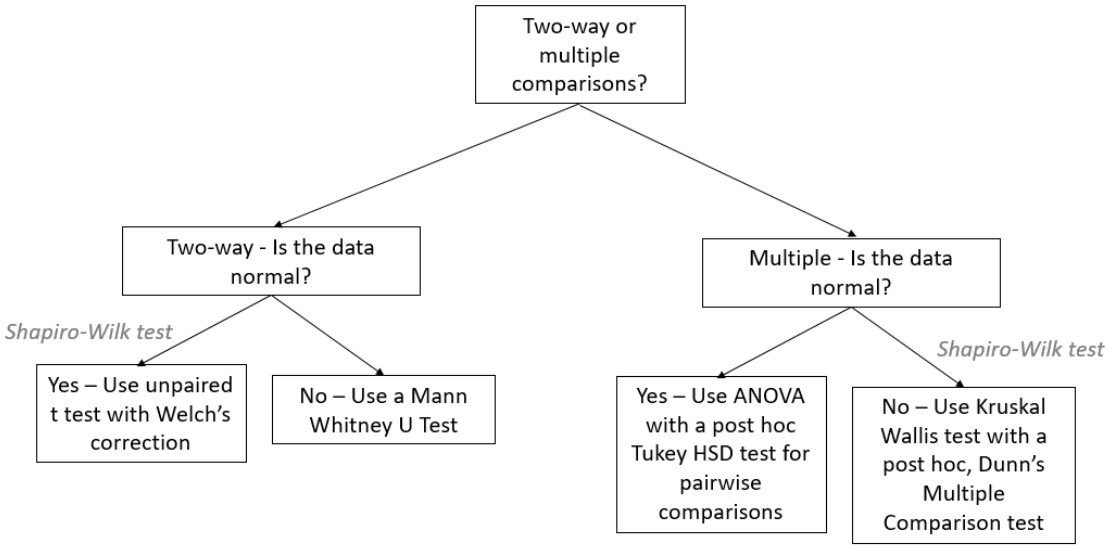

Figure 2.3: Flowchart showing the circumstances in which different statistical tests were applied (unless otherwise stated).

The Shapiro-Wilk test was used to test whether the data was normally distributed.

3 Chapter 3: Characterisation of embryoid bodies: identifying the cell types that might influence motoneuron maturation.

3.1 Introduction: No motoneuron is an island

'No man is an island, entire of itself; every man is a piece of the continent, a part of the main'

[Meditation XVII, Devotions upon Emergent Occasions by John Donne, 1624]

John Donne observes that humans are social animals, shaped by the cultures and people around them. Similarly, motoneurons do not reach a mature state or fulfil their function in isolation. Indeed, ESC-derived motoneurons transplanted alone into peripheral nerve were unable to form connections with and elicit muscle contraction when stimulated (Greensmith and Bryson labs, unpublished; Magown et al., 2017). In contrast, ESC-derived motoneurons within an embryoid body (EB) containing other cell types, innervated and formed NMJs with the muscle, enabling muscle contraction when the graft was stimulated (Bryson et al., 2014; Magown et al., 2016, 2017; Yohn et al., 2008). Thus, it seems that interaction with other cell types is important to motoneuron maturation within the EBs. The aim of this Chapter was to identify what cell types are present within the EB that might influence motoneuron maturation.

3.1.1 Motoneurons develop alongside spinal interneurons

In vivo, motoneurons develop and mature alongside many different cell populations such as spinal interneurons, forming connections and making up networks, including those involved in locomotion. Of particular interest are so-called 'last order' interneurons that synapse with motoneurons and so can directly control their activity. Such interneurons can be excitatory, inhibitory or neuromodulatory, may be ipsilateral or commissural, and may receive descending inputs or inputs from sensory afferents (Brownstone and Bui, 2010). Ventral spinal interneurons can be divided broadly into 4 categories based on lineage, V0-3 (Brownstone and Bui, 2010; Jessell, 2000). These categories can be further divided based on neurotransmitter type. For example, V2a interneurons are excitatory whereas V2b interneurons are inhibitory. Interneurons play a role in the generation and propagation of patterns of spontaneous activity, which is purportedly important for the development of spinal cord circuitry, in particular motoneuron axon pathfinding and integration into developing circuits (Blankenship and Feller, 2010; Kastanenka and Landmesser, 2010; Kirkby et al.,

2013; Warp et al., 2012). It is only when motoneurons are active that they acquire the mature characteristics essential for them to develop morphologically (Kalb and Hockfield, 1992) and form functional contacts NMJs (Gonzalez-Islas and Wenner, 2006; Witzemann, 2006). Spinal interneurons, therefore, are candidates for influencing motoneuron maturation and enabling function reinnervation of target muscles following engraftment of EBs.

3.1.2 The differentiation of spinal neuron subtypes *in vitro*.

By manipulating the concentrations of developmental patterning factors (Chapter 1: General Introduction, Section 1.4), it is possible to direct the differentiation of stem cells towards specific spinal fates. Wichterle et al. (2002) demonstrated that manipulation of the concentrations of retinoic acid (RA) and sonic hedgehog (or smoothened agonist (SAG)) could be used to direct the differentiation of embryonic stem cells (ESCs) into motoneurons *in vitro.* Hereafter this protocol is referred to as the 5-day RA/SAG differentiation protocol and it achieved yields of 20-30% Hb9-positive motoneurons. Of these motoneurons, 70% co-expressed isl1 and Lhx3, an expression profile suggestive of medial MMC motoneurons (Rousso et al., 2008) and a rostral cervical identity. In support of this, only a small proportion co-expressed Lhx1 with Hb9, as is characteristic of LMC motoneurons (Wichterle et al., 2002). Furthermore, Soundararajan et al., (2006) demonstrated that when motoneurons derived from the RA/SAG differentiation protocol were transplanted into the chick neural tube, they expressed medial MMC transcription factors, extended axons to targets appropriate to medial MMC motoneurons, and had electrophysiological properties similar to host medial MMC motoneurons (Soundararajan et al., 2006). Different subtypes of motoneurons are generated by manipulating differentiation conditions. For example, ESCs differentiated at lower densities for longer periods and exposed to RA at a later time point produced lower yields of motoneurons with a caudal brachial and thoracic identity (Peljto et al., 2010).

Since sonic hedgehog acts in a graded manner, other spinal interneurons are found in the EBs generated with the RA/SAG differentiation protocol, including V2a interneurons co-expressing Chx10 and Lhx3 (Brown et al., 2014; Wichterle et al., 2002), V2b interneurons expressing Gata3 (Brown et al., 2014) and putative V0/1 interneurons expressing Lhx1 in the absence of Hb9

(Soundararajan et al., 2006; Wichterle et al., 2002). Changing the relative concentrations of SAG affects EB composition; low concentrations generate EBs with high proportions of more medial V1 interneurons and low proportions of V3 interneurons, whereas higher concentrations generate EBs with low proportions of V1 interneurons and high proportions of V3 interneurons (Hoang et al., 2018; Sternfeld et al., 2017). While V2 interneuron yield is regulated by SAG concentration (Brown et al., 2014), the proportion of EBs comprising V2a interneurons remains low across a range of SAG concentrations (Sternfeld et al., 2017) unless Notch1 signalling is inhibited (Brown et al., 2014). This is because, in the presence of Notch1 signalling, the V2 progenitors favour V2b subtypes over V2a subtypes. Notch signalling also regulates diversification of V1 interneuron subtypes. Notch inhibition of EBs treated with V1 interneuron-favouring concentrations of SAG and RA increases the generation of Renshaw cells at the expense of Foxp2-expressing V1 interneurons, without changing the overall number of V1 interneurons generated (Hoang et al., 2018). Thus, changing the Shh and Notch signalling molecules that EBs are exposed to affects the dorsoventral identity (Hoang et al., 2018; Sternfeld et al., 2017; Wichterle et al., 2002; Xu and Sakiyama-Elbert, 2015) and diversification of the spinal interneurons generated (Brown et al., 2014; Hoang et al., 2018), respectively.

As discussed in Chapter 1 (Section 1.6.4), interneurons present within the EBs form microcircuits that give rise to and modulate spontaneous activity, significantly impacting graft-derived muscle contraction (Magown et al., 2017). Spontaneous activity is known to promote spinal cord development *in vivo* (Kastanenka and Landmesser, 2010, 2013; Montague et al., 2017; Personius et al., 2007; Spitzer et al., 2000b) so activity derived from microcircuits containing interneurons within the EBs (Magown et al., 2017) may promote maturation of the engrafted motoneurons.

3.1.3 Don’t forget glia!

The 5-day RA/SAG differentiation protocol for ESC differentiation also generates astrocytes (Bryson et al., 2014; Sternfeld et al., 2017), although astrocytes are born later in the differentiation process than the neurons (Bryson et al., 2014). Increasingly, astrocytes are being recognised as active participants in CNS functioning. Along with canonical trophic functions such as metabolic support and

secretion of growth factors, astrocytes are crucial for circuit formation and function (Allen and Eroglu, 2017; Haim and Rowitch, 2016). Astrocytes promote and regulate synapse formation by the secretion of synaptogenic factors such as thrombospondins (Christopherson et al., 2005) and by contact-mediated mechanisms (Barker et al., 2008). In addition to the general facilitation of synapse formation, spatially and functionally defined populations of astrocytes express different complements of axon guidance molecules (e.g. Semaphorin 3A in ventral spinal astrocytes), guiding the formation of sensory-motor circuits in the spinal cord (Haim and Rowitch, 2016; Molofsky et al., 2014). In some circuits, astrocytes also have a striking role in circuit function (Chapter 1: General Introduction, Section 1.8.6). Given the emerging role of astrocytes in both the development and mature functioning of neural circuits and given the presence of astrocytes in the EBs produced with the 5-day RA/SAG differentiation protocol, astrocytes are a promising candidate cell type capable of influencing ESC-derived motoneuron maturation within EBs.

3.2 Aims of this Chapter

Motoneurons in EBs generated by the 5-day RA/SAG differentiation protocol engrafted into denervated nerves can successfully reinnervate target muscles. When stimulated, these MNs can induce muscle contraction (Bryson et al., 2014; Magown et al., 2016, 2017). In contrast, grafts of purified motoneurons do not form functional NMJs with target muscles (Bryson, personal communication). I therefore examined EBs generated using the 5-day RA/SAG differentiation protocol (Bryson et al., 2014; Magown et al., 2017) in order to identify the cell types that may be promoting this capability.

The specific aims of this chapter were therefore to:

1. Characterise the ventral spinal neuron populations within EBs differentiated with the 5-day RA/SAG differentiation protocol.
2. Identify the most abundant interneuron subtype in the EBs as a candidate cell type that influences motoneuron maturation.
3. Establish an *in vitro* model to assess the effect of co-culture with different cell types on motoneuron maturation.

3.3 Results

3.3.1 Characterisation of neuronal populations within the embryoid body

As motoneurons within engrafted EBs can successfully innervate and enable functional control of muscle (Bryson et al., 2014; Magown et al., 2016, 2017), whereas purified motoneurons cannot, it was important to identify the cell populations other than motoneurons generated by the 5-day RA/SAG differentiation protocol (described in Chapter 2: Materials and Methods, Section 2.2).

The 5-day RA/SAG differentiation protocol used in the Bryson and Magown studies was developed by Wichterle, et al. (2002), and has been shown to produce ventralised spinal cell types, including motoneurons with MMC characteristics (Soundararajan et al., 2006), interneurons (Soundararajan et al., 2006; Sternfeld et al., 2017; Wichterle et al., 2002) and astrocytes (Bryson et al., 2014). To identify candidate cell types capable of influencing motoneuron maturation, I first characterised the spinal cell populations present in the EBs, as well as the timing of their generation. Due to the absence of dorsalising differentiation factors, it was assumed that only ventral spinal cell types would be generated by the 5-day RA/SAG differentiation protocol and only markers of ventral spinal cell populations were examined. During spinal cord development, different types of spinal interneurons are born at different times. Therefore, in the present study, the EBs were examined at two time points, day 5 and day 9, by labelling for a panel of antibodies against markers of spinal ventral neuron populations (Alaynick et al., 2011). Antibodies against markers of the various candidate ventral spinal cell populations were validated by testing their expression in spinal cord tissue at time points and in areas that the various cell populations are known to be present. Though there was some cross-reactivity of the secondary antibody with the spinal vasculature, the antibodies against Dbx1 (marker of p0 progenitors), Evx1 (postmitotic marker of V0 interneurons), En1 (postmitotic marker of V1 interneurons), Chx10 (postmitotic marker of V2a interneurons), Hb9 (postmitotic marker of motoneurons) and Nkx2.2 (marker of p3 progenitors) showed expected localisation of nuclear labelling in spinal cord tissue (Figure 3.1). The antibody against Gata3, the marker of V2b interneurons, did not show the expected pattern

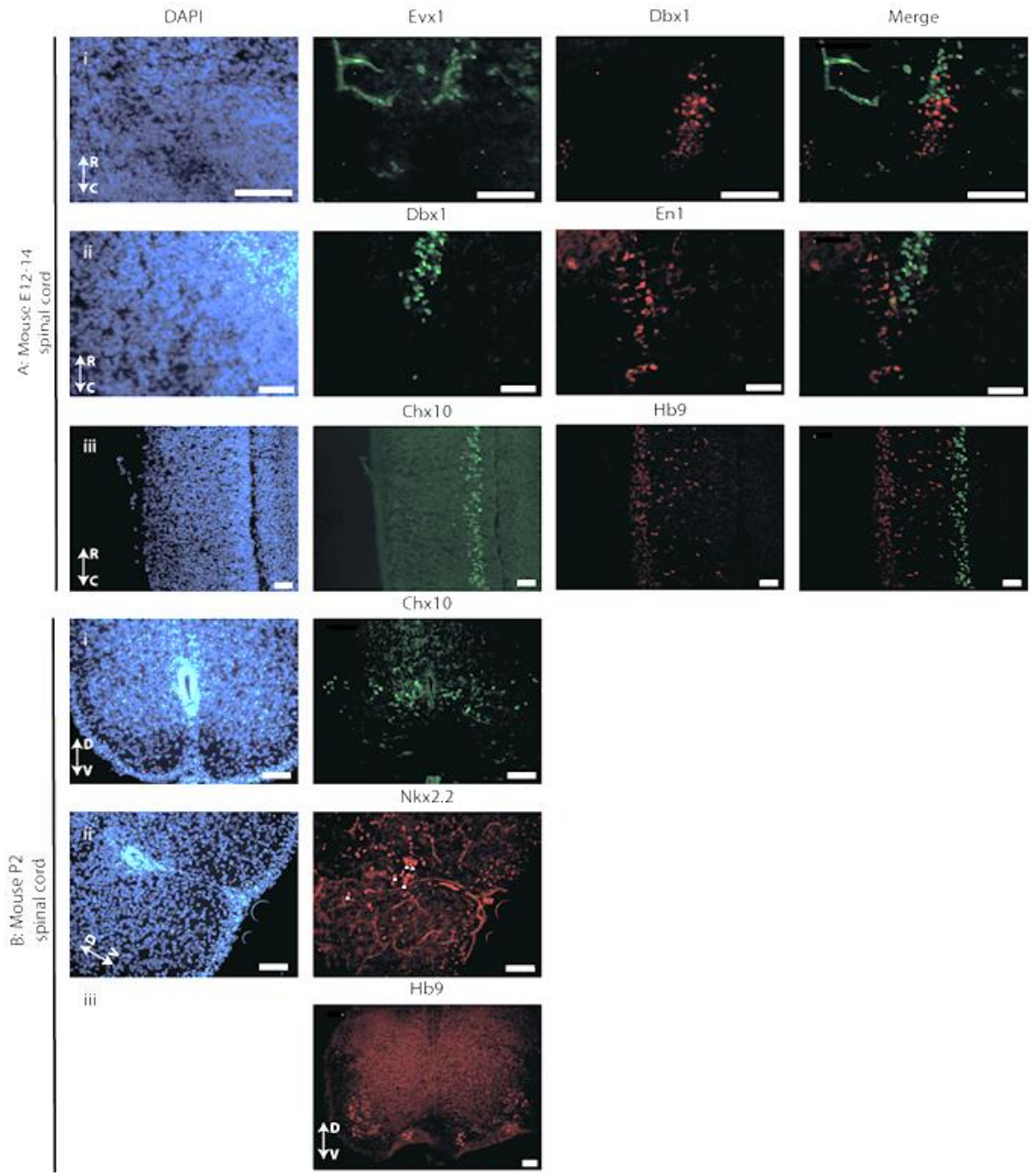

Figure 3.1: Validation of antibodies in longitudinal sections of mouse E12-14 spinal cord (A) or transverse sections of mouse P2 spinal cord (B).

R and C stand for Rostral and Caudal, respectively. D and V stand for Dorsal and Ventral, respectively. Note that there was non-specific binding of the secondary antibody to the vasculature in many of the slices as clearly seen in top left of Ai and throughout Bii. The white arrowheads in Bii indicate a selection of Nkx2.2-positive nuclei visible in the image. Scale bars = 50µm

of labelling at either time point. Therefore, except for the Gata3 antibody, I concluded that the antibodies were appropriate for use in the study. Most markers were nuclear and positive nuclei within the EBs were counted using spots function on Imaris; for more details see Chapter 2: Materials and Methods, Section 2.10.1.

3.3.1.1 Nuclear neuronal NeuN labelling appeared in EBs at the later time point

The neuronal content of the EBs was determined using the neuronal marker, NeuN. Nuclei labelled for NeuN were observed at day 9. Compared to day 9, the distribution of NeuN labelling on day 5 was more diffuse (Figure 3.2 A). On day 5, 2 ± 3% of each EB section was made up of cells with NeuN+ nuclei, which increased to 29 ± 13% by day 9 (Figure 3.2 B; p = 6.3e-09, Mann-Whitney U test; n = 26 day 5 and n = 27 day 9 EB sections from three differentiations).

3.3.1.2 Medial spinal neuronal populations (V0, V1, V2a) were rarely observed

Few markers of ventral interneuron subtypes born medially in the spinal cord were observed in the EBs produced by the 5-day RA/SAG differentiation protocol. V0 interneurons are a mix of inhibitory and excitatory interneurons which settle in the ventromedial spinal cord (Rybak et al., 2015). The progenitor V0 interneuron marker Dbx1 (Alaynick et al., 2011) was not expressed in EB sections at either day 5 or day 9 (at least 18 EB sections from two differentiations for each time point). The same was true for the postmitotic marker of glutamatergic V0 interneurons, Evx1 (Alaynick et al., 2011) (at least six EB sections from two differentiations for each time point).

En1 is a postmitotic marker (Alaynick et al., 2011) for ipsilaterally-projecting, inhibitory V1 interneurons in the spinal cord (Rybak et al., 2015). A small number of En1+ cells were observed in 20% of day 5 and 40% of day 9 EBs. The average number of En1+ cells per EB section was 1 on both day 5 and day 9 (Figure 3.3 A; at least 10 EB sections from two differentiations for each time point).

V2a interneurons are excitatory spinal interneurons involved in locomotion that co-express the transcription factors Chx10 and Lhx3 (Alaynick et al., 2011; Rybak et al., 2015). Small numbers of Chx10+/Lhx3+ cells were observed in 14% of day 5 and 28% of day 9 EBs (Figure 3.3 B; n = 22 EB sections for day 5 and n = 18 EB sections for day 9 from two differentiations). The average number of Chx10+/Lhx3+ cells per EB section observed was 4 on day 5 and 6 on day 9 (at least 18 EB sections from two differentiations). Note that the Lhx3-only nuclei

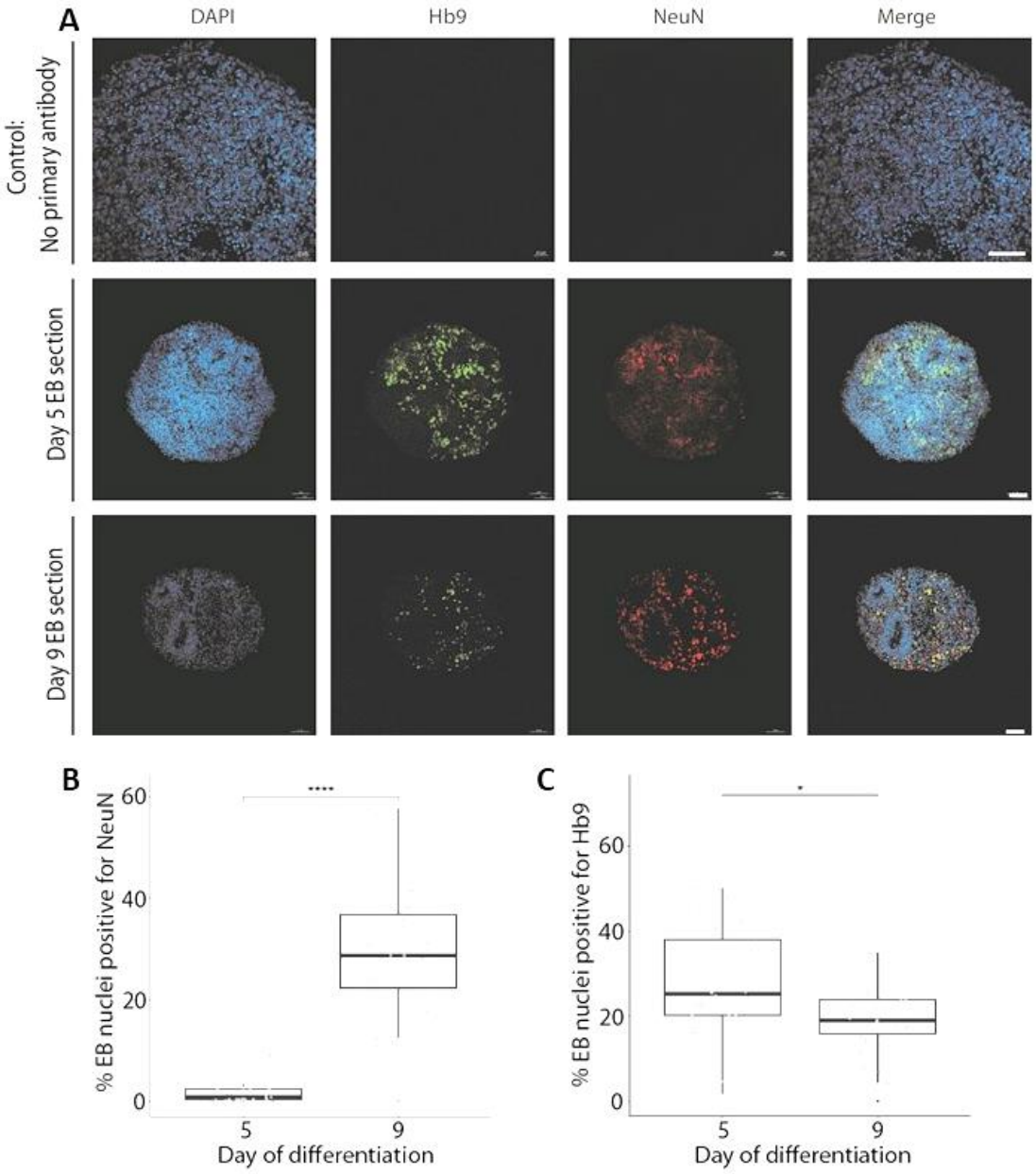

Figure 3.2: The expression of the neuronal marker NeuN and motoneuronal marker Hb9 in EB sections at day 5 and day 9 of differentiation.

A: EB sections were labelled for Hb9 (green), NeuN (red) and the nuclear marker DAPI (blue). In negative control sections (top row), the primary antibodies were omitted. Scale bars = 50μM. B: Expression of NeuN in neuronal nuclei increases between day 5 and day 9 of differentiation (n = 26 day 5 EB sections and n = 27 day 9 EB sections from three differentiations). C: Hb9-expressing motoneurons are present at both timepoints, but they comprised a lower proportion of cells in the EB sections on day 9 than day 5 (n = 26 EB sections for day 5 and n = 27 EB sections for day 9 from three differentiations). To determine significance, a non-parametric Mann Whitney U test was used. The bold horizontal line in boxplots shows the median. * = $p<0.05$, ** = $p<0.01$, *** = $p<0.001$, and **** = $p<0.0001$.

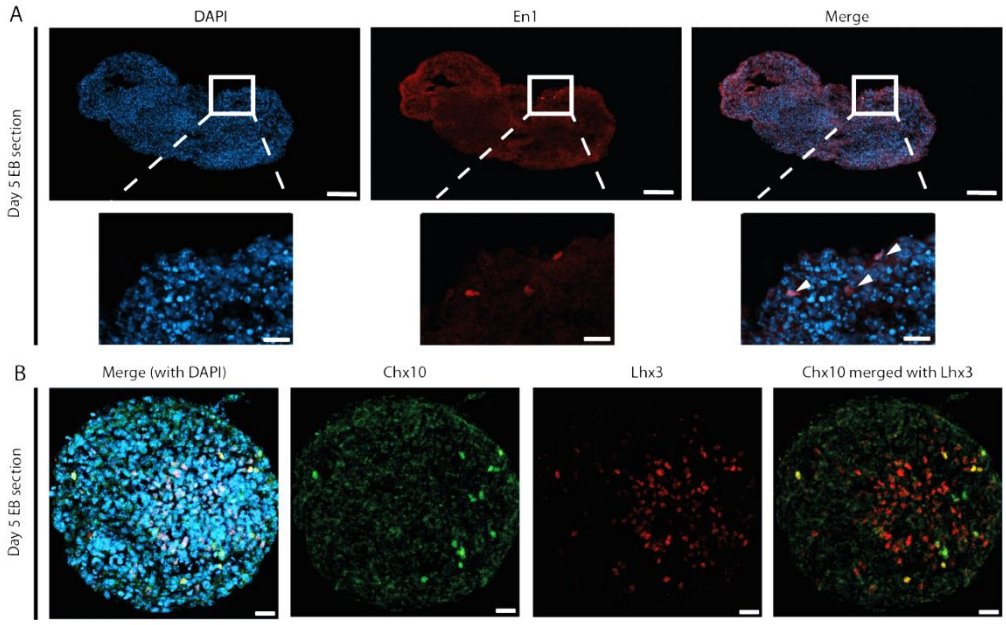

Figure 3.3: Examples of V1 and V2a interneurons in day 5 EB sections.

A: Sections were labelled for the V1 interneuron marker En1 (red) and the nuclear marker DAPI (blue). An EB section containing three V1 interneurons with nuclei labelled with En1 is shown. These cells are indicated in the merge image by white arrowheads. Top row scale bar = 100µm, bottom row scale bar = 20 µm. B: An EB section labelled for the V2a interneuron markers Chx10 (green) and Lhx3 (red), and the nuclear marker DAPI (blue). Scale bar = 20 µm.

observed in Figure 3.3 B are probably motoneurons.

These results suggest that the 5-day RA/SAG differentiation protocol did not produce large numbers of V0, V1 or V2a interneurons.

3.3.1.3 Motoneurons represented a large proportion of cells in the EBs

As might be expected given the concentrations of RA and SAG used, spinal cell types born in more ventral progenitor regions are likely to be produced in larger numbers by the 5-day RA/SAG differentiation protocol. Hb9 is a motoneuronal marker and was expressed in EB sections on both day 5 and day 9 (Figure 3.2). On day 5, 28 ± 12% of cells in EB sections expressed the Hb9 marker (Figure 3.2 B), suggesting that about a third of cells produced by the 5-day RA/SAG differentiation protocol were motoneurons. This is similar to previous studies (Bryson et al., 2014; Sternfeld et al., 2017; Wichterle et al., 2002) and to the proportion determined by Fluorescently-Activated Cell Sorting (FACS) of EBs differentiated from ESCs that only express *Hb9::CD14-IRES-GFP* (31% yield of motoneurons from day 5 EBs; see Section 3.3.2.1). Between day 5 and day 9,

the proportion of the EB sections comprising Hb9-expressing cells decreased from 28 ± 12% on day 5 to 22 ± 14% on day 9 (Figure 3.2 B; p = 0.02, Mann-Whitney U test; n = 26 EB sections for day 5 and n = 27 EB sections for day 9 from three differentiations). It is possible that this reflects a loss of motoneurons between these two time points or alternatively, as motoneurons are not continuously produced and cells within the EB keep proliferating, that motoneurons become diluted by other cell types.

On day 9, NeuN was expressed in the nucleus (Section 3.3.1.1). NeuN expression can be used to distinguish alpha from gamma motoneurons as gamma motoneurons have very low NeuN expression (Deardorff et al., 2013; Friese et al., 2009; Shneider et al., 2009). Co-expression of NeuN with Hb9 was observed in 58 ± 8% of Hb9-expressing cells (Figure 3.2), indicating that roughly two thirds of Hb9-expressing cells were likely alpha motoneurons. Those cells that expressed Hb9 but not NeuN could have been gamma motoneurons.

Islet 1 (isl1) is another motoneuron marker, expressed in all motoneuron subtypes except lateral LMC motoneurons (Rousso et al., 2008). Isl1 was expressed in EB sections at both time points (Figure 3.4 A). Similar to Hb9 expression, the proportion of EB sections comprising Isl1-expressing cells decreased significantly, from 41 ± 19% at day 5 to 23 ± 7% at day 9 (Figure 3.4 B; p = 0.0008, Welch's Two Sample t test; n = 18 EB sections each for day 5 and day 9 from two differentiations). The similarity in this trend supports the possibility that the proportion of cells that are motoneurons was reduced by day 9.

There was a significantly larger proportion of Isl1-expressing cells than Hb9-expressing cells in EBs at day 5 (Figure 3.2 B and C; p = 0.01 for day 5; Welch's Two Sample t test) but no significant difference between the two markers by day 9 (p = 0.15, Mann Whitney U test). This finding suggests either that not all Isl1-expressing cells were motoneurons or that not all motoneurons expressed Hb9 (see Section 3.4.1 for a discussion of this).

3.3.1.4 V3 interneurons were abundant in the EBs

V3 interneurons are mainly excitatory commissural interneurons that are thought to modulate the locomotor rhythm (Rybak et al., 2015). V3 interneuron progenitors express the marker Nkx2.2. Nkx2.2-expressing cells were observed in both day 5 and day 9 EB sections (Figure 3.4 A). The proportion of EB sections

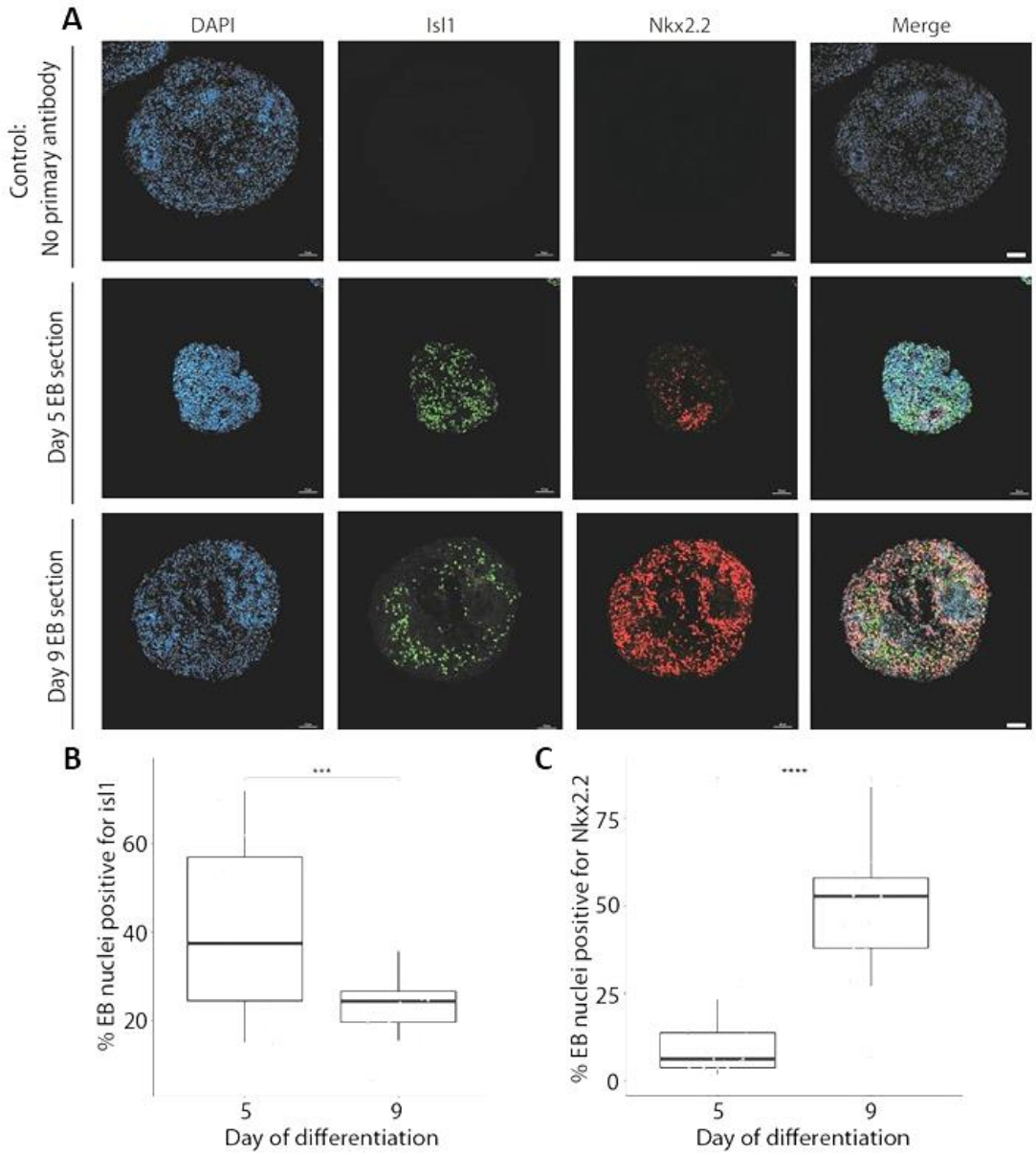

Figure 3.4: The expression of the motoneuron marker Isl1 and the V3 progenitor marker Nkx2.2 in EB sections at day 5 and 9 of differentiation.

A: EB sections were labelled for Isl1 (green), Nkx2.2 (red) and the nuclear marker DAPI (blue). In control sections (top row) the primary antibodies were omitted. Both isl1 and Nkx2.2 labelling was present at both time points. The proportion of nuclei that were Nkx2.2-positive increased significantly between day 5 and day 9. Scale bar = 20 µm. B: Isl1 is expressed by motoneurons and some dorsal spinal interneurons. Isl1-expressing nuclei were present at both time points but, as with Hb9-expressing cells, they comprised a significantly lower proportion of cells in the EB sections on day 9 than day 5 (n = 18 EB sections each for day 5 and day 9 from two differentiations). C: Nkx2.2 is a marker for V3 interneuron progenitors. There were significantly more Nkx2.2-positive nuclei on day 9 compared to day 5. Isl1 data was found to be normally distributed but the Nkx2.2 data was not. For normally distributed data, a Welch's Two Sample t test was used to determine significance. For non-normally distributed data, a non-parametric Mann Whitney U test was used. The bold horizontal line in boxplots shows the median. * = $p<0.05$, ** = $p<0.01$, *** = $p<0.001$, and **** = $p<0.0001$.

comprising Nkx2.2-expressing cells increased significantly from 10 ± 8% on day 5 to 46 ± 18% on day 9 (Figure 3.4 A and C; p = 1.04e-09, Mann-Whitney U test; n = 24 day 5 EB sections and n = 27 day 9 EB sections from three differentiations). This finding suggests that many Nkx2.2-expressing V3 interneurons are generated between day 5 and day 9 of the 5-day RA/SAG differentiation protocol, as suggested by Sternfeld, et al. (2017).

However, Nkx2.2 is not a V3 interneuron-specific marker. *In vivo,* the Nkx2.2-expressing progenitor pool also generates spinal oligodendrocytes (Jarrar et al., 2015), and in the developing hindbrain they give rise to oligodendrocytes and serotonergic neurons (Alaynick et al., 2011; Briscoe et al., 1999; Carcagno et al., 2014; Gotoh et al., 2012). A transgenic ESC line that expressed tdTomato under the promoter of the V3 interneuron-specific marker, Sim1, (Sternfeld et al., 2017) was used to generate EBs and further investigate the V3 interneuron population. EB sections were labelled for Nkx2.2 and an antibody was used to amplify the endogenous tdTomato. Figure 3.5 shows that not all Nkx2.2-positive nuclei were positive for the V3 interneuron-specific reporter, tdTomato. Therefore, it is likely the proportion of cells in the EBs that comprised V3 interneurons was lower than estimated by the Nkx2.2 labelling. Indeed, FACS of dissociated day 9 EBs according to the tdTomato reporter determined that 24 ± 6% of cells were V3 interneurons (n = 10 differentiations; see Chapter 2: Materials and Methods, Section 2.4.2 for more details about FACS) compared to the 46 ± 18% Nkx2.2-positive cells as counted from labelled sections (Figure 3.4 C).

Taken together, these results demonstrate that the 5-day RA/SAG differentiation protocol significantly ventralises the spinal cell identities of cells produced within the EB, with the ventral-most neuronal populations being the most highly represented. Due to the high numbers generated by the 5-day RA/SAG differentiation protocol, V3 interneurons were identified as a candidate cell type that may significantly influence motoneuron maturation in the EBs.

3.3.2 Establishing an *in vitro* model to assess the effect of co-culture with different cell types on motoneuron maturation

The first step to establishing an *in vitro* model to study motoneuron maturation was to produce and culture pure populations of motoneurons, V3 interneurons and astrocytes.

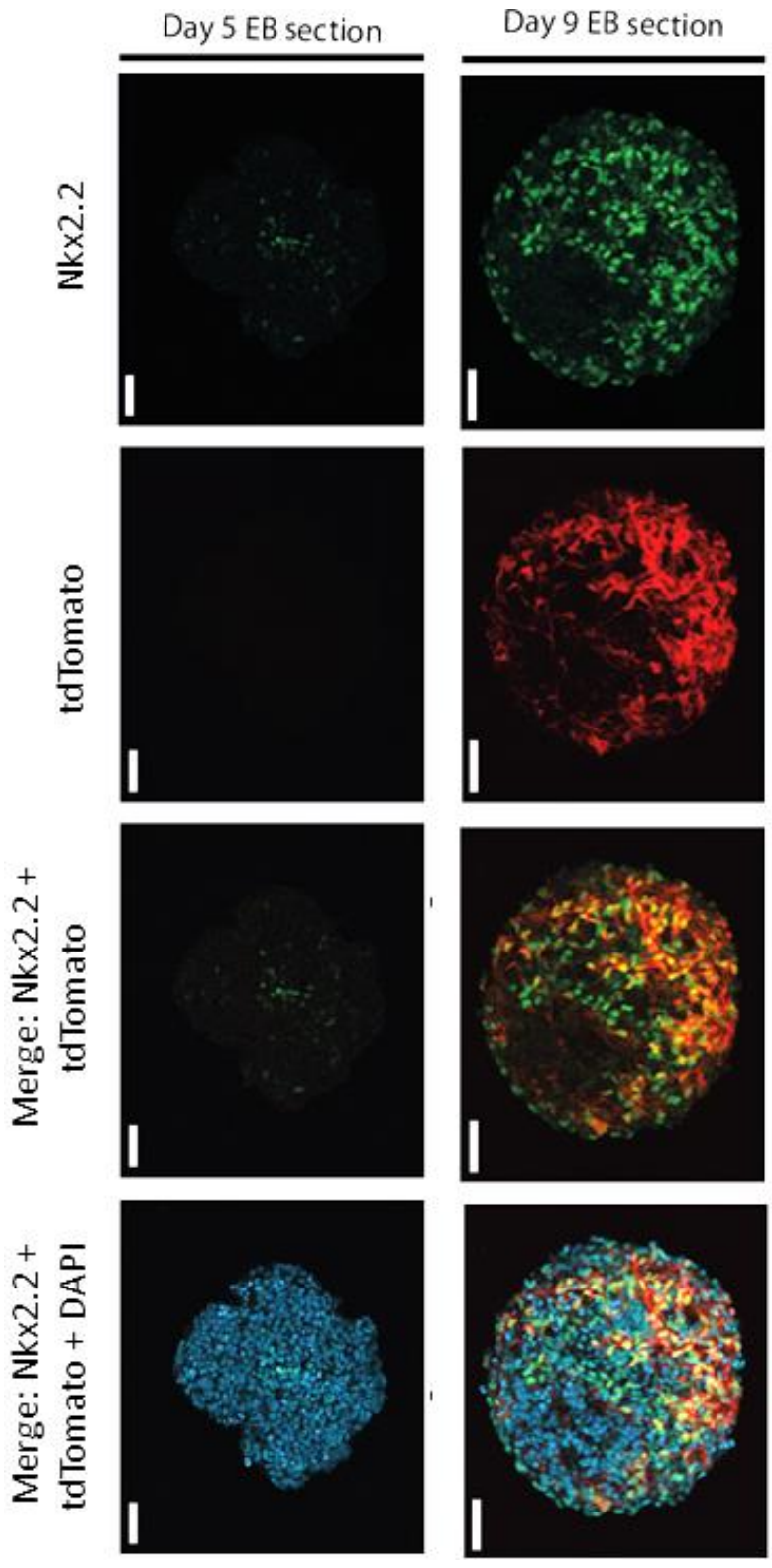

Figure 3.5: tdTomato-positive V3 interneurons only comprised a proportion of the Nkx2.2-positive cell population in the EB sections.

Left column: There were no tdTomato-positive V3 interneurons (red) in the day 5 EBs and very few Nkx2.2-positive cells (green). Right column: On day 9, many tdTomato-positive V3 interneurons and Nkx2.2-positive cells were observed in the EB section. Not all Nkx2.2-positive nuclei were also labelled for tdTomato, demonstrating that not all Nkx2.2-positive cells were V3 interneurons. DAPI is in blue. Vertical scale bars = 50µm. Images are tile scans taken on a confocal LSM800 with a 20x objective.

3.3.2.1 Motoneuron purification

Once differentiated, motoneurons were purified from day 5 C9G-derived EBs by Magnetically-Activated Cell Sorting (MACS; Chapter 2: Materials and Methods, Section 2.4.1). This involved sorting out motoneurons by attaching antibodies with magnetic beads to the CD14 tag expressed specifically in motoneurons under the Hb9 promoter. Before sorting, the EBs were treated with the antimitotic agent, mitomycin-C (MMc) (2μM for 2 hours at 37 °C) to prevent dividing cells from contaminating the cultures (Magown et al., 2016). This treatment did not affect the yield of motoneurons achieved (MN yield = 20.7 ± 9.6% (n = 10) for the non-treated condition and MN yield = 16.3 ± 4.7% (n = 15) for the MMc-treated condition; p = 0.41, Mann Whitney U test,). Pooling together MMc-treated and non-treated differentiations, the MACS purification method resulted in a motoneuron yield of 19 ± 7 % (n = 25 differentiations).

To investigate the effectiveness of the MACS protocol, the result of MACS was compared to FACS (Chapter 2: Materials and Methods, Section 2.4.2). Motoneurons from the C9G ESC line could not be sorted by FACS according to the GFP reporter expressed under the Hb9 promoter as they expressed a second fluorescent protein with an overlapping emission spectrum (ChR2-YFP under the Cag promoter). To overcome this, another cell line was used that contained only the *Hb9::CD14-IRES-GFP* transgene (the H14IG#13 line; for details of ESC lines used, see Chapter 2: Materials and Methods, Table 2.1). The CD14 tag was used to purify the motoneurons by MACS and the GFP reporter used to purify the motoneurons by FACS. FACS achieved a significantly higher yield of motoneurons than MACS (FACS motoneuron yield = 31 ± 8 %; MACS motoneuron yield = 20 ± 9 %; p = 0.003, paired t test; n = 3 differentiations for each method). FACS sorting of MACS-sorted motoneuron populations showed a purity of 91 ± 3 % was achieved by MACS-sorting (n = 3 differentiations).

To further probe the effectiveness and sensitivity of the MACS protocol, the cytoplasmic GFP expression (driven by the Hb9 promoter) of the MACS-purified cell population and the cell population not captured by the purification process (the flowthrough population) was compared. Although C9G cells express both GFP and YFP, GFP is predominantly cytoplasmic whereas the YFP is membranous due to its attachment to the membrane ion channel, ChR2 (Figure 3.6 A). Therefore, despite some overlap between the YFP and GFP emission

spectra, it was possible to distinguish the two fluorophores by a combination of carefully selected confocal microscope settings and intracellular reporter location. MACS-purified and flowthrough cells were plated on PLO- and laminin- coated coverslips and imaged live 24 hours after plating (Chapter 2: Material and Methods, Section 2.6). Live imaging was necessary as fixation with 4% paraformaldehyde quenched the endogenous fluorescence (data not shown). The MACS-purified cell population was significantly enriched for cells with high mean GFP intensity, i.e. motoneurons (mean GFP intensity = 6 ± 7 a.u. in the flowthrough condition compared to mean GFP intensity = 16 ± 14 a.u. in the MACS-purified condition; $p < 2.2e-16$, Mann Whitney U test; n = 841 flowthrough cells and n = 950 MACS-purified cells from three differentiations; Figure 3.6 B i). Both the minimum and maximum intensities were also greater in the MACS-purified condition (Figure 3.6 B ii and I, respectively; for both, $p < 2.2e-16$, Mann Whitney U test). However, the presence of cells with high intensities of cytoplasmic GFP in the flowthrough population suggested that the MACS purification process was not sensitive, so that not all motoneurons were captured by the MACS process. Indeed, FACS of the flowthrough population revealed 12 ± 2% were unsorted motoneurons (n = 3 differentiations). Thus, while MACS achieved high levels of purity, it was not a highly sensitive method.

3.3.2.2 Validation of motoneuron identity in culture

The evidence that MACS-purified cells were motoneurons was multi-facetted. Firstly, the GFP/YFP-positive cells purified by MACS were predominantly neuronal according to their BTIII labelling and morphology (Figure 3.7) and, when plated on astrocytic monolayers, had relatively large cell bodies when compared with V3 interneurons (Figure 3.8). Secondly, as GFP is expressed under the Hb9 promoter in the C9G cell line, enrichment of cells with higher mean GFP intensity implied enrichment for neurons expressing Hb9 (Figure 3.6 A and B i; Section 3.3.2.1). However, Hb9 is expressed transiently during development in many ventral horn neurons as well as potentially dorsal horn neurons, but expression persists only in motoneurons and a small population of excitatory, ventral medial neurons found in lower thoracic and upper lumbar segments (Caldeira et al., 2017; Dougherty and Ha, 2019; Wilson et al., 2005). Indeed, among the MACS-purified, GFP-positive cells, GFP intensity at 24 hours varied widely, which may indicate that some Hb9 expression was reduced. Therefore, to ensure the

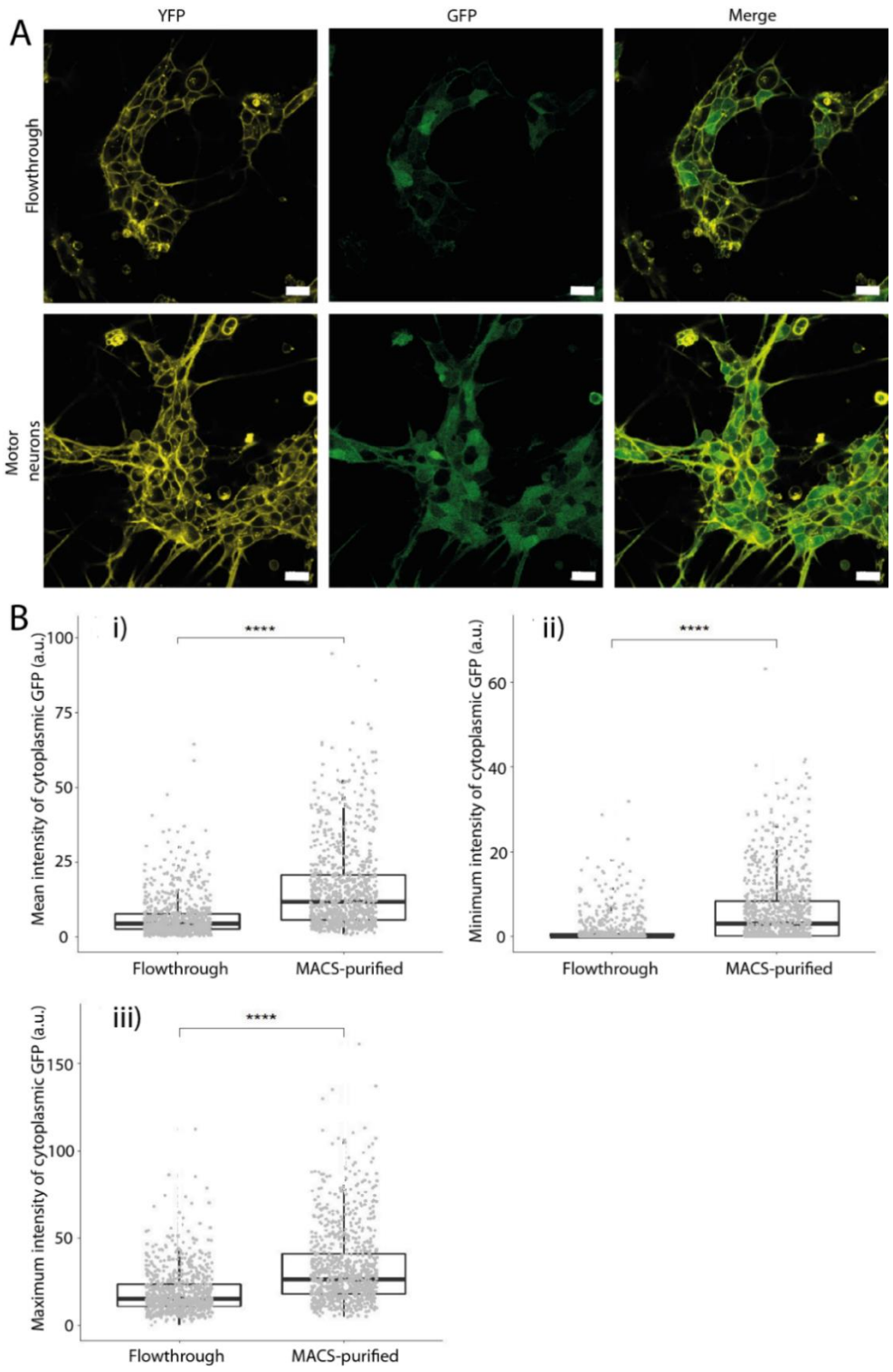

Figure 3.6: Efficacy and sensitivity of the MACS purification protocol

A: Endogenous GFP (green) and YFP (yellow) expression in live C9G cells imaged 24 hours after purification and plating. The YFP had a distinctly membranous distribution whereas the distribution of GFP was cytoplasmic. Scale bars = 20μM. B: Quantification of mean (i), minimum (ii) and maximum (iii) GFP intensity of a line drawn across the cytoplasm (bounded by the YFP-positive membrane). n = 841 and 950 for the flowthrough and MACS-purified cell populations, respectively, from three differentiations. **** = $p<0.0001$. The bold horizontal line in boxplots shows the median. These images were acquired using a Leica DMR epiflourescence microscope.

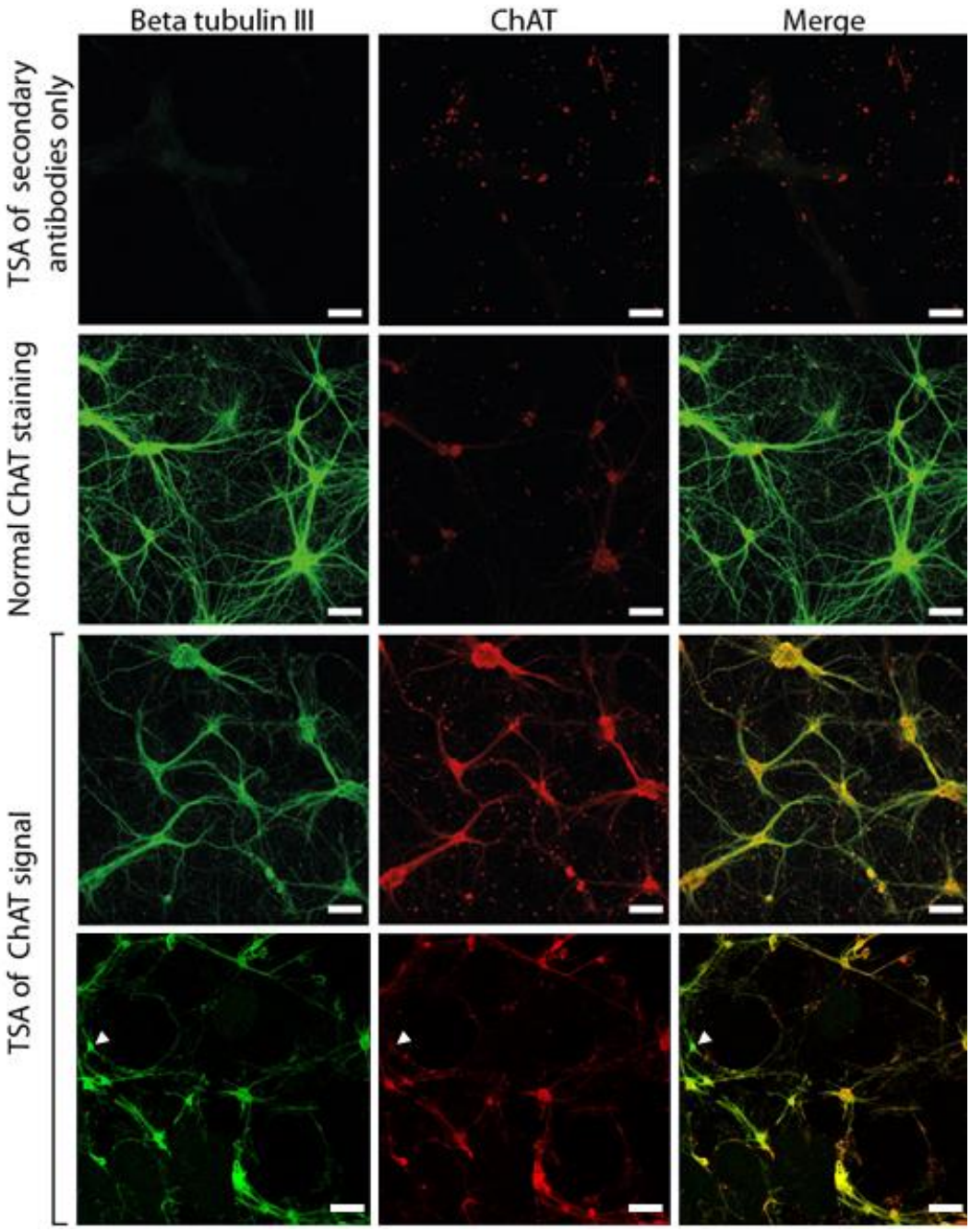

Figure 3.7: Week 3 motoneurons plated on an astrocyte monolayer were predominantly neuronal and expressed choline acetyltransferase (ChAT)

ESC-derived motoneurons were plated on a monolayer of ESC-derived astrocytes and cultured for 3 weeks before labelling for the neuronal marker, beta tubulin III, and ChAT. ChAT is a marker of cholinergic neurons such as motoneurons. ChAT labelling without amplification was faint (second row) so tyramide signal amplification (TSA) was used (bottom two rows). Of 15 randomly selected fields of view from four labelled and amplified coverslips from two differentiations, only one BTIII-positive neuron was found that did not express detectable levels of ChAT (white arrowhead in bottom row of images). Scale bar = 100µm. These images were obtained using a Plan-Neofluar 10x/0.3 objective on an LSM500 laser scanning microscope (Zeiss). Microscope settings for ChAT: excitation wavelength = 543nm, laser power = 15%, pinhole = 92µm. Microscope settings for YFP/GFP: excitation wavelength = 488, laser power = 30%, pinhole = 100 µm.

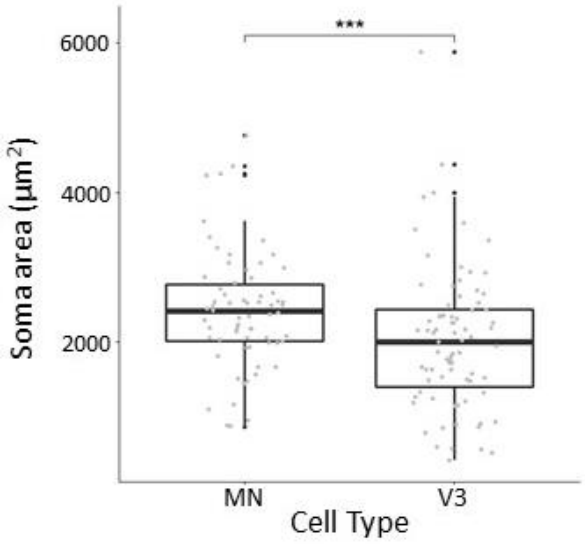

Figure 3.8: Motoneurons were significantly larger than V3 interneurons.

The soma area of motoneurons (MN) and V3 interneurons (V3) in week 2 cultures containing motoneurons, V3 interneurons and astrocytes (MN+V3+as) were measured and compared. For motoneurons, n = 66 from four differentiations and for V3 interneurons, n = 79 from three differentiations. The bold horizontal line in boxplots shows the median. Data was not normally distributed, so a non-parametric Mann Whitney U test was used to determine statistical significance. * = p<0.05, ** = p<0.01, *** = p<0.001, and **** = p<0.0001.

motoneuron identity of MACS-purified neurons, the expression of motoneuron markers was examined. MACS-purified neurons labelled with an antibody against GFP were found to express other motoneuron markers such as choline acetyltransferase (ChAT) (Figure 3.7; week 3 co-cultures) and vesicular Acetylcholine Transporter (vAChT) (Figure 3.9; week 2 co-cultures) when plated on astrocyte monolayers. For both labellings, there was a limited amount of labelling in the secondary-only negative control that likely represents the secondary antibody binding to debris from dead/dying cells (Figure 3.9 A; Figure 3.7). These data confirm that the MACS-purified cell population was motoneuronal.

3.3.2.3 V3 interneuron generation and purification

V3 interneurons were generated from the 'Vic_1244' (#1244) ESC line (Chapter 2: Materials and Methods, Table 2.1), which expresses tdTomato under the *Sim1* promoter and was kindly donated by the Pfaff lab, Salk Institute for Biological Studies (Sternfeld et al., 2017). Vic_1244 ESCs were expanded in feeder-free conditions and differentiated initially according to the 5-day RA/SAG

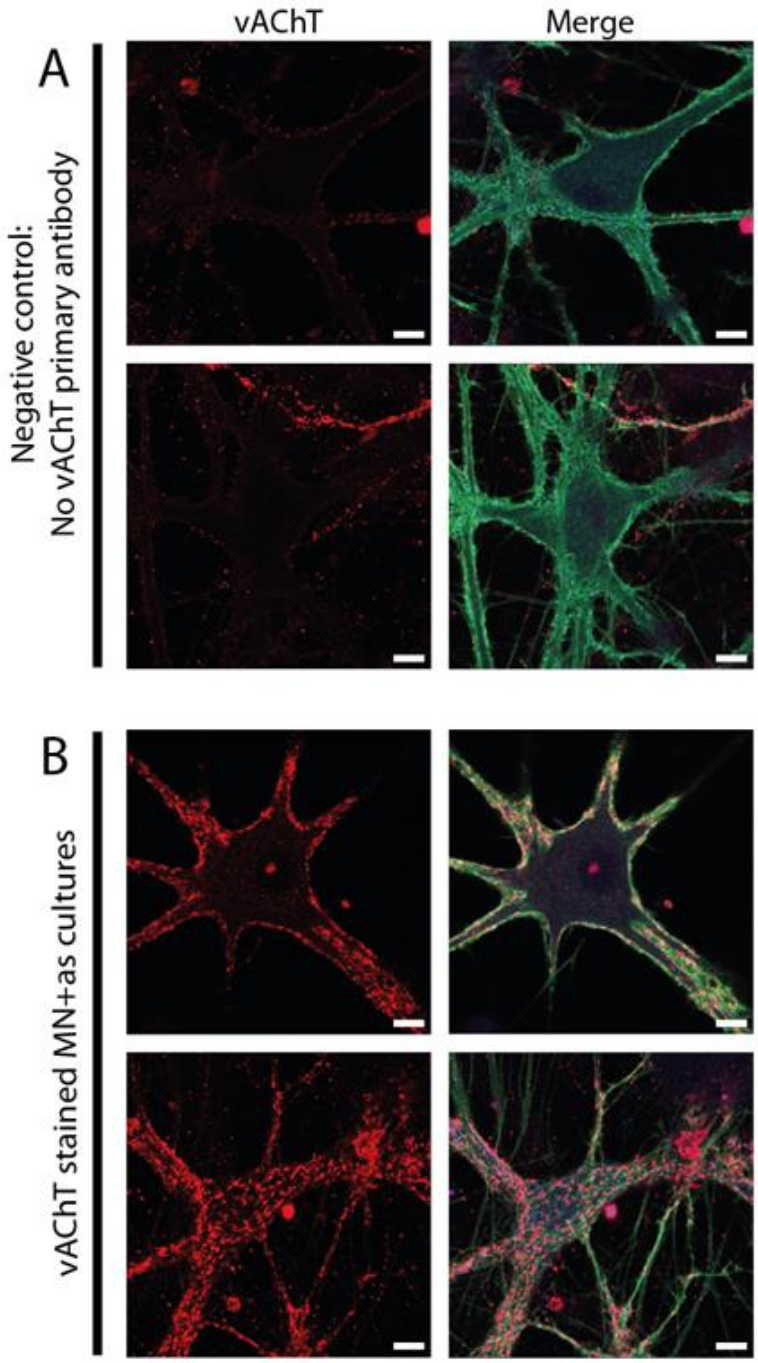

Figure 3.9: Week 2 motoneurons plated on an astrocyte monolayer expressed vesicular acetylcholine transporter (vAChT).

ESC-derived motoneurons were plated on a monolayer of ESC-derived astrocytes and cultured for 2 weeks before labelling for YFP/GFP (green) and vAChT (red). vAChT is a presynaptic marker of cholinergic neurons such as motoneurons. A: Two motoneurons in MN+as co-cultures labelled without the primary vAChT antibody as a negative control. B: Two motoneurons in MN+as co-cultures labelled with all primary antibodies. vAChT puncta decorated the membrane of the motoneurons; the images on the bottom row shows a cross section through the cell membrane against the glass of the coverslip. Scale bars = 10µm. These images were obtained using a Plan-Apochromat 63x/1.40 Oil DIC M27 objective on an LSM800 laser scanning microscope (Zeiss). Microscope settings for VAChT: excitation wavelength = 561nm, laser power = 0.1%, pinhole = 40µm. Microscope settings for YFP/GFP: excitation wavelength = 488, laser power = 0.1%, pinhole = 48µm.

differentiation protocol. On day 5, Vic_1244 EBs were resuspended in ADFNK and cultured for a further 4 days (changing the media every other day). On day 9, the Vic_1244 EBs were MMc-treated and dissociated. The yield of Vic_1244 cells was reduced by 74 ± 28 % if Glutamax was not included in the feeder-free media (n = 3 differentiations). V3 interneurons were purified from the dissociated EBs by FACS of the tdTomato reporter; the yield was 24 ± 6 % V3 interneurons (n = 10 differentiations). The purity of the FACS-purified population was 93 ± 2 % (n = 3 differentiations).

3.3.3 Maintaining the purity of motoneuron co-cultures

An *in vitro* co-culture model of motoneurons with the candidate cell types, V3 interneurons and astrocytes was established with four conditions as described in Chapter 2: Materials and Methods, Section 2.5: i) motoneurons alone (MN alone); ii) motoneurons with V3 interneurons (MN+V3); iii) motoneurons on an astrocyte monolayer (MN+as); and iv) motoneurons with V3 interneurons on an astrocyte monolayer (MN+V3+as). Division of astrocytes was occasionally observed in the co-cultures so immunofluorescence experiments were undertaken to determine the proportion of neurons in the cultures that were derived from dividing population of astrocytes. These contaminant neurons would express the neuronal marker beta-tubulin III (BTIII) but neither YFP (a marker for the MACS-purified C9G cell population; detected using a GFP antibody) nor tdTomato (a marker of the FACS-purified Sim1-positive V3 interneuron population; detected using an mCherry antibody). The proportions of BTIII-positive neurons expressing either GFP, tdTomato or neither were measured in the four co-culture conditions one week after plating. As expected, in the MN alone culture condition, all BTIII-positive cells were GFP-positive and there were no contaminant BTIII-only cells (n = 66 neurons from four differentiations; Figure 3.10). In the MN+V3 co-culture condition, 3 ± 6 % were contaminant, BTIII-only cells (n = 103 neurons from three differentiations; Figure 3.10). In the MN+as co-culture condition, 6 ± 5 % were contaminant, BTIII-only cells (n = 89 neurons from three differentiations; Figure 3.10). In the MN+V3+as co-culture condition, 2 ± 2 % were contaminant, BTIII-only cells (n = 109 neurons from three differentiations; Figure 3.10). There was no significant difference between the proportions of contaminant neurons in the different co-culture conditions ($p = 0.114$, Kruskal Wallis test), suggesting that the presence of astrocytes did not increase the amount of contaminant neurons in

the co-cultures. These data show that, after seven days, co-cultures comprising MMc-treated differentiated cells remained >92% pure.

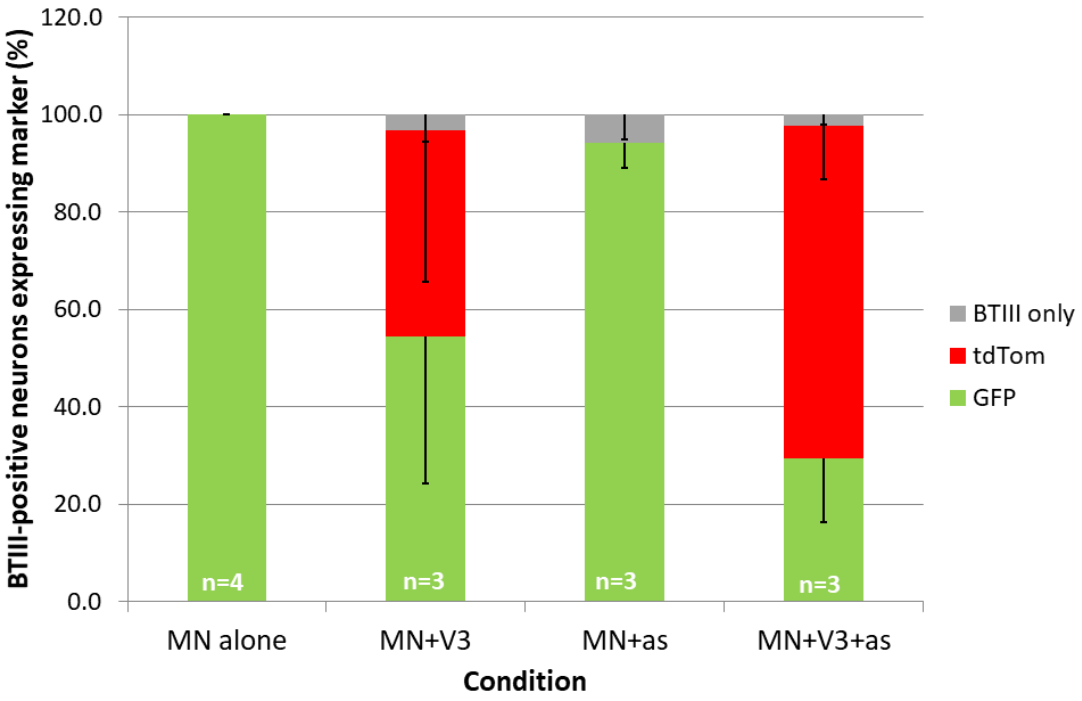

Figure 3.10: Co-cultures remain >92% pure after >7 days in culture.

Division of astrocytes was occasionally observed in the co-cultures so week 1 co-cultures were labelled to look for contaminant neurons from the H6 ESC line. Contaminant neurons would express the neuronal marker beta tubulin 3 (BTIII) but not the C9G ESC line reporter YFP/GFP or the Vic_1244 ESC line reporter tdTomato. This figure shows the proportion of BTIII-positive neurons that were YFP/GFP-positive motoneurons (green), tdTomato-positive V3 interneurons (red) or BTIII only-positive contaminant neurons (dark grey). No significant difference was found between the proportions of contaminant neurons in the different co-culture conditions ($p = 0.114$, Kruskal Wallis test). Error bars show the negative standard deviation. The n stated in white at the base of each bar represents the number of differentiations considered for that condition.

3.4 Discussion

The results presented in this Chapter show that the 5-day RA/SAG differentiation protocol ventralised the identity of neurons produced. Thus, neurons from the more medial V0, V1 and V2 progenitor domains were not observed in the EBs in large numbers, if at all, whereas motoneurons and V3 interneurons from the more ventral pMN and p3 progenitor domains respectively, comprised a large proportion of EBs. Consistent with previous reports (Sternfeld et al., 2017; Xu and Sakiyama-Elbert, 2015), V3 interneurons were generated later than motoneurons. Because of their abundance in the EBs, V3 interneurons were identified as a candidate cell type for further investigation.

MACS resulted in >91% pure populations of motoneurons but motoneuron yields were not as high as when sorted by FACS. The motoneuronal identity of purified cells was confirmed by morphology and the expression of various neuronal and motoneuronal markers. MMc-treatment of EBs and co-cultures effectively prevented the contamination of co-cultures with dividing cells such that co-cultures were still >92% pure after seven days in culture.

3.4.1 EB composition

The assumption that only ventral spinal populations were generated by the 5-day RA/SAG differentiation protocol was validated as more medial ventral cell types, such as V0 and V1 interneurons, were either absent or rarely observed in the EBs, similar to previous reports (Sternfeld et al., 2017; Wichterle et al., 2002). In contrast to this finding, some groups reported the presence of V0 and V1 interneurons in EBs as defined by Lim1 expression in the absence of Hb9 (Soundararajan et al., 2006; Wichterle et al., 2002) or indirectly by GABA- and glycin- ergic modulation of spontaneous muscle activity elicited by engrafted EBs (Magown et al., 2017). However, Lim1 is not a specific marker for V0 and V1 interneurons (Alaynick et al., 2011); it is also present in other types of interneuron (Alaynick et al., 2011) and there is evidence that it is present in other brain areas during development (Allen Brain Atlas: Developing Mouse Brain: Lim1/Lhx1). Therefore, the cells expressing Lim1 observed by other groups may not have been V0 and V1 interneurons. Alternatively, the disparity could arise due to the time course of expression of the markers. For example, one of the markers used, Dbx1, is only expressed at the progenitor stage (Alaynick et al., 2011); the

expression of this marker may already be switched off by day 5 of the RA/SAG differentiation protocol.

V2a interneurons were rarely observed in the EB sections. V2a interneurons were also detected in day 5 EBs by Wichterle, et al. (2002), although this group did not provide a quantification of their data. They suggest that the variability in the SAG concentration that individual EBs are exposed to could increase the variability of EB composition, such that V2a interneurons can be occasionally observed. The rarity of V2a interneurons could be because, without Notch inhibition, p2 progenitors favour generating the V2b subtypes rather than the V2a subtype in the RA/SAG differentiation protocol (Brown et al., 2014). In the experiments described in this Chapter, the V2b interneuron population was not examined because an effective antibody for the V2b marker Gata3 could not be sourced.

Motoneurons comprised approximately a third of the cells generated by the 5-day RA/SAG differentiation protocol, a result in agreement with FACS results and previous reports (Bryson et al., 2014; Sternfeld et al., 2017; Wichterle et al., 2002). There was a decrease in the proportion of EB sections labelled with both motoneuron markers (Hb9 and isl1) between day 5 and day 9. This could suggest that motoneuron genesis ceased after day 5 while the size of the EB continues to increase as other cell types are born, effectively diluting the motoneuron content of the EBs. *In vivo*, motoneuron genesis ceases around E11 (Arber et al., 1999; Nornes and Carry, 1978). Day 9 EBs have post-E12 characteristics as they express nuclear NeuN labelling, which is first observed in vivo at E12 (Li et al., 2016). Assuming the temporal relationships of the generation of different cells types are similar in the EB and *in vivo*, this supports the proposal that motoneuron genesis may have ceased by day 9 in EBs. An alternative explanation for motoneurons making up a smaller proportion of EB sections is motoneuron death between day 5 and day 9. *In vivo*, developmental programmed death of motoneurons due to competition for target-derived trophic factors is well documented (Dekkers et al., 1994; Milligan et al., 1994; Oppenheim, 1991). Indeed, between E13-18 in mice, 67% of the motoneurons initially present in the lumbar spinal cord die (Lance-Jones, 1982). As the day 9 EBs show other characteristics of post-E12 spinal cord (e.g. nuclear NeuN expression), it is possible that a similar process of programmed cell death was happening within the EB as the cells matured.

Significantly more Isl1-expressing cells than Hb9-expressing cells were observed in the EBs. This may be because not all Isl1-expressing cells were motoneurons (i.e. also express Hb9) (Wichterle et al., 2002). The Isl1-only expressing cells could be dI3 interneurons, which are known to express Isl1 postmitotically (Alaynick et al., 2011). Given the concentration of SAG present during the differentiation, however, it seems unlikely that dorsal interneuron populations would have been generated. Alternatively, these Isl1-expressing cells could be PGC and medial LMC motoneurons, which express Isl1 but only low levels of Hb9 (Rousso et al., 2008); perhaps these low levels were below the threshold set for detection of Hb9 labelling.

Nkx2.2-expressing cells were found in the EB sections and more were generated by day 9 of the protocol than day 5, as reported by Sternfeld et al. (2017). A proportion of these were V3 interneurons, as defined by Sim1 promoter-driven tdTomato expression. The abundance of motoneurons and V3 interneurons from the ventral progenitor domains compared to interneurons from more dorsal progenitor domains is consistent with the findings of Wichterle et al. (2002), who found that increasing concentrations of SAG caused a dorsal-to-ventral shift in the expression profile of progenitor cell transcription factor markers in EBs.

3.4.2 Validation of motoneuron identity

As, Hb9 is transiently expressed in non-motoneuronal neurons during development and persistently in a small population of excitatory interneurons in the ventral medial spinal cord (Caldeira et al., 2017; Wilson et al., 2005), it was necessary to verify the motoneuronal identity of MACS-purified cells using other markers. MACS-purified cells were confirmed to be motoneurons according to several criteria: i) they were found to be almost exclusively neuronal, expressing neuronal markers; ii) they were cholinergic, as determined by the expression of vAChT and ChAT; iii) had high cytoplasmic GFP expression (driven by the Hb9 promoter), and iv) as shown later in Chapter 5, they also demonstrated electrical firing properties characteristic of motoneurons.

GFP intensity was found to vary widely among the MACS-purified, GFP-positive cells. This may be because different motoneuron subtypes express different levels of Hb9 (Rousso et al., 2008), or it is possible that the GFP was broken down on a faster timescale than the Hb9. GFP-expressing cells were also present

in the flowthrough cell population, which is consistent with the finding that not all motoneurons were captured by MACS. Alternatively, it may be that some cells began expressing Hb9 in the 24 hours post-purification.

3.4.3 Studying the effect of co-culture on motoneuron maturation *in vitro*

The microenvironment of a motoneuron *in vivo* is extremely complex and it can be difficult to disentangle the different factors that influence motoneuronal maturation. When considering ESC-derived motoneurons present in a transplanted EB, this difficulty is compounded because the differentiation, surgery and recovery stages of the transplant can all influence the microenvironment of the transplanted motoneurons. In this study, these sources of variation were avoided by studying motoneuron maturation using an *in vitro* co-culture model. *In vitro,* the experimenter can manipulate culture conditions, enabling easier characterisation of factors that influence maturation. The use of an *in vitro* model also reduced the number of animals and time needed for such experiments. It was for these reasons that, in the next Chapters, the effect of the candidate cell types, astrocytes and V3 interneurons, on the maturation of ESC-derived motoneurons was studied using an *in vitro* co-culture model.

4 Chapter 4: The effect of astrocytes and V3 interneurons on the morphological and synaptic maturation of motoneurons *in vitro.*

4.1 Introduction

As described in Chapter 1 (Section 1.5.1), the size, morphological complexity and connectivity of motoneurons change during development *in vivo* and these changes are essential for motoneuron function. Many aspects of this development can be recapitulated *in vitro.* For example, Takazawa et al (2012) differentiated human ESCs into motoneurons using a 31-day differentiation process and investigated motoneuronal morphological development over the next 9 days in mixed culture. They found a significant increase in soma area, neurite branch order and dendritic arbour size between day 1 and day 9 (Takazawa et al., 2012). Other studies of ESC-derived (Miles et al., 2004) and iPSC-derived (Toma et al., 2015) murine motoneurons in mixed cultures or ESC-derived motoneurons cultured with ESC-derived astrocytes (Bryson et al., 2014) also demonstrated an increase in motoneuronal size as indicated by increased capacitance. Moreover, purified primary embryonic motoneurons cultured *in vitro* with either Schwann cells or astrocytes formed synapses (Ullian et al., 2004a) and displayed spontaneous synaptic activity (Sternfeld et al., 2017; Ullian et al., 2004a; Zhang et al., 2009) with both glutamatergic and cholinergic components (Ullian et al., 2004a; Zhang et al., 2009). Thus, some elements of motoneuronal morphological development occur in the absence of the 'normal' physiological milieu. Therefore, in this Chapter, the effects of co-culture with the candidate cell types, astrocytes and V3 interneurons, on motoneuron size, morphology and synapse formation were investigated using an *in vitro* co-culture model.

4.1.1 How do astrocytes affect motoneuron size, morphology and synapse formation?

Astrocytes are essential to the formation of motoneuron structure, morphology and connectivity. For example, the large soma size and functional characteristics of fast motoneurons in the spinal cord is maintained by the modulation of extracellular K^+ ions by surrounding astrocytes (Kelley et al., 2018). In terms of dendritic morphology, in *Drosophila*, the absence of glia was found to disrupt motoneuronal dendritic morphology (Landgraf et al., 2003), though gross circuit structure was unaffected (Hosoya et al., 1995; Landgraf et al., 2003). Given the

importance of excitatory activity in the development of the dendritic arbour (Chapter 1: General Introduction, Section 1.6.2) and the importance of astrocytes to synapse formation and excitatory-inhibitory balance in the spinal cord (Molofsky et al., 2014) (Chapter 1: General Introduction, Section 1.8), it is not surprising that the motoneuronal dendritic arbours were found to be abnormal in *glial cell missing* mutant *Drosophila* (Landgraf et al., 2003).

4.1.2 Synapses formed by V3 interneurons onto motoneurons in the spinal cord and their role

There is *in vitro* evidence that the release of synaptogenic signals from astrocytes is regulated by interactions with neurons. For example, the release of some synaptogenic molecules is regulated by glutamate; SPARC secretion is stimulated by glutamate (Jones et al., 2011), which, as SPARC decreases AMPA receptor levels, provides a homeostatic mechanism to decrease synaptic excitability in the response to increased activity. In a similar way, the release of TNFα, which increases synaptic AMPA receptors, is decreased by glutamate (Stellwagen and Malenka, 2006), again homeostatically limiting excitability. Furthermore, experimental interventions that reduced excitability, such as knocking out glutamate release in cortical neurons (Morel et al., 2014) or dark-rearing (Müller, 1990), caused a delay in the structural maturation of cortical astrocytes. However, there is a lack of direct evidence of these mechanisms *in vivo*.

Such homeostatic mechanisms mean that, at least *in vitro,* the synaptogenic potential of astrocytes may be affected by the types of neuron they interact with. V3 interneurons provide strong glutamatergic drive to motoneurons (Chopek et al., 2018; Sternfeld et al., 2017) and this increased glutamatergic signalling could negatively regulate synapse formation in V3 interneuron-containing co-cultures.

4.2 Aims of this Chapter

Given that motoneuronal size, dendritic morphology and synaptic connectivity change during development *in vivo*, influenced by both astrocytes and activity, the aim of the experiments described in this Chapter was to determine whether and how co-culture of ESC-derived motoneurons with either astrocytes, V3 interneurons or both affected motoneuronal soma size, the number and diameter of primary neurites (as measures of dendritic complexity), and/or synapse formation within the co-cultures. The effect of co-culture with astrocytes on V3 interneuron soma size and primary neurite number and diameter was also investigated.

4.3 Results

To investigate the effect of co-culture on morphological maturation and synapse formation, motoneurons were cultured *in vitro* either alone (MN alone), with astrocytes (MN+as), with V3 interneurons (MN+V3), or with both astrocytes and V3 interneurons (MN+V3+as). The various co-culture conditions were generated from pure populations of motoneurons, astrocytes and V3 interneurons from C9G, H6 and Vic_1244 ESCs respectively (for details see Chapter 2: Materials and Methods, Sections 2.2, 2.3, 2.4 and 2.5). Co-cultures were examined 2 weeks after motoneurons were plated, as at this timepoint, motoneurons in all co-culture conditions showed signs of electrophysiological maturity, such as the ability to fire repetitively (Chapter 5).

4.3.1 The effects of co-culture with astrocytes and V3 interneurons on motoneuron size and morphology.

To investigate motoneuronal size and morphology, motoneuron co-cultures were labelled (Chapter 2: Materials and Methods, Section 2.8) with antibodies against GFP, to mark the C9G-derived motoneurons, and tdTomato, to mark the V3 interneurons (Figure 4.1 and Figure 4.2). Note that the GFP antibody cross-reacts with the ubiquitous membranous YFP also expressed by the C9G ESC line. These same co-cultures were used to examine motoneuronal glutamatergic synapses formed in co-culture (Section 4.3.2), so they were also labelled for vesicular Glutamate Transporter 2 (vGluT2) and Homer1. Soma area and diameter were used as measures of motoneuronal soma size (Chapter 2: Materials and Methods, Section 2.10.2). In each co-culture, neurites from multiple motoneurons and V3 interneurons were overlapping making it extremely difficult to fully characterise the morphology of individual neurons. Therefore, the number and diameter of primary neurites, which have both been shown to correlate with dendritic complexity *in vivo* (Ulfhake and Cullheim, 1988; Ulfhake and Kellerth, 1981), were measured (Chapter 2: Materials and Methods, Section 2.10.2) and used as indicators of morphological complexity. The soma size and complexity of V3 interneurons in the MN+V3 and MN+V3+as conditions were also quantified. Figure 4.2 shows example images of V3 interneurons.

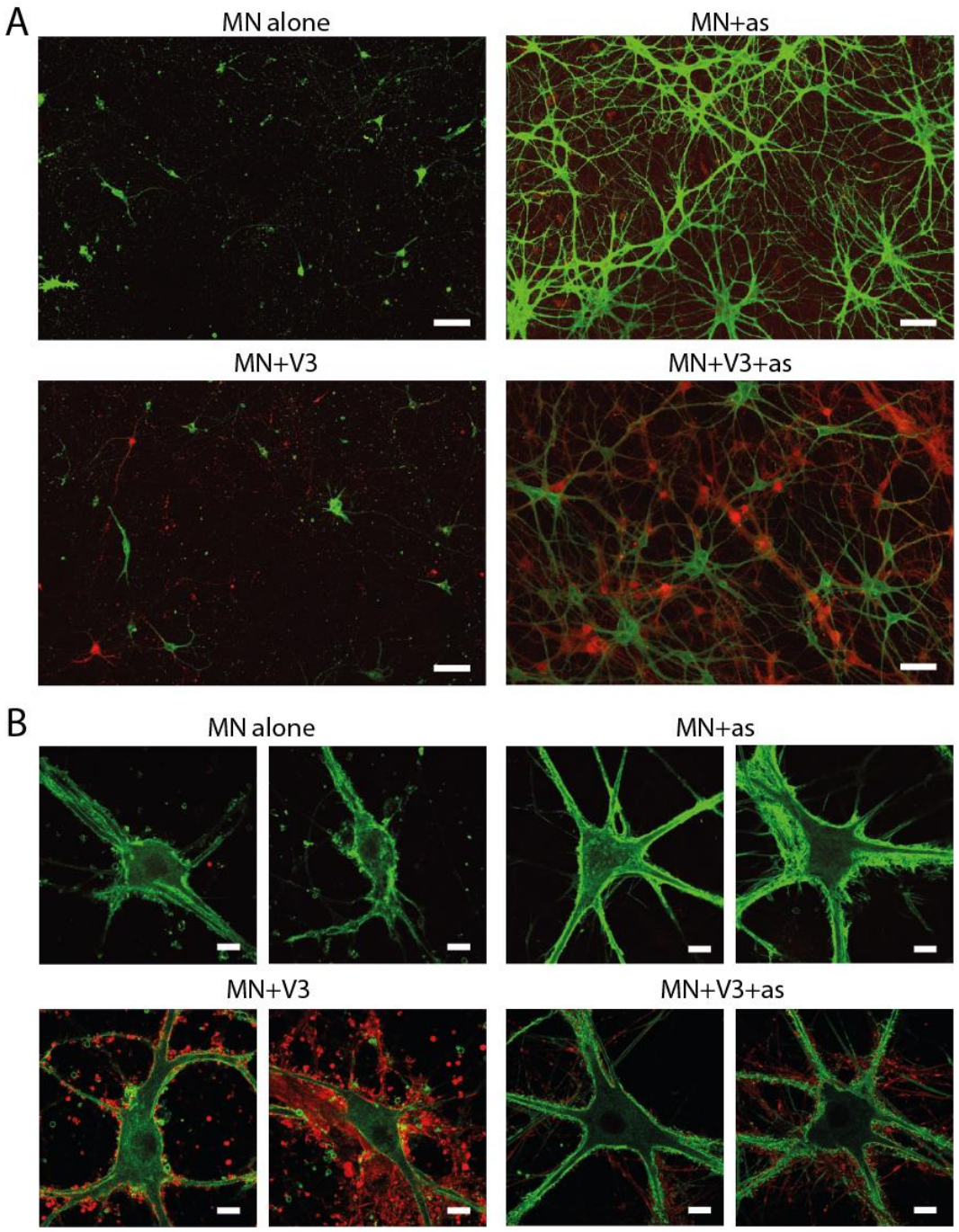

Figure 4.1: Example images of motoneurons in the four different culture conditions

Week 2 motoneuron cultures were labelled for GFP (green) and V3 interneurons were labelled for tdTomato (red). A: Example tile scans for each culture condition, taken with a 20x objective. Analysis of MN size and morphology was performed on tile scans such as these. Note that the low level of red seen in the MN+as condition because of non-specific binding of the secondary antibody to the astrocyte monolayer and debris; there was no tdTomato present in this condition. Scale bar = 100µm. B: Example high magnification images of the somatic and proximal dendritic compartments of individual motoneurons in each culture condition, taken with a 63x objective. Scale bar = 10µm. Cell survival was worse in the astrocyte-free culture conditions so neurons were sparser (A) and GFP- and extracellular tdTomato- positive debris could be seen (B) in the MN alone and MN+V3 conditions, respectively.

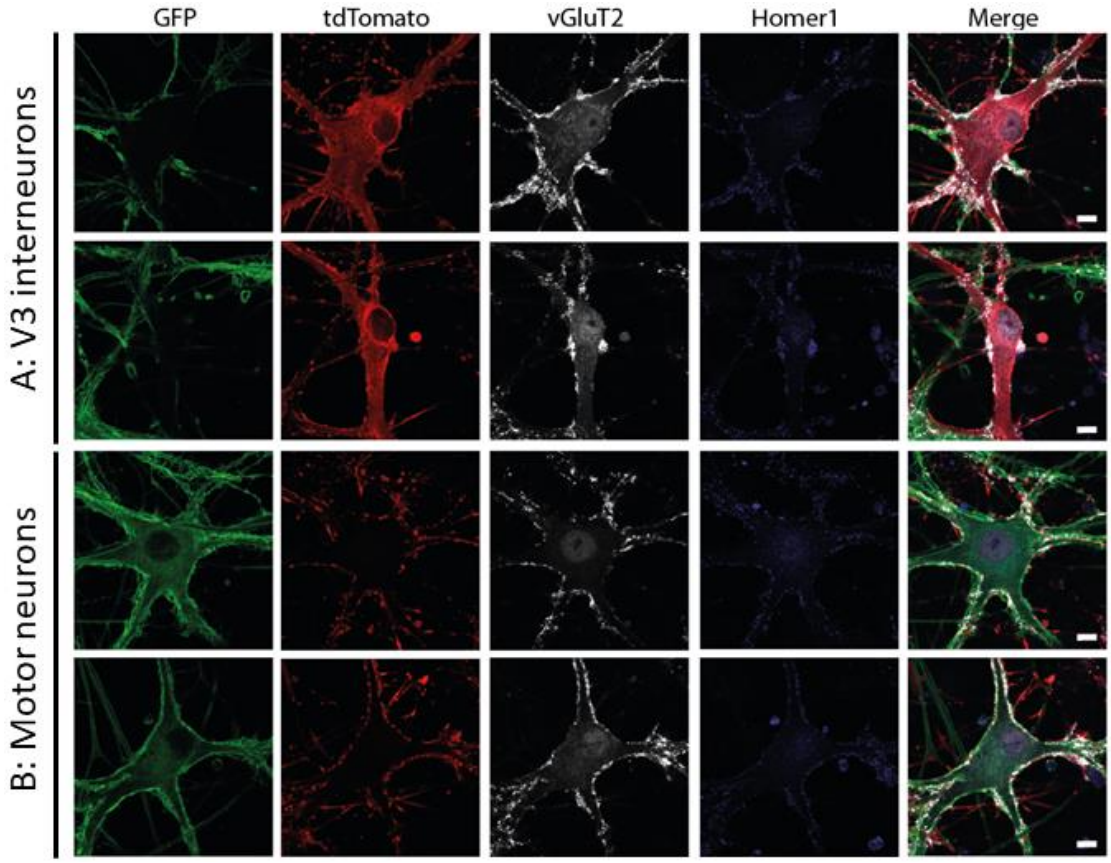

Figure 4.2: Immunofluorescent images of the somatic and proximal dendritic compartments of motoneurons (B) and V3 interneurons (A) labelled for markers of glutamatergic synapses.

Week 2 co-cultures were labelled for YFP/GFP (green), tdTomato (red), vGluT2 (white) and Homer1 (blue). Cytoplasmic vGluT2 (red) expression varied between cells of the same type. V3 interneurons (A) seemed to express slightly more cytoplasmic vGluT2 than motoneurons (B). However, the majority of vGluT2 labelling was membrane-bound (white puncta). All images were from cells in the MN+V3+as condition. vGluT2 = vesicular glutamate transporter 2. Scale bar = 10µm.

4.3.1.1 Co-culture with astrocytes increased neuronal survival

The first obvious effect of co-culture condition was an increase in neuronal survival (Figure 4.1 A and Figure 4.3; $p = 0.002$ in an ANOVA test). To determine which cell-type was affecting survival, a post hoc Tukey HSD test was performed. Co-culture with astrocytes significantly increased neuronal survival (Figure 4.3; 4.3 ± 1.0% for the MN+as condition compared to 0.8 ± 0.4% in the MN alone condition; $p = 0.028$ in a post hoc Tukey HSD test). In contrast, the presence of V3 interneurons in the cultures did not affect neuronal survival (Figure 4.3; $p = 0.74$ comparing the MN alone with the MN+V3 condition and $p = 0.55$ comparing the MN+as with the MN+V3+as condition in post hoc Tukey HSD tests).

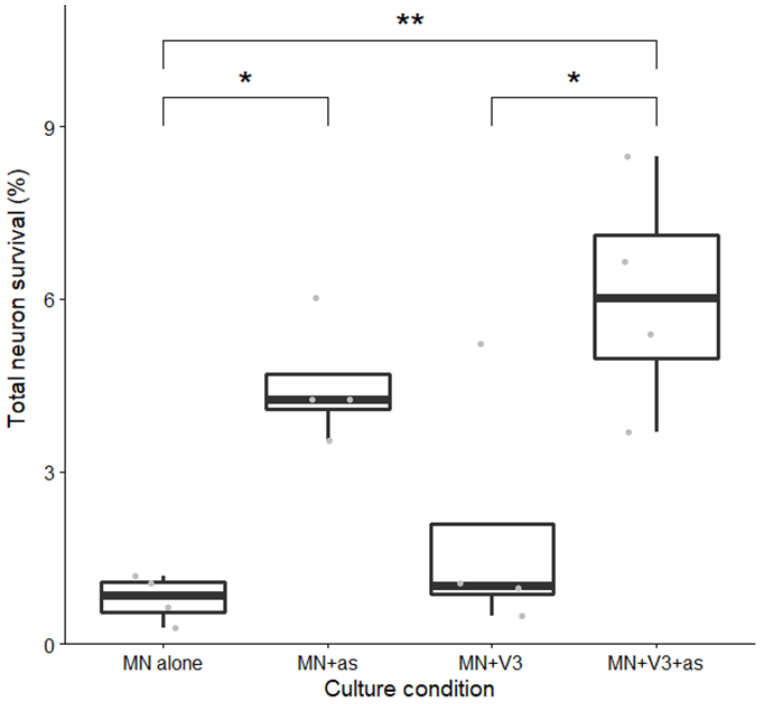

Figure 4.3: Co-culture with astrocytes increased total neuronal survival.

Percentage neuron survival was determined in week 2 co-cultures from images such as those shown in Figure 4.1 A. A uniform distribution of neurons across the coverslip was assumed. For each condition, n = 4 coverslips, each from a different differentiation. Neuronal survival was calculated as described in Chapter 2: Material and Methods, Section 2.10.2. Significance was determined with an ANOVA followed by a post hoc Tukey HSD Multiple Comparison tests. Bold horizontal lines in the boxplots show the median. * = p<0.05, ** = p<0.01, *** = p<0.001, and **** = p<0.0001

4.3.1.1 Neurons co-cultured with astrocytes had larger somas

Co-culture with astrocytes also increased the soma size of motoneurons (Figure 4.4 A and C). Motoneuronal soma area in the MN+as condition was significantly larger than in the MN alone condition (2690 ± 915μm^2 compared to 1120 ± 509μm^2, respectively; p < 2e-16 in a Kruskal-Wallis test and p < 2e-16 comparing the MN+as with the MN alone condition in a post-hoc Dunn's Multiple Comparison test; Figure 4.4 A). The same was true of motoneuronal soma diameter (30 ± 7μm compared to 20 ± 4μm in the MN+as and MN alone conditions, respectively; p < 2e-16 in a Kruskal-Wallis test and p < 2e-16 in a post-hoc Dunn's Multiple Comparison test; Figure 4.4 C).

The effect of astrocytes on soma size was not specific to motoneurons. V3 interneuron soma size was also increased by co-culture with astrocytes (Figure 4.4 B and D). The soma area of V3 interneurons in the MN+V3+as culture condition was significantly larger than in the MN+V3 culture condition (2020 ±

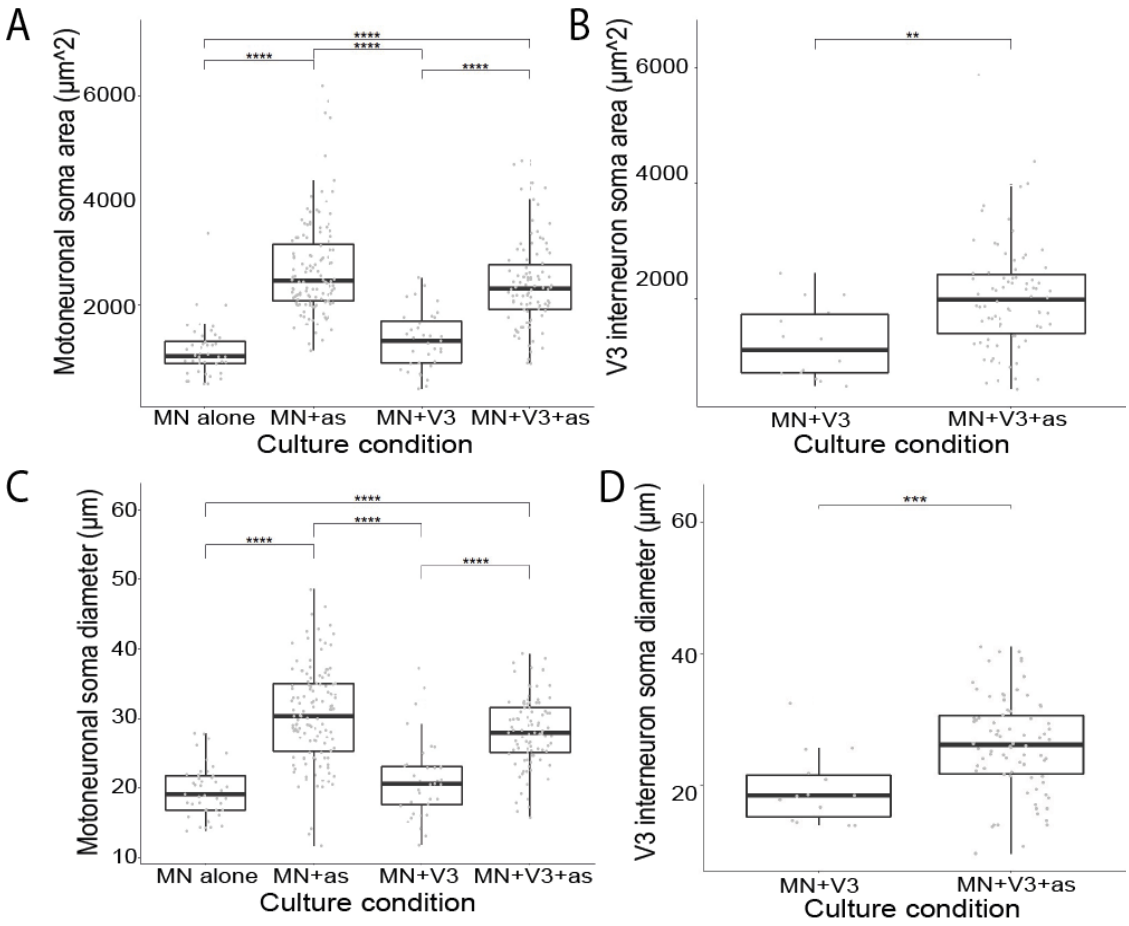

Figure 4.4: The effect of co-culture with different cell types on the soma size of motoneurons (A and C) and V3 interneurons (B and D)

A: Co-culture with astrocytes significantly increased motoneuronal soma area but co-culture with V3 interneurons had no effect. B: Co-culture with astrocytes significantly increased the soma area of V3 interneurons. C: Co-culture with astrocytes significantly increased motoneuronal soma diameter but co-culture with V3 interneurons had no effect. D: Co-culture with astrocytes significantly increased the soma diameter of V3 interneurons. For motoneurons, n = 44 for the MN alone condition, n = 128 for the MN+as condition, n = 35 for the MN+V3 condition and n = 135 for the MN+V3+as condition from four, four, three and five different differentiations, respectively. For V3 interneurons, n = 14 for the MN+V3 condition and n = 78 for the MN+V3+as condition from three different differentiations. The assumption of normality was violated for the motoneuronal data as tested by a Shapiro-Wilk test. Therefore, for the motoneuron data, a non-parametric, Kruskal Wallis test was used followed by a post hoc, Dunn's Multiple Comparison test. The V3 interneuron diameter data was found to be normally distributed by a Shapiro-Wilk test so a Welch's Two Sample t test was used to determine significance. The V3 interneuron soma area data was not found to be normally distributed by a Shapiro-Wilk test and so a Mann Whitney U test was performed to determine significance. Bold horizontal lines in the boxplots show the median. * = $p<0.05$, ** = $p<0.01$, *** = $p<0.001$, and **** = $p<0.0001$. Example images of V3 interneurons can be seen in Figure 4.2.

953μm^2 compared to 1220 ± 656μm^2, respectively; p = 0.0023, Mann Whitney U test; Figure 4.4 B) as was the soma diameter (26 ± 7μm compared to 20 ± 5μm, respectively; p = 0.0006, Welch's Two Sample t test; Figure 4.4 D). These data show that co-culture with astrocytes significantly increased the soma size of both motoneurons and V3 interneurons.

4.3.1.1 Neurite complexity was increased by co-culture with astrocytes

Characterisation of morphology in cat hindlimb motoneurons has shown that many aspects of dendrite morphology, including the number of dendritic terminals, the dendritic membrane area and the dendritic volume, are positively correlated with the diameter of the primary (also called 1st order or stem) dendrites (Cullheim et al., 1987; Ulfhake and Cullheim, 1988; Ulfhake and Kellerth, 1981, 1983). A similar correlation has been demonstrated in other types of motoneuron (Cameron et al., 1985; Fukunishi et al., 1999; Nüñez-Abades et al., 1994). Therefore, while dendrites and axons could not be distinguished in these co-cultures, the mean primary neurite diameter of cultured neurons was used as an indicator of neurite arbour size in different co-culture conditions. The number of primary neurites was also compared between co-culture conditions.

Co-culture with astrocytes had a significant effect on these measures of neuronal morphology. The mean primary neurite diameter was significantly larger when motoneurons were co-cultured with astrocytes (Figure 4.5 A; 5.4 ± 1.6μm compared to 8.7 ± 2.0μm in the MN alone and MN+as conditions, respectively; p = 2.3e-15 in a Kruskal-Wallis test and p = 8.4e-9 in a post-hoc Dunn's Multiple Comparison test comparing the MN+as and MN alone conditions). Similarly, the number of primary motoneuronal neurites was significantly increased in the MN+as condition compared to the MN alone condition (Figure 4.5 B; 5.7 ± 1.5 neurites compared to 2.8 ± 1.2 neurites, respectively; p < 2.2e-16 in a Kruskal-Wallis test and p < 2e-16 in a post-hoc Dunn's Multiple Comparison test comparing the MN+as and MN alone conditions).

The effect of astrocytes on the morphology of V3 interneurons was similar to that on motoneurons. In the MN+V3+as condition, V3 interneurons had a significantly larger mean primary neurite diameter than in the MN+V3 condition (Figure 4.5 C; 8.5 ± 1.9μm compared to 6.3 ± 2.2μm in the MN+V3+as and MN+V3 conditions, respectively; p = 0.003, Welch's Two Sample t test). Moreover, the number of

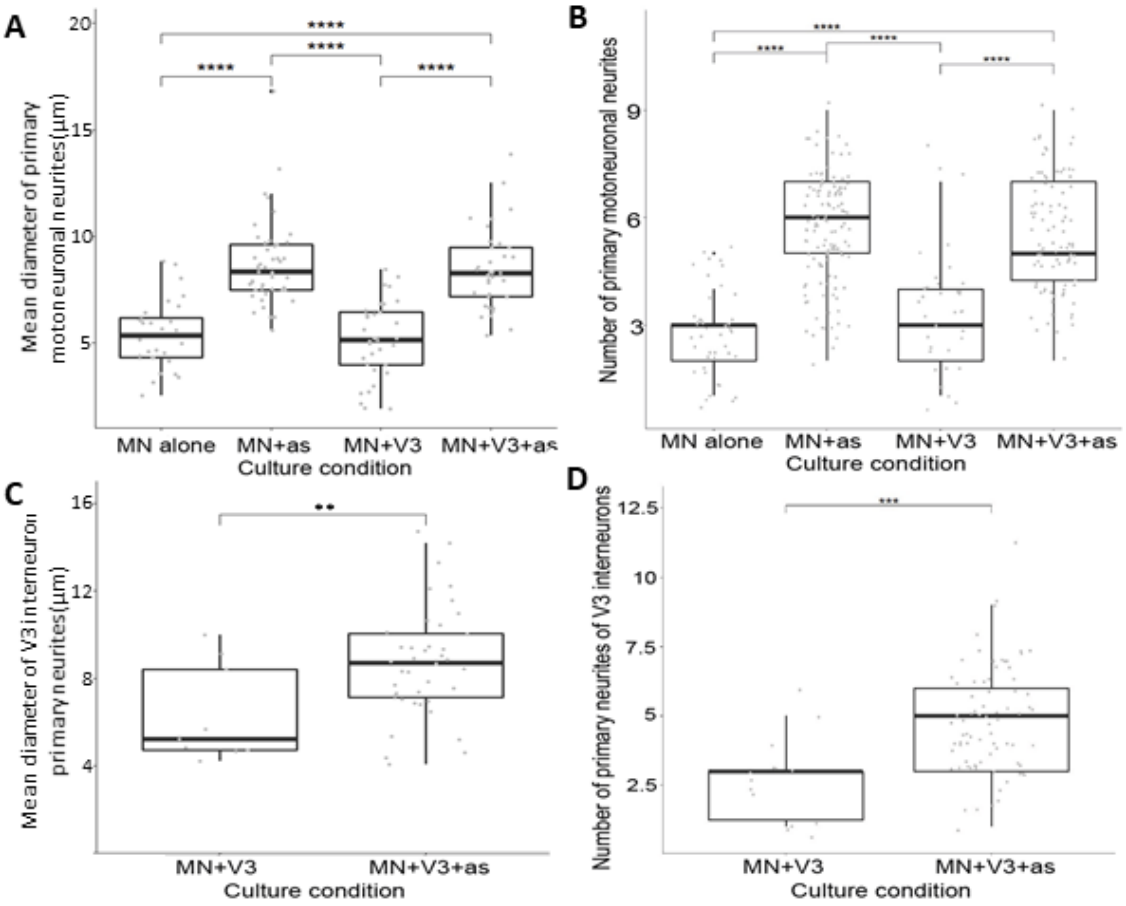

Figure 4.5: The effect of co-culture with different cell types on the number and diameter of primary neurites in motoneurons and V3 interneurons.

Co-culture with astrocytes significantly increased the mean primary neurite diameter (A) and number (B) of motoneurons, but co-culture with V3 interneurons did not have an effect. Similarly, co-culture with astrocytes significantly increased V3 interneuron mean primary neurite diameter (C) and neurite number (D). Mean neurite diameter = average of the diameter of all primary neurites of a neuron. A: For motoneurons, n = 28 for the MN alone condition, n = 45 for the MN+as condition, n = 33 for the MN+V3 condition, and n = 35 for the MN+V3+as astrocyte condition from three different differentiations. B: For motoneurons, n = 44 for the MN alone condition, n = 128 for the MN+as condition, n = 35 for the MN+V3 condition and n = 135 for the MN+V3+as condition from four, four, three and five differentiations, respectively. C: For V3 interneurons, n = 11 for the MN+V3 condition and n = 40 for the MN+V3+as condition from three different differentiations. D: For V3 interneurons, n = 14 for the MN+V3 condition and n = 78 for the MN+V3+as condition from three different differentiations.

The data in A and B was not normally distributed according to a Shapiro-Wilk test so a non-parametric, Kruskal Wallis test was used followed by a post hoc Dunn's Multiple Comparison test to determine significance. The data in C was not normally distributed so significance was determined using a Mann Whitney U test. The data in D was found to be normally distributed so a Welch's Two Sample t test was used. Bold horizontal lines in the boxplots show the median. * = $p<0.05$, ** = $p<0.01$, *** = $p<0.001$, and **** = $p<0.0001$. Example images of V3 interneurons can be seen in Figure 4.2.

primary neurites of V3 interneurons was significantly increased in the MN+V3+as culture condition compared to the MN+V3 culture condition (4.8 ± 1.9 neurites compared to 2.7 ± 1.5 neurites, respectively; p = 0.0002, Mann Whitney U test; Figure 4.5 D). Thus, co-culture with astrocytes had a significant effect on the morphology of both motoneurons and V3 interneurons.

4.3.1.1 No effect of co-culture with V3 interneurons on motoneuronal soma size or neurite morphology

In contrast to astrocytes, co-culture with V3 interneurons had no significant effect on motoneuronal soma area or diameter (p = 0.33 and 0.26, respectively, in a post-hoc Dunn's Multiple Comparison test comparing the MN alone and MN+V3 conditions; Figure 4.4 A and C). Similarly, V3 interneurons did not affect mean primary motoneuronal neurite diameter or the number of primary motoneuronal neurites (p = 1 and 0.29, respectively, in a post hoc Dunn's test comparing the MN alone and MN+V3 conditions; Figure 4.5 A and B).

To investigate the possibility of an astrocyte-dependent effect of V3 interneurons, the MN+as condition was compared to the MN+V3+as condition. No effect was observed on motoneuronal soma area or motoneuronal soma diameter (p = 0.11 and 0.065, respectively, in a post-hoc Dunn's Multiple Comparison test comparing the MN+V3+as to the MN+as condition; Figure 4.4 A and C). Neither were the mean primary motoneuronal neurite diameter nor the number of primary motoneuronal neurites (p = 1 and 0.48, respectively, in a post-hoc Dunn's Multiple Comparison test comparing the MN+V3+as to the MN+as condition; Figure 4.5 A and B) affected by V3 interneurons in an astrocyte-dependent manner. These data show that V3 interneurons had no effect on the measures of motoneuronal soma size or morphology, irrespective of the presence of astrocytes.

4.3.2 The effects of co-culture with astrocytes and V3 interneurons on motoneuronal synapse formation.

To investigate the effect of astrocytes and V3 interneurons on the number of motoneuronal synapses formed, co-cultures were labelled for a presynaptic marker, a postsynaptic marker, GFP (to mark the motoneurons), and then either tdTomato (to positively identify the V3 interneurons) or a second presynaptic marker. The postsynaptic marker used was a postsynaptic density protein, Homer1 (Hayashi et al., 2009). Two presynaptic markers were used: vGluT2,

which labels glutamatergic terminals, and vAChT, which labels cholinergic terminals. A synapse was defined as a presynaptic marker within 0.35µm of a postsynaptic Homer1 puncta. Examples of different kinds of synapse are shown in Figure 4.6. The motoneuronal density of synapses in the somatic and proximal dendritic compartments were examined (example images of compartments analysed in Figure 4.2) and the different co-culture conditions compared (Chapter 2: Materials and Methods, Section 2.10.3). Some coverslips had distinctive extracellular tubular Homer1-positive debris on them. These were excluded firstly because the Homer1 debris skewed the analysis, giving a falsely inflated value for Homer1 puncta density, and secondly because the presence of such debris suggests that the cells on the coverslip were unhealthy. Such debris was found predominantly in the MN+V3+as condition (2/5 MN+V3+as coverslips labelled) and was accompanied by a paucity of Homer1 puncta and an absence of any synapses.

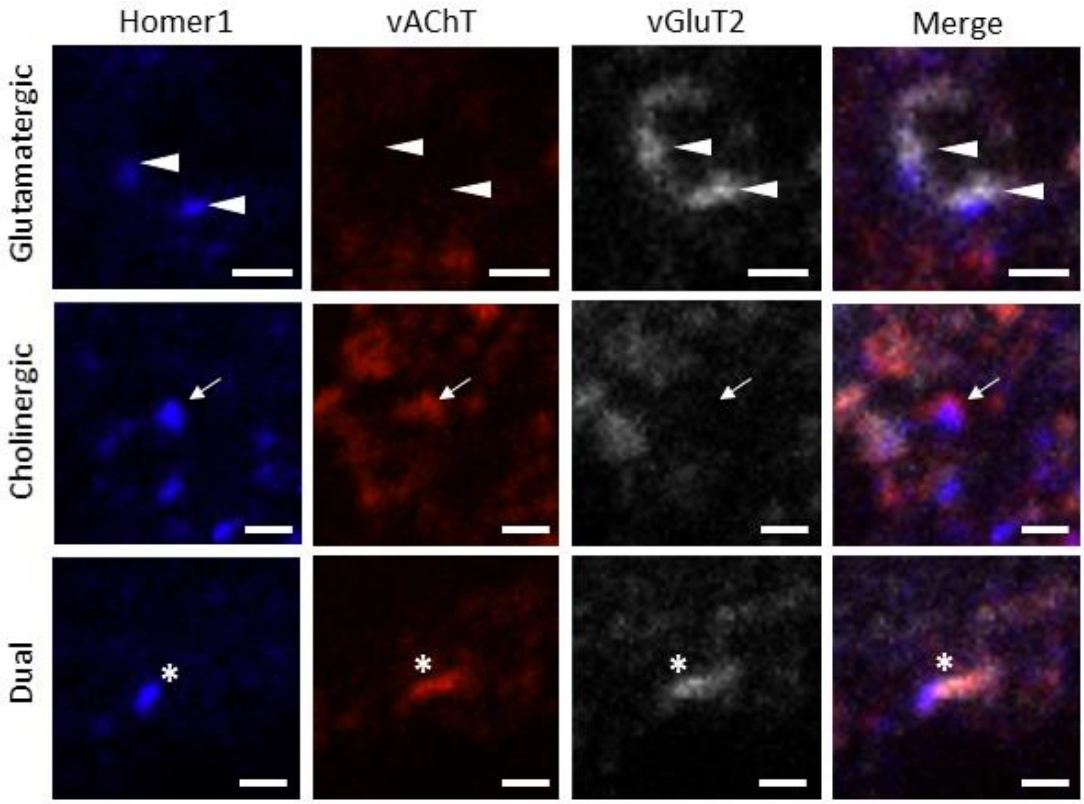

Figure 4.6: Example motoneuronal synapses labelled for either cholinergic markers, glutamatergic markers or both.

These synapses are from a motoneuron in a week 2 MN+as co-culture. Top row: An example of two glutamatergic synapses (arrowheads). Middle row: An example of a cholinergic synapse (arrows). Bottom row: An example of a 'dual synapse' labelled for both vAChT and vGluT2 (asterisks). Scale bars = 1µm.

4.3.2.1 Astrocytes promoted synapse formation in motoneuron co-cultures.

As has been previously demonstrated (Ullian et al., 2004b), astrocytes dramatically increased synapse formation in the *in vitro* motoneuron co-cultures. In astrocyte-containing co-cultures, the density of motoneuronal Homer1 puncta was significantly increased compared to the MN alone condition (0.04 ± 0.04 puncta/μm^2); this was true of both the MN+as (0.10 ± 0.05 puncta/μm^2) and the MN+V3+as (0.12 ± 0.05 puncta/μm^2) conditions (Figure 4.7 A; p = 8.2e-05 in a Kruskal-Wallis test, p = 0.002 and 0.0001 for MN+as and MN+V3+as conditions respectively compared to MN alone in a post-hoc Dunn's Multiple Comparison test). Co-culture with astrocytes also increased the density of motoneuronal cholinergic synapses (defined by presynaptic vAChT labelling; 0.05 ± 0.03 synapses/μm^2 in the MN+as condition) compared to the MN alone condition (0.01 ± 0.01 cholinergic synapses/μm^2; p = 1.7e-10 in a Kruskal-Wallis test and p = 7.3e-07 in a post-hoc Dunn's Multiple Comparison test comparing the MN alone and MN+as conditions; Figure 4.7 B). However, in the presence of astrocytes there was no statistically significantly increase in the density of motoneuronal glutamatergic synapses (Figure 4.7 C; p = 3.0e-09 in a Kruskal-Wallis test and p = 0.09 in a post-hoc Dunn's Multiple Comparison test comparing the MN+as and MN alone conditions). While this shows that co-culture with astrocytes did not affect somatic and proximal dendritic glutamatergic motoneuronal synapses, no conclusions can be drawn about more distal dendritic or axonic synapses. These data show that astrocytes were synaptogenic in co-cultures with ESC-derived motoneurons, although the regulation of different types of synapses was not uniform.

4.3.2.1 V3 interneurons increased the density of glutamatergic synapses and decreased the density of cholinergic synapses in an astrocyte-dependent manner.

While V3 interneurons did not affect motoneuronal homer1 puncta or synapse density (Figure 4.7; MN+V3 condition compared to the MN alone condition), there was an astrocyte-dependent effect of V3 interneurons on synapse formation. To investigate this effect, the MN+V3+as and MN+as conditions were compared. The addition of V3 interneurons to the co-culture resulted in a higher density of motoneuronal glutamatergic synapses in the MN+V3+as (0.07 ± 0.03 synapses/μm^2) compared to the MN+as condition (0.01 ± 0.02 synapses/μm^2;

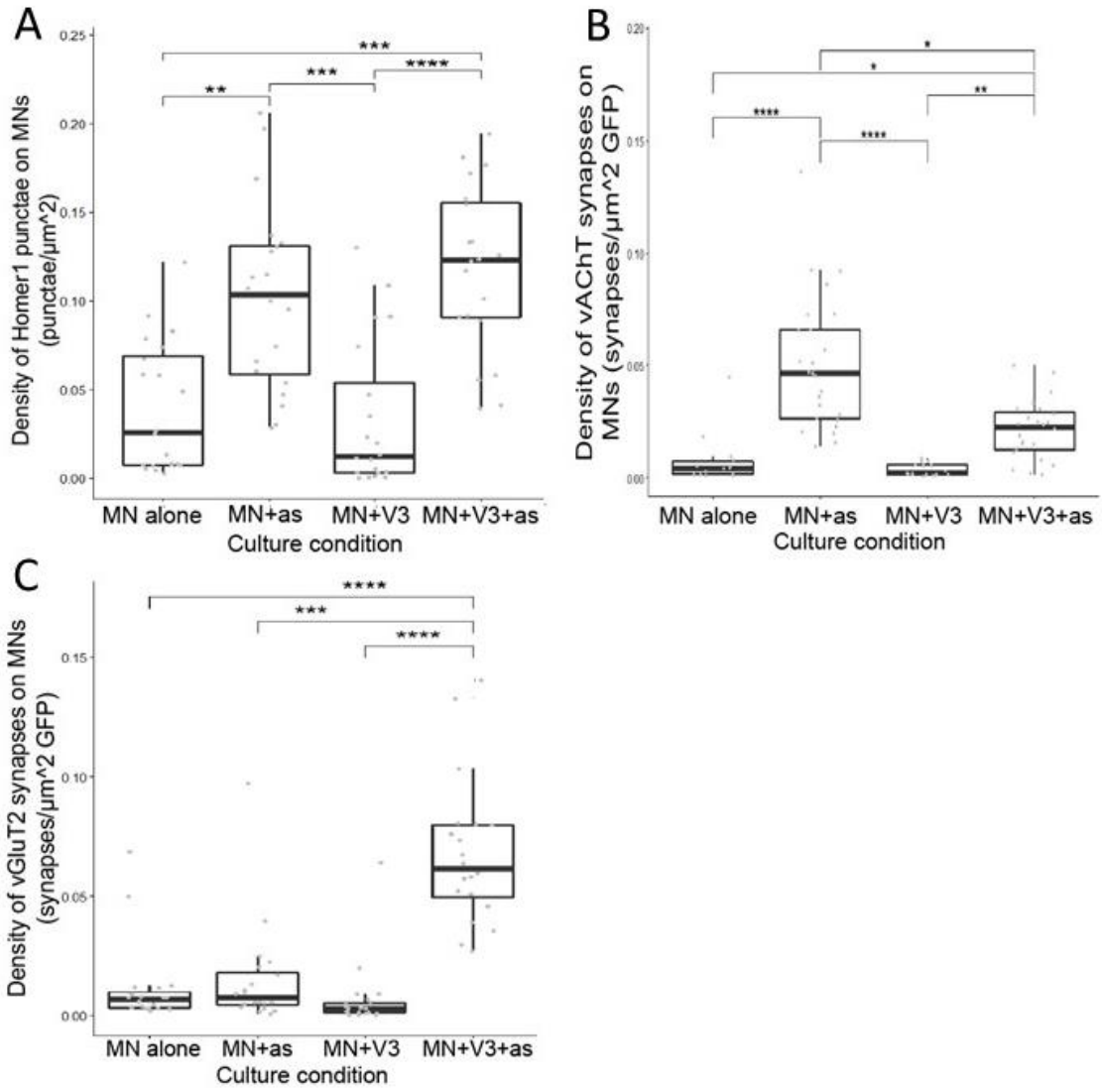

Figure 4.7: The effect of co-culture with astrocytes and V3 interneurons on the motoneuronal density of Homer1 puncta, cholinergic synapses and glutamatergic synapses.

A: Astrocytes increased the density of motoneuronal Homer1 puncta but V3 interneurons had no effect. n = 20 motoneurons from four differentiations (except the MN+V3+as conditions that had 20 motoneurons from three differentiations). B: Astrocytes increased the density of motoneuronal cholinergic synapses. V3 interneurons decreased the density of cholinergic synapses in an astrocyte-dependent manner. n = 15 motoneurons for the MN alone and MN+V3 conditions from two differentiations and n = 25 for the MN+as and MN+V3+as conditions from three differentiations. C: V3 interneurons increased the density of motoneuronal glutamatergic synapses in an astrocyte-dependent manner but neither V3 interneurons nor astrocytes had any effect alone. n = 20 motoneurons from four differentiations (except the MN+V3+as conditions that had 20 motoneurons from three differentiations). A motoneuronal synapse was defined as a GFP-positive Homer1 puncta that was <0.35µm from a presynaptic marker (vAChT or vGluT2). Bold horizontal lines in the boxplots show the median. * = p<0.05, ** = p<0.01, *** = p<0.001, and **** = p<0.0001.

p = 0.0002 in a post-hoc Dunn's Multiple Comparison test comparing the MN+V3+as and MN+as conditions; Figure 4.7 C), as might be expected given that V3 interneurons are glutamatergic. In contrast, there was a significant reduction in the density of cholinergic synapses in the MN+V3+as condition (0.02 ± 0.01 synapses/μm^2) compared to the MN+as condition (0.05 ± 0.03 synapses/μm^2; p = 0.01 in a post-hoc Dunn's Multiple Comparison test comparing the MN+V3+as and MN+as conditions; Figure 4.7 B). Thus, as well as the expected astrocyte-dependent promotion of on glutamatergic synapse formation, co-culture with V3 interneurons reduced the density of motoneuronal cholinergic synapses.

4.3.2.2 Dual synapses labelled for both cholinergic and glutamatergic presynaptic markers

In astrocyte-containing cultures, there was a persistent population of synapses labelled for both cholinergic and glutamatergic presynaptic markers (Figure 4.6, bottom row); these were defined as Homer1 puncta abutted by (<0.35µm from) both vGluT2 and vAChT labelling. Note that the vAChT and vGluT2 labelling may or may not be co-localised at such a 'dual synapse'. This population of 'dual synapses' are interesting because, from electrophysiological experiments, motoneurons are known to form synapses with mixed neurotransmitter identity with Renshaw cells (Lamotte d'Incamps et al., 2017). Despite the reduction in cholinergic synapse density in MN+V3+as co-cultures (Figure 4.7 B) and despite V3 interneurons having no effect on motoneuronal vAChT density (Figure 4.8 A), the population of 'dual synapses' was increased two-fold in the presence of V3 interneurons, from 0.008 ± 0.007 synapses/μm^2 in the MN+as condition to 0.02 ± 0.02 synapses/μm^2 in the MN+V3+as condition (Figure 4.8 B; p = 1.7e-05, Mann Whitney U test). In the MN+as condition, 33.4% ± 21.1% of Homer1 puncta apposed to vAChT labelling (cholinergic synapses) were dual synapses – i.e. also apposed to vGluT2 labelling – and 67.8 ± 19.3% of Homer 1 puncta apposed to vGluT2 labelling (glutamatergic synapses) were dual synapses – i.e. also apposed to vAChT labelling. The percentage of cholinergic synapses that were dual synapses was significantly larger in the MN+V3+as condition than in the MN+as condition (Figure 4.8 C; 67.1 ± 14.1% in the MN+V3+as condition; p = 1.7e-08, Mann Whitney U test). Conversely, the proportion of glutamatergic synapses that were dual synapses was significantly smaller in the presence of

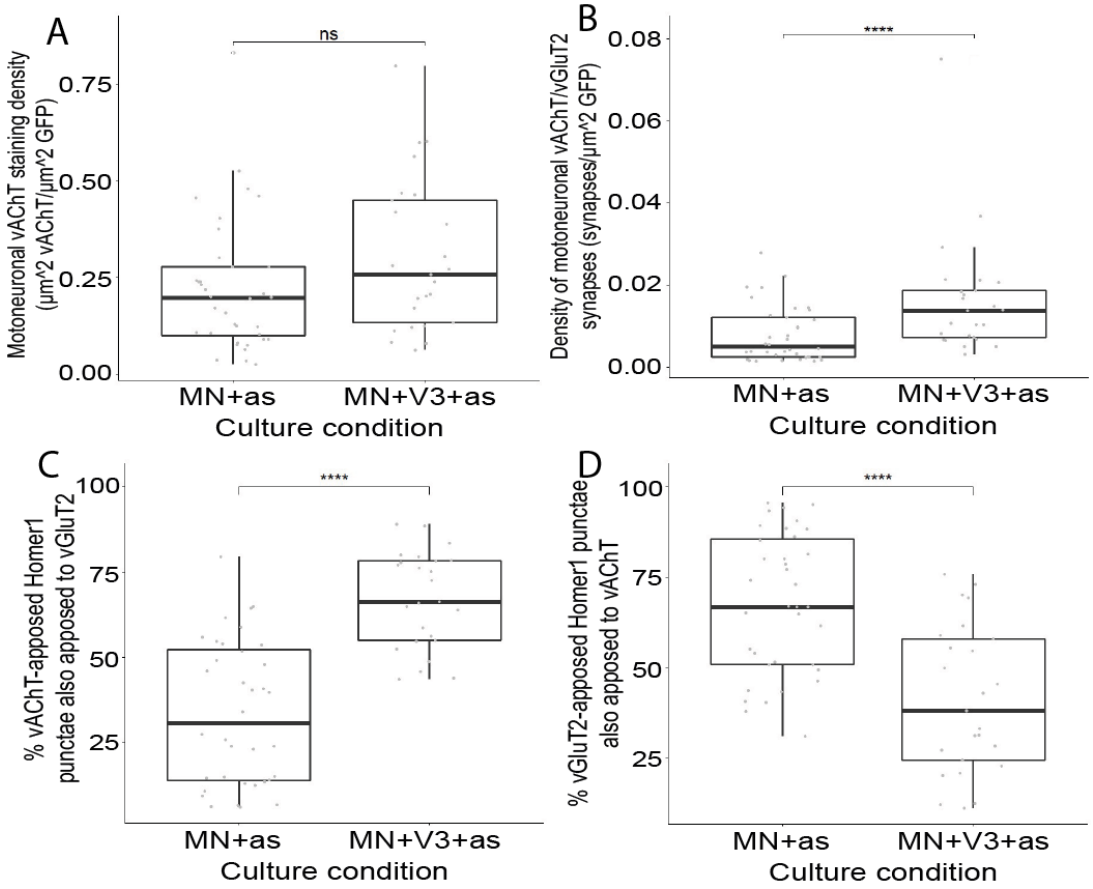

Figure 4.8: The astrocyte-dependent effect of co-culture with V3 interneurons on motoneuronal synapses labelled for both cholinergic and glutamatergic markers.

A: Co-culture with V3 interneurons had no effect on the density of vAChT expressed by motoneurons (defined as GFP-positive vAChT labelling). B: There was a small but significant increase in the number of motoneuronal synapses labelled for both vAChT and vGluT2 when motoneurons were co-cultured with V3 interneurons. C and D: The proportion of cholinergic and glutamatergic synapses that were also labelled for vGluT2 and vAChT, respectively. Note that it was difficult to resolve GFP and tdTomato labelling in the dense neuronal projections; this meant that it was difficult to determine the density of GFP-positive (motoneuronal) vAChT and vGluT2 labelling accurately. The motoneuronal vAChT labelling density could be measured because V3 interneurons did not express vAChT and so the lack of resolution did not prevent accurate measurement. However, it was difficult to distinguish the high intensity vGluT2 labelling in V3 interneurons (co-localised with tdTomato) from the fainter motoneuronal vGluT2 labelling (co-localised with GFP). Therefore, the effect of V3 interneurons on motoneuronal vAChT density could be measured and is shown in panel A, but not the effect on motoneuronal vGluT2 density. n = 36 and n = 25 motoneurons for the MN+as and MN+V3+as culture conditions respectively from two differentiations. A motoneuronal synapse was defined as a GFP-positive Homer1 puncta that was <0.35µm from a presynaptic marker. Bold horizontal lines in the boxplots show the median. ns = not significant, * = p<0.05, ** = p<0.01, *** = p<0.001, and **** = p<0.0001.

V3 interneurons (Figure 4.8 D; 41.2 ± 20.4% in the MN+V3+as condition; p = 3.4e-05, Mann Whitney U test). The population of dual synapses observed here suggests the formation of such synapses with mixed neurotransmitter identity was not dependent on the presence of Renshaw cells as there were no Renshaw cells in these co-cultures.

As mentioned above, while occasionally a motoneuronal synapse was found in which a Homer1 punctum was abutted by two separate terminals each labelled for either vAChT or vGluT2 but not both, predominantly dual synapses comprised presynaptic vesicles with co-localised vAChT and vGluT2 labelling (Figure 4.6). Indeed, 17.9 ± 14.6% and 36.6 ± 17.2% of motoneuronal vAChT labelling was colocalised with vGluT2 labelling in the MN+as and MN+V3+as culture conditions respectively (p = 7.5e-05, Mann Whitney U test). Conversely, 36.6 ± 20.4% and 26.4 ± 18.6% of motoneuronal vGluT2 labelling was colocalised with vAChT labelling in the MN+as and MN+V3+as culture conditions respectively (p = 0.05, Mann Whitney U test). This suggests that glutamatergic and cholinergic markers were generally, though not exclusively, colocalised and trafficked in the same terminals and that co-culture with V3 interneurons increased the extent of colocalization.

4.4 Discussion

4.4.1 Summary

Neuronal survival, soma size and morphological complexity of both motoneurons and V3 interneurons were all increased by co-culture with astrocytes. Furthermore, motoneurons in astrocyte-containing cultures had increased density of postsynaptic markers and cholinergic synapses in the somatic and proximal dendritic compartments. In contrast, co-culture with V3 interneurons had no effect on neuronal survival, motoneuronal soma size or morphological complexity. Nor did V3 interneurons independently affect motoneuronal synapse formation, though there was an astrocyte-dependent effect of V3 interneurons. In the presence of astrocytes, co-culture with V3 interneurons modulated the balance of glutamatergic and cholinergic synapses in the somatic and proximal dendritic compartments of motoneurons, increasing the density of glutamatergic synapses – unsurprising, given V3 interneurons are glutamatergic – and decreasing the density of cholinergic synapses. Dual synapses, labelled for both cholinergic and glutamatergic presynaptic markers, were present in the cultures, and dual synapse density was increased by co-culture with V3 interneurons in an astrocyte-dependent manner.

4.4.2 The effect of co-culture with astrocytes on neuronal soma size and neurite complexity

The improved neuronal survival, increased motoneuronal soma size and motoneuronal primary neurite diameter caused by co-culture with astrocytes is broadly consistent with recently published results in human iPSC-derived motoneuron/astrocyte *in vitro* co-cultures (Taga et al., 2019). However, unlike the results in this Chapter, Taga et al. (2019) showed no astrocyte-dependent increase in primary neurite number of motoneurons. The reason for the discrepancy is unclear. It may be a species-specific difference or due to differences in culture medium; Taga et al. (2019) enriched the culture medium with the cell adhesion molecule, laminin, which is known to promote neurite extension (Lander et al., 1985) and may be responsible for the higher number of primary neurites in the astrocyte-free condition.

Astrocytes also affect motoneuron morphology during *in vivo* development. Factors and channels expressed in ventral spinal astrocytes have been shown to

improve the survival (Molofsky et al., 2014) and increase the soma size (Kelley et al., 2018) of large alpha motoneurons, thus increasing the average soma size of the whole motoneuronal population. In the present case, however, the effect was not specific to motoneurons; V3 interneuron soma size was also increased. This lack of specificity suggests that the effect on soma size and neuronal survival in this case was due to non-specific support provided by astrocytes, such as trophic support.

4.4.3 Astrocytes had a permissive effect on synapse formation.

Consistent with previous studies *in vitro* (Taga et al., 2019; Ullian et al., 2004a), co-culture with astrocytes had a profound effect on synapse formation, likely due to their synaptogenic properties. Astrocytes promote synaptogenesis both through the secretion of synaptogenic factors and by contact-mediated mechanisms (Allen and Eroglu, 2017). For example, thrombospondins – large oligomeric extracellular matrix proteins – have been shown to promote neurite outgrowth of many neuronal subtypes *in vitro* (DeFreitas et al., 1995; Neugebauer et al., 1991; O'Shea et al., 1991; Osterhout et al., 1992). Furthermore, while V3 interneurons did affect the balance of cholinergic and glutamatergic synapses, the effects were astrocyte-dependent, suggesting the presence of astrocytes was permissive. The permissive importance of astrocytes to synapse formation was further explored in primary cultures of RGCs during development by Barker et al. (2008). They found that embryonic (E17) RGCs were able to form but not receive synapses until E19, at which stage astrocytes are generated. Additionally, they found that direct contact with astrocytes was sufficient to induce synaptic receptivity in E17 RGCs by altering the distribution of synaptic adhesion molecules. Therefore, it is likely that the presence of astrocytes in co-cultures was permissive for the formation of motoneuronal synapses and the same may be true in the present study.

4.4.4 The relevance of the synaptogenic properties of astrocytes to their effects on morphological complexity.

The synaptogenic properties of astrocytes may be related to the astrocyte-dependent increase in the number and diameter of primary neurites, in both motoneurons and V3 interneurons. In addition to increasing the density of synapses at this time point, co-culture with astrocytes promoted the formation of

neuronal networks with spontaneous excitatory activity as demonstrated in Chapter 5, Section 5.3.2.2.3. Activity has been shown to increase dendritic elaboration in motoneurons, both during development (Kalb and Hockfield, 1992) and in adulthood (Gazula et al., 2004). It may be that astrocytes increase the neurite outgrowth in these cultures by promoting the formation of active synaptic networks.

Due to the strong excitatory drive provided to motoneurons by V3 interneurons (Sternfeld et al., 2017) and the role excitatory activity has been shown to play in increasing the size and complexity of the dendritic arbour (Inglis et al., 1998, 2002; Kalb and Hockfield, 1992), it was surprising that V3 interneurons had no significant effect on the number or diameter of primary neurites. This may be because there was already spontaneous excitatory activity present astrocyte-containing cultures (Chapter 5, Section 5.3.2.2.3), likely due to the astrocyte-dependent formation of motoneuron-to-motoneuron synapses, and V3 interneuron-derived activity did not have an additional effect.

4.4.5 In an astrocyte-dependent manner, V3 interneurons change the balance of glutamatergic and cholinergic synapses.

In vivo, V3 interneurons form monosynaptic glutamatergic synapses with motoneurons (Chopek et al., 2018; Zhang et al., 2008b) and can be characterised by their vGluT2 expression (Xu et al., 2015). Therefore, it was not surprising that co-culture with V3 interneurons (in the presence of astrocytes) significantly increased the density of motoneuronal glutamatergic synapses. In contrast, co-culture with V3 interneurons significantly decreased the density of motoneuronal cholinergic synapses in the proximal dendritic and somatic compartments, meaning either that fewer motoneuronal cholinergic synapses were formed in the presence of V3 interneurons or that the cholinergic synapses were redistributed to the distal dendrites of the motoneurons. These effects of V3 interneurons on motoneuronal synapse formation and/or distribution could be due to the increase in the level of glutamate caused by the increased spontaneous glutamatergic activity in the co-cultures from the V3 interneurons (Chapter 5). Glutamate has been shown to affect synapse formation, elimination and plasticity by regulating astrocytic factors in a putatively homeostatic manner (Allen and Eroglu, 2017); indeed, knocking out *vGluT2* (and therefore a great portion of glutamatergic transmission) caused malformation of excitatory synapses in the brainstem of

E18.5 mutant mice (Wallén-Mackenzie et al., 2006). In another example, treatment of hippocampal astrocytes with glutamate caused a two-fold increase in astrocytic SPARC expression (Jones et al., 2011). SPARC has been shown to prevent the maturation of (Albrecht et al., 2012) and promote the elimination of (López-Murcia et al., 2015) autaptic cholinergic synapses in primary cultures of rat neonatal superior cervical ganglion neurons *in vitro*. These results are supported by *in vivo* evidence; the injection of a SPARC-derived peptide in to the tail of *Xenopus tropicalis* tadpoles caused the reversible elimination of cholinergic NMJs (López-Murcia et al., 2015). Thus, the increased amount of glutamate in the more spontaneously active MN+V3+as co-cultures might cause a reduction in the density of motoneuronal cholinergic synapses.

4.4.6 The expression of vGluT2 by motoneurons

While it is clear from electrophysiological experiments that motoneurons form synapses with a glutamatergic component *in vitro* (Chapter 5, Section 5.3.2.2.3; Sternfeld et al., 2017; Ullian et al., 2004a) and *in vivo* (Bhumbra et al., 2014; Lamotte d'Incamps et al., 2017; Mentis et al., 2005), the results from studies looking at motoneuronal expression of vesicular glutamate transporters such as vGluT2 are mixed. Some studies present evidence from immunohistochemical (Borgius et al., 2010; Herzog et al., 2004; Nishimaru et al., 2005) and in situ hybridisation (Herzog et al., 2004; Landry et al., 2004) experiments supporting the expression of vGluT2 (and vGluT1) in rodent spinal motoneurons. Others failed to find evidence of vGlut2 (or vGluT1) in mammalian spinal motoneurons by immunohistochemical methods (Liu et al., 2009; Mentis et al., 2005; Oliveira et al., 2003) or by in situ hybridisation methods (Gezelius et al., 2006; Kullander et al., 2003; Oliveira et al., 2003). The discrepancy may, in some cases, be due to the method by which motoneurons were identified; Mentis et al (2005) used the combination of vAChT labelling and retrograde labelling to identify motor axon terminals. As has been demonstrated in this Chapter, presynaptic vGluT2 and vAChT labelling does not necessarily overlap in motoneurons. Moreover, neurotransmission at different synapses in the same spinal motoneurons may have different neurotransmitter dependencies (Bhumbra and Beato, 2018; Lamotte d'Incamps et al., 2017), meaning vAChT labelling may not be sufficient to label all motoneuronal synapses. Furthermore, it has been speculated that some of the methods used may not be sensitive enough to detect low levels of

mRNA or protein expression (Oliveira et al., 2003), though this has been disputed (Gezelius et al., 2006). In the present study, vGluT2 labelling was observed in ESC-derived motoneurons cultured *in vitro*. However, the presence of vGluT2 expression in spinal motoneurons remains an unresolved question.

4.4.7 The glutamatergic postsynaptic marker, Homer1, apposed the presynaptic cholinergic marker, vAChT.

Motoneurons in culture expressed the presynaptic cholinergic marker, vAChT. Surprisingly, vAChT often apposed the postsynaptic glutamatergic marker, Homer1. Homer1 is enriched at excitatory synapses (Brakeman et al., 1997; Xiao et al., 1998) and facilitates synaptic glutamate signalling (Brakeman et al., 1997; Tu et al., 1998; Xiao et al., 1998) and glutamatergic receptor cycling (Nakano-Kobayashi et al., 2014). Without labelling for a postsynaptic marker specific to cholinergic synapses, it is impossible to determine whether these vAChT/Homer1 synapses expressed a mix of glutamate and acetylcholine receptors postsynaptically or only glutamatergic receptor machinery. Indeed, the lack of a postsynaptic marker for cholinergic synapses in these experiments meant the values of cholinergic synapse density might be underestimated.

4.4.8 Dual synapses

In astrocyte-containing co-cultures, there was a small population of motoneuron-to-motoneuron synapses labelled for both cholinergic and glutamatergic presynaptic markers. Motoneurons are known to form synapses of mixed neurotransmitter identity with Renshaw cells *in vivo* (Bhumbra et al., 2014). However, there were no Renshaw cells present in these co-cultures, so the presence of dual synapses was surprising. Usually, vAChT and vGluT2 labelling co-localised, though occasionally single Homer1 puncta were apposed to separate vAChT and vGluT2 vesicles. The co-localisation of presynaptic vAChT and vGluT2 (and other neurotransmitter transporters) in motoneurons has been observed in electroplaques of *Torpedo californica*; indeed, in this study 88% of vAChT-positive vesicles were also positive for vGluT2 (Li and Harlow, 2014). Here, a smaller percentage of vAChT-positive vesicles were found to be positive for vGluT2 (17.9 ± 14.6% in the MN+as condition and 36.6 ± 17.2% in the MN+V3+as condition). In contrast to the results presented here and by Li and Harlow (2014), Herzog et al (2004) found no or less overlap between vGluT2 and

vAChT vesicles in adult rat motoneurons and proposed that individual motoneuronal collaterals contained either one or the other. The source of this discrepancy could be the differing species (rat vs mouse), differing ages (adult vs embryonic), or differing model (primary vs stem cell-derived motoneurons). Furthermore, as mentioned above, the presence of vGluT2 in motoneurons at all remains a controversial issue.

The dual-labelled synapse population increased in the presence of V3 interneurons (in an astrocyte-dependent manner) despite the concurrent reduction of cholinergic synapses (at least in the somatic and proximal dendritic compartments). The persistence of the dual-labelled population may indicate that they were active and therefore resistant to the activity-dependent competition, which often plays a role in synapse elimination (Chung and Barres, 2012).

5 Chapter 5: The effect of co-culture with astrocytes and V3 interneurons on the development of electrophysiological properties in motoneurons

5.1 Introduction: The electrophysiological maturation of stem cell-derived motoneurons *in vitro*

The electrophysiological properties of motoneurons change significantly during *in vivo* development and are essential for motoneuron function (Chapter 1: General Introduction, Section 1.5.2). Many aspects of *in vivo* electrophysiological motoneuronal maturation also occur in murine ESC-derived (Miles et al., 2004) and iPSC-derived (Toma et al., 2015) motoneurons in mixed stem cell-derived cultures *in vitro*; these include a decrease in input resistance, increase in capacitance, increase in firing frequency and an increase in the proportion of motoneurons capable of repetitive firing. Therefore, electrophysiological properties can be used as an indicator of motoneuron maturation, and co-culture of motoneurons with other cell types can be used to parse out which elements of electrophysiological maturation are cell intrinsic and which are influenced by other cells such as V3 interneurons and/or astrocytes.

To investigate the cell intrinsic elements of electrophysiological maturation, McCreedy et al (2015) purified motoneurons from an ESC line transgenically-altered to be puromycin resistant by puromycin-selection and monitored their electrophysiological properties over time *in vitro*. The pure motoneuron cultures developed repetitive firing in response to depolarising current pulses and displayed Spike Frequency Adaptation (SFA). They also demonstrated motoneuronal voltage-gated Na^+, K^+ and Ca^{2+} currents and the presence of functional AMPA, glycine and GABA receptors. This demonstrated that a level of motoneuronal maturation could be achieved without the presence of or contact with any other cell type. However, the motoneuron culture media included many growth factors normally released by non-neuronal cells, which are known to influence motoneuron maturation. Indeed, pure populations of ESC-derived motoneurons cultured with pure populations of astrocytes displayed many of the same signs of maturation that are observed in mixed stem cell culture and *in vivo* (Bryson et al., 2014; Machado et al., 2019). Astrocytes regulate the electrophysiological properties of motoneurons by manipulating the extracellular concentrations ions, including K^+ ions (Kelley et al., 2018), Ca^{2+} ions (Morquette

et al., 2015). Therefore, while it is known that motoneurons mature electrophysiologically *in vitro* to some extent when cultured both with and without other cell types, it is unclear which of these processes of maturation were cell-autonomous.

5.2 Aims of this Chapter

Given the importance of motoneuronal electrophysiology to motoneuron maturation and function, and the role that activity and astrocytes play in modulating it, in this Chapter I aimed to determine the effects of co-culturing ESC-derived motoneurons with astrocytes and V3 interneurons, separately and together, on the maturation of passive and active motoneuronal electrophysiological properties *in vitro*.

5.3 Results

To investigate the role of V3 interneurons (V3) and astrocytes (as) in motoneuron (MN) maturation *in vitro*, co-cultures of pure populations of the different cell types were produced from ESCs in different combinations: MN alone, MN+as, MN+V3 and MN+V3+as (Chapter 2: Materials and Methods, particularly Section 2.5). The development of motoneuronal electrophysiological properties in each culture condition was measured by single cell patch-clamp (Chapter 2: Materials and Methods, Section 2.12) and compared. In the astrocyte-free conditions, cultured cells generally did not survive beyond 2 weeks *in vitro*, so electrophysiological properties for these conditions were measured in weeks 1 and 2. Neurons in the astrocyte-containing conditions survived up to week 4, so electrophysiological properties for these conditions were measured in weeks 1, 2, 3 and 4. The method by which each electrophysiological property was determined is described in Chapter 2: Materials and Methods, Section 2.12.1. The dot-line graphs in Figure 5.1 show the change in each motoneuronal electrophysiological property discussed between week 1 and week 2 for each co-culture condition.

5.3.1 Development of motoneuronal electrophysiological properties over time

When pure populations of ESC-derived MNs were cultured alone *in vitro*, many electrophysiological properties developed (Table 5.1) on a trajectory comparable to that reported for embryonic and postnatal MNs *in vivo*, indicating that some aspects of electrophysiological maturation are cell type-autonomous. To investigate these effects in my model, I first looked at the development of electrophysiological properties in the MN alone condition between week 1 and week 2.

5.3.1.1 RMP and passive membrane properties

As motoneuron morphology develops over time, so do the resting electrophysiological properties. Motoneurons in the MN alone condition showed an RMP of -59 ± 7mV in week 1. Consistent with findings from ESC-derived MNs in mixed cultures (Miles et al., 2004), the RMP became more hyperpolarised over time (-71 ± 6mV in week 2; $p = 0.0006$, Welch's Two Sample t test; Table 5.1), indicating that the potassium equilibrium potential and the permeability of channels open at this potential changed in motoneurons from week 1 to week 2. As has been unfailingly observed in studies of motoneuron development *in vivo*

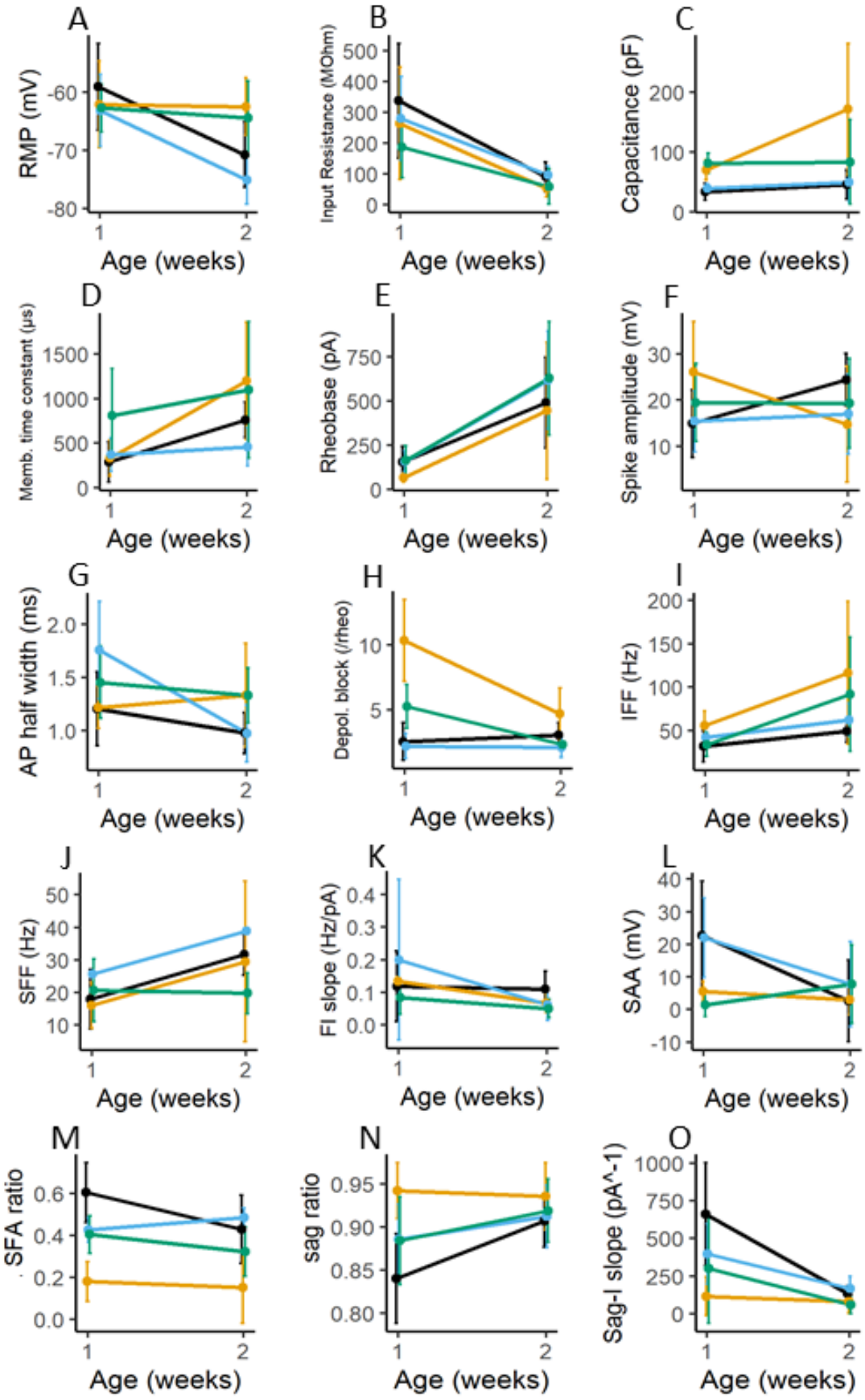

Figure legend on next page…

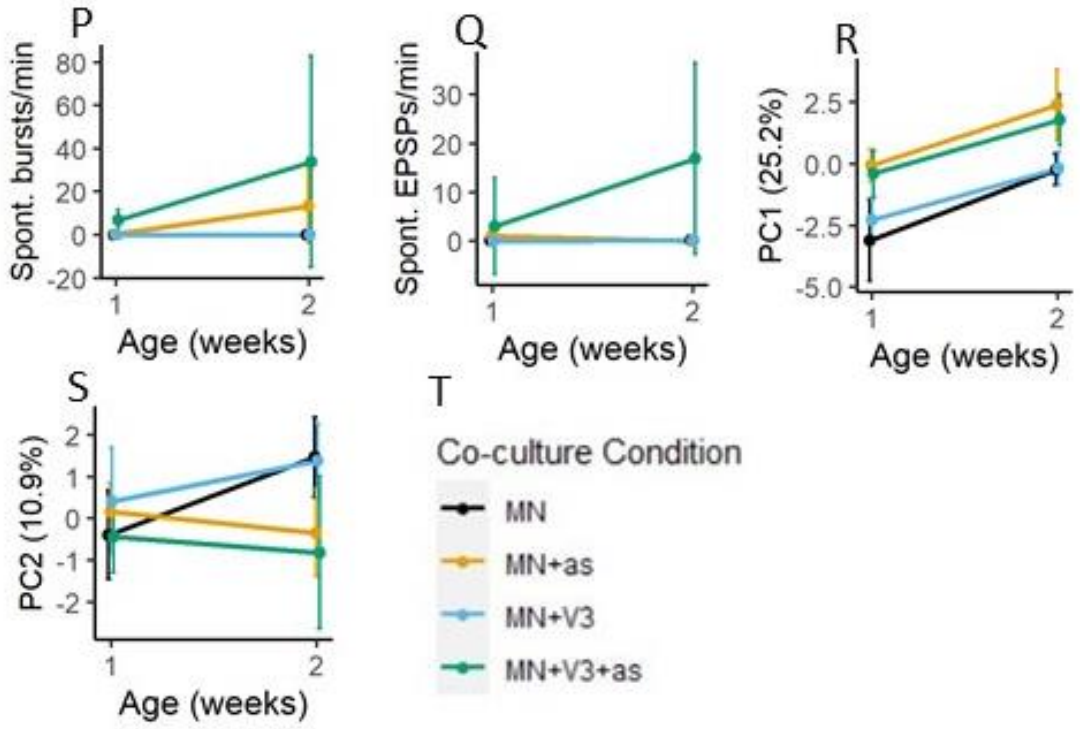

Figure 5.1: Plots showing the change in motoneuronal electrophysiological properties between week 1 and week 2 for different co-culture conditions.

Each point is the mean for that co-culture condition and the error bars represent standard deviation. AP = Action Potential. A: RMP = resting membrane potential. B: input resistance. C: Capacitance. D: memb. time constant = membrane time constant E: Rheobase. F: Spike amplitude = AP amplitude at rheobase. G: AP half width. H: depol. block (/rheo) = multiple of rheobase at which depolarisation block occurred. I: IFF = Initial Firing Frequency. J: SFF = Steady-state Firing Frequency. K: FI slope = SFF-current slope. L: SAA = Spike Amplitude Adaptation. M: SFA ratio = spike frequency adaptation ratio. N: sag ratio = sag ratio. O: sag-I slope = sag-current slope. P: spont. bursts/minute = spontaneous burst frequency (bursts/min). Q: spont. EPSPs/minute = spontaneous EPSP frequency (EPSPs/min), PC = principle components. PC1 (R) and PC2 (S) derived from a dimensionality reduction analysis of the results described in Section 5.3.5. The % in brackets shows the variance of the dataset captured by the PC. n of each property can be found in the respective tables. T: The legend. MN alone = black, MN+as = yellow, MN+V3 = blue, and MN+V3+as = green.

Table 5.1: Electrophysiological properties of motoneurons cultured alone *in vitro*

Values are given as the mean ± standard deviation (n). ∞ denote a comparison between weeks 1 and 2; p<0.05 = ∞, p<0.01 = ∞∞, p<0.001 = ∞∞∞.

Co-culture condition: MN alone		
Electrophysiological property	**Week 1**	**Week 2**
Proportion motoneurons that fire	14/14 (100%)	7/8 (88%)
Proportion motoneurons that display repetitive firing	10/14 (71%)	6/7 (86%)
Proportion motoneurons that sustain firing to the end of a 500ms square pulse	8/14 (57%)	5/7 (71%)
Proportion of motoneurons which can sustain firing that display depolarisation block	8/8 (100%)	(2/5) (40%)
Proportion of motoneurons firing doublets or triplets at rheobase	0/14 (0%)	0/7 (0%)
Proportion of motoneurons displaying rebound action potentials	2/13 (15%)	0/7 (0%)
Resting membrane potential (mV)	-59 ± 7 (14)	-71 ± 6 (8) $^{\infty\infty\infty}$
Input resistance (MOhm)^	338 ± 187 (14)	91 ± 48 (8) $^{\infty\infty\infty}$
Capacitance (pF)^	34 ± 14 (13)	46 ± 24 (8)
Membrane time constant (µs)^	286 ± 226 (13)	762 ± 198 (8) $^{\infty\infty\infty}$
Rheobase (pA)^	154 ± 90 (14)	491 ± 259 (7) $^{\infty\infty\infty}$
Action potential amplitude at rheobase (mV)	15 ± 7 (14)	24 ± 6 (7) $^{\infty\infty}$
Action potential half width (ms)^	1.2 ± 0.4 (11)	1.0 ± 0.2 (5)
Multiple of rheobase at which depolarisation block occurs^	2.56 ± 1.45 (8)	3.08 ± 0.93 (2)
Spike amplitude adaptation at 2 x rheobase (mV)^	23 ± 17 (9)	3 ± 13 (5) $^{\infty}$
Initial firing frequency (IFF) (Hz)	31.7 ± 18.1 (9)	49.0 ± 12.9 (5) $^{\infty}$
Steady-state firing frequency (SFF) (Hz)	17.8 ± 9.1 (5)	31.7 ± 6.3 (5) $^{\infty}$
FI slope (SFF) (Hz/pA)^	0.12 ± 0.11 (7)	0.11 ± 0.05 (5)
Spike frequency adaptation ratio (SFA)^	0.60 ± 0.14 (8)	0.43 ± 0.17 (5)
Sag ratio	0.84 ± 0.05 (13)	0.91 ± 0.03 (7) $^{\infty\infty}$
Slope of sag ratio-current graph (pA^{-1})^	663 ± 342 (13)	132 ± 53 (7) $^{\infty\infty\infty}$
Spontaneous burst frequency (bursts/min)^	0.00 ± 0.00 (14)	0.00 ± 0.00 (8)
Spontaneous EPSP frequency (EPSPs/min)^	0.25 ± 0.94 (14)	0.25 ± 0.71 (8)
PC1^	-3.11 ± 1.65 (14)	-0.23 ± 0.63 (8) $^{\infty\infty\infty}$
PC2^	-0.39 ± 1.06 (14)	1.47 ± 0.96 (8) $^{\infty\infty\infty}$

and *in vitro* (Table 1.4 in Chapter 1), the input resistance decreased over time (from 338 ± 187MOhms to 91 ± 48MOhms; p = 0.0002, Mann Whitney U test; Table 5.1), likely reflecting increased density and maturation of channels open at this potential over time. However, in contrast to previous studies of ESC-derived motoneurons in mixed culture (Miles et al., 2004), no significant change in capacitance was observed between motoneurons in week 1 and 2 in these MN alone co-cultures (from 34 ± 14pF to 46 ± 24pF; p = 0.3, Mann Whitney U test). As whole cell capacitance is related to neuronal size, this may indicate that motoneurons in the MN alone condition did not change in size between weeks 1 and 2 as would be expected. In addition, the membrane time constant increased between weeks 1 and 2 (from 286 ± 226µs to 762 ± 198µs; p = 0.0007, Mann Whitney U test), despite the observations in studies of motoneuron development *in vivo* that the membrane time constant decreased (Carrascal et al., 2005; Martin-Caraballo and Greer, 1999). An increase of membrane time constant means that the motoneurons were more able to sum consecutive stimuli and so less able to distinguish between stimuli. These data suggest that, although there were some commonalities, the passive membrane properties of ESC-derived MNs cultured alone did not mature in exactly the same way to those in mixed cultures or *in vivo*.

5.3.1.2 Active membrane properties

Although motoneuronal activity is influenced by the passive properties of the membrane, it depends on the action and interaction of voltage-dependent ion channels. As the ion channel complement expressed in the membrane changes during development, so do the active membrane properties (Figure 5.2; Table 5.1).

5.3.1.2.1 Sag and rebound action potentials

The hyperpolarisation-activated depolarising current (I_h) contributes to motoneuron firing and can be modulated by various neurotransmitters. The development of I_h can be investigated by looking at the emergence of sag potentials and Rebound Action Potentials (RAPs) (Figure 5.2 A and B, respectively). In motoneurons alone in culture, Ssag ratio was found to increase from week 1 to week 2 (from 0.84 ± 0.05 to 0.91 ± 0.03; p = 0.0020, Welch's Two Sample t test) and the slope of the sag ratio-current graph became

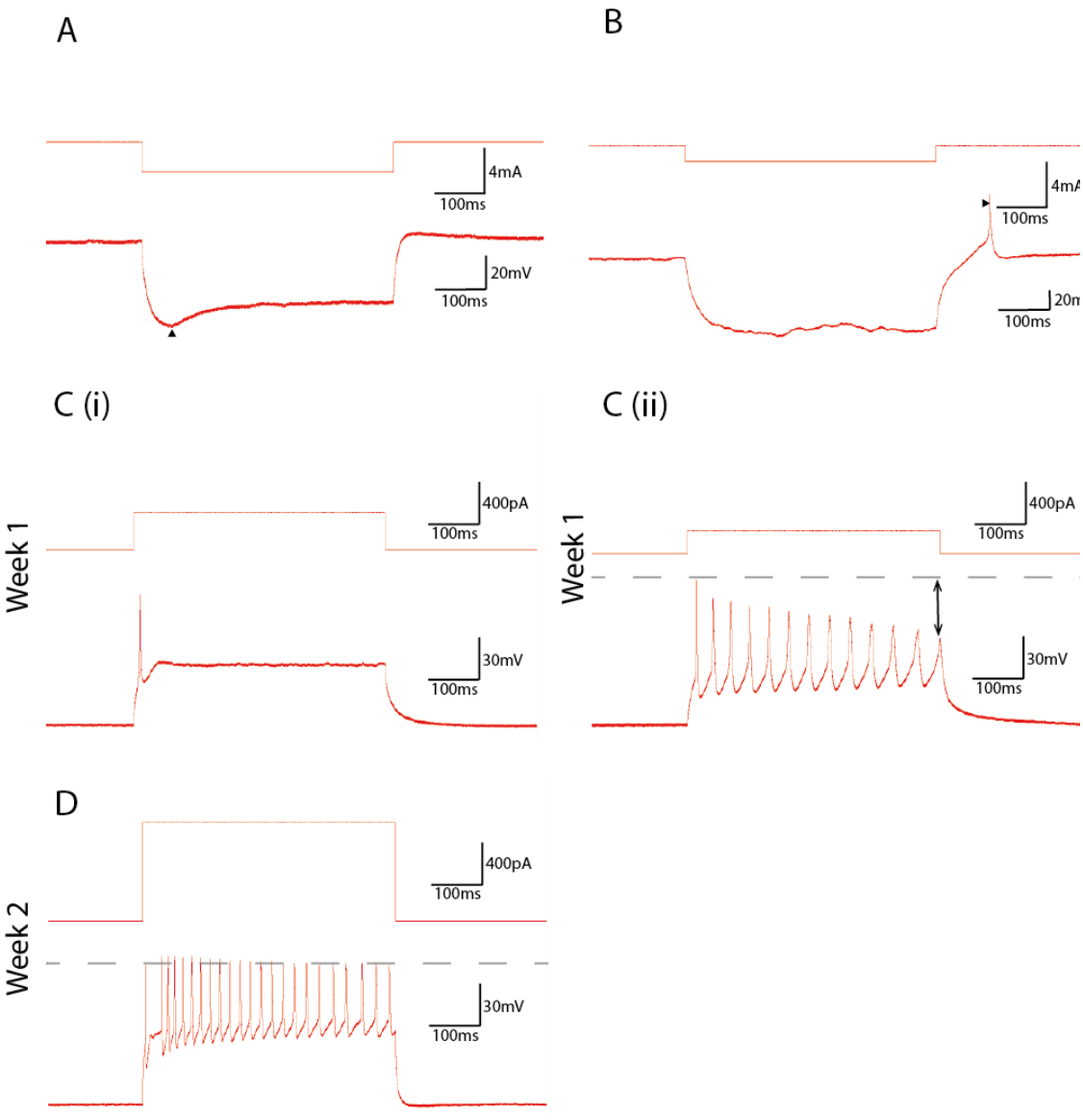

Figure 5.2: Active properties of motoneurons cultured alone.

In each panel, the upper trace shows the current injected and the lower trace shows the resulting change in voltage. A: During a 500ms hyperpolarising current injection, sag potential was observed (black arrowhead) in the MN alone condition. B: In some motoneurons in the MN alone condition, following a 500ms hyperpolarising current injection, there was a rebound depolarisation or a rebound action potential (black arrowhead). C: Traces from two different week 1 motoneurons in the MN alone condition recorded during a 500ms current injection at 2 x rheobase. (i) A motoneuron only capable of firing single action potentials. (ii) A motoneuron capable of firing repetitive action potentials and sustaining firing throughout the current pulse. Note the spike amplitude adaptation; the dashed line = first spike amplitude and the double-headed arrow = spike amplitude adaptation. D: Trace from a week 2 motoneuron in the MN alone condition recorded during a 500ms current injection at 2 x rheobase. Motoneurons at this time point were capable of sustained repetitive firing and had reduced spike amplitude adaptation (the dashed line = first spike). All traces were recorded from week 1 cultures except D.

significantly shallower (from 663 ± 342 in week 1 to 132 ± 53 in week 2; p = 2.6e-05, Mann Whitney U test). The proportion of motoneurons which displayed RAPs slightly decreased from week 1 to week 2 (2/13 in week 1 to 0/7 in week 2).

5.3.1.2.2 Firing properties

As motoneurons mature, they become more capable of firing action potentials at increasing frequencies (Table 1.4 in Chapter 1). In the MN alone co-culture conditions, all motoneurons recorded from were capable of firing action potentials, apart from one motoneuron examined at week 2 (Table 5.1). As observed in previous studies (Table 1.4 in Chapter 1), rheobase increased from week 1 to week 2 (from 154 ± 90pA to 491 ± 259pA; p = 0.0003, Mann Whitney U test), indicating that motoneurons became less excitable over time. The proportion of firing motoneurons capable of repetitive firing increased slightly between weeks 1 and 2 (10/14 in week 1 and 6/7 in week 2, Table 5.1), as did the initial and steady-state firing frequencies at 2 x rhoebase (IFF and SFF) (IFF: from 31.7 ± 18.1Hz in week 1 to 49.0 ± 12.9Hz in week 2; p = 0.042, Welch's Two Sample t test; SFF: from 17.8 ± 9.1Hz in week 2 to 31.7 ± 6.3Hz in week 2; p = 0.026, Welch's Two Sample t test) (compare Figure 5.2 Ci and C ii with Figure 5.2 D). However, there was no change in FI slope and no significant decrease in SFA ratio with time (Figure 5.3; p = 1 and 0.12 respectively, Mann Whitney U test; Table 5.1). The proportion of motoneurons that could sustain firing to the end of the pulse also increased slightly from week 1 to week 2 (8/14 in week 1 and 5/7 or in week 2; Table 5.1). The proportion of motoneurons able to fire repetitively that displayed depolarisation block within the range of current intensities tested decreased from week 1 to week 2 (8/8 in week 1 to 2/5 in week 2; Table 5.1), as did the spike amplitude adaptation (a numerical indicator of depolarisation block; from 23 ± 17mV in week 1 to 3 ± 13mV in week 2; p = 0.0290, Mann-Whitney U test; compare Figure 5.2C(ii) to Figure 5.2D). These findings indicate that motoneurons were more capable of repetitive firing over a larger range of stimulus intensities. Thus, excepting SFA ratio, the ability of ESC-derived motoneurons cultured alone matures to fire trains of repetitive action potentials in a similar way to that reported for motoneurons studied *in vivo*.

As the complement of ion channels expressed on a motoneuron matures, the shape of the action potential changes. For example, spike amplitude at rheobase

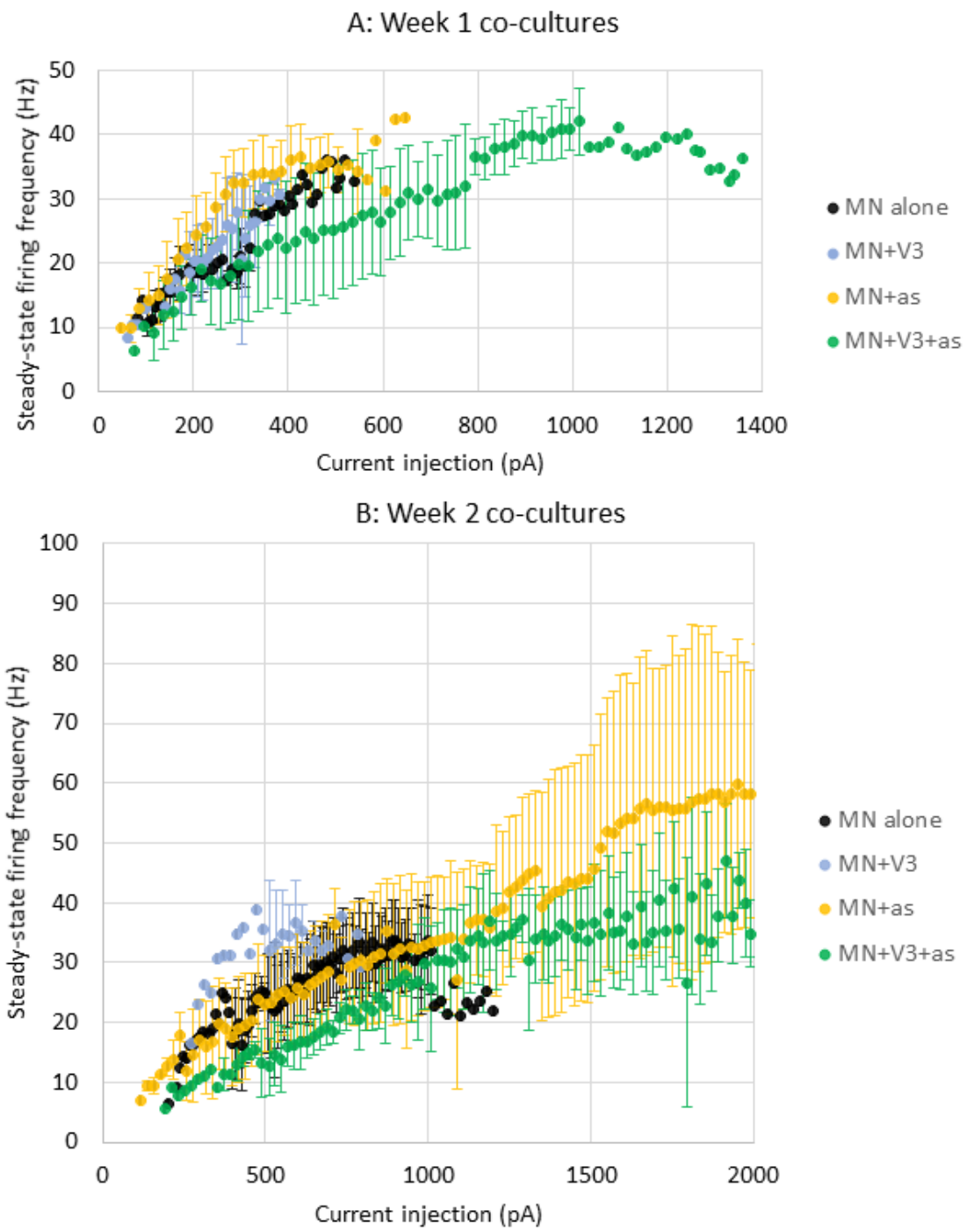

Figure 5.3: Plots of steady-state firing frequency (SFF) against current injected for each co-culture condition in week 1 (A) and week 2 (B).

The legend is on the right of each graph. Each point is the mean SFF for all motor neurons firing at that current intensity. Error bars show standard deviation at each current intensity. Points without an error bar thus suggest that only one motor neuron recorded from was firing at that current intensity. Note that the motor neurons were not driven to their maximum firing frequency so maximum SFF cannot be derived from these graphs.

increased (from 15 ± 7mV in week 1 to 24 ± 6mV in week 2; p = 0.0049, Welch's Two Sample t test). However, no significant change in action potential half-width was observed, despite previous findings both *in vivo* and *in vitro* indicating that a decrease was to be expected as motoneurons matured (Chapter 1: General Introduction, Table 1.4).

5.3.1.2.3 Absence of spontaneous activity in motoneurons cultured alone

As the spinal cord develops, spontaneous activity is observed in spinal neuronal networks. However, no spontaneous activity and few putative spontaneous EPSPs were observed in cultures of pure ESC-derived motoneurons (Table 5.1). No difference between weeks 1 and 2 was observed.

Altogether these data show that the maturation of some active and passive electrophysiological properties in ESC-derived MNs such as input resistance and rheobase did not require the presence of other cells in culture but that other properties such as spontaneous activity did not mature in these pure motoneuronal cultures.

5.3.2 The effect of astrocytes on individual electrophysiological properties of motoneurons and their development over time.

To investigate the effect of astrocytes on motoneuron maturation, pure populations of ESC-derived MNs were seeded onto pure, confluent layers of ESC-derived astrocytes (Chapter 2: Materials and Methods, Section 2.5). The development of motoneuronal electrophysiological properties in these 'MN+as' cultures was compared to that in the MN alone condition (Table 5.2). As concluded in Chapter 4, a striking effect of astrocytes was to prolong the neuronal survival in culture from 2 to 4 weeks. However, since neurons in the MN alone condition only survived until week 2, a comparison of motoneuronal electrophysiological properties was only possible for weeks 1 and 2.

5.3.2.1 Astrocytes affected the development of the motoneuronal RMP and passive membrane properties

The development of passive membrane properties of motoneurons cultured with astrocytes were in general comparable to motoneurons cultured alone. Thus, as observed in the MN alone condition, between weeks 1 and 2, motoneurons in the MN+as condition displayed a decrease in input resistance (from 265 ± 182MOhms to 54 ± 27MOhms; p = 0.021 in a Kruskal Wallis test for the MN+as

Table 5.2 Electrophysiological properties of motoneurons cultured with astrocytes *in vitro.*

Values are given as the mean ± standard deviation (n). ∞ denotes a comparison between weeks 1 and 2; p<0.05 = ∞, p<0.01 = ∞∞, p<0.001 = ∞∞∞. * denotes a significant difference compared to the MN alone culture condition at that time point. Note that comparisons were only made for weeks 1 and 2. p<0.05 = *, p<0.01 = **, p<0.001 = ***. ^ means that some data was not normally distributed according to a Shapiro-Wilk test so a non-parametric statistical test was used.

Co-culture condition: MN+as				
Electrophysiological property	**Week 1**	**Week 2**	**Week 3**	**Week 4**
Proportion motoneurons that fire	8/8	9/9	3/3	5/5
Proportion motoneurons that display repetitive firing	8/8 (100%)	9/9 (100%)	3/3 (100%)	5/5 (100%)
Proportion motoneurons that sustain firing to the end of a 500ms square pulse	8/8 (100%)	9/9 (100%)	3/3 (100%)	5/5 (100%)
Proportion of motoneurons which can sustain firing that display depolarisation block	6/8 (75%)	2/9 (22%)	n/a	n/a
Proportion of motoneurons firing doublets or triplets at rheobase	4/8 (50%)	4/9 (44%)	3/3 (100%)	2/4 (50%)
Proportion of motoneurons displaying rebound action potentials	3/5 (60%)	3/8 (38%)	0/3 (0%)	1/2 (50%)
Resting membrane potential (mV)	-62 ± 7 (8)	-62 ± 5 (9) *	-63 ± 3 (3)	-60 ± 7 (4)
Input resistance (MOhm)^	265 ± 182 (8)	54 ± 27 (9) ∞	49 ± 16 (3)	132 ± 111 (4)
Capacitance (pF)^	71 ± 17 (8) **	172 ± 110 (6)*	66 ± 48 (3)	69 ± 70 (4)
Membrane time constant (µs)^	332 ±203 (8)	1202 ± 660 (6)	1947 ± 349 (3) ∞	1666 ± 907 (4) ∞
Rheobase (pA)^	66 ± 27 (8)*	446 ± 389 (9) ∞	790 ± 710 (3) ∞	461 ± 452 (4)
Action potential amplitude at rheobase (mV)	26 ± 11 (8)*	15 ± 13 (9)	28 ± 19 (3)	0 ± 26 (4)
Action potential half width (ms)^	1.2 ± 0.2 (5)	1.3 ± 0.5 (6)	n/a	0.7 ± 0.3 (2)
Multiple of rheobase at which depolarisation block occurs^	10.34 ± 3.16 (6)**	4.71 ± 1.97 (2)	n/a	n/a
Spike amplitude adaptation at 2 x rheobase (mV)^	6 ± 3 (8)	3 ± 5 (8)	4 ± 2 (3)	7 ± 10 (3)
Initial firing frequency (IFF) (Hz)	55.9 ± 16.3 (8)*	116.6± 82.4 (8)	124.1 ± 18.1 (3)	89.5 ± 80.5 (3)
Steady-state firing frequency (SFF) (Hz)	16.0 ± 7.1 (7)	29.5 ± 24.8 (8)	22.6 ± 17.6 (3)	31.6 ± 6.7 (3)
FI slope (SFF) (Hz/pA)^	0.13 ± 0.01 (8)	0.07 ± 0.03 (9)	0.03 ± 0.01 (3) ∞∞	0.03 ± 0.00 (3) ∞∞
Spike frequency adaptation ratio (SFA)^	0.18 ± 0.10 (8)***	0.15 ± 0.17 (9)*	0.07 ± 0.03 (3)	0.22 ± 0.26 (3)
Sag ratio	0.94 ± 0.03 (5)**	0.93 ± 0.04 (9)	0.98 ± 0.00 (3)	0.94 ± 0.04 (3)

Slope of sag ratio-current graph (pA^{-1})^	115.94 ± 129.01 (5)*	82.41 ± 78.27 (9)	31.83 ± 82.89 (3)	67.17 ± 32.25 (3)
Spontaneous burst frequency (bursts/min)^	0.50 ± 1.41 (8)	13.49 ± 17.09 (9)*	22.28 ± 7.88 (3)	46.67 ± 31.23 (5) ∞∞∞
Spontaneous EPSP frequency (EPSPs/min)^	1.08 ± 2.00 (8)	0.09 ± 0.27 (9)	0.00 ± 0.00 (3)	1.87 ± 2.47 (5)
PC1^	-0.08 ± 0.66 (8) ***	2.38 ± 1.44 (9) ** ∞∞	3.73 ± 0.96 (3) ∞∞	1.62 ± 0.90 (5)
PC2^	0.17 ± 0.68 (8)	-0.34 ± 1.04 (9)	-0.28 ± 2.51 (3)	-1.15 ± 1.74 (5)

condition and p = 0.025 in a post hoc Dunn's Multiple Comparison test between week 1 and 2; Table 5.2) and no change in capacitance (p = 0.073 in a Kruskal Wallis test). Despite mirroring developmental trajectory, capacitance was significantly higher in the MN+as condition compared to the MN alone condition in both week 1 (71 ± 17pF compared to 34 ± 14pF respectively; p = 7.7e-07 in a Kruskal Wallis test for week 1 and p = 0.007 in a post hoc Dunn's Multiple Comparison test of the MN alone and MN+as conditions) and week 2 (172 ± 110pF compared to 46 ± 24pF respectively; p = 0.0092 in a Kruskal Wallis test for week 2 and p = 0.013 in a post hoc Dunn's Multiple Comparison test of the MN alone and MN+as conditions). This is consistent with results presented in Chapter 4 which show that motoneurons in the MN+as condition were significantly bigger than in the MN alone condition. Although no significant change in membrane time constant was observed between weeks 1 and 2, there was a significant difference when week 1 was compared to weeks 3 and 4 in the MN+as condition (332 ± 203µs in week 1 to 1666 ± 907µs in week 4; p = 0.0043 in a Kruskal Wallis test for the MN+as condition and p = 0.026 and 0.028 in a post hoc Dunn's Multiple Comparison test of week 1 with weeks 3 and 4 respectively; Table 5.2). Thus, the trajectory of an increasing membrane time constant with time was maintained in the presence of astrocytes. However, the similarities in passive membrane properties between the two co-culture conditions were not universal. Unlike motoneurons cultured alone, the RMP of motoneurons cultured with astrocytes did not change between weeks 1 and 2. Indeed, the RMP in week 2 was significantly more depolarised in the MN+as condition than in the MN alone condition (-62 ± 5mV in week 2 MN+as co-cultures; p = 2.1e-05 as tested by ANOVA and p = 0.018 in a post hoc Tukey's HSD Multiple Comparison test; Table

5.2). This suggests that astrocytes prevented the hyperpolarisation of the RMP that occurred in the MN alone condition. Thus, the presence of astrocytes influenced the development of some motoneuronal passive membrane properties.

5.3.2.2 Astrocytes accelerated the development of motoneuronal active membrane properties

Astrocytes can influence the active as well as the passive electrophysiological properties of motoneurons (Kelley et al., 2018), even altering motoneuronal firing patterns in real time in response to sensory stimuli (Morquette et al., 2015).

5.3.2.2.1 The effect of astrocytes on motoneuronal sag and rebound action potentials

The properties of sag of motoneurons in the MN+as condition did not change over time as in the MN alone condition. In week 1, sag ratio was significantly higher in the MN+as condition (Table 5.2; 0.94 ± 0.03 compared to 0.84 ± 0.05 in the MN+as and MN alone conditions, respectively; $p = 0.0022$ as tested by ANOVA and $p = 0.0014$ in a post hoc Tukey's HSD Multiple Comparison test) and the slope of the sag ratio-current graph was significantly lower (Table 5.2; 115.94 ± 129.01 compared to 663 ± 342 in the MN+as and MN alone conditions, respectively; $p = 0.0016$ in a Kruskal Wallis test and $p = 0.0029$ in a post hoc Dunn's Multiple Comparison test). Indeed, the week 1 values of these properties in the MN+as condition were not found to be different from the week 2 values in the MN alone condition (Table 5.1). This could suggest that the maturation of sag properties in motoneurons occurred earlier in the presence of astrocytes. The proportion of motoneurons that displayed RAPs following hyperpolarisation decreased slightly from week 1 to 2 in the MN+as condition; the same trend observed in the MN alone condition. However, the proportion was higher in the MN+as condition (3/5 in week 1 and 3/8 in week 2; Table 5.2) than the MN alone condition (2/13 in week 1 to 0/7 in week 2; Table 5.2) in both weeks 1 and 2. Thus, the presence of astrocytes affected the development of hyperpolarisation-activated currents in the cultured motoneurons.

5.3.2.2.2 Coculture with astrocytes accelerated the maturation of motoneuronal firing properties

The maturation trajectory of some motoneuronal firing properties was similar in the MN+as condition as in the MN alone condition. For example, as in the MN

alone condition, rheobase increased with time in the MN+as condition (from 66 ± 27pA to 446 ± 389pA; p = 0.0033 in a Kruskal Wallis test and p = 0.012 in a post hoc Dunn's Multiple Comparison test between week 1 and 2; Figure 5.4). However, differences were also observed. In week 1, rheobase was significantly lower in the MN+as condition than the MN alone condition (66 ± 27pA compared to 154 ± 90pA respectively; p = 0.014 in a Kruskal Wallis test and p = 0.046 in a post hoc Dunn's Multiple Comparison test), suggesting that motoneurons were more excitable in the presence of astrocytes at this earlier time point. Furthermore, in recordings from motoneurons in the MN+as condition, the first spike at rheobase was sometimes a doublet or triplet (4/8 in week 1 and 4/9 in week 2; Figure 5.4; Table 5.2). This phenomena has also been observed in motoneurons *in vivo* (Martin-Caraballo and Greer, 1999; Walton and Fulton, 1986). Doublets or triplets were not observed in the MN alone condition, suggesting co-culture with astrocytes enabled ESC-derived motoneurons to display this type of firing in culture, perhaps by accelerating the development of the underlying ion channels.

The presence of astrocytes seemed to accelerate the maturation of most motoneuronal firing properties observed in the MN alone condition. In the MN+as condition, all motoneurons recorded from were capable of firing trains of action potentials that were sustained to the end of a 500ms square pulse at all time points (Table 5.2), in contrast to only 8/14 and 5/7 of motoneurons in the MN alone condition in weeks 1 and 2 respectively (Table 5.1). Unlike in the MN alone condition, IFF did not increase significantly over time but was already significantly higher in the MN+as condition than the MN alone condition in week 1 (Table 5.2; 55.9 ± 16.3Hz compared to 31.7 ± 18.1Hz, respectively; p = 0.0097 in an ANOVA and p = 0.013 in a post hoc Tukey's HSD test). This is likely related to the initial doublets/triplets observed in the MN+as condition, which have a shorter inter-spike interval. In a similar way, the SFA ratio in the MN+as condition was significantly lower than in the MN alone condition (Table 5.2; for week 1, 0.18 ± 0.10 compared to 0.60 ± 0.14, and for week 2, 0.15 ± 0.17 compared to 0.43 ± 0.17 in the MN+as and MN alone conditions, respectively; for weeks 1 and 2 respectively, p = 9.2e-05 and 0.0070 in a Kruskal Wallis test and p = 2.9e-05 and 0.031 in a post hoc Dunn's Multiple Comparison test). A lower SFA ratio indicates more pronounced SFA in the MN+as conditions, which is sometimes considered

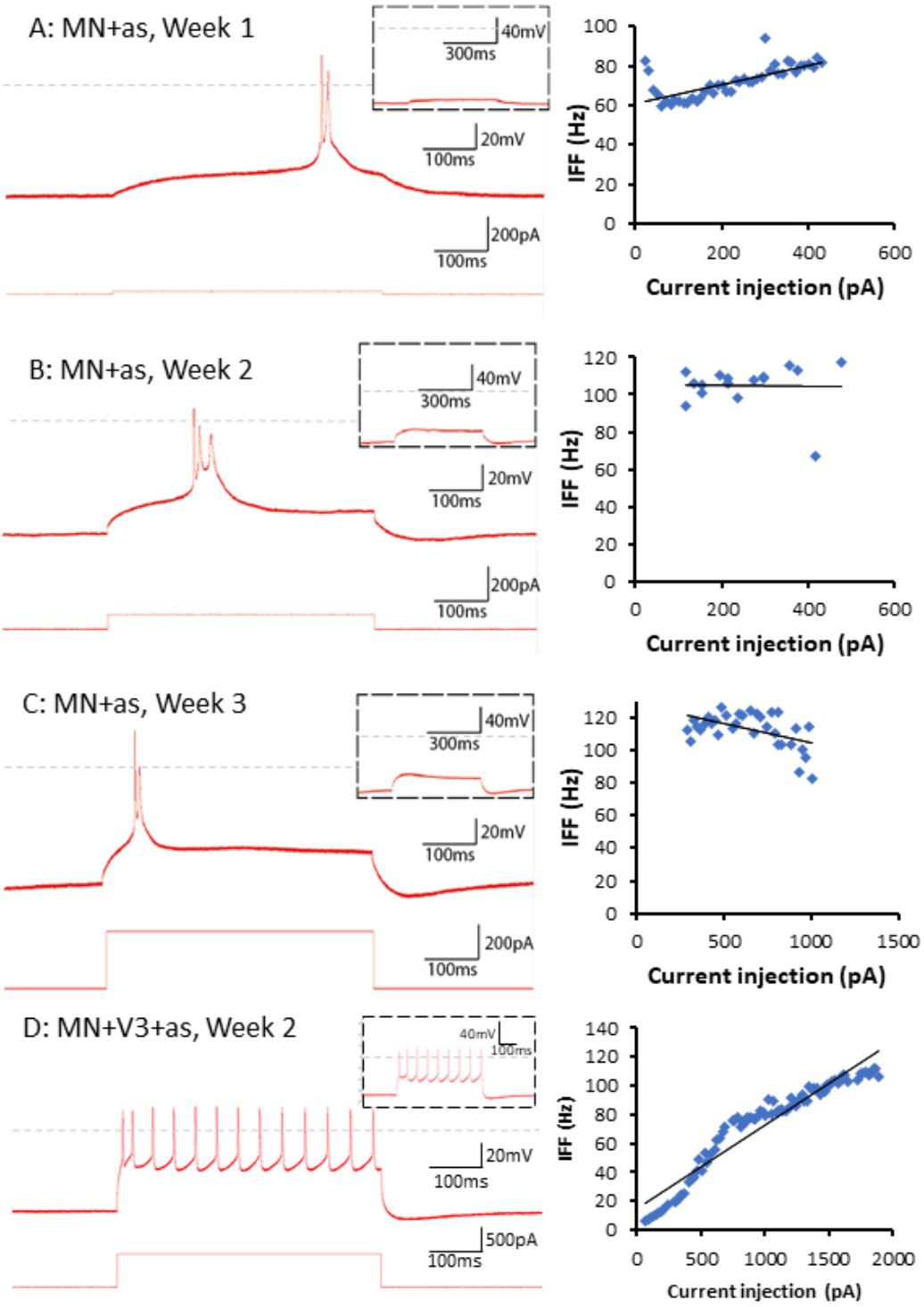

Figure 5.4: Examples of doublets and triplets elicited by a 500ms square current pulse at rheobase in the MN+as condition (A-C) and at 6 x rheobase in the MN+V3+as condition (D).

In each panel, the lower trace shows the current injected and the upper trace shows the resulting change in voltage. The dashed grey lines show 0mV. For A-C, the box in the top right corner of each figure show the trace given by a current injection 20pA below rheobase. Note that rheobase increases with time. For D, the box in the top right corner shows a trace taken at four times rheobase when there was no doublet at the beginning of the pulse. The graph on the right is plot of IFF against current for that motoneuron. Note the S-shaped FI plot in D. The age and culture condition of each motoneuron is shown in each panel.

to indicate more mature motoneurons (Takazawa et al., 2012). Additionally, fewer motoneurons displayed depolarisation block in the MN+as condition at both time points (6/8 in week 1 and 2/9 in week 2; Table 5.2) and depolarisation block occurred at a significantly greater multiple of rheobase (In week 2, 10.34 ± 3.16 for compared to 2.56 ± 1.45 for the MN+as and MN alone conditions, respectively; $p = 0.0002$ in a Kruskal Wallis test of week 2 data and $p = 0.0011$ in a post hoc Dunn's Multiple Comparison test). This suggests astrocytes enabled motoneurons to fire over a wider range of stimulus intensities. Indeed, FI slope was significantly reduced by week 3 and 4 in the MN+as condition (Table 5.2 and Figure 5.3; $p = 0.0004$ in a Kruskal Wallis test for the MN+as condition and $p = 0.074$, 0.0041 and 0.0054 in a post hoc Dunn's Multiple Comparison test comparing week 1 with weeks 2, 3 and 4, respectively). A shallower FI slope means that each increase in injected current resulted in a smaller increase in firing frequency and thus stimulus intensity is more sensitively encoded into frequency by the motoneuron. No decrease in FI slope over time was observed in the MN alone condition (Table 5.1 and Figure 5.3; $p = 0.39$, Mann Whitney U test) or any other culture condition.

The maturation of motoneuronal action potential morphology was also accelerated by the presence of astrocytes in the culture. Motoneuronal action potential amplitude at rheobase in the MN+as condition did not change significantly between weeks 1 (26 ± 11mV) and 2 (15 ± 13mV) but it was higher in week 1 than in the MN alone condition (Table 5.2; $p = 0.0203$ in an ANOVA and $p = 0.0201$ in a post hoc Tukey's HSD test). Together, these data suggest that astrocytes accelerate and facilitate various aspects of maturation of motoneuronal firing properties in culture.

5.3.2.2.3 Astrocyte-containing cultures developed spontaneous, glutamatergic motoneuronal activity

The most obvious difference in the motoneurons of astrocyte-containing cultures was the emergence of spontaneous activity in week 2 (Figure 5.5 A and C; Table 5.2; 13.49 ± 17.09 bursts/minute). In contrast, no spontaneous activity was observed at any time point in the MN alone condition. Furthermore, there was a significant increase in spontaneous burst frequency in week 4 (46.67 ± 31.23 bursts/min) compared to week 1 (0.50 ± 1.41bursts/min) in the MN+as condition

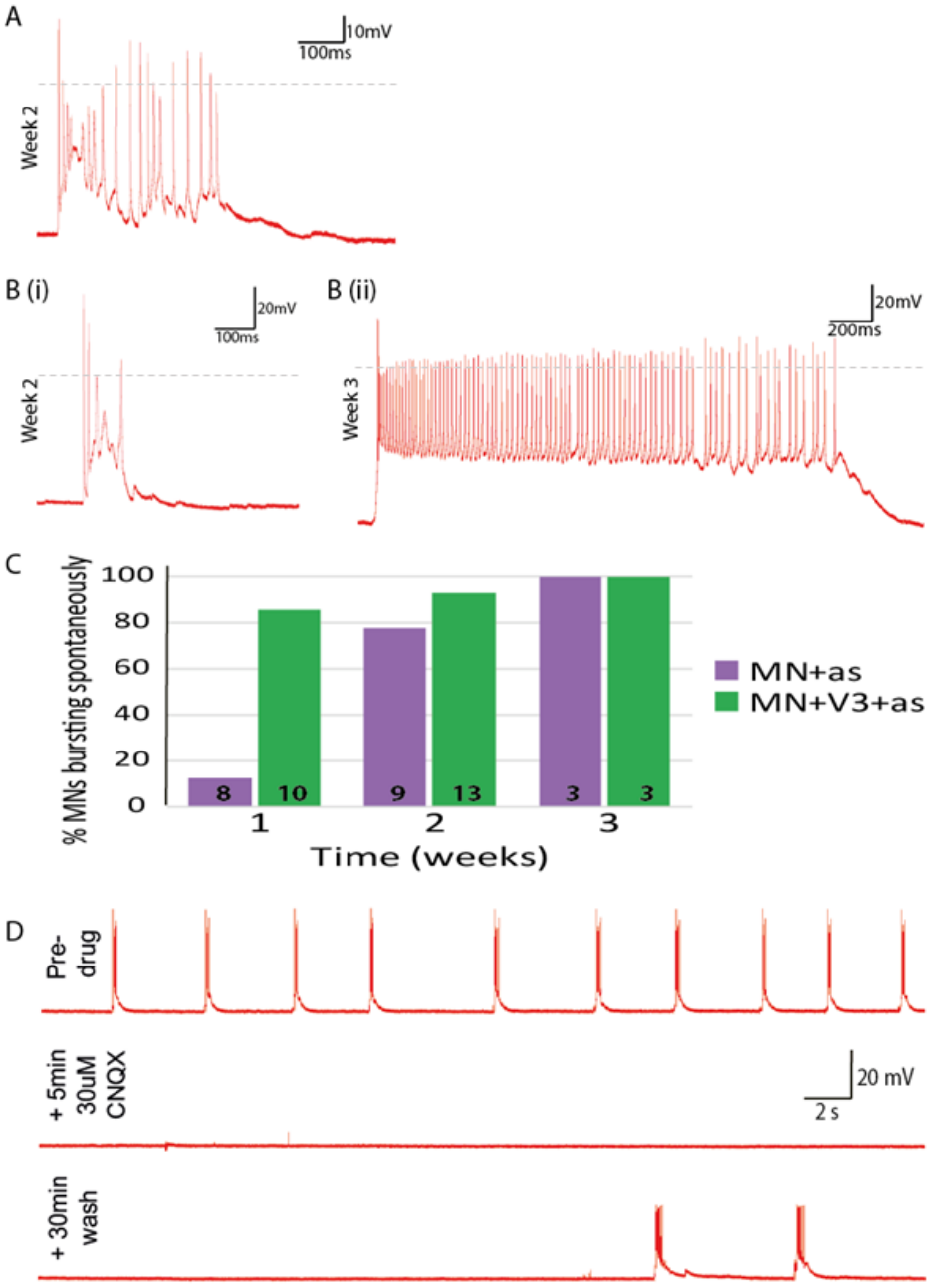

Figure 5.5: Glutamatergic spontaneous activity occurred in astrocyte-containing cultures.

A: An example of spontaneous bursts in a week 2 motoneuron in a MN+as culture. B: Examples of spontaneous bursts in motoneurons in MN+V3+as cultures; (i) week 2, (ii) week 3. C: A timeline of the development of spontaneous activity measured by single cell patch-clamping in the astrocyte-containing co-culture conditions. D: CNQX completely eliminated spontaneous activity in 3-5min. Spontaneous activity was restored after 20-30 minutes of washing. Data shown is from a week 2 MN+V3+as culture. n = 13 for MN+as condition and n = 17 for MN+V3+as condition. Dashed grey lines in A and B show 0mV.

(Table 5.2; p = 0.0011 in a Kruskal Wallis test and p = 0.0009 in a post hoc Dunn's Multiple Comparison test). To confirm that spontaneous activity was not caused by activation of the ChR2 expressed by the C9G ESC-derived motoneurons, spontaneous burst frequency was compared between MN+as cultures containing motoneurons derived from C9G ESCs and those containing motoneurons derived from ChR2-less H14IG#13 ESCs. No significant difference in spontaneous burst frequency was observed (Figure 5.6). These data indicate that spontaneous burst frequency of motoneurons in the presence of astrocytes increased over time (Figure 5.5C).

Receptor antagonists were used to determine the neurotransmitter dependency of the spontaneous activity. Figure 5.5D shows an example of the regular spontaneous bursts of activity in motoneurons that were eliminated by the addition of AMPA receptor antagonist, cyanquixaline (CNQX, 30μM) (n = 13 for MN+as condition). The presence of glutamatergic spontaneous activity in MN+as co-cultures suggests that motoneurons formed active glutamatergic synapses with other motoneurons in the co-cultures. In some motoneurons, single action potentials elicited by a 20ms square current pulse would be reproducibly followed by a burst of action potentials (Figure 5.7 Ai) that were also sensitive to CNQX (Figure 5.7 Aii; n=1 for MN+as and n=1 for MN+V3+as condition). Presumably, these bursts indicate that the motoneuron being recorded from was connected with itself via glutamatergic synapses, either autaptically or via other neurons. In contrast to CNQX, the inhibitors of cholinergic signalling, mecamylamine (50μM) and atropine (~100μM), had no consistent effect on the frequency of or characteristics of motoneuronal spontaneous activity in the MN+as condition (Figure 5.8). These data show that the spontaneous activity observed was glutamatergic and, while cholinergic signalling may have had some effect, it varied between motoneurons. Thus, the addition of astrocytes to the co-cultures led to the formation of spontaneously active, glutamatergic networks in culture.

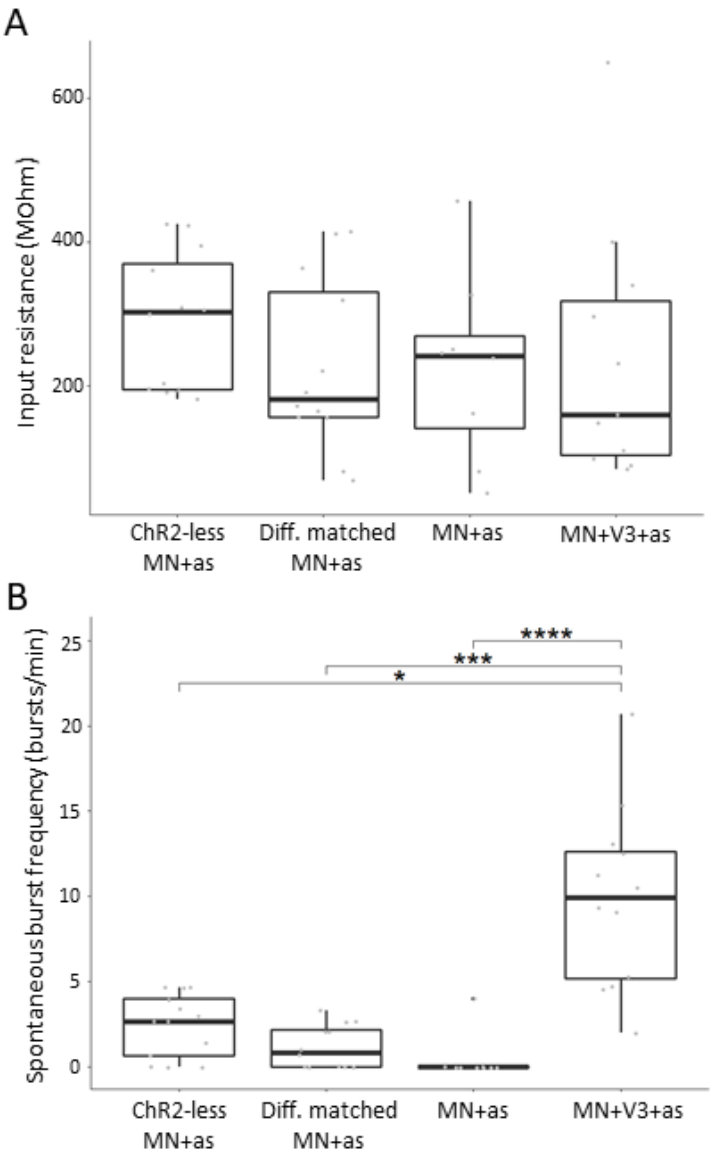

Figure 5.6: The presence of ChR2 in the C9G ESC-derived motoneurons did not affect spontaneous burst frequency.

To determine whether the spontaneous activity observed in the MN+as cultures was due to activity of channelrhodopsin-2 (ChR2) expressed in the C9G ESC line, MN+as cultures containing motoneurons derived from ChR2-less H14IG#13 ESCs (ChR2-less MN+as; n = 13 motoneurons from three differentiations) were compared to MN+as cultures containing motoneurons derived from C9G ESCs in week 1, including differentiation-matched MN+as cultures (diff. matched MN+as; n = 12 motoneurons from four differentiations) and historical MN+as cultures (MN+as; n = 9 motoneurons from three differentiations). All MN+as cultures were compared to historical MN+V3+as cultures (MN+V3+as; n=12 motoneurons from four differentiations) to check that the astrocyte-dependent effect of V3 interneurons on spontaneous bursts frequency was robust to the presence/absence of ChR2. A shows that neither ChR2 nor V3 interneurons affected motoneuronal input resistance (an indicator of cell size and ion channel density). B) There were no significant differences in spontaneous burst frequency between the ChR2-less MN+as condition and either the differentiation matched or historical MN+as conditions. There was a significant difference between each MN+as condition and the historical MN+V3+as condition. Bold horizontal lines in the boxplots show the median. * = $p<0.05$, ** = $p<0.01$, *** = $p<0.001$, and **** = $p<0.0001$.

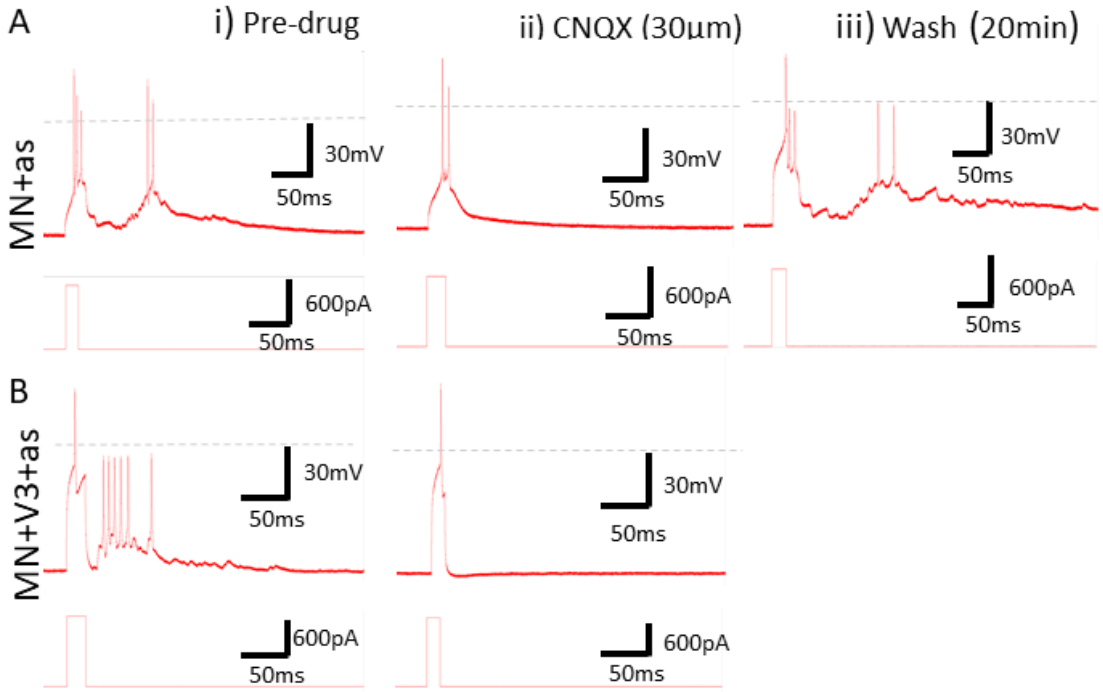

Figure 5.7: Evoked action potentials caused spontaneous network activity that was sensitive to CNQX (30µM).

Action potentials were elicited from motoneurons by the injection of a 20ms square current. Dashed grey lines show 0mV. In some motoneurons, the evoked action potentials were reproducibly followed by a burst of spontaneous action potentials or EPSPs (Ai) and Bi)). This non-evoked bursting was sensitive to CNQX (A ii and B ii) and could be restored following washout of the drug (A iii). In each panel, the upper trace shows the voltage change in response to a short square current, shown in the lower trace. Note that in A, the pulse evoked doublets and triplets instead of single action potentials; this was unaffected by CNQX.

5.3.3 V3 interneurons had a minimal effect on electrophysiological properties of motoneurons and their development over time

To investigate the effect of V3 interneurons on motoneuron maturation *in vitro*, ESC-derived motoneurons were seeded onto 2-day old cultures of pure V3 interneurons (Chapter 2: Materials and Methods, Section 2.5). The development of motoneuronal electrophysiological properties in this 'MN+V3' culture condition was compared to that in the MN alone condition and some limited effects on motoneuron firing properties were observed. For example, motoneurons in the MN+V3 condition displayed a more limited ability to sustain repetitive firing over a range of current intensities compared to the MN alone condition; indeed, all motoneurons in the MN+V3 condition displayed depolarisation block (Table 5.3) at a current intensity less than 2 x rheobase, meaning that SFF at 2 x rheobase could not be measured. Additionally, action potential half width was increased in

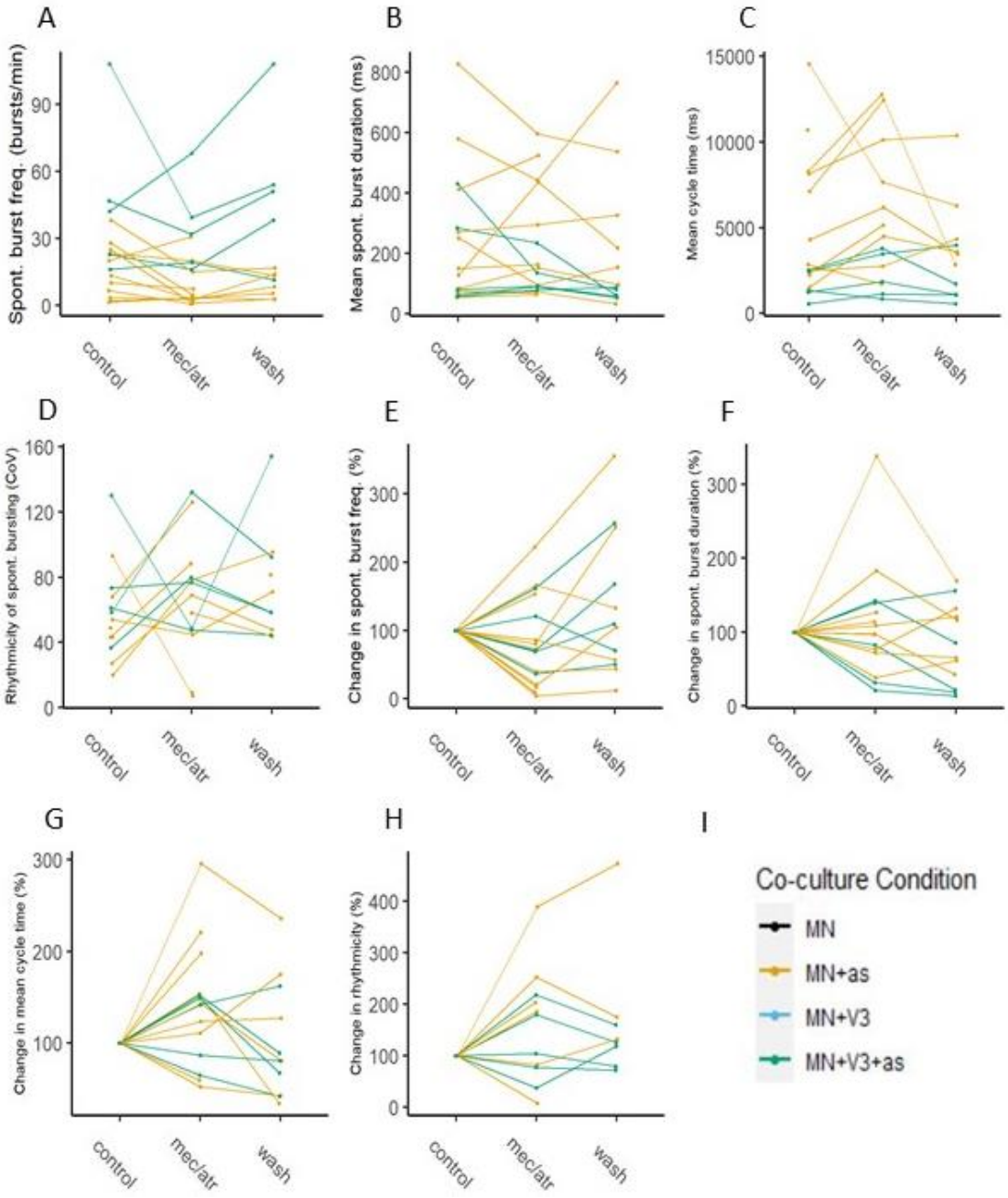

Figure 5.8: Cholinergic receptor blockers had no consistent effect on motoneuronal spontaneous activity.

Week 2 motoneurons were patched and their spontaneous activity recorded before (control), during wash-in of mecamylamine (50 μM) and atropine (~50μM) (mec/atr) and after washout (wash). Cells were exposed to mec/atr for on average 8.7 ± 4.3 minutes and washed for an average of 9.6 ± 6.5 minutes (mean ± standard deviation). Each line on the graphs represents a different motoneuron. For MN+as, 12 motoneurons from 7 networks/coverslips were recorded from and, for MN+V3+as, 4 motoneurons from 2 networks/coverslips were recorded from. E-H show the change in each characteristic as a percentage of the control recording. Regarding D, low CoV indicates low variation of cycle time and therefore high rhythmicity of firing.

Table 5.3: Electrophysiological properties of motoneurons cultured with V3 interneurons *in vitro.*

Values are given as the mean ± standard deviation (n). ∞ denotes a comparison between weeks 1 and 2; p<0.05 = ∞, p<0.01 = ∞∞, p<0.001 = ∞∞∞. * denotes a significant difference compared to the MN alone culture condition at that time point. Note that comparisons were only made for weeks 1 and 2. p<0.05 = *, p<0.01 = **, p<0.001 = ***. ^ means that some data was not normally distributed according to a Shapiro-Wilk test so a non-parametric statistical test was used.

Co-culture condition: MN+V3		
Property	**Week 1**	**Week 2**
Proportion motoneurons that fire	10/10 (100%)	10/10 (100%)
Proportion motoneurons that display repetitive firing	9/10 (90%)	7/10 (70%)
Proportion motoneurons that sustain firing to the end of a 500ms square pulse	5/10 (50%)	4/10 (40%)
Proportion of motoneurons which can sustain firing that display depolarisation block	5/5 (100%)	4/4 (100%)
Proportion of motoneurons firing doublets or triplets at rheobase	0/10 (0%)	0/10 (0%)
Proportion of motoneurons displaying rebound action potentials	0/9 (0%)	0/10 (0%)
Resting membrane potential (mV)	-63 ± 6 (10)	-75 ± 4 (10) ∞∞∞
Input resistance (MOhm)^	281 ± 137 (10)	98 ± 29 (10) ∞∞∞
Capacitance (pF)^	39 ± 8 (10)	50 ± 33 (9)
Membrane time constant (µs)^	369 ± 191 (10)	460 ± 215 (9)
Rheobase (pA)^	159 ± 60 (10)	619 ± 278 (10) ∞∞∞
Action potential amplitude at rheobase (mV)	15.37 ± 6.61 (10)	16.93 ± 8.71 (10)
Action potential half width (ms)^	1.8 ± 0.5 (8)*	1.0 ± 0.3 (9) ∞∞
Multiple of rheobase at which depolarisation block occurs^	2.23 ± 0.96 (5)	2.10 ± 0.76 (4)
Spike amplitude adaptation at 2 x rheobase (mV)^	22 ± 12 (10)	8 ± 13 (5)
Initial firing frequency (IFF) (Hz)	41.9 ± 12.8 (9)	62.2 ± 19.1 (5)
Steady-state firing frequency (SFF) (Hz)	25.6 (1)	39.0 (1)
FI slope (SFF) (Hz/pA)^	0.20 ± 0.25 (5)	0.06 ± 0.05 (3)
Spike frequency adaptation ratio (SFA)^	0.43 ± 0.06 (4)	0.48 ± 0.04 (3)
Sag ratio	0.89 ± 0.04 (9)	0.91 ± 0.04 (10)
Slope of sag ratio-current graph (pA^{-1})^	397.40 ± 199.28 (9)	165.48 ± 83.25 (10) ∞∞
Spontaneous burst frequency (bursts/min)^	0.00 ± 0.00 (10)	0.00 ± 0.00 (10)
Spontaneous EPSP frequency (EPSPs/min)^	0.00 ± 0.00 (10)	0.22 ± 0.70 (10)
PC1^	-2.28 ± 0.80 (10)	-0.18 ± 0.67 (10) ∞∞∞
PC2^	0.41 ± 1.29 (10)	1.38 ± 0.89 (10) ∞

the MN+V3 condition in week 1 (1.8 ± 0.5ms compared to 1.2 ± 0.4ms in the MN+V3 and MN alone conditions, respectively; p = 0.13 in a Kruskal Wallis test and p = 0.028 in a post hoc Dunn's Multiple Comparison test; Table 5.3). Moreover, unlike in the MN alone condition, there was a significant reduction in action potential half width from week 1 to 2 (p = 0.0025, Mann Whitney U test; Table 5.3). There was no significant difference in action potential half width between the two conditions in week 2, suggesting that the developmental narrowing of the action potential was delayed in the MN+V3 condition but 'caught up' by week 2. However, apart from these differences, a direct comparison between the MN alone and MN+V3 conditions at each time point did not reveal any significant differences in either passive membrane or firing properties. These data indicate that V3 interneurons had a negligible effect on motoneuron maturation and that any effect slowed maturation rather than accelerating it.

5.3.4 There was an astrocyte-dependent effect of V3 interneurons on the electrophysiological properties of motoneurons

V3 interneurons are an important excitatory component in spinal motor circuits and affect the balance of cholinergic and glutamatergic synapses formed by motoneurons *in vitro* (Chapter 4, Section 4.3.2.1). However, the formation of synapses in these *in vitro* cultures was astrocyte-dependent (Chapter 4, Section 4.3.2.1). To investigate astrocyte-dependent effects of V3 interneurons on motoneuronal electrophysiological development, pure populations of ESC-derived motoneurons were seeded onto pure cultures of 2-day old V3 interneurons on a confluent layer of astrocytes (Chapter 2: Materials and Methods, Section 2.5). These 'MN+V3+as' cultures were compared with MN+as cultures (¥ in Table 5.4).

5.3.4.1 The maturation of motoneuronal firing properties was affected by V3 interneurons in an astrocyte-dependent manner

While no astrocyte-dependent effect of V3 interneurons on passive motoneuronal membrane properties was observed (Table 5.4), there was a complex effect on motoneuronal firing properties. In some ways, motoneurons in MN+V3+as cultures were less mature than in MN+as cultures; for example, fewer motoneurons were capable of sustained repetitive firing in weeks 1 and 2 (12/14 in week 1 and 10/13 in week 2 for the MN+V3+as condition compared to all motoneurons in the MN+as condition; Table 5.4 and Table 5.2). There were also

Table 5.4: Electrophysiological properties of motoneurons cultures with V3 interneurons and astrocytes in vitro.

Values are given as the mean ± standard deviation (n). ∞ denotes a comparison between weeks 1 and the other time points; p<0.05 = ∞, p<0.01 = ∞∞, p<0.001 = ∞∞∞. * denotes a significant difference compared to the MN alone culture condition at that time point. Note that comparisons were only made for weeks 1 and 2. p<0.05 = *, p<0.01 = **, p<0.001 = ***. ¥ denotes a significant difference compared to MN+as condition for that time point; p<0.05 = ¥, p<0.01 = ¥¥, p<0.001 = ¥¥¥. ^ means that some data was not normally distributed according to a Shapiro-Wilk test so a non-parametric test was used.

Co-culture Condition: MN+V3+as				
Electrophysiological property	**Week 1**	**Week 2**	**Week 3**	**Week 4**
Proportion motoneurons that fire	14/14	13/13	3/3	5/5
Proportion motoneurons that display repetitive firing	12/14 (86%)	10/13 (77%)	3/3 (100%)	2/2 (100%)
Proportion motoneurons that sustain firing to the end of a 500ms square pulse	12/14 (86%)	10/13 (77%)	3/3 (100%)	2/2 (100%)
Proportion of motoneurons which can sustain firing that display depolarisation block	10/12 (83%)	1/10 (10%)	n/a	n/a
Proportion of motoneurons firing doublets or triplets at rheobase	0/12 (0%)	0/10 (0%)	2/3 (67%)	1/2 (50%)
Proportion of motoneurons displaying rebound action potentials	1/10 (10%)	1/9 (11%)	1/2 (50%)	0/2 (0%)
Resting membrane potential (mV)	-63 ± 4 (14)	-64 ± 6 (14)	-73 ± 12 (3)	-73 ± 9 (5) ¥ ∞
Input resistance^ (MOhm)	188 ± 100 (14)	59 ± 57 (14) ∞∞	30 ± 22 (3) ∞	111 ± 55 (4)
Capacitance (pF)^	82 ± 17 (14)***	84 ± 71 (14)	84 ± 53 (3)	51 ± 36 (4)
Membrane time constant (µs)^	812 ± 525 (14)**	1101 ± 767 (14)	1592 ± 756 (3)	677 ± 638 (4)
Rheobase (pA)^	163 ± 83 (12) ¥	629 ± 323 (10) ∞∞	651 ± 452 (3)	400 ± 409 (2)
Action potential amplitude at rheobase (mV)	19 ± 8 (12)	19 ± 10 10)	21 ± 17 (3)	5 ± 31 (2)
Action potential half width (ms)^	1.5 ± 0.3 (8)	1.3 ± 0.3 (3)	1.4 (1)	1.5 ± 0.4 (2)
Multiple of rheobase at which depolarisation block occurs^	5.26 ± 1.68 (10)	2.33 (1)	n/a	n/a
Spike amplitude adaptation at 2 x rheobase (mV)^	1 ± 4 (11)**	8 ± 12 (8)	1 ± 6 (2)	-1 (1)
Initial firing frequency (IFF) (Hz)	33.8 ± 13.6 (11) ¥	91.7 ± 65.7 (9)	64.7 ± 76.8 (2)	95.0 ± 3.6 (2)
Steady-state firing frequency (SFF) (Hz)	20.6 ± 9.6 (8)	19.7 ± 6.2 (7)	33.3 ± 23.0 (2)	44.9 ± 17.8 (4) ∞
FI slope (SFF) (Hz/pA)	0.09 ± 0.05 (12)	0.05 ± 0.03 (10)	0.09 ± 0.03 (3)	0.10 ± 0.06 (2)
Spike frequency adaptation ratio (SFA)^	0.40 ± 0.09 (12)¥	0.32 ± 0.11 (10)	0.46 ± 0.40 (3)	0.31 ± 0.28 (2)
Sag ratio	0.88 ± 0.05 (10)	0.92 ± 0.04 (9)	0.91 ± 0.05 (2)	0.98 ± 0.01 (2)

Slope of sag ratio-current graph (pA^{-1})^	300.97 ± 366.09 (10)*	59.75 ± 59.04 (9)	99.67 ± 100.43 (2)	19.90 ± 40.48 (2)
Spontaneous burst frequency (bursts/min)^	6.73 ± 4.83 (13)*** ¥¥¥	33.99 ± 49.11 (13)*** ∞	19.56 ± 14.26 (3)	64.08 ± 44.41 (5) ∞
Spontaneous EPSP frequency (EPSPs/min)^	3.11 ± 9.88 (14)**	16.96 ± 19.60 (14)** ¥¥¥	1.22 ± 1.58 (3)	11.93 ± 18.15 (5)
PC1^	-0.41 ± 0.93 (14) ***	1.78 ± 1.05 (14) ** ∞∞∞	1.80 ± 1.50 (3)	1.07 ± 0.86 (5)
PC2^	-0.43 ± 0.86 (14)	-0.82 ± 1.83 (14)*	0.25 ± 1.45 (3)	0.16 ± 0.58 (5)

no motoneurons that fired doublets or triplets at rheobase in the MN+V3+as condition in week 1 and 2, such as those seen in the MN+as condition (Figure 5.4). However, 2/10 motoneurons in the MN+V3+as condition in week 2 had an S-shaped IFF-I plot, indicating that doublets arose at higher intensity current injection (Figure 5.4 D). The lack of high frequency doublets/triplets may be the reason that IFF was significantly lower in the MN+V3+as condition than in the MN+as condition in week 1 (33.8 ± 13.6Hz compared to 55.9 ± 16.3Hz; p = 0.0097 in an ANOVA and p = 0.018 in a post hoc Tukey HSD Multiple Comparison test; Table 5.4), though no significant difference was observed between the two conditions in weeks 2, 3 or 4. Furthermore, SFA was less marked; the SFA ratio in week 1 was significantly higher in the MN+V3+as condition compared to the MN+as condition (0.40 ± 0.09 compared to 0.18 ± 0.10, respectively; p = 9.2e-05 in a Kruskal Wallis test and p = 0.04 in a post hoc Dunn's Multiple Comparison test; Table 5.4). However, the maturation of rheobase seemed to be accelerated in the MN+V3+as condition. Rheobase was higher in the MN+V3+as condition compared to the MN+as condition in week 1 (163 ± 83pA compared to 66 ± 27pA; p = 0.014 in a Kruskal Wallis test and p = 0.026 in a post hoc Dunn's Multiple Comparison test). There was no significant difference observed in rheobase between the two conditions in weeks 2, 3 or 4 (Table 5.4). Thus, the astrocyte-dependent effects of V3 interneurons on motoneurons sometimes seemed to sometimes promote and sometimes to prevent maturation of motoneuronal firing properties.

5.3.4.2 *The development of spontaneous activity in motoneuron was accelerated by V3 interneurons in an astrocyte-dependent manner.*

Spontaneous activity was observed in motoneurons in the MN+V3+as condition. Similar to the MN+as condition, the activity was eliminated completely with CNQX and restored following washout (Figure 5.5 D, n = 17), but not consistently affected by mec/atr (Figure 5.8). This glutamatergic spontaneous activity occurred sooner in the MN+V3+as condition (week 1) than the MN+as condition (week 2) (Figure 5.5 C); spontaneous burst frequency was found to be higher in week 1 in the MN+V3+as condition (6.73 ± 4.83 bursts/minute compared to 0.50 ± 1.41 bursts/minute in the MN+V3+as and MN+as conditions, respectively; p = 1.4e-07 in a Kruskal Wallis test and p = 0.0006 in a post hoc Dunn's Multiple Comparison test), but there was no significant difference observed in weeks 2, 3 or 4 (Table 5.4). Moreover, the increase in spontaneous burst frequency over time occurred by week 2 in the MN+V3+as condition (from 6.73 ± 4.83 bursts/minute in week 1 to 33.99 ± 49.11 bursts/minute in week 2; p = 0.012 in a Kruskal Wallis test and p = 0.048 in a post hoc Dunn's Multiple Comparison test; Table 5.4), earlier than in the MN+as condition (week 4; Table 5.2). In addition, by week 2, spontaneous EPSP frequency was higher in the MN+V3+as condition compared to the MN+as condition (16.96 ± 19.60 EPSPs/minute compared to 0.09 ± 0.27 EPSPs/minute in the MN+V3+as and MN+as conditions, respectively; p = 3.7e-05 in a Kruskal Wallis test and p = 0.0009 in a post hoc Dunn's Multiple Comparison test; Table 5.4). When taken together with an increased spontaneous burst frequency in week 1, this may indicate increased excitatory drive from V3 interneurons to motoneurons in the MN+V3+as condition.

Despite accelerating the emergence of spontaneous activity in an astrocyte-dependent manner, V3 interneurons did not have a noticeable effect on the characteristics of motoneuronal spontaneous glutamatergic activity (Figure 5.9; Table 5.5 and Table 5.6). Apart from an decrease mean spontaneous burst duration in week 2 in the MN+V3+as condition compared to the MN+as condition (p = 0.046, Mann-Whitney U test), there were no significant differences in mean burst duration, mean cycle time or rhythmicity between the two conditions (Table 5.5 and Table 5.6). However, the amount of time the motoneuron had been in the recording chamber affected spontaneous burst duration (Figure 5.10; p = 0.003 for comparison of spontaneous burst duration at t_0 and t_{max}), which may have

confounded the analysis of spontaneous burst characteristics. The reason for the reduction in spontaneous burst duration with time in the recording chamber was unclear.

Taken together, these results suggest that V3 interneurons affected the maturation of motoneuronal firing properties and accelerated the development of spontaneous activity in an astrocyte-dependent manner, although approximately the same level of maturation was achieved eventually.

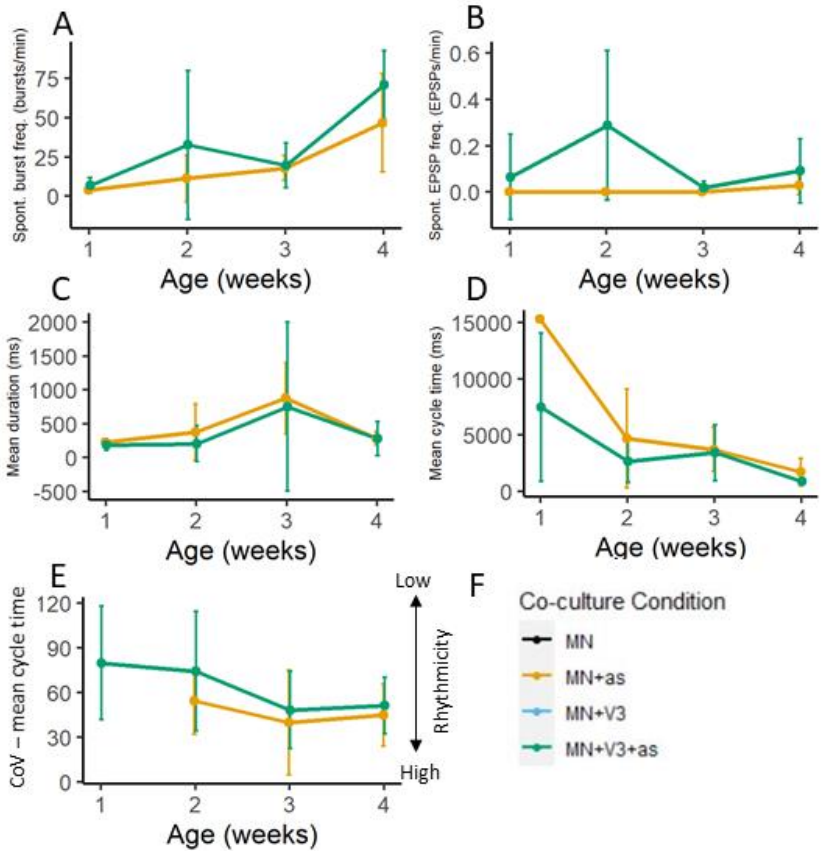

Figure 5.9: V3 interneurons did not affect the characteristics of the motoneuronal spontaneous glutamatergic activity.

Comparison of spontaneous bursts characteristics in MN+as and MN+V3+as conditions: spontaneous burst frequency (A), spontaneous EPSP (putative) frequency (B), mean spontaneous burst duration (C), mean cycle time (D) and rhythmicity (CoV = Coefficient of Variation of mean cycle time; a higher CoV means lower rhythmicity). F is the legend. Error bars are the standard deviation. n are shown in Table 5.5 and Table 5.6.

Table 5.5: Characteristics of spontaneous motoneuronal bursts in MN+as co-cultures.

Values are given as the mean ± standard deviation (n). ^ means that some data was not normally distributed according to a Shapiro-Wilk test so a non-parametric statistical test was used.

Co-culture condition: MN+as				
Property of spontaneous activity	**Week 1**	**Week 2**	**Week 3**	**Week 4**
Mean spontaneous burst duration (ms)^	224 (1)	375 ± 414 (7)	878 ± 526 (6)	284 ± 97 (5)
Mean cycle time (ms)^	15332 (1)	4679 ± 4402 (4)	3710 ± 1956 (6)	1696 ± 1235 (5)
Rhythmicity (CoV for cycle time)^	n/a	54.3 ± 22.3 (3)	40.0 ± 35.2 (6)	45.0 ± 20.7 (5)

Table 5.6: Characteristics of spontaneous motoneuronal bursts in MN+V3+as co-cultures.

Values are given as the mean ± standard deviation (n). ∞ denotes a comparison between weeks 1 and other time points; p<0.075 = ∞, p<0.05 = ∞∞, p<0.01 = ∞∞∞, p<0.001 = ∞∞∞∞. * denotes a significant difference compared to the MN+as culture condition at that time point. Note that comparisons were only made for weeks 1 and 2. p<0.075 = *, p<0.05 = **, p<0.01 = ***, p<0.001 = ****. ^ means that some data was not normally distributed according to a Shapiro-Wilk test so a non-parametric statistical test was used.

Co-culture condition: MN+V3+as				
Property of spontaneous activity	**Week 1**	**Week 2**	**Week 3**	**Week 4**
Mean spontaneous burst duration (ms)^	180 ± 74 (14)	204 ± 265 (15)**	753 ± 1250 (4)	279 ± 251 (5)
Mean cycle time (ms)^	7448 ± 6601 (12)	2651 ± 1904 (15) ∞∞	3417 ± 2499 (4)	863 ± 225 (5) ∞∞∞
Rhythmicity (CoV for cycle time)^	79.9 ± 38.2 (10)	74.4 ± 40.1 (14)	48.4 ± 25.9 (4)	51.4 ± 18.8 (5)

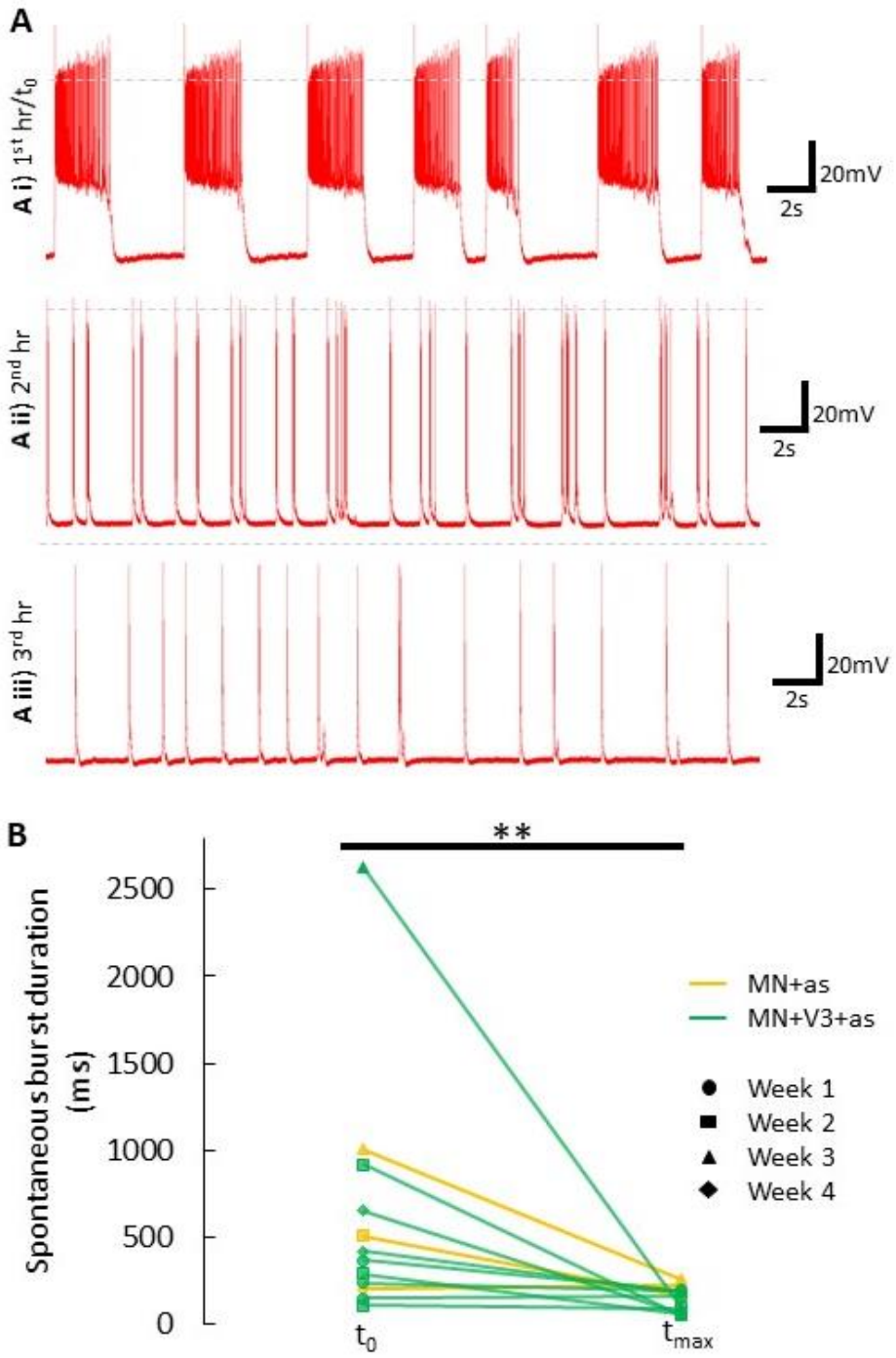

Figure 5.10: Systemic change in spontaneous burst duration with the time the motoneuron had been in the recording chamber.

A: Recordings of spontaneous activity from three different motoneurons in a week 3 MN+V3+as co-culture. The top trace (i) was from the first motoneuron patched on that coverslip and displayed long spontaneous bursts. The middle trace (ii) was recorded from a second motoneuron in the second hour and the bottom trace (iii) from a third motoneuron in the third hour. A systematic reduction in spontaneous burst duration over time can be seen. B: There was a significant reduction in mean spontaneous burst duration between motoneurons recorded from at t_0 and $t_{max,}$ where t was number of hours since the first motoneuron was patched. t_{max} = 2 ± 1 (1-6) hours (binned by hour and given as mean ± standard deviation (range)). Data was found to be non-parametric using a Shapiro-Wilk Test so significance was determined using a Mann Whitney U test. ** = $p<0.01$. Dashed grey lines show 0mV.

5.3.5 Dimensionality reduction by principle component analysis showed co-culture with astrocytes affected electrophysiological maturation of motoneurons over time

To gain a more wholistic picture of the effect of co-culture with V3 interneurons and astrocytes on the maturation of motoneuronal electrophysiological properties, Principle Component Analysis (PCA) was used to reduce the number of dimensions in the dataset (Chapter 2: Materials and Methods, Section 2.12.2.2). The PCA method required missing data within the dataset to be imputed by various methods depending on the reason for the data absence; data missing completely at random was dealt with either by casewise deletion or population mean imputation as appropriate, missing values for depolarisation block were imputed as described in the Chapter 2: Materials and Methods, Section 2.12.2.2, and data missing seemingly due to a lack of astrocytes in the cultures manner was imputed with the mean of astrocyte-free condition (astrocyte-mean imputation). The imputation methods are further described and discussed in the Chapter 2: Materials and Methods, Section 2.12.2.2.2. The robustness of the conclusions drawn from the analysis to this last, astrocyte-mean imputation, was demonstrated by comparison with analyses of datasets created using different imputation methods for this particular missing data (Figure 5.11).

The PCA produced 18 Principle Components (PCs). The first two PCs together captured 36% of the variability in the dataset. The remaining 16 principle components accounted for less than 10% of the variability each. Therefore, only the first two PCs were considered in the present analysis. Many electrophysiological, both passive and firing, properties contributed to each of these two principle components. Notably, slope of the sag ratio-current graph, input resistance, sag ratio, SFA ratio and multiple of rheobase at which depolarisation block occurred each contributed to >10% of PC1 (Figure 5.12E), and the time the motoneuron had been in the recording chamber and rheobase contributed to >10% of PC2 (Figure 5.12F). No variable contributed to >13% of either PC.

There was an effect of time on both PC1 and PC2; a significant increase was observed between week 1 and 2 in the MN alone condition for both (from -3.11 ± 1.65 and -0.39 ± 1.06 in week 1 to -0.23 ± 0.63 and 1.47 ± 0.96 in week 2 for PC1

and PC2, respectively; Table 5.1), verifying that these PCs could be used to investigate the change of electrophysiological properties with time. Indeed, PC1 changed significantly between weeks 1 and 2 in every culture condition (Table 5.1, Table 5.2, Table 5.3, Table 5.4); this may indicate a facet of electrophysiological development that was common to all co-culture conditions.

To investigate the effect of astrocytes, the differences between PCs 1 and 2 in motoneurons from the MN alone and MN+as culture conditions were considered. In both weeks 1 and 2, the MN alone and MN+as data clustered separately when PC2 was plotted against PC1 (Figure 5.12 A). Furthermore, though both conditions displayed an increase in PC1 over time (Table 5.2), a significant difference was observed between PC1 of the two culture conditions at both time points (Table 5.2; $p = 2.3e-06$ in a Kruskal Wallis test for week 1 and $p = 0.0002$ in a post hoc Dunn's Multiple Comparison test; $p = 2.1e-05$ in a Kruskal Wallis test for week 2 and $p = 0.0017$ in a post hoc Dunn's Multiple Comparison test). PC1 of week 1 motoneurons in MN+as cultures were comparable to PC1 of week 2 motoneurons in MN alone cultures (-0.08 ± 0.66 and -0.23 ± 0.63 respectively; Figure 5.12 A; Table 5.2). This may indicate that, while motoneurons in the two culture conditions were maturing along the same trajectory electrophysiologically, co-culture with astrocytes accelerated that maturation.

In contrast, the presence of astrocytes in culture seemed to prevent a change in motoneuronal PC2 over time. The increase of PC2 between weeks 1 and 2 seen in the MN alone condition was not observed in the MN+as condition (Figure 5.12A). Indeed, there was no significant change in PC2 between the two time points where astrocytes were present (Table 5.2). One of the two main variables that contributed strongly to PC2 was the time that the motoneuron had spent in the recording chamber during the patching process. Therefore, the lack of change in PC2 in the MN+as condition may indicate an increased resilience to deterioration during incubation in the recording chamber – i.e. increased cell health. These data show that astrocytes affect both motoneuronal electrophysiological properties and the trajectory of their development over time.

V3 interneurons did not alter the change in PCs 1 and 2 over time; overlap was observed between the Euclidean ellipses of the MN alone and MN+V3 conditions at both time points (Figure 5.12 B) and no significant differences were observed

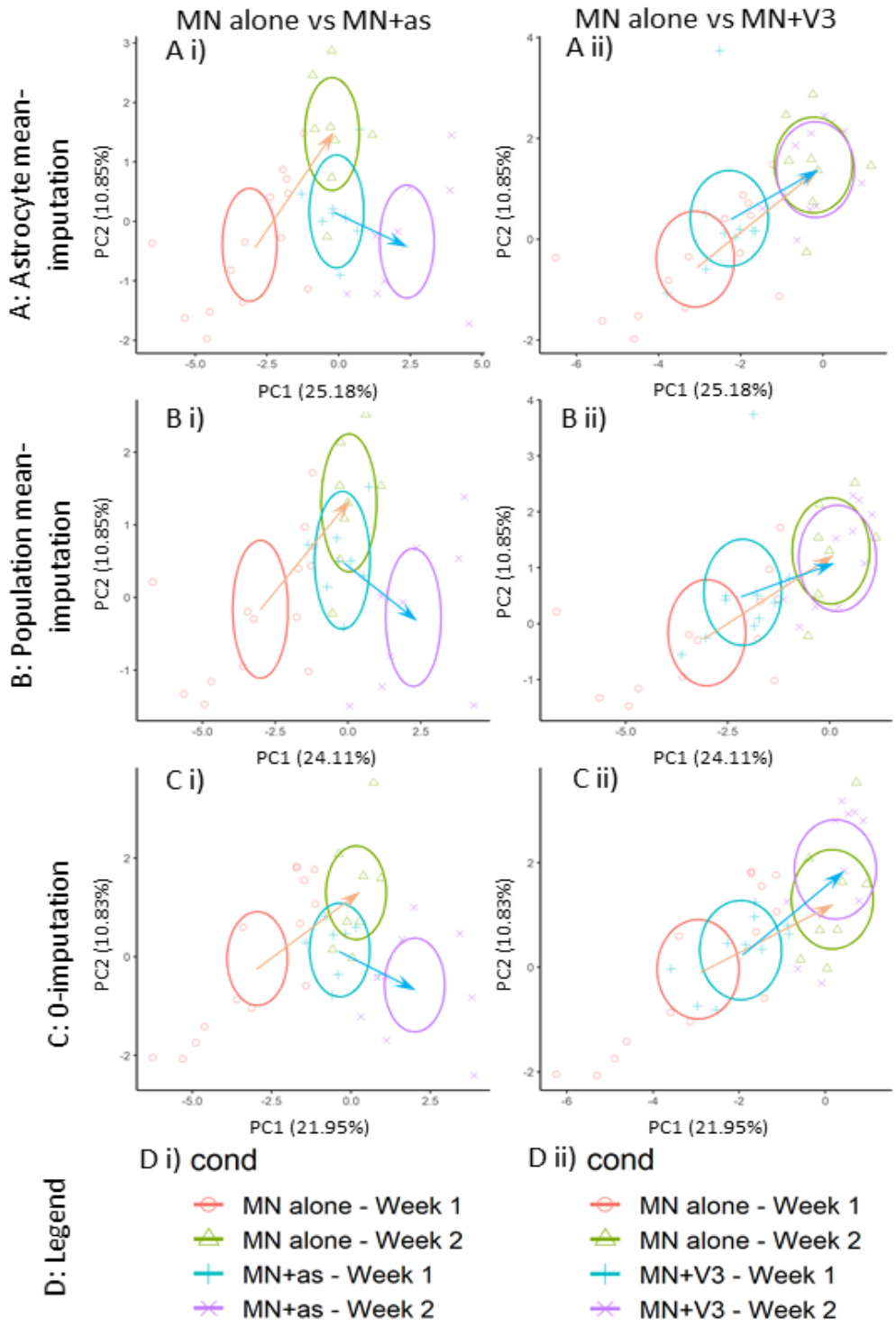

Figure 5.11: Conclusions drawn from the PCA analysis were robust to different methods of imputing missing data (specifically, data MAR in 2 of Chapter 2: Materials and Methods, Section 2.12.2.2.2).

The graphs show PC1 (x axes) and PC2 (y axes) in weeks 1 and 2; for each condition, the trajectory of development of the PCs is denoted with an arrow. The ellipses are Euclidean ellipses. The left-hand column (i) shows the comparison between the MN alone and MN+as conditions, and the right-hand column (ii) shows the comparison between the MN alone and MN+V3 conditions. D shows the legend for each comparison; cond = condition. The method of imputation used in section 5.3.5 was the astrocyte-mean imputation method (A). This was compared to the population mean-imputation method (B) and the 0-imputation method (C).

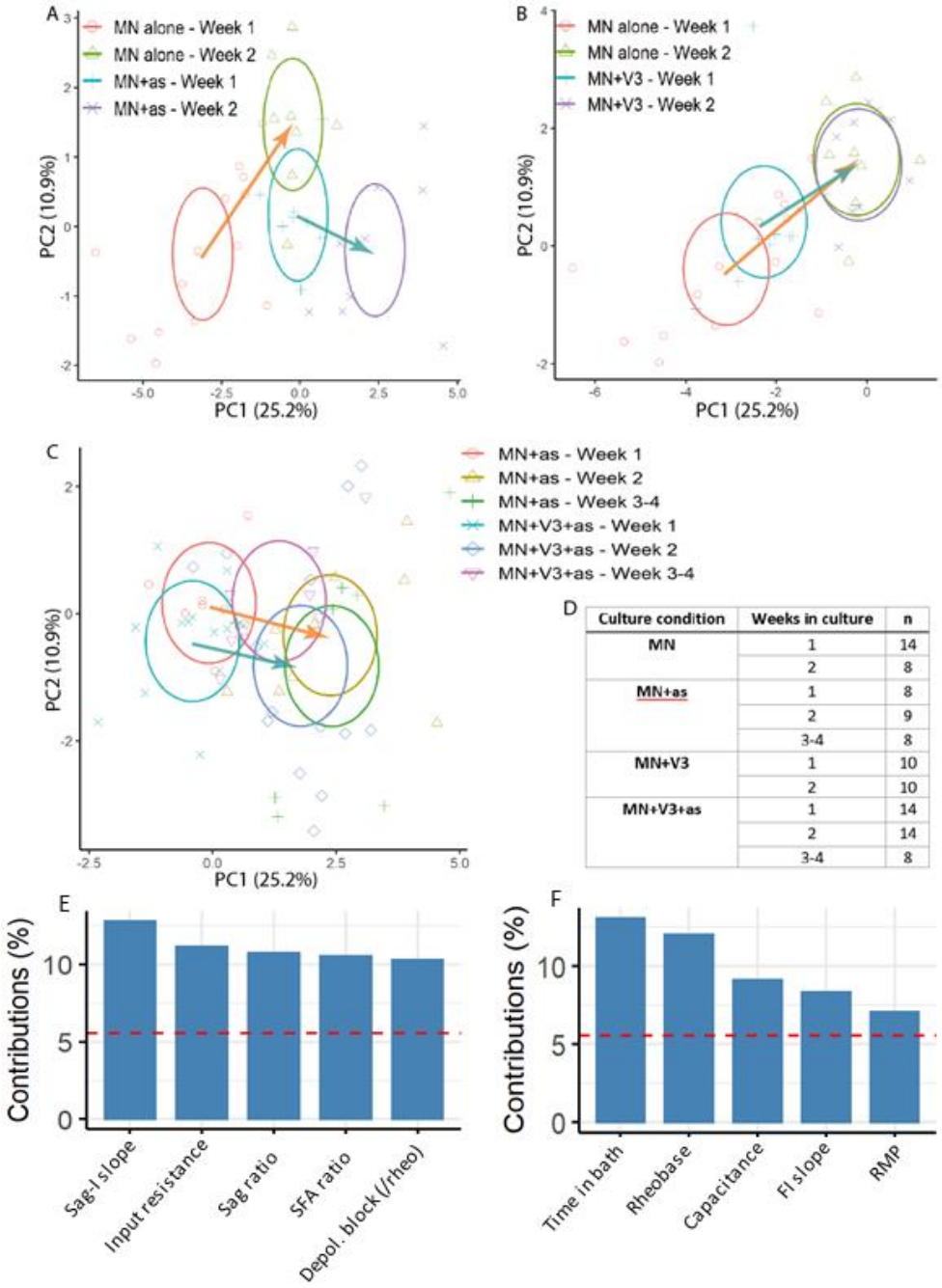

Culture condition	Weeks in culture	n
MN	1	14
	2	8
MN+as	1	8
	2	9
	3-4	8
MN+V3	1	10
	2	10
MN+V3+as	1	14
	2	14
	3-4	8

Figure 5.12: PCA of motoneuronal electrophysiological properties in motoneurons co-cultured alone or with astrocytes (as) and/or V3 interneurons (V3).

Arrows show change in PCs between weeks 1 and 2. Ellipses are Euclidean ellipses. A: The trajectory of PC development was different in the MN alone condition (orange arrow) compared to the MN+as condition (turquoise arrow). B: The trajectory of PC development was not different in the MN alone condition (orange arrow) compared to the MN+V3 condition (turquoise arrow). C: The trajectory of PC development was not different in the MN+as condition (orange arrow) compared to the MN+V3+as condition (turquoise arrow). D: Number of motoneurons in each co-culture condition included in the PCA analysis. E and F show the 5 variables that contribute most to PC1 and PC2, respectively. FI slope refers to the primary slope of SFF plotted against current as in Figure 5.3. 'Time in bath' refers to the time the motoneuron had spent in the recording chamber before being patched. The red dashed line corresponds to the expected value if the contribution where uniform.

between those two culture conditions in either PC. A similar observation was made when the MN+as and the MN+V3+as conditions were compared (Figure 5.12 C); again, a significant difference was not observed. This ruled out an astrocyte-dependent effect of V3 interneurons on the two PCs. These results together suggest that the presence of astrocytes, but not V3 interneurons, significantly affected the maturation of electrophysiological properties in motoneurons.

5.4 Discussion

5.4.1 Summary

The results presented in this Chapter show that the maturation of some motoneuron electrophysiological properties occurred in pure populations of ESC-derived motoneurons *in vitro*, without the influence of other cell types. However, higher levels of electrophysiological maturity were achieved and on a shorter time scale when the motoneurons were co-cultured with astrocytes. Furthermore, glutamatergic, spontaneous activity occurred only in motoneuron cultures that contained astrocytes. In contrast, on their own, V3 interneurons had a little or no effect on the maturation of motoneuronal electrophysiological properties. However, in the presence of astrocytes, V3 interneurons accelerated the development of glutamatergic, spontaneous activity in the motoneuron co-cultures. There were also complex, astrocyte-dependent effects of V3 interneurons on the active electrophysiological properties of motoneurons in culture; in some ways seeming to improve and in others seeming to regress motoneuronal maturation. Thus, the electrophysiological maturation of motoneurons was, in the most part, accelerated and improved by their interaction with astrocytes and V3 interneurons.

5.4.2 Developmental reduction of action potential half width

Trends in motoneuronal electrophysiological development observed in this Chapter were generally consistent with observations in the literature. However, this was not always the case. For example, while consistent evidence across multiple motoneuron subtypes and culture models has shown that action potential duration/half width decreases during development (Chapter 1: General Introduction, Table 1.4), here, motoneuronal action potential half width did not reduce between week 1 and week 2 in any of the culture conditions except the MN+V3 condition. One reason for this discrepancy could be the time points selected. Bryson et al (2014), using the same model and ESC line as in the MN+as culture condition, showed a decrease in action potential half width between 3 and 7 Days *In Vitro* (DIV). As the first time point used in this Chapter was week 1 – i.e. 7-13 DIV – it is likely that the expected reduction in action potential duration had already taken place at this stage. The observation of wider action potentials in week 1 in MN+V3 condition compared to the MN alone

condition and of a reduction in half width between week 1 and 2, suggests that the addition of V3 interneurons to the motoneuron co-culture slowed the maturation of the ion conductances responsible for narrowing of the motoneuronal action potential.

5.4.3 In the presence of astrocytes, motoneurons displayed initial doublets/triplets and V3 interneurons modulate this feature of motoneuronal firing.

In vivo, doublets (and triplets) are often observed in slow and fast motoneurons at the beginning of a movement/burst of action potentials, both in experimental models (Bączyk et al., 2013; Gorassini et al., 2000; Mrówczyński et al., 2010) and humans. They represent a highly conserved mechanism to rapidly enhance the force of muscles at the beginning of a contraction (Mrówczyński et al., 2015). A study of ESC-derived motoneurons *in vitro* showed that doublets could be elicited by activating Ca_V1-type Ca^{2+} channels and were eliminated when these channels were blocked (Miles et al., 2004). In this Chapter, doublets/triplets were predominantly observed in the MN+as condition, resulting in a higher IFF than in the MN alone condition. This finding is consistent with the known role of astrocytes in facilitating higher frequencies of motoneuronal firing *in vivo* by modulating extracellular ion concentrations (Kelley et al., 2018; Morquette et al., 2015) and calcium signalling (Morquette et al., 2015). However, in the MN+as condition, the doublet threshold was exclusively 1 x rheobase, whereas *in vivo* the doublet threshold is most commonly 2-3 x rheobase (Mrówczyński et al., 2010, 2015). In contrast to the MN+as condition, doublets/triplets were less frequent in the MN+V3+as condition, particularly at earlier timepoints. Where doublets/triplets were observed in week 2 (2/10 motoneurons), the doublet threshold was higher at approximately 1.5 x and 4.5 x rheobase, which is more in the range to be expected from the literature. It seems that V3 interneurons modulate this feature of motoneuronal firing. Indeed, *in vivo,* descending supraspinal inputs and networks in the spinal cord are thought to modulate doublets/triplets *in vivo* (Gorassini et al., 2000; Mrówczyński et al., 2015).

5.4.4 The effect of astrocytes on motoneuronal electrophysiological development and health may be due to release of trophic factors and spontaneous activity.

The presence of astrocytes in the motoneuronal cultures promoted motoneuron health and survival, increased the maturation of both passive and active electrophysiological properties, and was necessary for the emergence of spontaneous activity. These effects could be due to various mechanisms. While motoneurons in astrocyte-free cultures are exposed to GDNF (expressed by the C9G ESC line under the ubiquitous CAG promoter and included in the culture media), astrocytes express and release many additional neurotrophic factors which promote neuronal health and prevent programmed cell death (Ang et al., 1992; Taylor et al., 2007; Yamanaka and Komine, 2018). Furthermore, astrocytes are necessary for the generation of spontaneous motoneuronal activity in the co-cultures, most likely because of their essential role in synapse formation (Chapter 4). Indeed, glial cells, including astrocytes, have been shown to express and secrete various synaptogenic factors, such as thrombospondin, that are essential for the formation of synapses *in vitro* (Allen and Eroglu, 2017; Christopherson et al., 2005; Ullian et al., 2004a). In addition to their role in synapse formation, astrocytes have an important role in maintaining synaptic transmission. For example, as discussed in Chapter 1: General Introduction, Section 1.8.2, astrocytes play an important role in controlling the concentration of glutamate in the synaptic cleft (Hill et al., 2016; Tzingounis and Wadiche, 2007). They also modulate the extracellular concentration of ions, which dramatically affects neuronal firing and circuit function (as described in Chapter 1: General Introduction, Sections 1.8.3 and 1.8.6; Kelley et al., 2018; Morquette et al., 2015). The roles astrocytes play in synaptic formation and transmission likely underly the marked influence of astrocytes on electrophysiological maturation and the emergence of spontaneous motoneuronal activity observed in these co-cultures.

The astrocyte-dependent spontaneous activity itself may also have improved electrophysiological development and motoneuronal health. *In vivo,* spontaneous activity influences the maturation of spinal circuitry (Montague et al., 2017; Warp et al., 2012) and, in the cortex, spontaneous activity prevents programmed motoneuronal death (Golbs et al., 2011; Heck et al., 2008; Nimmervoll et al., 2013). Thus, astrocytes may have affected motoneuron health and

electrophysiological maturation both directly by the expression of neurotrophic factors and indirectly by enabling motoneuronal spontaneous activity.

5.4.5 The neurotransmitter dependency of spontaneous activity in motoneurons

Perhaps surprisingly for a neuronal population often considered to be predominantly cholinergic, motoneuronal spontaneous activity was eliminated by exposure to a glutamate receptor blocker. As purified motoneuron and astrocytes populations were used to generate the cultures, the presence of activity in the MN+as condition indicated the presence of glutamatergic motoneuron-to-motoneuron synaptic connections. Such motoneuronal glutamatergic activity has been previously observed in mixed cultures (Sternfeld et al., 2017; Zhang et al., 2009) and in motoneurons on glial cells (Sternfeld et al., 2017; Taga et al., 2019; Ullian et al., 2004a), and motoneurons are known to form reciprocal glutamatergic synapses with other motoneurons in the mature spinal cord (Bhumbra and Beato, 2018). However, despite the spontaneous glutamatergic activity observed in these cultures, the experiments described in Chapter 4, Section 4.3.2.1 found no significant increase in the density of motoneuronal glutamatergic (vGluT2-positive) synapses in the somatic and proximal dendritic compartments in the MN+as condition when compared to the silent MN alone condition at the same time point. This was an unexpected finding because astrocytes are known to release synaptogenic molecules that induce the formation of both silent and active glutamatergic synapses (Allen and Eroglu, 2017). It may be that the glutamatergic synapses responsible for this activity were not located in the somatic or proximal dendritic compartments, but rather in the distal dendritic or axonal compartments, meaning they were not captured by the analysis undertaken in Chapter 4. Indeed, early anatomical tracing studies showed that, although sometimes found on proximal dendrites, most axon collaterals in the motor nuclei terminated in the neuropil (Cullheim et al., 1977). Another possibility is that glutamatergic transmission was mediated by a mechanism not involving vGluT2. In support of this possibility was the astrocyte-dependent increase in the motoneuronal density of puncta positive for Homer1, a marker of glutamatergic synapses.

To investigate the role of cholinergic neurotransmitters in the cultures, non-selective antagonists of nicotinic and muscarinic cholinergic receptors,

mecamylamine and atropine, were added together to the cultures. While the antagonists often affected the burst frequency and burst characteristics of the spontaneous activity of motoneurons, the effects varied from one motoneuron to the next. This is in contrast to previous experiments in primary cultures of embryonic rat motoneurons that found that, while addition of mecamylamine and atropine did not affect mean burst frequency, mean burst duration was decreased (Zhang et al., 2009), though the authors did not report the effects on individual cultures. One reason for the variable effects of the blockers in this Chapter could be that different cholinergic receptors have different effects on spontaneous motoneuronal activity. For example, muscarinic M2 and M3 receptors have opposing effects on spinal locomotor circuits. During M2 receptor blockade, locomotor burst frequency and frequency variance decreased, and burst duration increased. Conversely, during M3 receptor blockade, frequency variance increased and locomotor burst duration decreased (Nascimento et al., 2019). As the antagonists used in this Chapter were non-selective, the effect would depend on the balance of M2 and M3 receptors (and any other cholinergic receptors present) expressed by each motoneuron. Further investigation of the impact of cholinergic signalling on the spontaneous activity in these cultures would require the use of more selective cholinergic receptor antagonists.

5.4.6 The effect of co-culture with V3 interneurons on motoneuronal spontaneous activity

As excitatory interneurons that connect monosynaptically with motoneurons and are involved in stabilising spinal rhythm-generating networks (Chopek et al., 2018; Zhang et al., 2008b), V3 interneurons are a prime candidate for the modulation of motoneuronal spontaneous activity. Indeed, Sternfeld et al. (2017) studied the effect of motoneuron, V3 interneuron and inhibitory V1 interneuron co-culture on spontaneous network activity *in vitro*. From their experiments, they generated a model predicting that in a co-culture with a high excitation/inhibition ratio (such as the MN+V3+as networks used in this Chapter), the excitatory drive of V3 interneurons would dominate, increasing the burst frequency and rhythmicity. In agreement with the model, spontaneous burst frequency was increased in the MN+V3+as condition compared to the MN+as condition in week 1. However, by week 2 there was no significant difference. Moreover, V3 interneurons had no impact on the rhythmicity of the spontaneous activity.

However, the results in this Chapter were obtained by intracellular electrophysiology, a low throughput technique compared to calcium imaging, as in the study by Sternfeld et al. (2017). In the next chapter, calcium imaging was used to further investigate whether V3 interneurons modulate motoneuronal spontaneous activity.

6 Chapter 6: The effect of co-culture with V3 interneurons on motoneuronal spontaneous calcium activity

6.1 Introduction

Spontaneous activity in the spinal cord has been shown to be important for motoneuron maturation *in vivo*, affecting axon guidance (Kastanenka and Landmesser, 2010), dendritic morphology (Kalb and Hockfield, 1992) and the formation of spinal circuitry (Montague et al., 2017; Warp et al., 2012). Magown et al. (2017) found that peripherally-engrafted EBs sometimes contained microcircuits that were spontaneously active, resulting in spontaneous muscle contractions. Therefore, it has been suggested that activity of peripherally-engrafted ESC-derived motoneurons is necessary for the formation of functional NMJs (Bryson et al., 2016) and that the failure of engrafted purified motoneurons to form functional NMJs (Bryson, personal communication), was due to a lack of motoneuron activity within the graft. Indeed, in the previous Chapter, I showed that purified, ESC-derived motoneurons cultured alone were not active, and that the presence of astrocytes was fundamental to the generation of spontaneous motoneuron activity *in vitro*.

While motoneurons plated with astrocytes display spontaneous activity (Sternfeld et al., 2017; Ullian et al., 2004a), this activity is modulated by interaction with other interneurons present. For example, co-culturing motoneurons with inhibitory V1 interneurons reduced spontaneous burst amplitude and synchronicity while increasing network complexity. Synchronous bursting was restored by the addition of V3 interneurons to motoneuron-V1 interneuron-astrocyte co-cultures, suggesting that V3 interneurons provide a strong excitatory drive that dominates network output (Sternfeld et al., 2017). Different patterns of spontaneous activity, which have been shown to arise at different times during development (Yvert et al., 2004), may have functional consequences. For example, it has been shown that different manipulations of the frequency of spontaneous motoneuron activity have different effects on motor circuit formation (Hanson et al., 2008). Therefore, in this Chapter, the effect of co-culture with V3 interneurons on spontaneous activity in motoneuron co-cultures was further investigated.

Single cell patch clamp techniques, as used in Chapter 5, are low throughput and do not allow observations of spontaneous activity at a network level (Buzsáki, 2004; Wei et al., 2020). In contrast, calcium imaging enables the observation of multiple neurons in a network concurrently, including information about the temporal and spatial relationship of activity in different neurons (Grienberger and Konnerth, 2012). Motoneurons have been shown to demonstrate spontaneous calcium activity in zebrafish (Warp et al., 2012), in chick (Montague et al., 2017; O'donovan et al., 1998), in mouse ESC-derived cultures (Sternfeld et al., 2017), and in human ESC-derived (Bianchi et al., 2018) and iPSC-derived (Boulting et al., 2011; Karumbayaram et al., 2009) cultures.

6.2 Aims of this Chapter

Given these limitations of single cell patch clamp techniques, in this Chapter, calcium imaging was used to gain further insight into the effect of co-culture of ESC-derived motoneurons with V3 interneurons on spontaneous network activity

6.3 Results

During electrophysiological experiments, spontaneous activity was observed in motoneurons cultured with astrocytes from week 2 onwards. To investigate the effect of co-culture with V3 interneurons on the pattern and characteristics of spontaneous activity, motoneurons were cultured with and without V3 interneurons in the presence of astrocytes (the MN+V3+as and MN+as conditions, respectively; see Chapter 2: Materials and Methods, Section 2.5). Week 2 and 3 motoneuron cultures were loaded with the green fluorescent calcium binding dye, Fluo-8 AM, and calcium activity in the somas of motoneurons and V3 interneurons was recorded (Chapter 2: Materials and Methods, Section 2.13; Figure 6.1). The expression of tdTomato by V3 interneurons enabled them to be distinguished from motoneurons (Figure 6.1 A ii). The ESC-derived motoneurons expressed ChR2 but there was no evidence that ChR2-dependent calcium activity could be activated with the microscope settings used. Indeed, many of the cultured motoneurons were silent, with no motoneurons (cultured with astrocytes alone) showing any spontaneous calcium activity until week 3 in the absence of V3 interneurons. The astrocytes formed a monolayer under the neurons and were out of the plane of recording in these experiments. When examined, astrocytes rarely showed any calcium activity unless the laser power exceeded 10%, in which case the laser caused a calcium wave that propagated throughout the astrocytic syncytia. For this reason, even though the astrocytes were out of plane, the laser power was kept at or below 10%.

6.3.1 The presence of V3 interneurons accelerated the emergence of synchronous spontaneous glutamatergic calcium activity.

Motoneurons in both the MN+as and the MN+V3+as co-culture conditions displayed spontaneous calcium activity (Figure 6.2 A i-iii and B i-iv, respectively). However, in the presence of V3 interneurons, motoneuronal spontaneous calcium activity arose earlier; while no activity was observed in week 2 MN+as co-cultures (Table 6.1), 7/8 Fields Of View (FOVs) examined in week 2 MN+V3+as co-cultures contained neurons with spontaneous calcium activity (across two coverslips from two differentiations; Table 6.1). By week 3, spontaneous calcium activity was observed in both co-culture conditions (12/26 FOV on five coverslips from five differentiations in the MN+as condition and 15/20

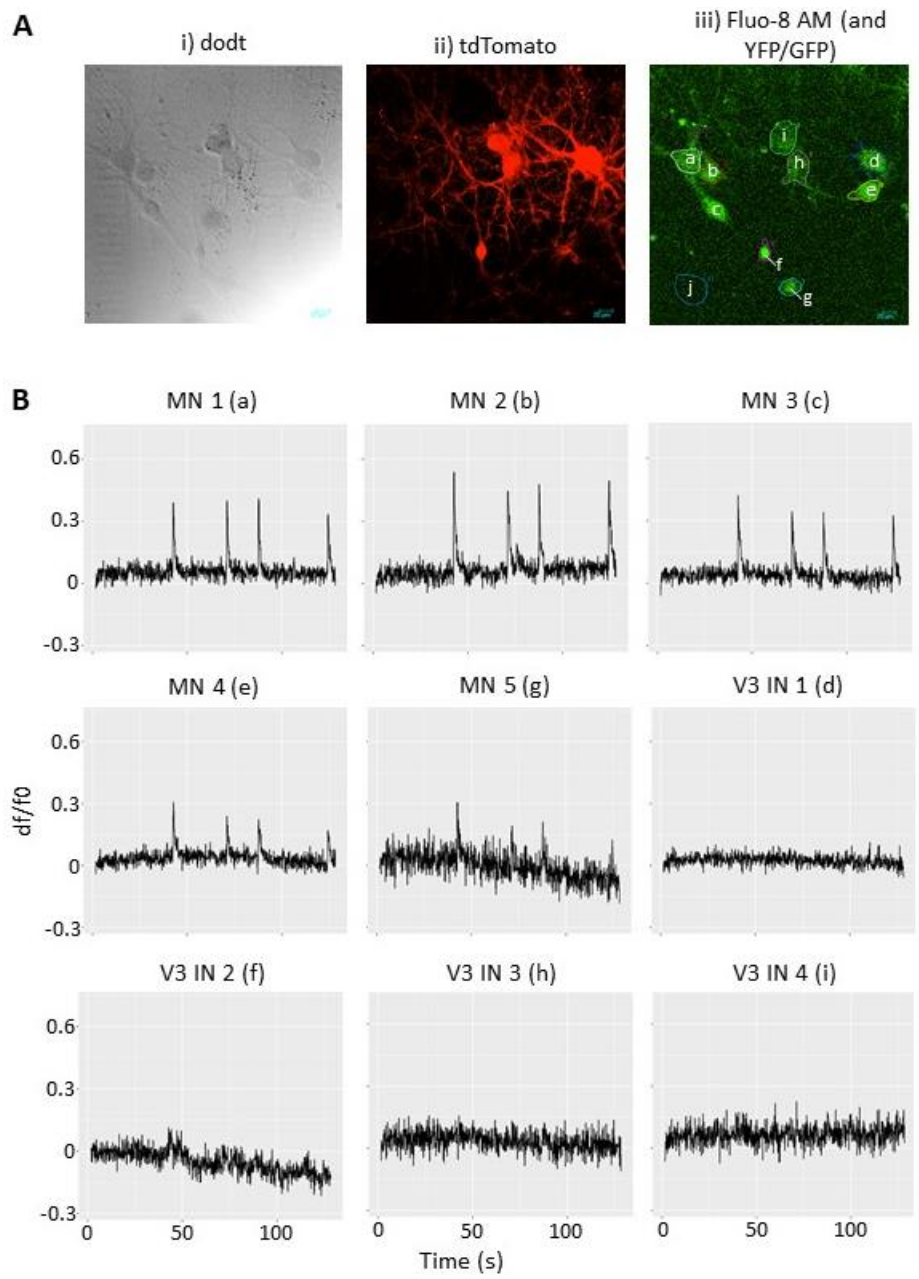

Figure 6.1: Example calcium activity in a MN+V3+as co-culture.

A: A Field Of View (FOV) from a week 2 MN+V3+as co-culture. All neurons somas were visible in the dodt image (A i). TdTomato-positive V3 interneurons were distinguished by tdTomato expression (A ii). All cells were loaded with the green fluorescent calcium dye, Fluo-8 AM, and the motoneurons and V3 interneurons are both visible in A iii because the dye was fluorescing due to spontaneous calcium activity. The astrocytes were below the plane of the image. Regions Of Interest (ROI; labelled a-j in A iii were drawn around the cell bodies as observed in the dodt image (A i) and the Fluo-8 AM signal was recorded over time in each ROI. ROI j served as a measure of background fluorescence. The background was subtracted and df/f0 was calculated for each ROI (B). In this particular culture, four synchronous calcium events were observed in the five motoneurons and the V3 interneurons did not display calcium activity. Imaging settings for A: A resonant galvo was used. Dwell time = 0.4µs/px, frame period = 0.066s, scan line period = 0.063ms. Images are 1024x1024 pixels with 0.386µm/pixel. For dodt (A i), tdTomato (A ii) and Fluo-8 AM (A iii) images respectively, the excitation wavelength was 720, 1100 and 860nm, the laser power was 70, 30 and 100, and the PMT gain was 128, 548 and 605.

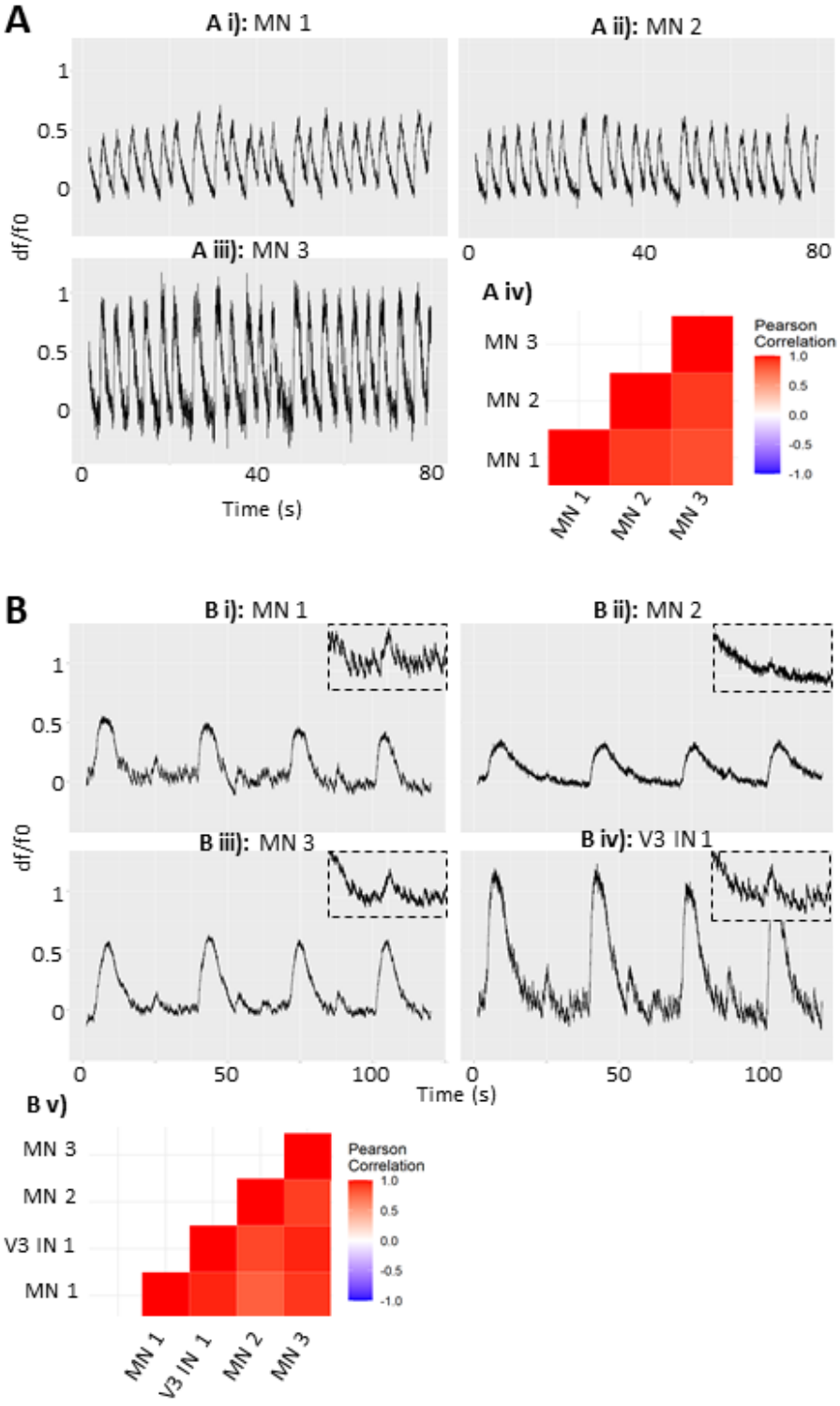

Figure 6.2: Calcium bursting in both the MN+as and MN+V3+as conditions were predominantly correlated.

Example recordings from bursting neurons in a single FOV in week 3 MN+as (A i-iii) and MN+V3+as (B i-iv) co-cultures. The traces in B i-iv between 12.5s and 37.5s have been expanded in the boxes in the top right of each trace and outlined with a black dashed line. These show the small, short events of the long+short pattern in the MN+V3+as condition more clearly. Note that non-bursting neurons in each FOV have not been included in the figure. Bursting was correlated in both the MN+as and the MN+V3+as condition, as illustrated by the heat maps of Pearson correlation coefficients in A iv and B v respectively.

Table 6.1: Correlation of bursting neurons in MN+as and MN+V3+as co-cultures.

FOV = field of view on a coverslip; c = Pearson correlation coefficient. n/a means co-cultures of this age did not display spontaneous activity

Condition	**MN+as**			**MN+V3+as**		
Age	Week 1	Week 2	Week 3	Week 1	Week 2	Week 3
# differentiations	1	1	5	2	2	4
# coverslips	2	1	5	2	2	7
# FOVs with any bursting neurons	0/5	0/6	12/26	0/7	7/8	15/20
# FOVs with multiple bursting neurons	n/a	n/a	10/12	n/a	3/7	13/15
# Not correlated FOVs with multiple bursting neurons ($c < 0.3$)	n/a	n/a	1/10	n/a	0/3	2/13
# mostly correlated FOVs with multiple bursting neurons ($0.3 < c < 0.6$)	n/a	n/a	0/10	n/a	0/3	3/13
# correlated FOVs with multiple bursting neurons ($c > 0.6$)	n/a	n/a	9/10	n/a	3/3	8/13

FOV on six coverslips from four differentiations in the MN+V3+as condition). Thus, as observed in electrophysiological experiments in Chapter 5, the presence of V3 interneurons accelerated the emergence of motoneuronal spontaneous activity in the co-cultures.

The spontaneous calcium activity in ESC-derived co-cultures of V3 interneurons, motoneurons and V1 interneurons measured by Sternfeld et al. (2017) was highly correlated. Similarly, between active neurons in one FOV on a coverslip, spontaneous calcium activity was predominantly correlated; the neurons in both the MN+as and MN+V3+as culture conditions burst synchronously (Figure 6.2 A iv and B v, respectively; Table 6.1; Pearson correlation coefficient >0.6). That is, if a neuron had calcium bursts, it burst at the same time as other bursting neurons. The synchronous spontaneous calcium activity was eliminated by the addition of

the AMPA receptor antagonist, CNQX, and was restored on washout in both the MN+as and MN+V3+as conditions (Figure 6.3), demonstrating that the spontaneous calcium activity was glutamate-dependent.

6.3.2 The presence of V3 interneurons affected the pattern of spontaneous calcium activity.

The pattern of spontaneous activity has been shown to change throughout spinal cord development *in vivo* (Yvert et al., 2004), so the effect of V3 interneurons on the pattern of spontaneous calcium activity *in vitro* was examined. In the MN+V3+as culture condition only, a distinctive pattern of spontaneous calcium activity was observed whereby low amplitude, short duration calcium events were interspersed by regular, higher amplitude, longer duration calcium events (example in Figure 6.2 B i, iii and iv). Hereafter, this pattern is referred to as the 'long+short' pattern. While the calcium event duration histogram for the MN+as condition had one peak between 0-3s (Figure 6.4 A), the long calcium events in the MN+V3+as condition led to a bimodal calcium event duration histogram with two peaks, one between 0-1s and another between 3-8s (Figure 6.4 B). This long+short pattern was observed on 4/7 coverslips and in 8/11 FOVs on those coverslips in the MN+V3+as condition, compared to 0/3 coverslips (0/7 FOVs) in the MN+as condition. It should be noted that, despite the numerical evidence of correlation, not every short calcium event was present in every bursting neuron in an FOV (Figure 6.2 B ii and iii). It is unclear whether this was because the neuron truly did not fire or whether the events did not cause sufficient somatic calcium influx to be detected by the calcium dye in those neurons.

6.3.3 Spontaneous calcium event frequency and event characteristics

To further investigate the effect of V3 interneurons on the spontaneous calcium activity of motoneurons, calcium event frequency, the proportion of calcium events that were long (>3s), and various event characteristics of each bursting neuron were measured. These included mean event amplitude, mean event duration, mean event cycle time, variation in event amplitude, variation in event duration, variation in event cycle time (i.e. the inverse of rhythmicity).

The first step of the analysis was to decide on the appropriate statistical unit. Calcium imaging data were collected from individual neurons (motoneurons and V3 interneurons) in FOVs on coverslips. As spontaneous calcium activity

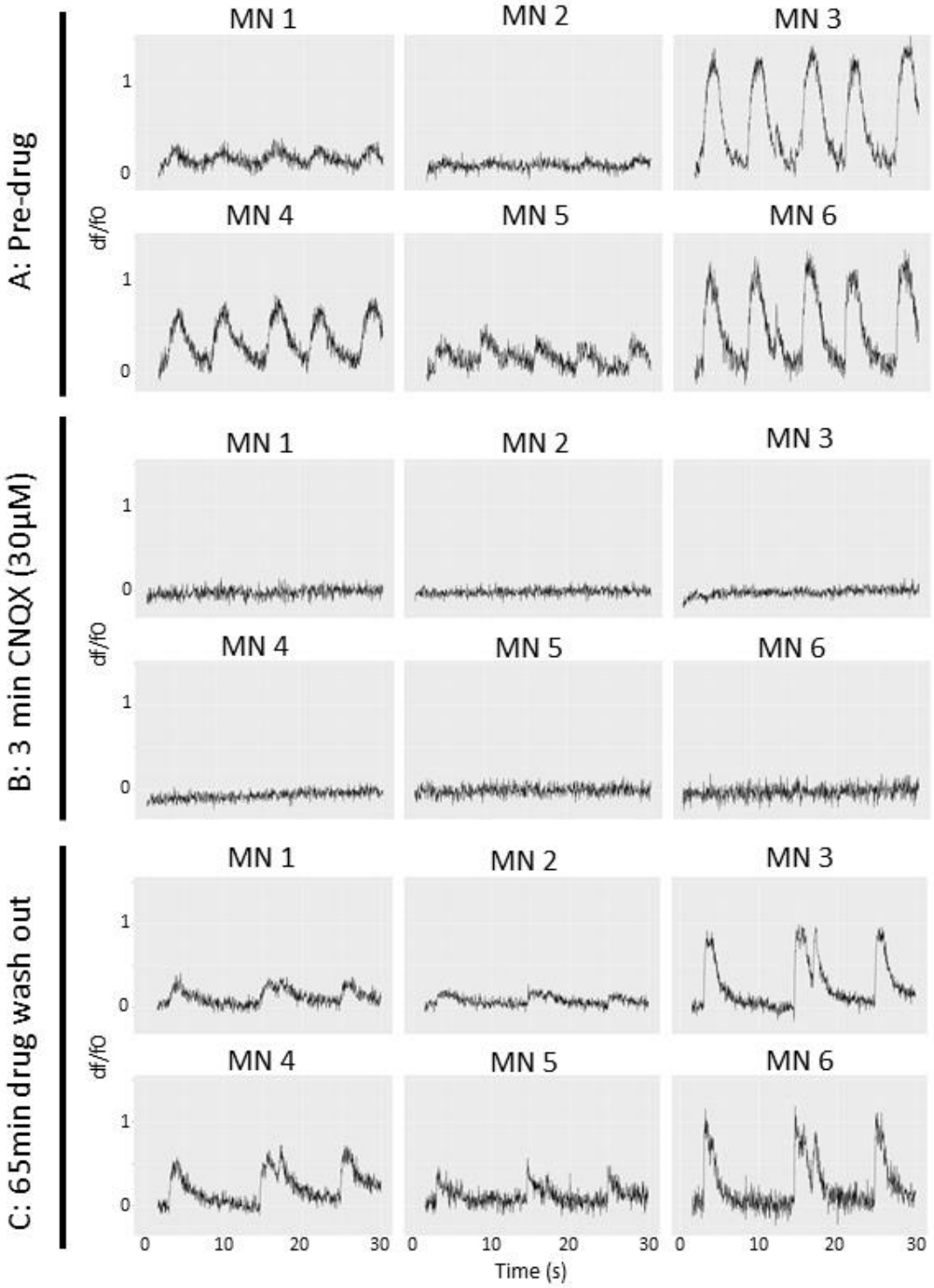

Figure 6.3: Spontaneous calcium activity in motoneuron co-cultures was eliminated by glutamatergic receptor antagonist, CNQX.

In this example, motoneurons in a week 3 MN+as co-culture displayed spontaneous calcium activity (A). Addition of CNQX (30µM, 3min) eliminated this activity (B). Washout of the drug (65min) restored the spontaneous calcium activity in the motoneurons (C). n = 4 repeats from three separate coverslips/differentiations for the MN+as co-culture condition and n = 5 repeats from four separate coverslips/differentiations for the MN+V3+as co-culture condition.

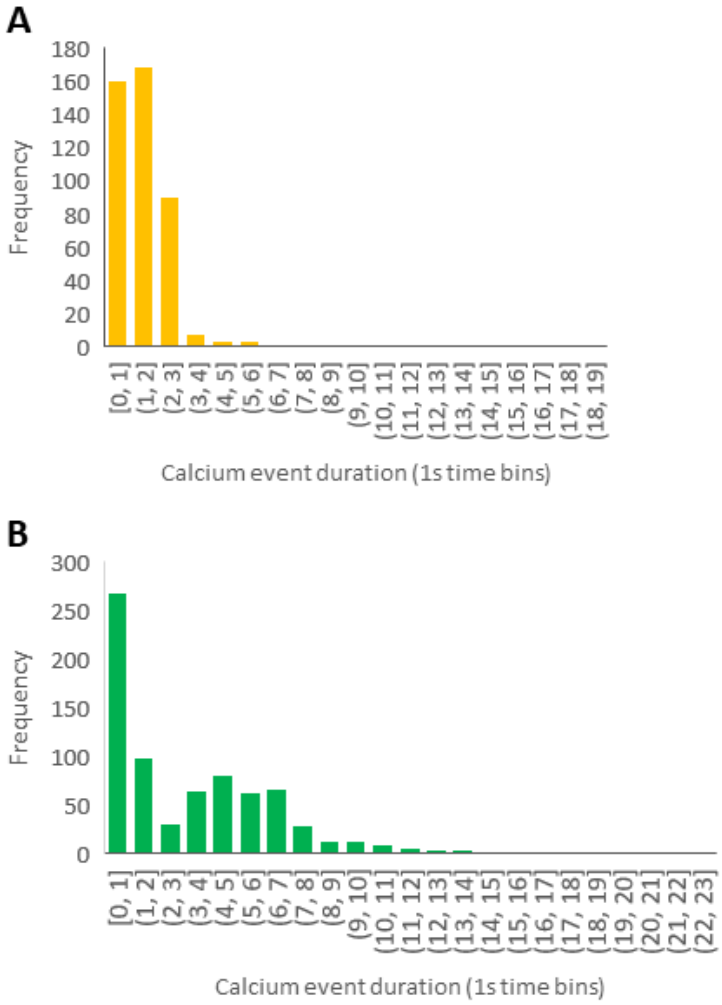

Figure 6.4: Calcium event duration histograms illustrating the long+short pattern of spontaneous calcium activity in the MN+V3+as condition.

Histograms of the duration of all calcium events recorded in the MN+as (A; yellow) and MN+V3+as (B; green) conditions. This included 440 calcium events from 24 motoneurons in the MN+as condition, and 750 calcium events from 37 motoneurons and 42 V3 interneurons in the MN+V3+as condition. The long+short pattern in the MN+V3+as condition means the calcium event duration histogram is bimodal.

between bursting neurons in a FOV was correlated, individual bursting neurons were not considered statistically independent and FOV averages were calculated. As there was no evidence that bursting neurons in different FOVs on the same coverslip were not also correlated, it could be suggested that coverslip averages should be calculated and used as the statistical unit. However, there was large variation of event characteristics between FOVs at different locations recorded at different times on the same coverslip. Furthermore, periodic recordings from neurons in one FOV showed the calcium event frequency and event characteristics varied greatly overtime. The variance of FOV averages was

not significantly different to the variance of coverslip averages using an F test (or a Conover test for the non-parametric datasets) and, as illustrated in Figure 6.5, the median and inter quartile ranges were similar between FOV averages and coverslip averages datasets. The assumption of equal variance between the FOV averages and coverslip averages being upheld eliminated the need to summarise the data at the level of the coverslip, which would also reduce sample size and therefore the statistical power of the results. Therefore, FOV averages were used in the rest of the analysis described.

Bursting cultures were observed both in week 2 and 3 in the MN+V3+as co-culture condition. No significant effect of age was observed in spontaneous calcium event frequency or in the various event characteristics. Therefore, week 2 and week 3 MN+V3+as cultures were pooled together in the rest of the analyses described.

Motoneurons and V3 interneurons a) within the same FOV and b) on the same coverslip were not found to be significantly different in spontaneous calcium event frequency or in the various event characteristics, using paired statistical tests. However, only motoneurons were included in the rest of the analyses described.

6.3.3.1 The effect of co-culture with V3 interneurons on spontaneous calcium event frequency and characteristics in motoneurons

Initially, the effect of V3 interneurons on the FOV averages of motoneuronal calcium event frequency and event characteristics was explored. The presence of V3 interneurons in the co-cultures significantly reduced the frequency of motoneuronal calcium events (4.56 ± 2.71 events/minute compared to 11.8 ± 4.33 events/minute in the MN+V3+as and MN+as conditions, respectively; $p = 0.003$ in a Welch's Two Sample t test; Figure 6.6 A, Table 6.2). Similarly, mean event cycle time was increased in the MN+V3+as condition (12.9 ± 7.5s compared to 6.2 ± 2.5s in the MN+V3+as and MN+as conditions, respectively; $p = 0.008$ in a Mann Whitney U test; Figure 6.6 B, Table 6.2). These findings were likely linked to the presence of more long calcium events in the MN+V3+as condition than in the MN+as condition due to the long+short pattern (Figure 6.4). Indeed, though there was no significant increase in mean calcium event duration (Figure 6.6 C), the proportion of calcium events that were long (>3s) was significantly higher in the MN+V3+as condition (0.47 ± 0.38 compared to

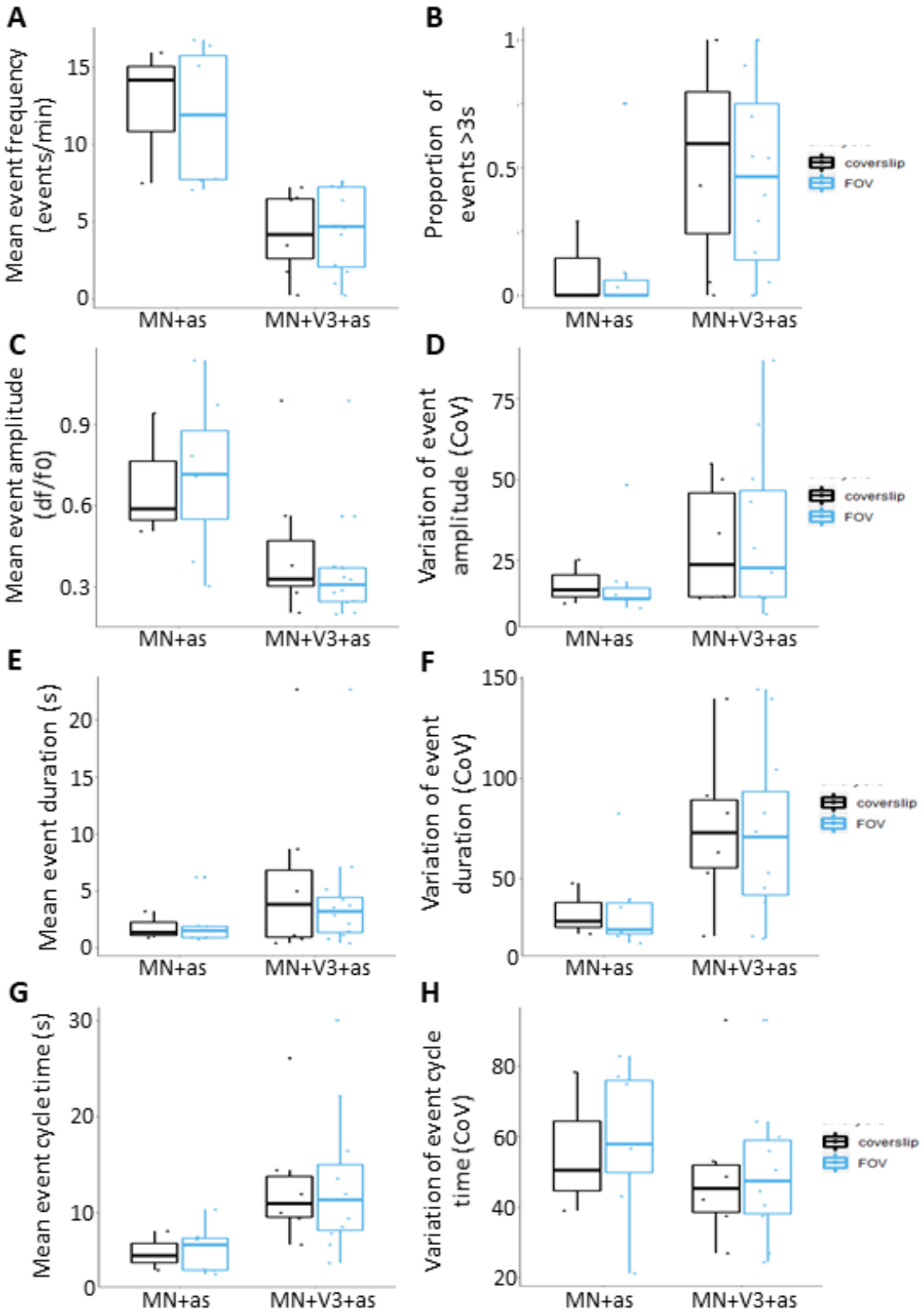

Figure 6.5: Comparison of motoneuronal calcium event frequency and event characteristics summarised by FOV (blue) and by coverslip (black).

There was no significant difference between the variance of the data summarised by FOV and the data summarised by coverslip for any event characteristics or for calcium event frequency in either the MN+as or the MN+V3+as condition. The normality of the data was tested with a Shapiro-Wilk test. An F test was used for the parametric data and a Conover test was used for the non-parametric data.

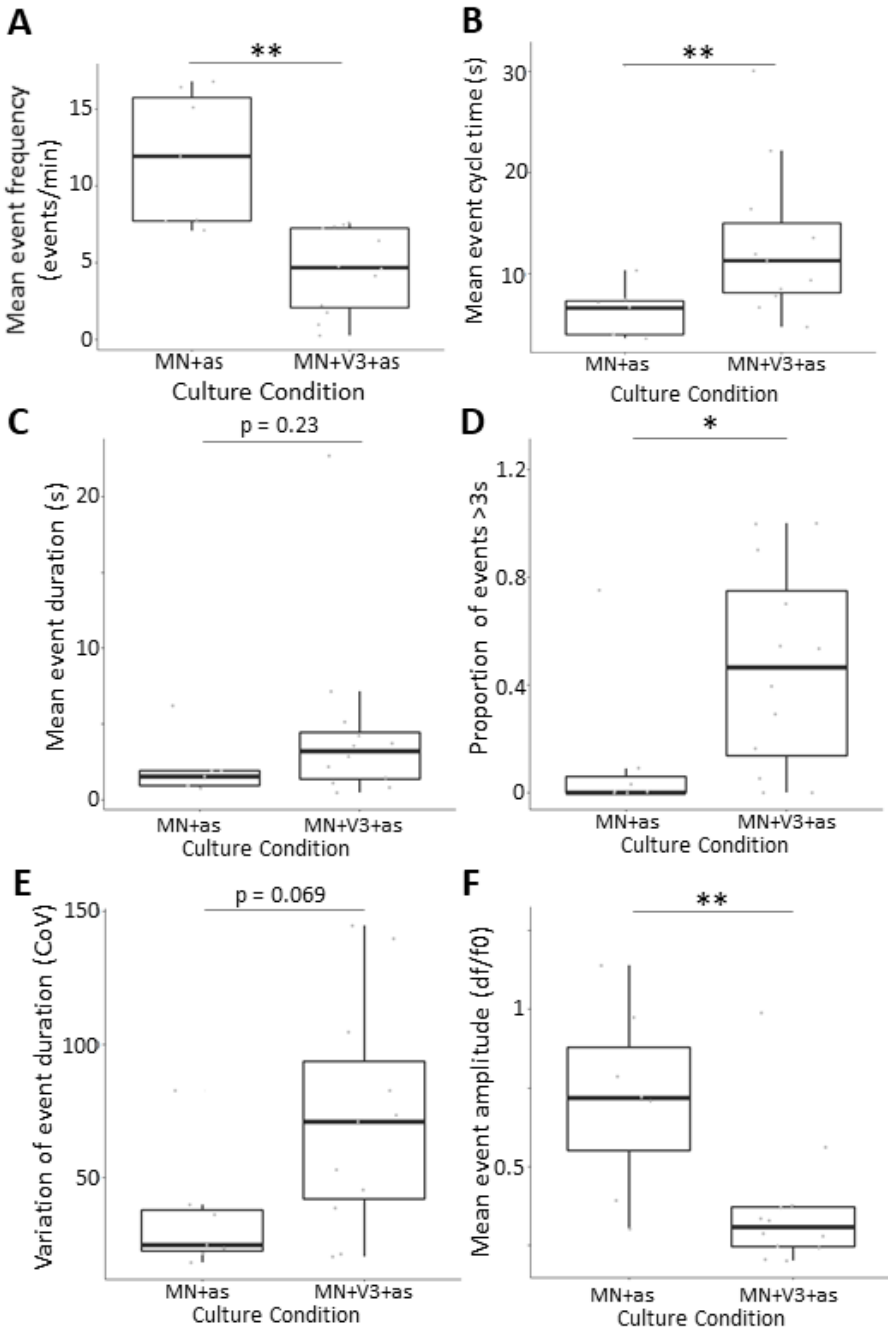

Figure 6.6: The effect of co-culture with V3 interneurons on the calcium event frequency and event characteristics of motoneurons on astrocytes.

The characteristics of calcium events were averaged to produce a mean value for each bursting motoneuron. As calcium activity between bursting motoneurons within each FOV was correlated, event characteristics were further averaged such that each point in the plots represents an FOV average. Co-culture with V3 interneurons decreased motoneuronal calcium event frequency (A), increased mean event cycle time (B), increased the proportion of events that were longer than 3s (D) and decreased mean even amplitude (F). Mean event duration (C) and the variation of event duration (E) were unaffected by co-culture with V3 interneurons. The Coefficient of Variation (CoV) is the (standard deviation/mean)*100. As the data (except the variability of event cycle time) was found to be non-parametric using a Shapiro-Wilk test, a Mann Whitney U test was used to determine statistical significance, except for variability of event cycle time for which a Welch's Two Sample t test was used. Bold horizontal lines in the boxplots show the median. * - $p<0.05$, ** - $p<0.01$.

Table 6.2: The effect of co-culture with V3 interneurons on motoneuronal calcium event frequency and event characteristics.

CoV = coefficient of variation; mean ± standard deviation (n); * - p<0.05, ** - p<0.01

Co-culture condition	**MN+as**	**MN+V3+as**
Statistical unit	FOV averages	
Event frequency (events/min)	11.8 ± 4.33 (7)	4.56 ± 2.71 (12)**
Proportion of calcium events that were >3s	0.12 ± 0.28 (7)	0.47 ± 0.38 (12)*
Variability of event amplitude (CoV)	18.7 ± 13.3 (7)	33.5 ± 25.4 (11)
Mean event duration (s)	2.0 ± 1.9 (7)	4.6 ± 6.0 (12)
Variability of event duration (CoV)	35.1 ± 22.4 (7)	72.2 ± 43.0 (11)
Mean cycle time (s)	6.2 ± 2.5 (7)	12.9 ± 7.5 (11)**
Variability of cycle time or rhythmicity (CoV)	59.0 ± 21.7 (7)	49.7 ± 20.1 (10)
Mean event amplitude (df/f0)	0.72 ± 0.30 (7)	0.37 ± 0.22 (12)**
Variability of event amplitude (CoV)	18.7 ± 13.3 (7)	33.5 ± 25.4 (11)

0.12 ± 0.28 in the MN+as condition; p = 0.044 in a Mann Whitney U test; Table 6.2, Figure 6.6 D). Despite the long and short calcium events observed in the MN+V3+as condition but not the MN+as condition (Figure 6.4, Figure 6.6 D), no significant difference was observed in the variability of calcium event duration (p = 0.069 in a Mann Whitney U test; Table 6.2, Figure 6.6 E). Motoneuron calcium event amplitude was also affected by the presence of V3 interneurons in the co-cultures. In the MN+V3+as condition, mean event amplitude was significantly smaller than in the MN+as condition (0.37 ± 0.22 df/f0 compared to 0.72 ± 0.30

df/f0 in the MN+V3+as and MN+as conditions, respectively; p = 0.01 in a Mann Whitney U test; Table 6.2, Figure 6.6 F).

Because seemingly distinct long and short calcium events were observed in the MN+V3+as condition (Figure 6.4, Figure 6.6 D), calcium events were separated into long events (>3s) and short events (<3s), and their event characteristics analysed and compared (Figure 6.7). Note that only 3 FOVs in the MN+as condition contained any long events and only 2 had enough long events to find a value for many of the event characteristics (Table 6.3), so statistical comparisons with this group were underpowered, which is likely why significant differences were rarely observed between the MN+as, long group and any of the other groups. Short events in the MN+V3+as condition had significantly smaller amplitudes than short events in the MN+as condition (Table 6.3, Figure 6.7 A; p = 0.008 using a post hoc Dunn's Multiple Comparison test) and long events in both conditions (Table 6.3, Figure 6.7 A; p = 0.0005 and 0.018 for comparing MN+V3+as, short group with the MN+as and MN+V3+as long groups, respectively, using a post hoc Dunn's Multiple Comparison test). In contrast, short events in the MN+as condition were not significantly different in amplitude from long events in either condition. This suggests that co-culture with V3 interneurons introduced low amplitude, short events in addition to a larger proportion of long events. The long events observed in the MN+V3+as condition were found to be more rhythmic (have a lower variability of event cycle time) than short events both in the MN+as condition and the MN+V3+as condition (Table 6.3, Figure 6.7 B; p = 0.017 and p = 0.001 comparing the MN+V3+as, long group with the MN+as, short and MN+V3+as, short groups, respectively, with a post hoc Tukey HSD Multiple Comparison test). Thus, motoneurons co-cultured with V3 interneurons displayed a pattern of low amplitude, short calcium events interspersed by long, rhythmic calcium events that was not observed in the MN+as condition.

6.3.4 Comparing spontaneous activity recorded by calcium imaging and single cell patch clamp methods

Having identified the long+short pattern of spontaneous calcium activity introduced by co-culture with V3 interneurons, the patterns and characteristics of spontaneous activity recorded by single cell patch clamping (as described in Chapter 5) were re-examined. Co-culture with V3 interneurons led to earlier emergence of spontaneous activity regardless of experimental method. However,

Table 6.3: The effect of co-culture with V3 interneurons on the characteristics of long and short motoneuronal calcium events.

Coefficient of Variation (CoV); values expressed as mean ± standard deviation (n). See Figure 6.7 for information about significant differences.

Co-culture condition	**MN+as**		**MN+V3+as**	
Statistical unit	FOV averages			
Length of calcium events (<3s = short and >3s = long)	short	long	short	long
Mean event amplitude (df/f0)	0.62 ± 0.24 (7)	1.26 ± 0.11 (3)	0.2 ± 0.07 (10)	0.52 ± 0.28 (10)
Variability of event amplitude (CoV)	16.8 ± 8.52 (7)	16.1 ± 15.6 (2)	19.9 ± 13.7 (9)	12.8 ± 3.35 (6)
Variability of event duration (CoV)	33.5 ± 20.0 (7)	29.7 ± 37.4 (2)	44.5 ± 21.0 (9)	21.8 ± 5.68 (6)
Mean cycle time (s)	8.9 ± 7.9 (7)	15.5 ± 8.7 (2)	15.7 ± 7.8 (9)	26.0 ± 15.7 (8)
Variability of cycle time/Rhythmicity (CoV)	59.2 ± 22.7 (7)	40.4 ± 34.2 (2)	71.5 ± 24.9 (8)	18.4 ± 10.5 (6)

spontaneous calcium activity emerged a week later than spontaneous firing recorded by patch clamping in both co-culture conditions (week 3 vs week 2 for the MN+as condition and week 2 vs week 1 in the MN+V3+as condition, respectively; Table 6.1; Figure 5.5 C in Section 5.3.2.2.3 of Chapter 5). This observation may in part be due to the low n for differentiations in weeks 1 and 2 for both conditions in the calcium imaging experiments. However, the later time course was upheld in differentiations/coverslips that were excluded from the analysis for various reasons (see Chapter 2: Materials and Methods, Section 2.13.2).

Similar to calcium imaging experiments, a long+short bursting pattern of spontaneous activity was sometimes observed in single cell patch clamp recordings of motoneurons in the MN+V3+as co-culture condition (1/13 and 2/5 motoneurons in week 2 and 4 MN+V3+as co-cultures, respectively; example in Figure 6.8 A) but never in motoneurons in the MN+as co-culture condition. However, the proportion of motoneurons showing the long+short spontaneous burst pattern was likely to be an underestimate because, in single cell patch clamping experiments, spontaneous burst duration and was significantly affected

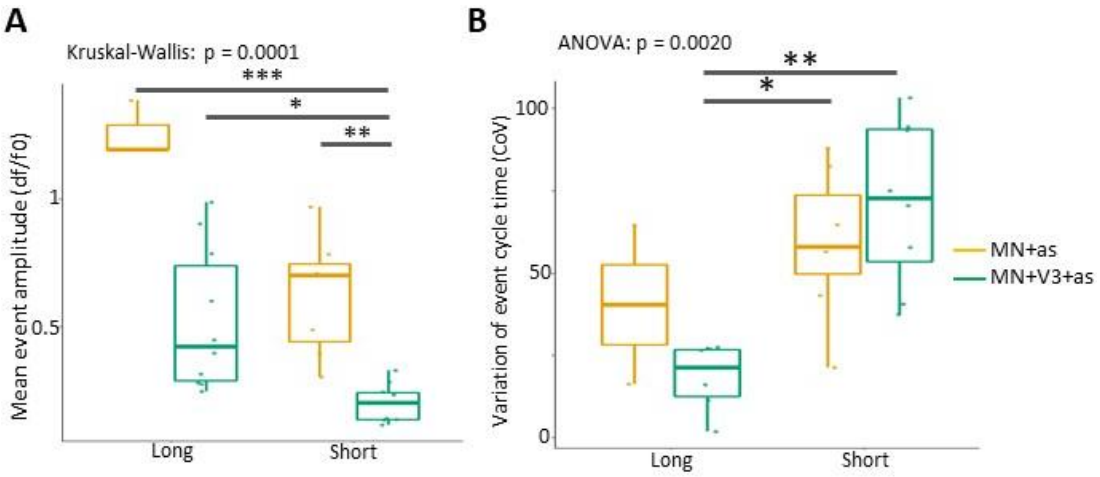

Figure 6.7: Long calcium events of motoneurons in the MN+V3+as condition had higher rhythmicity.

Motoneuronal calcium events were separated by length (long>3s and short<3s) and the different sets of calcium events were analysed using FOV averages (the mean for all bursting motoneurons in an FOV). A: Long events in both the MN+as (yellow) and the MN+V3+as (green) condition and short events in the MN+as condition had significantly larger amplitudes than short events in the MN+V3+as condition. B: There was significantly lower variation of event cycle time in long in the MN+V3+as condition compared to short events in both conditions. As variation of event cycle time is an inverse measure of rhythmicity, this suggests long events in the MN+V3+as condition were more rhythmic. Statistical differences were determined using either ANOVA with a post hoc Tukey HSD test, or, if the data was found to be non-parametric using a Shapiro-Wilk test, a Kruskal-Wallis test with a post hoc Dunn's test. For n, see Table 6.3. * = $p<0.05$, ** = $p<0.01$, *** = $p<0.001$.

by the amount of time a coverslip had spent in the recording chamber (Chapter 5, Section 5.3.4.2, Figure 5.10). In contrast, no significant effect of time on calcium event duration was observed in the calcium imaging experiments (Figure 6.8 B).

Furthermore, spontaneous event characteristics differed between calcium imaging and single patch clamping experiments. As spontaneous burst duration in the single cell patch clamping experiments was reduced with increasing time spent in the recording chamber, only the first motoneuron patched on each coverslip (at t_0) was included in this analysis. Spontaneous event frequency was significantly reduced in calcium imaging experiments compared to single cell patch clamping experiments in both conditions (Figure 6.8 C; Table 6.4). Mean spontaneous burst duration was longer in calcium imaging experiments compared to single cell patch clamping experiments (Figure 6.8 C; Table 6.4). Although some increase in burst duration would be expected due to the kinetics

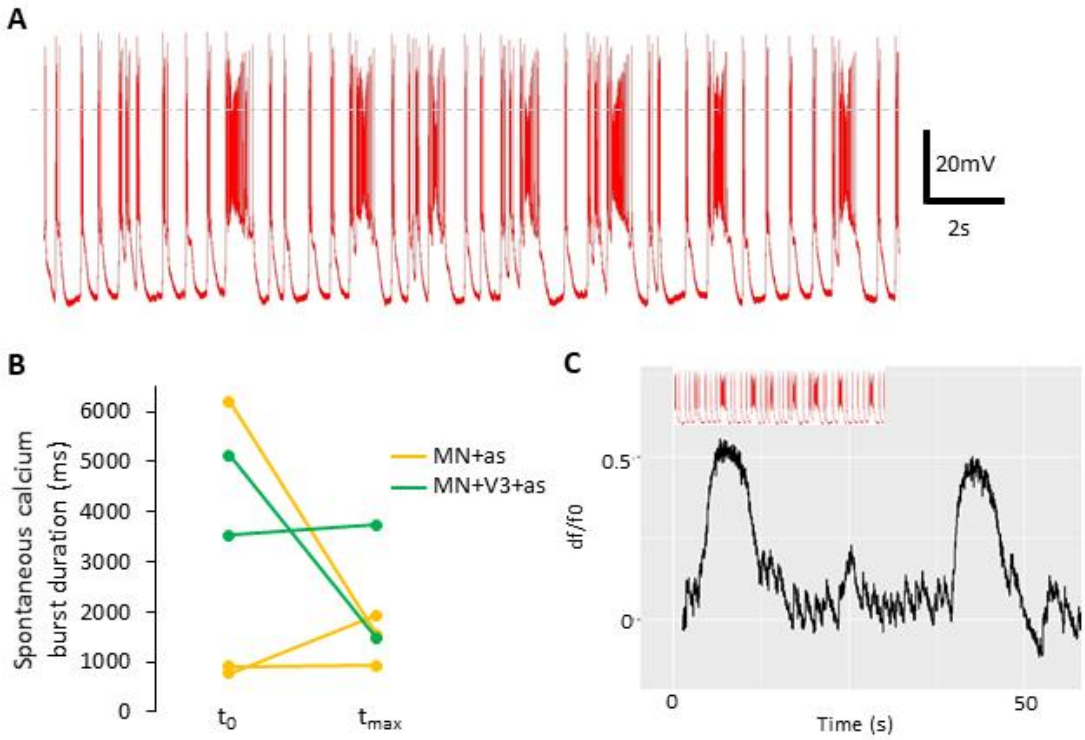

Figure 6.8: Comparing spontaneous activity recorded by single cell patch-clamping and calcium imaging.

A: An example trace from a week 4 motoneuron in the MN+V3+as co-culture condition that showed a putative long+short pattern of spontaneous activity. The dashed grey line shows 0mV. B: The amount of time a motoneuron had spent in the recording chamber did not significantly affect the mean spontaneous calcium burst duration ($p = 0.3$, paired t test). C: A comparison of the timescales of the spontaneous activity recorded by single cell patch clamping shown in A (red trace, top left) and spontaneous calcium activity of a week 3 motoneuron in the MN+V3+as co-culture condition (black trace, MN 1 also shown in Figure 6.2 B i).

Table 6.4: Comparing spontaneous burst characteristics in calcium imaging and patch clamping experiments.

The statistical unit of the calcium imaging data was the FOV average. The statistical unit of the patch clamping data was individual motoneurons, each the first recorded on their coverslip (at t_0). Age was not found to affect either spontaneous burst frequency or mean spontaneous burst duration for either experimental method or co-culture condition so data from different ages were pooled together. Values expressed as mean ± standard deviation (n); * denotes a comparison between the event characteristic recorded by the calcium imaging and patch clamping methods. * = $p<0.05$, ** = $p<0.01$, *** = $p<0.001$, **** = $p<0001$.

Event characteristic	Co-culture condition	Calcium imaging	Patch clamping
Spontaneous burst frequency (bursts/min)	MN+as	11.8 ± 4.3 (7)	31.2 ± 29.4 (8)*
	MN+V3+as	4.6 ± 2.7 (12)	20.5 ± 22.0 (12)**
Mean spontaneous burst duration (ms)	MN+as	2024 ± 1903 (7)	537 ± 342 (8)*
	MN+V3+as	4607 ± 6019 (12)	568 ± 694 (12)****

of the calcium dye this should have been in the order of hundreds of milliseconds (Lock et al., 2015) rather than thousands (Table 6.4). These discrepancies make it difficult to directly relate spontaneous firing recorded by single cell patch clamping to spontaneous calcium activity. Nevertheless, these data represent further evidence that the presence of V3 interneurons affected the pattern of spontaneous activity in the motoneuron co-cultures.

6.3.5 Co-culture with V3 interneurons did not affect bursting order variability

In vivo, V3 interneurons form layered microcircuits with motoneurons, putatively feeding information to motoneurons (Chopek et al., 2018). The correlation of spontaneous calcium events in the co-cultures (Figure 6.2; Table 6.1) suggests the neural networks in the co-cultures were also structured in some way. To further characterise network structure and to investigate the origin of the spontaneous calcium activity, calcium event onset was quantified for each neuron and bursting order between neurons established for each FOV. The null hypothesis was that bursting order was disorderly or random, with no neuron consistently bursting before another. A consistent bursting order would indicate more structured network activity with information flowing between neurons in a set direction. Furthermore, 'leader' neurons that consistently fired first were looked for as potential pacemaker neurons, driving the activity. For each coverslip, the FOV with the most neurons bursting and the most calcium events was selected for analysis. Calcium events only present in one or two neurons and neurons that did not fire consistently during each calcium event were excluded from the analysis. Note that, because low amplitude, short calcium events in MN+V3+as FOVs displaying the long+short calcium activity pattern were less consistent between bursting neurons in the FOV, these exclusion criteria resulted in predominantly high amplitude, long calcium events being included in the MN+V3+as co-culture condition. To visualise the bursting order, start times for each calcium event in each cell were compared. For a given calcium event, the start time in the neuron that fired first was designated T_0 and the latency between the start times of that event in other neurons and T_0 was determined (Chapter 2: Materials and Methods, Equation 3). In the resulting plots of latency of event onset against Event ID, the points at which the lines cross over indicate a change

in bursting order. Changes in bursting order were observed in every FOV, indicating that bursting order was not consistent. Example plots for a FOV in the MN+V3+as condition and MN+as condition can be seen in Figure 6.9 A and Figure 6.10 B, respectively. Though there were no leader neurons that consistently fired first during every calcium event, in some FOVs neurons were observed that predominantly led the other neurons. For instance, in the example plot for a week 3 MN+as co-culture (Figure 6.10 B), MN 5 predominantly appeared to lead whereas MN 8 appeared to follow.

To investigate the extent of variability in bursting order in each FOV, the variance of the bursting order across the calcium events was determined for each neuron and compared with that of a randomly generated dataset (e.g. Figure 6.9 B i compared with ii, and Figure 6.10 C i compared with ii). For the majority of FOVs in both conditions, there was no significant difference in the bursting order variance between the real bursting order data and the randomly generated bursting order data (Table 6.5; example in Figure 6.9 C). One reason for this could be that the bursting order was random. Alternatively, this may be because the number of bursting neurons and calcium events were too small in some FOVs for any difference in bursting order variance to be seen. Three FOVs, one from the MN+as condition and two from the MN+V3+as condition (including the FOV with a consistent bursting order), showed significantly lower bursting order variance than in the randomly generated dataset, suggesting these FOVs had non-random bursting orders (Table 6.5; example in Figure 6.10 D).

To investigate the effect of V3 interneurons on the randomness of bursting order, the extent of randomness was calculated for each FOV according to Equation 4 in Chapter 2: Materials and Methods. There was no significant difference in the extent of bursting order randomness between the MN+as and MN+V3+as conditions (Table 6.5; Figure 6.10 E; $p = 0.55$, Welch's Two Sample t test). These data suggest that, apart from a few exceptions, the bursting order of neurons in co-culture was random and that the presence of V3 interneurons had no effect on this.

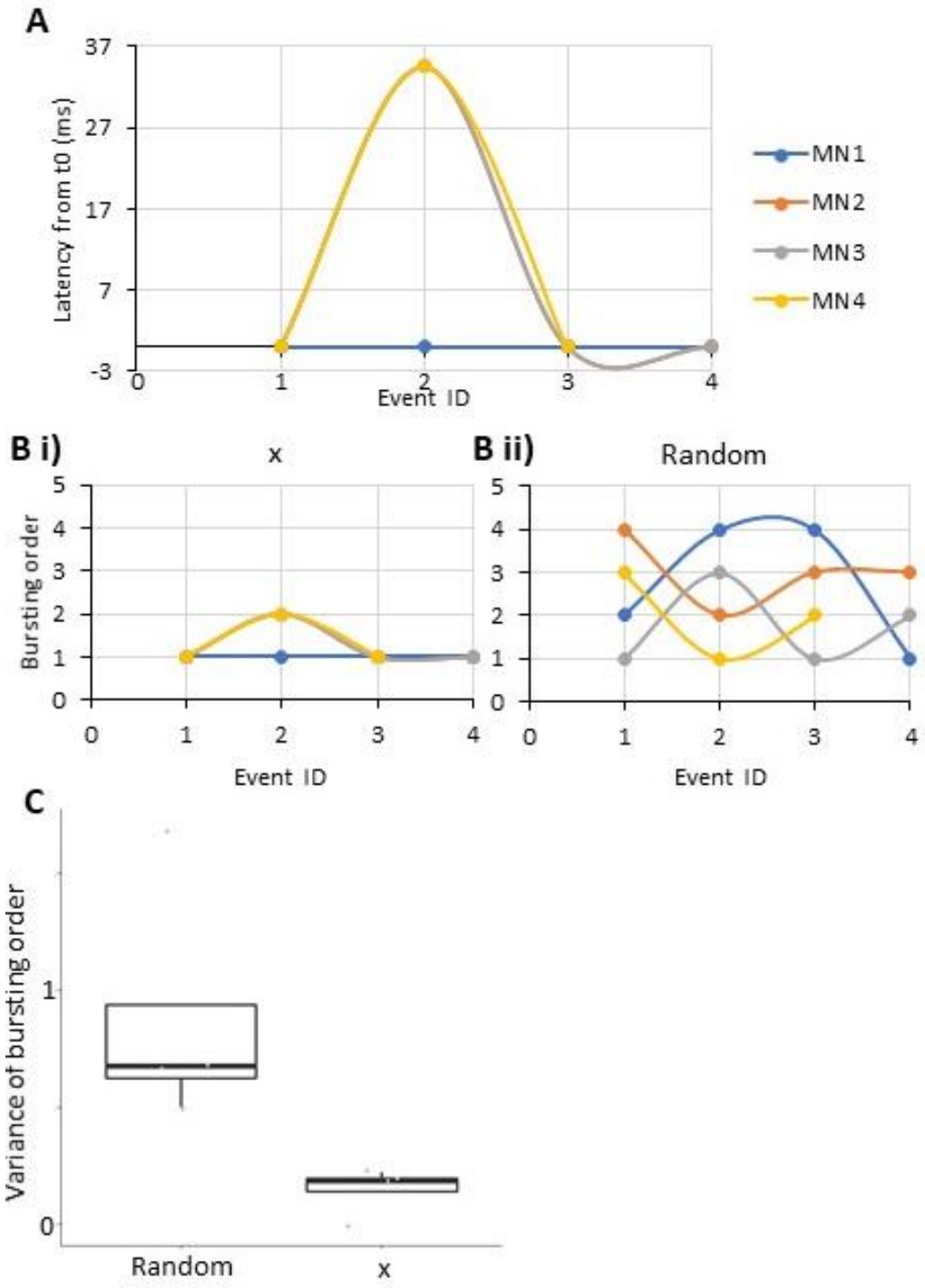

Figure 6.9: Variability in bursting order for calcium events recorded from an example FOV in a week 2 MN+V3+as co-culture. df/f0 data for this FOV is shown in Figure 6.1.

A: The latency between the calcium event start times of different neurons for each calcium event where the neuron at T_0 had the earliest start time for that calcium event. Note that in this FOV, MN 1 appeared to lead the other neurons. B: The change in bursting order in the FOV (x; B i) and in a randomly generated dataset (B ii). C compares the variance in bursting order for each neuron between the FOV (x) and the randomly generated dataset (Random). No significant difference in bursting order variance was found between x and Random using a Welch's Two Sample t-test ($p = 0.07$).

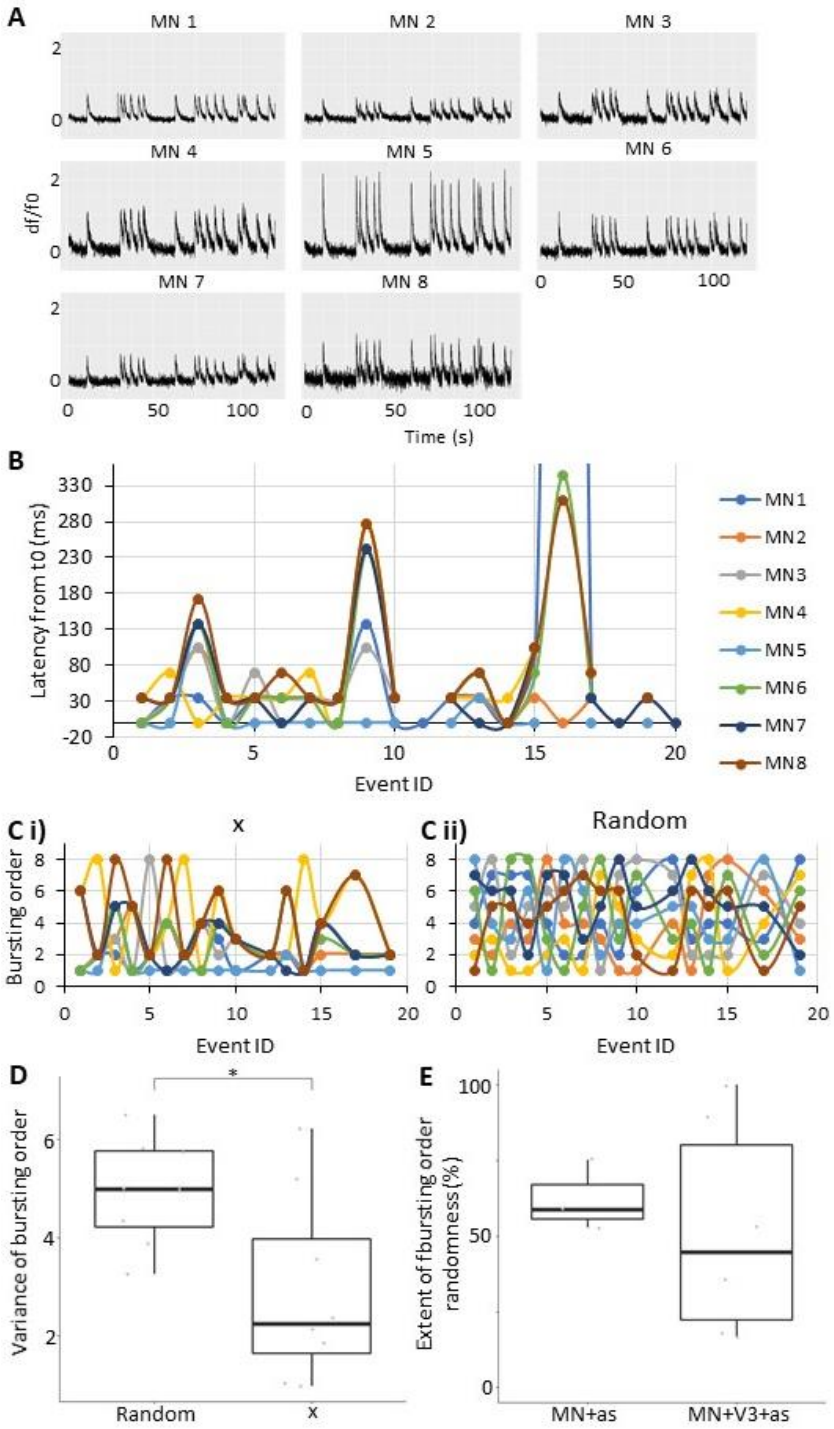

Figure 6.10: Variability in bursting order for calcium events recorded from an example FOV in a week 3 MN+as co-culture.

A: df/f0 showing calcium events. B: The latency between the event start times of different neurons for each event where the neuron at T_0 had the earliest start time for that event. At event 16, the latency from T_0 of MN 1 was 2138ms. Note that in this FOV, MN 5 appears to lead the other neurons. C: The change in bursting order in the FOV (x; C i) and in a randomly generated dataset (C ii). D compares the variance in bursting order for each neuron between the FOV (x) and the randomly generated dataset (Random). There was a significant reduction in bursting order variance found in x compared to Random using a Welch's Two Sample t-test ($p = 0.02$; * in D). E: The presence of V3 interneurons had no significant difference on the extent of bursting order randomness using a Welch's Two Sample t test ($p = 0.55$).

Table 6.5: The effect of co-culture with V3 interneurons on variability of bursting order.

Values given as mean ± standard deviation (min-max).

Co-culture condition	MN+as	MN+V3+as
Neurons included per FOV	5 ± 4 (2-8)	7 ± 3 (4-12)
Calcium events included per FOV	18.7 ± 3.8 (16-23)	5.8 ± 3.3 (3-12)
FOVs with a significantly more variable bursting order than random	1/3	2/6
Extent of randomness of the bursting order (%)	62.3 ± 11.6 (3)	52.3 ± 35.6 (6)

6.4 Discussion

6.4.1 Summary

Spontaneous, glutamatergic calcium activity was observed in the somas of motoneuron co-cultures and, in most cultures, the activity of different bursting neurons within a FOV was correlated. The presence of V3 interneurons led to an earlier onset of spontaneous calcium activity and introduced a new pattern of calcium activity into the co-cultures in which long, higher amplitude, rhythmic events were interspersed by short, low amplitude, arrhythmic events. The presence of these long calcium events led to a decrease in event frequency and an increase in mean cycle time in the MN+V3+as condition. Bursting order of neurons in an FOV was not consistent between calcium events, although in some FOVs the bursting was not completely random either. The presence of V3 interneurons did not introduce more ordered bursting.

6.4.2 Somatic calcium transients

In this Chapter, spontaneous somatic calcium transients were observed in both the MN+as and MN+V3+as co-culture conditions. The main determinant of somatic calcium signals are voltage-gated calcium channels with some NMDA component (Bengtson et al., 2010; Grienberger and Konnerth, 2012). Somatic calcium transients have an important role in the regulation of gene transcription and protein expression (Bengtson et al., 2010; Ibata et al., 2008; Lyons and West, 2011; Montague et al., 2017), which affects development of the nervous system. For example, spontaneous calcium activity affected the maturation of the facial and abducens motor nuclei in embryonic chick spinal cord due to interactions with type II cadherins and gap junctions; perturbing cadherin- and gap junction- dependent interactions disrupted spontaneous calcium activity whereas inhibition of spontaneous calcium activity prevented proper nucleogenesis and reduced cadherin expression (Montague et al., 2017). Therefore, the impacts of V3 interneurons on motoneuronal spontaneous somatic calcium activity may have affected gene and protein expression.

6.4.3 Spontaneous activity differed between patch clamping and calcium imaging experiments.

Methods used for measuring spontaneous activity in the spinal cord include intracellular and/or extracellular recordings (Buntschu et al., 2020; Rosato-Siri et al.,

2004), calcium imaging (Montague et al., 2017; Warp et al., 2012), tracking the expression of a gene regulated by activity (Kalb and Hockfield, 1992), and measuring ventral root activity (Yvert et al., 2004) or muscle movements (Kastanenka and Landmesser, 2010; Magown et al., 2017). In this Thesis, both single cell patch clamping (see Section 6.3.4 and Chapter 5) and calcium imaging were used to record spontaneous activity in the motoneuron co-cultures. The advantage of patch clamping is direct electrical access to the inside of the cell, enabling activity to be recorded by high temporal fidelity, signal-to-noise ratio and dynamic range (Peron et al., 2015; Wei et al., 2020). However, patch clamping only allows access to one or at most a few neurons at a time (Buzsáki, 2004). Therefore, spontaneous network activity was investigated by calcium imaging, which enables the somatic calcium transients of whole populations of neurons to be recorded. However, calcium imaging imposes a transformation that is affected by non-linearities in intracellular calcium dynamics and the calcium indicator kinetics (Bengtson et al., 2010; Grienberger and Konnerth, 2012; Scheuss et al., 2006; Yuste and Denk, 1995), meaning somatic calcium imaging only indirectly reports neuronal activity (Grienberger and Konnerth, 2012; Peron et al., 2015) and has a lower signal-to-noise ratio and dynamic range (Peron et al., 2015). The dependence on intracellular calcium dynamics also means that coupling between spikes and calcium-dependent fluorescence likely varies between neurons (Chen et al., 2013; Maravall et al., 2000; Wei et al., 2020). Therefore, although calcium imaging and electrophysiological techniques are often treated interchangeably, somatic calcium transients are not a direct proxy for action potentials and inferring neuronal spiking activity from calcium transients is fraught with difficulty, as recently demonstrated by Wei et al. (2020). Comparing neuronal spikes measured electrophysiologically and calcium-dependent fluorescence of matched neural populations in behaving mice, the authors found multiple discrepancies between their analyses of the two forms of data, including in elements with relevance to conclusions about the relationship of neural activity to behaviour, such as single neuron selectivity and population decoding. Only a fraction of this variability was accounted for by the slow dynamics of the calcium indicators and commonly used spike inference algorithms. The development of more accurate spike inference models is complicated by the variation in calcium influx and extrusion rates between individual neurons (Maravall et al., 2000; Wei et al., 2020). Therefore, although calcium imaging enables

concurrent recording from multiple neurons, it is hard to directly relate calcium activity to true neuronal activity.

The non-linear relationship between somatic calcium transients and neuronal action potentials was likely the reason that mean spontaneous burst duration was longer in calcium imaging experiments compared to single cell patch clamping in this Chapter. An example of regenerative somatic calcium activity in response to action potentials was observed in rat CA1 pyramidal neurons by Bengtson et al (2010); a train of action potentials (measured by patch clamping the neuron) in response to a burst of synaptic activity caused a regenerative calcium signal that lasted long after the cessation of EPSPs. Perhaps the disparity between spike and calcium event duration in this Chapter was due to a similarly regenerative calcium signal. However, Sternfeld et al. (2017) performed simultaneous calcium imaging and extracellular electrical recordings of activity in cultured ESC-derived V3 interneurons and found that calcium activity did not exceed the duration of action potential trains. The reason for the discrepancy between the results in this Chapter and the results of Sternfeld et al. (2017) is unclear; perhaps the putative regenerative calcium transients were introduced only by the presence of motoneurons in co-culture. The only way to truly determine the relationship between spontaneous neuronal activity and spontaneous calcium activity in the co-cultures would be to perform similar simultaneous calcium imaging and patch clamp experiments.

In both co-culture conditions, spontaneous somatic calcium activity emerged a week later than the spontaneous firing measured by patch clamping. The absence of spontaneous calcium activity at a time point when motoneurons in co-culture were known to be firing suggests either that this calcium activity was below the level of detection of the calcium indicator or that the underlying calcium currents, likely voltage-gated calcium channels (Grienberger and Konnerth, 2012), developed later than the currents responsible for spontaneous activity observed in patch clamp experiments. The emergence of somatic spontaneous calcium activity a week after spontaneous firing may represent a second stage of maturation in which gene transcription becomes coupled with spontaneous neuronal firing. It would be interesting to find out whether the emergence of spontaneous firing and spontaneous somatic calcium bursts in the spinal cord are similarly staggered *in vivo*.

Despite the differences between the methods, the impact of V3 interneurons on spontaneous activity was robust between single cell patch clamping and calcium imaging experiments. In both, co-culture with V3 interneurons accelerated the emergence of spontaneous activity in the cultures and introduced a long+short pattern of spontaneous activity in some neurons.

6.4.4 Emergence of spontaneous activity was accelerated by the presence of V3 interneurons.

As in the patch clamp experiments described in Chapter 5, co-culture with V3 interneurons led spontaneous somatic calcium activity to arise a week earlier than in the MN+as condition. This may be because of the strong excitatory drive provided by the V3 interneurons (Sternfeld et al., 2017). Indeed, an increased amount of excitatory synapses can lead networks to be hyperexcitable and prone to spontaneous episodes (Blankenship and Feller, 2010; Marchetti et al., 2005). Perhaps the increased activity (caused by the presence of V3 interneurons) accelerated the development of the voltage-gated calcium channels and NMDA receptors that likely underly the spontaneous somatic calcium activity (Bengtson et al., 2010; Grienberger and Konnerth, 2012). However, the accelerated emergence may also be an artefact of the way the culture was set up. As V3 interneurons are born later in the EB than motoneurons (as demonstrated in Chapter 3), the differentiation of V3 interneurons was begun a week prior to motoneuron differentiation and the V3 interneurons were plated three days before the motoneurons. It may be that the V3 interneurons were therefore more mature and more capable of forming synapses and initiating spontaneous activity than the motoneurons in the MN+as condition.

6.4.5 V3 interneurons were not ‘leader’ neurons.

Both *in vitro* and *in vivo,* V3 interneurons have been implicated in driving motoneuron activity and contributing to the locomotor rhythm (Chopek et al., 2018; Danner et al., 2017; Sternfeld et al., 2017; Zhang et al., 2008b). However, V3 interneurons did not consistently burst before other neurons in the same FOV. Indeed, though pseudo-leader neurons that predominantly fired first were observed in some FOVs, bursting order was found to be disorderly irrespective of the presence of V3 interneurons; although the results in the MN+V3+as co-culture condition may have been statistically underpowered as the exclusion criteria led to fewer calcium events being included in FOVs that displayed the long+short activity pattern. Given the correlation of bursting,

the disorderliness of bursting order was unexpected. It is possible that the true 'leader' neurons lay outside the FOVs recorded from. Alternatively, subthreshold calcium activity or differences in calcium extrusion and intake that varied between neurons and over time may have combined additively with synaptic input, affecting onset from burst to burst. A third option is that the spontaneous calcium activity may have been correlated via gap junctions, as with spontaneously active motor neurons belonging to the same motor pool *in vivo* (Montague et al., 2017; Personius et al., 2001). The effect of carbenoxolone, a putative gap junctional blocker, was explored but carbenoxolone appeared to be toxic to the cells (data not shown); indeed, carbenoxolone has many off-target effects on neurons so is not a wholly reliable tool to explore the influence of gap junctions (Connors, 2012). Nonetheless, although V3 interneurons accelerated the emergence of spontaneous activity, it seems unlikely that the spontaneous calcium activity in these co-cultures was driven by leader V3 interneurons.

6.4.6 Co-culture with V3 interneurons introduced a more mature pattern of activity

In the spinal cord, manipulating spontaneous activity has been shown to have fundamental functional impacts. For example, manipulating the frequency of spontaneous firing affected the accuracy of axon pathfinding decisions and targeting (Hanson et al., 2008), and disrupting spontaneous calcium activity by manipulating cadherin or gap junction expression disturbed nucleogenesis (Montague et al., 2017). In this Chapter, the emergence of a different pattern of motoneuronal spontaneous activity – with long, higher amplitude, rhythmic events were interspersed by short, low amplitude, arrhythmic events – was observed only in co-cultures containing V3 interneurons. The long+short pattern was observed both in calcium imaging and patch clamp experiments, though on different timescales (Figure 6.8). No such pattern was observed in the experiments of Sternfeld et al. (2017) that examined spontaneous calcium bursting in co-cultures of ESC-derived V3 interneurons, motoneurons and V1 interneurons, though they showed no recordings from V3 interneuron-motoneuron co-cultures in the absence of V1 interneurons. The reason for the absence of small calcium events in their experiments could also be that they were below the detection level of the calcium indicators used (GCamp3 and Oregon Green 488 BAPTA-1-AM) or due to the smoothing of the calcium signals with a 1s-wide running mean filter. Indeed, applying a similar filter to my own calcium imaging data rendered many small calcium events indistinguishable.

The potential functional significance of the long+short pattern of activity observed is unclear. While examining the day-by-day evolution of spontaneous activity in the embryonic mouse spinal cord by ventral root recordings, Yvert et al. (2004) observed a similar long+short pattern of spontaneous activity transiently at E14, synchronised across the spinal cord. Long episodes at different levels of the spinal cord had different tonicity and the long+short pattern preceded the emergence of more erratic and spatially segregated spontaneous activity. For this reason, Yvert et al. (2004) suggested that the long+short pattern was an important step in the maturation of the spinal cord towards more functional, segregated networks. Direct comparisons cannot be drawn between the spontaneous activity observed in the spinal cord and the spontaneous calcium activity observed in the motoneuronal co-cultures in this Thesis; the spontaneous activity observed in mouse embryonic spinal cord was recorded using a very different method with no information about calcium transients and the burst durations observed were much longer than in the co-cultures. However, it is possible that the long+short pattern of spontaneous activity observed in the V3 interneuron-containing culture condition represents a more mature bursting pattern. Using *in vitro* co-culture models with a muscle compartment, it would be interesting to explore the functional impact of the different patterns of spontaneous activity, such as that introduced by V3 interneurons, on the gene expression and NMJ formation of motoneurons.

7 General Discussion

ALS is a progressive, fatal neurodegenerative disease with typical symptom onset at ages over 50 (Chiò et al., 2011). Disease progression is aggressive with patients surviving, on average, one to five years from diagnosis (Oskarsson et al., 2018). Limb, respiratory and bulbar-innervated muscles of patients become atrophied and eventually paralysed as motoneurons degenerate (Peters et al., 2015; Petrov et al., 2017). Current treatments for ALS confer only marginal benefits. For example, the most commonly prescribed drug for ALS is Riluzole, which extends life by 2-3 months (Bellingham, 2011; Miller et al., 2002). There are currently no approved treatments that restore muscle function already lost due to ALS progression.

Our group is exploring a novel strategy to restore function to paralysed muscles that involves the peripheral engraftment of healthy, optogenetic ESC-derived motoneurons to enable reinnervation of denervated muscles and control of muscle contraction by exogeneous optical stimulation (Bryson et al., 2014). This method overcomes limitations of other methods, such as the safety concerns surrounding non-specific electrical stimulation of degenerating host motoneurons (DiPALS Writing Committee et al., 2015). To improve the therapeutic feasibility of this experimental treatment strategy, optimising the composition of the peripheral graft is important to 1) ensure safety, and 2) ensure and improve functional innervation of the target denervated muscles. Embryoid Bodies (EBs), which have been used to successfully restore muscle function in mouse models, contain a variety of cells alongside motoneurons (Sternfeld et al., 2017; Wichterle et al., 2002). These include undifferentiated cells that could be tumorigenic (Magown et al., 2016) and therefore must be excluded from any optimised or therapeutic graft. Moreover, the Greensmith, Bryson and Brownstone labs have found that peripherally-engrafted purified motoneuron grafts, which excluded all other cell types, did not functionally innervate muscles and control muscle contraction (Magown et al., 2017 and Bryson et al, unpublished observations). This led to the hypothesis that the remaining cellular milieu in the EB contained cell types that were important to the maturation and therefore performance of the engrafted motoneurons.

In this Thesis, astrocytes and spinal V3 interneurons were identified as candidate cell types due to their abundance in EBs generated by the 5-day RA/SAG protocol and their influence on motoneuron maturation was investigated in an *in vitro* co-culture model. Co-culture on a monolayer of ESC-derived astrocytes profoundly promoted the maturation of motoneurons, increasing neuronal survival, soma size, and the number and complexity of neuronal neurites. The electrophysiological maturation of motoneurons was also accelerated by the presence of astrocytes. Furthermore, astrocytes had synaptogenic properties, increasing the density of motoneuronal cholinergic synapses that formed in the somatic and proximal dendritic compartments, and enabling spontaneous, glutamatergic activity in the motoneurons. In contrast, co-culture of motoneurons with V3 interneurons alone had little to no effect on any of the indicators of motoneuron maturation measured. However, there was an astrocyte-dependent effect of V3 interneurons that increased and decreased motoneuronal glutamatergic and cholinergic synapse density, respectively. Furthermore, motoneurons co-cultured with V3 interneurons in the presence of astrocytes developed spontaneous glutamatergic activity earlier and sometimes displayed a different, long+short pattern of spontaneous activity. The long+short activity pattern was characterised by long, higher amplitude, rhythmic events interspersed by short, low amplitude, arrhythmic events. The promotion of spontaneous activity by co-culture with astrocytes and V3 interneurons (in an astrocyte-dependent manner) is significant because of the importance of spontaneous activity in the maturation of motoneurons and the neuromuscular system *in vivo*. Taken together, the results of this Thesis suggest that the inclusion of astrocytes and, to a lesser extent, V3 interneurons in peripheral motoneuron grafts may improve the ability of engrafted motoneurons to functionally innervate host muscle by promoting spontaneous activity and thereby accelerating their maturation in the graft.

7.1 Astrocytes promote motoneuron maturation *in vitro*

Astrocytes promoted ESC-derived motoneuron maturation in a variety of ways. First and foremost, consistent with previous results, *in vitro* neuron survival was improved by co-culture with astrocytes, likely due to the secretion of trophic factors (Taylor et al., 2007). Furthermore, the presence of astrocytes led to an increase in motoneuron soma size and dendritic complexity that broadly corroborated recent results obtained

in human iPSCs. In fact, the impact of co-culture was perhaps even more dramatic in these experiments because, in contrast to the results of Taga et al. (2019), co-culture with astrocytes increased primary dendrite number in addition to the other measures of motoneuron size and complexity.

As has previously been demonstrated (Taga et al., 2019; Ullian et al., 2004a), the expression of synaptic molecules and synapse formation was promoted by co-culture of motoneurons with astrocytes. Specifically, increased cholinergic synapse density in the somatic and proximal dendritic compartments was observed in astrocyte-containing cultures compared to motoneurons cultured alone. The function of these cholinergic synapses was not elucidated as the effect of non-specific cholinergic receptor blockers on spontaneous activity was not consistent.

The inclusion of astrocytes in motoneuron co-cultures lead to the emergence of spontaneous activity, as has been previously observed in co-cultures of motoneurons *in vitro* (Sternfeld et al., 2017; Taga et al., 2019; Ullian et al., 2004a) and in cortical neurons (Kayama et al., 2018). Unlike previous reports in primary mixed motoneuron cultures (Ullian et al., 2004a) and purified human iPSC-derived motoneuron and astrocyte co-cultures (Taga et al., 2019), spontaneous activity was completely eliminated by a glutamate receptor antagonist in both single cell patch clamp and calcium imaging experiments. This suggests that there was no cholinergic component to the spontaneous activity. Given that the presence of astrocytes did not increase glutamatergic synapse density in the somatic and proximal dendritic compartment of the motoneurons, it is likely either that the glutamatergic synapses responsible were either formed on distal dendrites or that a glutamate transporter other than vGluT2 was involved. The glutamatergic motoneuron-to-motoneuron synapses in these purified motoneuron-astrocyte co-cultures are reminiscent of glutamatergic synapses responsible for recurrent excitation in the spinal cord, which similarly show purely glutamatergic synaptic transmission (Bhumbra and Beato, 2018). *In vivo,* spontaneous activity is known to contribute to axon guidance and outgrowth (Gordon, 2016; Hanson et al., 2008; Kastanenka and Landmesser, 2010), the formation of neuromuscular and spinal circuits (Montague et al., 2017; Personius et al., 2007) and the regulation of synaptic strength (Gonzalez-Islas and Wenner, 2006). In particular, increased excitatory activity has been shown to profoundly affect maturation of dendritic

morphology in motoneurons (Fogarty et al., 2016; Kalb and Hockfield, 1990a, 1990b, 1992; Zhang et al., 2008a). Therefore, it is possible that the emergence of glutamatergic spontaneous activity underlies the effects of astrocytes on motoneuron morphology.

Spontaneous calcium activity in the form of somatic calcium transients was also observed in astrocyte-containing co-cultures, though it showed different dynamics to spontaneous activity recorded by single cell patch clamping. Spontaneous calcium activity is observed in spinal neural networks *in vivo* (Montague et al., 2017; O'donovan et al., 1998). Somatic calcium transients are known to affect gene transcription (Bengtson et al., 2010; Ibata et al., 2008; Lyons and West, 2011), so its emergence in astrocyte-containing co-cultures likely denotes further changes in maturation. Indeed, spontaneous calcium activity has been directly related to the expression of cell adhesion proteins important for nucleogenesis in the chick brainstem (Montague et al., 2017). Consistent with similar recordings from ESC-derived motoneurons co-cultured with astrocytes (Sternfeld et al., 2017), spontaneous calcium activity astrocyte co-cultures was correlated between motoneurons. However, synchrony was not observed in recordings of spontaneous activity of human IPSC-derived motoneurons co-culture with astrocytes made with multi-electrode arrays (Taga et al., 2019); the discrepancy could be due to different species (mouse vs human), different models (ESC vs iPSC), or because calcium activity and electrical activity are not necessarily directly related (Wei et al., 2020). *In vivo*, synchronised spontaneous activity is observed at particular stages of spinal cord development (Rosato-Siri et al., 2004; Yvert et al., 2004) and contributes to delaying synaptic elimination within a motor pool (Personius et al., 2007) and nucleogenesis (Montague et al., 2017).

In addition to promoting spontaneous activity, ESC-derived astrocytes were found to influence both passive and active electrophysiological properties of ESC-derived motoneurons. The increase in motoneuron capacitance in astrocyte-containing cultures likely reflected increased motoneuron size shown in Chapter 4. Co-culture with astrocytes increased the proportion of motoneurons capable of sustained repetitive firing and that display rebound action potentials, increased action potential amplitude, and led to the emergence of doublets and triplets at the beginning of trains

of action potentials. These properties of ESC-derived motoneurons co-culture with astrocytes are associated with more mature motoneurons in electrophysiological experiments *in vitro* and *in vivo* (see Chapter 1: General Introduction, Table 1.4 for references) and initial doublets/triplets are a conserved mechanism for rapidly enhancing muscle force at the beginning of a contraction (Mrówczyński et al., 2015). Thus, astrocytes were found to be fundamental to the electrophysiological, as well as the morphological and synaptic, maturation of ESC-derived motoneurons *in vitro.*

The role of astrocytes in motoneuron maturation *in vitro* is consistent with the role of astrocytes during motoneuron development, promoting motoneuron survival (Kelley et al., 2018), morphological maturation (Taga et al., 2019), synaptic formation (Taga et al., 2019; Ullian et al., 2004a), and circuit formation (Molofsky et al., 2014) and function (Morquette et al., 2015). However, there are other glial cell types that may also promote motoneuron maturation, some of which show similarly promising results *in vitro.* For example, co-culturing primary spinal motoneurons on sciatic Schwann cell monolayers improved motoneuron survival and axon extension (Hyung et al., 2015) and increase synapse formation and synaptic activity (Ullian et al., 2004a) in 2D *in vitro* co-cultures. Moreover, during peripheral nerve injury *in vivo*, myelinating Schwann cells transdifferentiate to secrete trophic factors that promote neuronal survival and form Bands of Büngner, which provide trophic and physical support for regrowing axons (Boerboom et al., 2017). Indeed, the Greensmith lab has found that purified ESC-derived motoneuron aggregates grafted into denervated sciatic nerve extended axons into the muscle, likely supported by host Schwann cells (Bryson, unpublished observations). However, there was evidence of terminal axonal sprouting and stimulation of the graft did not result in muscle contraction, indicative of inactive and immature motoneurons. This suggests that Schwann cells within the denervated peripheral nerve were not sufficient to enable synapse formation and motoneuron activity to encourage successful innervation of NMJs by the purified motoneuron graft. Schwann cells have been shown to behave differently in 2D and 3D *in vitro* cultures (Cattin et al., 2015), so perhaps transdifferentiated Schwann cells in the peripheral nerve were not as synaptogenic as Schwann cells in 2D *in vitro* co-cultures. Alternatively, the environment in the peripheral nerve may have inhibited synapse formation altogether, blocking the synaptogenic effects of the Schwann cells. Indeed,

while the environment in the peripheral nerve has been shown to promote remyelination and axon regeneration, porcine decellularised Extracellular Matrix (ECM) of the peripheral nerve inhibited synapse formation in dorsal root ganglion-Schwann cell *in vitro* co-cultures to a greater extent than decellularised ECM from spinal cord (Zou et al., 2018). Thus, despite promising *in vitro* results, Schwann cells are not a good candidate for improving the functional muscle innervation of motoneurons in ESC-derived peripheral grafts. This underlines the importance of following up the *in vitro* evidence outlined in this Thesis and other studies with *in vivo* studies of the benefit of including astrocytes in the ESC-derived motoneuron grafts.

7.2 V3 interneurons affected synapse complement and spontaneous activity pattern

The results presented in this Thesis show that V3 interneurons had no effect on motoneuron maturation *in vitro* in the absence of astrocytes. However, there was an astrocyte-dependent effect, perhaps because the astrocytes enabled synapses to form between the V3 interneurons and the motoneurons. V3 interneurons affected the balance of cholinergic and glutamatergic synapses onto the somatic and proximal dendritic compartment of motoneurons. V3 interneurons are glutamatergic neurons that project monosynaptically onto motoneurons *in vivo* (Chopek et al., 2018; Zhang et al., 2008b), so the increase in glutamatergic synapse density is unsurprising. However, there is a concurrent reduction in cholinergic synapse density, whether due to translocation of cholinergic synapses to distal dendrites, reduction in cholinergic synapse formation, or increase in cholinergic synapse elimination. This may be due to the increased levels of glutamate released by V3 interneurons affecting the expression of astrocytic synapse regulators (Jones et al., 2011), leading to the elimination of cholinergic synapses (Albrecht et al., 2012; López-Murcia et al., 2015).

In addition to affecting the complement of motoneuronal synapses, V3 interneurons (in astrocyte-containing cultures) had some effects on the active electrophysiological properties of motoneurons. For example, motoneurons co-cultured with V3 interneurons had higher rheobase and did not display initial doublets and triplets at all in the first two weeks. These effects suggest that motoneurons are less excitable in the presence of V3 interneurons. However, there was also an increase in spontaneous activity at earlier time points, both in terms of bursts and EPSP frequency, suggesting

an increase in excitability. Indeed, V3 interneurons have been shown to provide strong excitatory input to motoneurons both *in vitro* (Sternfeld et al., 2017) and *in vivo* (Chopek et al., 2018). Activity can drive homeostatic changes in electrophysiological properties (O'Leary and Wyllie, 2011), which may be the reason for the seemingly contradictory effect of V3 interneurons on rheobase and initial doublet/triplets.

Co-culture of V3 interneurons accelerated the emergence of spontaneous glutamatergic activity and introduced a new activity pattern in both calcium imaging and single cell patch clamp experiments. Given somatic calcium transients induce gene transcription (Bengtson et al., 2010; Ibata et al., 2008; Lyons and West, 2011), it would be interesting to investigate whether the altered activity pattern introduced by V3 interneurons affects gene expression, by comparing gene expression of motoneurons in the MN+as and MN+V3+as co-culture conditions in week 3 or 4 (when calcium activity was observed in both conditions). Previous experiments have indicated that patterns of spontaneous activity with a mix of long and short duration, and high and low amplitude calcium bursts only occurs in co-cultures containing inhibitory interneurons (Sternfeld et al., 2017). However, the results in Chapter 6 suggest that varying the source of spontaneous glutamatergic activity (either from other motoneurons or from V3 interneurons) can be enough to alter the pattern of spontaneous activity. To further probe the roles of different subtypes of spinal interneuron in motoneuron activity, it would be interesting to explore whether other excitatory spinal interneurons give rise to different patterns of motoneuronal spontaneous activity.

7.3 Study Limitations

The effects of ESC-derived astrocytes and V3 interneurons on various indicators of *in vitro* motoneuron maturation have been effectively investigated and described in this Thesis. However, as with any study, there are limitations. A 2D *in vitro* co-culture model was used for this investigation as it was a reliable and consistent way of efficiently gathering data compared to producing and transplanting motoneuron grafts of differing compositions into mice. However, a 2D *in vitro* model is, of course, an imperfect representation of transplantation *in vivo*. For example, astrocytes have been shown to express more activation markers in 2D than in 3D cultures (East et al., 2009),

meaning the co-cultures used in this Thesis may have had some characteristics of an inflammatory environment. In some conditions, reactive astrocytes can be neurotoxic (Guttenplan et al., 2020; Li et al., 2019), which may be the reason that, while neurons survival was increased in the presence of astrocytes (Figure 4.3 in Chapter 4), they did not survive indefinitely (typically cultures were discarded 1 month after motoneuron plating). In contrast, peripherally-transplanted EBs containing motoneurons survive at least 11 months following transplantation (given the inclusion of GDNF and ciliary neurotrophic factor in the implant medium) (Yohn et al., 2008). Thus, as with any model, the extent to which the 2D *in vitro* co-culture model used in this Thesis was representative of the peripheral ESC-derived motoneuron transplant is limited.

Furthermore, the high degree of overlapping neurite extension in the co-cultures meant the dendritic and axonal structure of individual neurons was difficult to distinguish, particularly in astrocyte-containing co-cultures. Therefore, immunocytochemical experiments predominantly focussed on the somatic and proximal dendritic neuronal compartments as these were easily identified and directly comparable between neurons. Primary neurite diameter was used as a proxy measure of neurite complexity as it has been shown to be strongly positively correlated with other measures of *in vivo* dendritic complexity in various subtypes of cat (Cameron et al., 1985; Cullheim et al., 1987; Fukunishi et al., 1999; Ulfhake and Cullheim, 1988; Ulfhake and Kellerth, 1981, 1983) and rat (Nüñez-Abades et al., 1994) motoneurons. The assumption adopted here was that the correlation observed in rat and cat motoneurons *in vivo* was also true of these mouse ESC-derived motoneurons *in vitro.* Despite using this proxy for neurite complexity, the lack of information about the distal dendritic and axonal compartments meant some of the results left unanswered questions. For example, despite motoneurons in MN+as co-cultures displaying spontaneous activity in week 2 as shown in Chapters 5 and 6, the presence of astrocytes did not increase the density of vGluT2-positive synapses in the somatic and proximal dendritic compartments compared to the MN alone control (Figure 4.7 in Chapter 4). There are several potential reasons for this: 1) astrocytes exert their effect by causing the baseline number of glutamatergic synapses to become active and this is sufficient to enable spontaneous glutamatergic activity, 2) synapses characterised by a glutamate transporter different from vGluT2 was responsible for the spontaneous

activity, or 3) the glutamatergic synapses responsible for this activity were on more distal dendrites and therefore not counted in this experiment. Examples of synapses between motor axon collaterals and other motoneurons in the literature are predominantly somatic and proximal dendritic (Cullheim et al., 1977; Mentis et al., 2005). However, this may similarly be because motoneuron somas were easier to label and locate. To draw any further conclusions about glutamatergic synapses between motoneurons, the synapses of two synaptically connected motoneurons would need to be mapped including the distal dendritic compartments.

7.4 Future work

While the results of this Thesis showed that V3 interneurons and particularly astrocytes play important roles in various aspects of motoneuron maturation *in vitro*, a multi-compartment model including muscle fibres would be needed to investigate how the presence of each of these cell types impacts muscle innervation by motoneurons. One such multi-compartment model of nerve-muscle connectivity (which included astrocytes) was used by Machado et al. (2019) to show that optically entraining ChR2-expressing motoneurons encouraged the formation of putative NMJs and synapses, though only cholinergic synapses were considered. Experiments in the Bryson and Greensmith groups are using similar multi-compartment models to investigate how well different motoneuron subtypes innervate muscle fibres and to further optimise culture conditions. Preliminary results have shown that co-culture with astrocytes was necessary for motoneuron survival in the microfluidic chamber, supporting the results presented in this Thesis that suggest that astrocytes are likely to be fundamental to the success of motoneuron grafts (Mclaughlin, Kourgiantaki & Bryson, unpublished observations). The multi-compartment NMJ model could be further used to explore the influence on motoneuron muscle innervation of different spontaneous activity patterns, such as those demonstrated in Chapter 6 or observed during spinal cord development (Yvert et al., 2004), either by introducing V3 interneurons into the nerve compartment alongside motoneurons or using patterned optical entrainment to mimic the influence of V3 interneurons on spontaneous motoneuron activity.

V3 interneurons were selected for study because of their prevalence in the EB, as demonstrated in Chapter 3. However, it is possible that other spinal interneurons may introduce different spontaneous activity patterns. For example, in addition to V3 interneurons, Sternfeld et al. (2017) investigated the impact of V1 interneurons on motoneuron circuit formation and activity. They found that co-culture of ESC-derived motoneurons with moderate amounts of ESC-derived V1 interneurons (with ESC-derived astrocytes) increased the variability of spontaneous calcium event amplitude, increased network complexity and decreased cellular synchrony; these effects were eliminated by an inhibitory antagonist (Sternfeld et al., 2017). Therefore, there is scope to investigate the role of other spinal interneurons in motoneuron maturation.

Further progression towards the therapeutic use of intraneural ESC-derived optogenetic motoneuron engraftment as a treatment for paralysis in ALS will require optimisation of the opsins used. The therapeutic utility of ChR2 has been called into question by results showing that expression of ChR2 led to immunogenicity, resulting in axonopathy (Miyashita et al., 2013), CNS motoneuron death and muscle atrophy (Maimon et al., 2018). Red-shifted opsins, such as ReaChR (Lin et al., 2013), are more sensitive, boast greater tissue penetrance with less energetic excitation wavelengths in the orange-red spectrum, and avoid the potentially cytotoxic effects of blue-violet light (Hockberger et al., 1999). Therefore, though more work needs to be done to ensure they are not immunogenic, red-shifted opsins are good candidates to take forward into an optogenetic stem cell-based therapy to restore muscle function in ALS.

The development of implantable optical pacemakers suitable for therapeutic use is also a necessary step towards the use of therapeutic optogenetics to restore muscle function. The method for optical stimulation used in initial experiments to enable optical control of muscle function in awake and freely moving rats (which expressed ChR2 in peripheral nerves) was tethered optical fibres connected to an external light source (Aravanis et al., 2007). However, the intermittent tethered systems do not offer the chronic, long-term stimulation of transplanted motoneurons and subsequent muscle activity required, as previously discussed, for the formation and maintenance of the NMJs (Bryson et al., 2016). To enable such translationally-relevant chronic, longitudinal stimulation experiments, fully implantable wirelessly-powered mini-LED devices have been developed (Wentz et al., 2011) and their use to optically stimulate

the brain, spinal cord and peripheral nerves of mice demonstrated (Montgomery et al., 2015). Optimisation of this technology for motor control is required such that a gradual ramping of light intensity can be used to recruit motoneurons and muscle in a physiological manner and avoid fatigue (Bryson et al., 2016). The development of wireless optical stimulators represents a great advance towards the reliable control of muscle function with optogenetics. Control of more complex motor functions with optogenetics could be achieved by using neural transplantation or viral transduction strategies to allow control of spatially separate opposable muscle groups and multiple opsins. To facilitate this, more sophisticated optical stimulators with multiple excitation wavelengths will need to be developed.

7.5 Concluding remarks.

This Thesis aimed to investigate the impact of co-culture with astrocytes and V3 interneurons on the maturation of ESC-derived motoneurons. The results show that astrocytes are fundamental for the *in vitro* maturation of ESC-derived motoneurons as determined by assessment of their morphology, synaptic connectivity and electrophysiological properties, and essential for the development of spontaneous glutamatergic activity. Co-culture with V3 interneurons modulated the synapses formed by motoneurons and the patterns of spontaneous motoneuronal glutamatergic activity in an astrocyte-dependent manner. Insights from these results could be used to optimise the cellular composition or patterns of optical entrainment of ESC-derived motoneuron-containing peripheral nerve grafts for the restoration of muscle function in ALS and other axonopathies.

8 Bibliography

Abe, K., Itoyama, Y., Sobue, G., Tsuji, S., Aoki, M., Doyu, M., Hamada, C., Kondo, K., Yoneoka, T., Akimoto, M., et al. (2014). Confirmatory double-blind, parallel-group, placebo-controlled study of efficacy and safety of edaravone (MCI-186) in amyotrophic lateral sclerosis patients. Amyotroph. Lateral Scler. Frontotemporal Degener. *15*, 610–617.

Acton, D., and Miles, G.B. (2015). Stimulation of glia reveals modulation of mammalian spinal motor networks by adenosine. PLoS One *10*.

Acton, D., Broadhead, M.J., and Miles, G.B. (2018). Modulation of spinal motor networks by astrocyte-derived adenosine is dependent on D_1-like dopamine receptor signaling. J. Neurophysiol. *120*, 998–1009.

Al-Chalabi, A. (2017). Perspective: Don't keep it in the family. Nature *550*, S112–S112.

Al-Majed, A.A., Neumann, C.M., Brushart, T.M., and Gordon, T. (2000). Brief electrical stimulation promotes the speed and accuracy of motor axonal regeneration. J. Neurosci. *20*, 2602–2608.

Alaynick, W.A., Jessell, T.M., and Pfaff, S.L. (2011). SnapShot: Spinal Cord Development. Cell *146*, 178-178.e1.

Albert, P.R. (2014). Light up your life: optogenetics for depression? J. Psychiatry Neurosci. *39*, 3–5.

Albrecht, D., López-Murcia, F.J., Pérez-González, A.P., Lichtner, G., Solsona, C., and Llobet, A. (2012). SPARC prevents maturation of cholinergic presynaptic terminals. Mol. Cell. Neurosci. *49*, 364–374.

Allan, D.W., and Greer, J.J. (1997). Development of phrenic motoneuron morphology in the fetal rat. J. Comp. Neurol. *382*, 469–479.

Allen, N.J., and Eroglu, C. (2017). Cell biology of astrocyte-synapse interactions. Neuron *96*, 697–708.

Allen, D.L., Harrison, B.C., Maass, A., Bell, M.L., Byrnes, W.C., and Leinwand, L.A. (2001). Cardiac and skeletal muscle adaptations to voluntary wheel running in the mouse. J. Appl. Physiol. *90*, 1900–1908.

Allen, N.J., Bennett, M.L., Foo, L.C., Wang, G.X., Chakraborty, C., Smith, S.J., and Barres, B.A. (2012). Astrocyte glypicans 4 and 6 promote formation of excitatory synapses via GluA1 AMPA receptors. Nature *486*, 410–414.

Almaas, R., Saugstad, O.D., Pleasure, D., and Rootwelt, T. (2002). Neuronal formation of free radicals plays a minor role in hypoxic cell death in human NT2-N neurons. Pediatr. Res. *51*, 136–143.

Almeida, S., Gascon, E., Tran, H., Chou, H.J., Gendron, T.F., DeGroot, S., Tapper, A.R., Sellier, C., Charlet-Berguerand, N., Karydas, A., et al. (2013a). Modeling key pathological features of frontotemporal dementia with C9ORF72 repeat expansion in iPSC-derived human neurons. Acta Neuropathol. *126*, 385–399.

Almeida, V., de Carvalho, M., Scotto, M., Pinto, S., Pinto, A., Ohana, B., and Swash, M. (2013b). Primary lateral sclerosis: Predicting functional outcome. Amyotroph. Lateral Scler. Front. Degener. *14*, 141–145.

Altschuler, S.M., Bao, X., and Miselis, R.R. (1994). Dendritic architecture of hypoglossal

motoneurons projecting to extrinsic tongue musculature in the rat. J. Comp. Neurol. *342*, 538–550.

Alvarez, F.J., and Fyffe, R.E.W. (2007). The continuing case for the Renshaw cell. J. Physiol. *584*, 31–45.

Alvarez, F.J., Jonas, P.C., Sapir, T., Hartley, R., Berrocal, M.C., Geiman, E.J., Todd, A.J., and Goulding, M. (2005). Postnatal phenotype and localization of spinal cord V1 derived interneurons. J. Comp. Neurol. *493*, 177–192.

Anderson, K.D. (2004). Targeting recovery: priorities of the spinal cord-injured population. J. Neurotrauma *21*, 1371–1383.

Ang, L.C., Bhaumick, B., Munoz, D.G., Sass, J., and Juurlink, B.H.J. (1992). Effects of astrocytes, insulin and insulin-like growth factor I on the survival of motoneurons in vitro. J. Neurol. Sci. *109*, 168–172.

Angeli, C.A., Edgerton, V.R., Gerasimenko, Y.P., and Harkema, S.J. (2014). Altering spinal cord excitability enables voluntary movements after chronic complete paralysis in humans. Brain *137*, 1394–1409.

Aravanis, A.M., Wang, L.-P., Zhang, F., Meltzer, L.A., Mogri, M.Z., Schneider, M.B., and Deisseroth, K. (2007). An optical neural interface: in vivo control of rodent motor cortex with integrated fiberoptic and optogenetic technology. J. Neural Eng. *4*, S143-56.

Arber, S., Han, B., Mendelsohn, M., Smith, M., Jessell, T.M., and Sockanathan, S. (1999). Requirement for the homeobox gene Hb9 in the consolidation of motor neuron identity. Neuron *23*, 659–674.

Arenkiel, B.R., Peca, J., Davison, I.G., Feliciano, C., Deisseroth, K., Augustine, G.J., Ehlers, M.D., and Feng, G. (2007). In vivo light-induced activation of neural circuitry in transgenic mice expressing channelrhodopsin-2. Neuron *54*, 205.

Arlow, R.L., Foutz, T.J., and McIntyre, C.C. (2013). Theoretical principles underlying optical stimulation of myelinated axons expressing channelrhodopsin-2. Neuroscience *248*, 541–551.

Arnold, E.S., Ling, S.-C., Huelga, S.C., Lagier-Tourenne, C., Polymenidou, M., Ditsworth, D., Kordasiewicz, H.B., McAlonis-Downes, M., Platoshyn, O., Parone, P.A., et al. (2013). ALS-linked TDP-43 mutations produce aberrant RNA splicing and adult-onset motor neuron disease without aggregation or loss of nuclear TDP-43. Proc. Natl. Acad. Sci. U. S. A. *110*, E736-45.

Ash, P.E.A., Bieniek, K.F., Gendron, T.F., Caulfield, T., Lin, W.-L., Dejesus-Hernandez, M., van Blitterswijk, M.M., Jansen-West, K., Paul, J.W., Rademakers, R., et al. (2013). Unconventional translation of C9ORF72 GGGGCC expansion generates insoluble polypeptides specific to c9FTD/ALS. Neuron *77*, 639–646.

Atasoy, D., Aponte, Y., Su, H.H., and Sternson, S.M. (2008). A FLEX switch targets Channelrhodopsin-2 to multiple cell types for imaging and long-range circuit mapping. J. Neurosci. *28*, 7025–7030.

Atkin, J.D., Farg, M.A., Walker, A.K., McLean, C., Tomas, D., and Horne, M.K. (2008). Endoplasmic reticulum stress and induction of the unfolded protein response in human sporadic amyotrophic lateral sclerosis. Neurobiol. Dis. *30*, 400–407.

Bączyk, M., Hałuszka, A., Mrówczyński, W., Celichowski, J., and Krutki, P. (2013). The influence of a 5-wk whole body vibration on electrophysiological properties of rat hindlimb spinal motoneurons. J. Neurophysiol. *109*, 2705–2711.

Baek, W., Kim, Y.S., Koh, S.H., Lim, S.W., Kim, H.Y., Yi, H.J., and Kim, H. (2012). Stem cell transplantation into the intraventricular space via an Ommaya reservoir in a patient with amyotrophic lateral sclerosis. J. Neurosurg. Sci. *56*, 261–263.

Bakels, R., and Kernell, D. (1993). Matching between motoneurone and muscle unit properties in rat medial gastrocnemius. J. Physiol. *463*, 307–324.

Bannwarth, S., Ait-El-Mkadem, S., Chaussenot, A., Genin, E.C., Lacas-Gervais, S., Fragaki, K., Berg-Alonso, L., Kageyama, Y., Serre, V., Moore, D.G., et al. (2014). A mitochondrial origin for frontotemporal dementia and amyotrophic lateral sclerosis through CHCHD10 involvement. Brain *137*, 2329–2345.

Barker, A.J., Koch, S.M., Reed, J., Barres, B.A., and Ullian, E.M. (2008). Developmental control of synaptic receptivity. J. Neurosci. *28*, 8150–8160.

Bayha, E., Jørgensen, M.C., Serup, P., and Grapin-Botton, A. (2009). Retinoic acid signaling organizes endodermal organ specification along the entire antero-posterior axis. PLoS One *4*, e5845.

Bayliss, D.A., Viana, F., Bellingham, M.C., and Berger, A.J. (1994). Characteristics and postnatal development of a hyperpolarization-activated inward current in rat hypoglossal motoneurons in vitro. J. Neurophysiol. *71*, 119–128.

Bayraktar, O.A., Fuentealba, L.C., Alvarez-Buylla, A., and Rowitch, D.H. (2014). Astrocyte development and heterogeneity. Cold Spring Harb. Perspect. Biol. *7*, a020362.

Beaumont, E., and Gardiner, P. (2002). Effects of daily spontaneous running on the electrophysiological properties of hindlimb motoneurones in rats. J. Physiol. *540*, 129–138.

Beckman, J.S., Carson, M., Smith, C.D., and Koppenol, W.H. (1993). ALS, SOD and peroxynitrite. Nature *364*, 584–584.

Bellingham, M.C. (2011). A review of the neural mechanisms of action and clinical efficiency of riluzole in treating amyotrophic lateral sclerosis: What have we learned in the last decade? CNS Neurosci. Ther. *17*, 4–31.

Belzil, V. V, Katzman, R.B., and Petrucelli, L. (2016). ALS and FTD: an epigenetic perspective. Acta Neuropathol. *132*, 487–502.

Bengtson, C.P., Freitag, H.E., Weislogel, J.-M., and Bading, H. (2010). Nuclear calcium sensors reveal that repetition of trains of synaptic stimuli boosts nuclear calcium signaling in CA1 pyramidal neurons. Biophys. J. *99*, 4066–4077.

Bensimon, G., Lacomblez, L., Meininger, V., and Group, the A.S. (1994). A controlled trial of riluzole in amyotrophic lateral sclerosis. N. Engl. J. Med. *330*, 585–591.

Berlowitz, D.J., Howard, M.E., Fiore, J.F., Vander Hoorn, S., O'Donoghue, F.J., Westlake, J., Smith, A., Beer, F., Mathers, S., and Talman, P. (2016). Identifying who will benefit from non-invasive ventilation in amyotrophic lateral sclerosis/motor neurone disease in a clinical cohort. J. Neurol. Neurosurg. Psychiatry *87*, 280–286.

Berry, J.D., Cudkowicz, M.E., Windebank, A.J., Staff, N.P., Owegi, M., Nicholson, K., McKenna-Yasek, D., Levy, Y.S., Abramov, N., Kaspi, H., et al. (2019). NurOwn, phase 2, randomized, clinical trial in patients with ALS: Safety, clinical, and biomarker results. Neurology *93*, e2294–e2305.

Bertrand, S., and Cazalets, J.R. (1998). Postinhibitory rebound during locomotor-like activity in neonatal rat motoneurons in vitro. J. Neurophysiol. *79*, 342–351.

Bhumbra, G.S., and Beato, M. (2018). Recurrent excitation between motoneurones propagates across segments and is purely glutamatergic. PLOS Biol. *16*, e2003586.

Bhumbra, G.S., Bannatyne, B.A., Watanabe, M., Todd, A.J., Maxwell, D.J., and Beato, M. (2014). The recurrent case for the Renshaw cell. J. Neurosci. *34*, 12919–12932.

Bialas, A.R., and Stevens, B. (2013). TGF-β signaling regulates neuronal C1q expression and developmental synaptic refinement. Nat. Neurosci. *16*, 1773.

Bianchi, F., Malboubi, M., Li, Y., George, J.H., Jerusalem, A., Szele, F., Thompson, M.S., and Ye, H. (2018). Rapid and efficient differentiation of functional motor neurons from human iPSC for neural injury modelling. Stem Cell Res. *32*, 126–134.

Bilsland, L.G., Sahai, E., Kelly, G., Golding, M., Greensmith, L., and Schiavo, G. (2010). Deficits in axonal transport precede ALS symptoms in vivo. Proc. Natl. Acad. Sci. U. S. A. *107*, 20523–20528.

Birger, A., Ben-Dor, I., Ottolenghi, M., Turetsky, T., Gil, Y., Sweetat, S., Perez, L., Belzer, V., Casden, N., Steiner, D., et al. (2019). Human iPSC-derived astrocytes from ALS patients with mutated C9ORF72 show increased oxidative stress and neurotoxicity. EBioMedicine *50*, 274–289.

Birsa, N., Bentham, M.P., and Fratta, P. (2020). Cytoplasmic functions of TDP-43 and FUS and their role in ALS. Semin. Cell Dev. Biol. *99*, 193–201.

Blankenship, A.G., and Feller, M.B. (2010). Mechanisms underlying spontaneous patterned activity in developing neural circuits. Nat. Rev. Neurosci. *11*, 18–29.

Blanquer, M., Moraleda, J.M., Iniesta, F., Gómez-Espuch, J., Meca-Lallana, J., Villaverde, R., Pérez-Espejo, M.Á., Ruíz-López, F.J., García Santos, J.M., Bleda, P., et al. (2012). Neurotrophic bone marrow cellular nests prevent spinal motoneuron degeneration in amyotrophic lateral sclerosis patients: a pilot safety study. Stem Cells *30*, 1277–1285.

Boerboom, A., Dion, V., Chariot, A., and Franzen, R. (2017). Molecular mechanisms involved in Schwann cell plasticity. Front. Mol. Neurosci. *10*, 38.

Boillee, S., Yamanaka, K., Lobsiger, C.S., Copeland, N.G., Jenkins, N.A., Kassiotis, G., Kollias, G., and Cleveland, D.W. (2006). Onset and progression in inherited ALS determined by motor neurons and microglia. Science (80-.). *312*, 1389–1392.

Bond, A.M., Bhalala, O.G., and Kessler, J.A. (2012). The dynamic role of bone morphogenetic proteins in neural stem cell fate and maturation. Dev. Neurobiol. *72*, 1068–1084.

Bond, L., Ganguly, P., Khamankar, N., Mallet, N., Bowen, G., Green, B., and Mitchell, C.S. (2019). A comprehensive examination of percutaneous endoscopic gastrostomy and its association with amyotrophic lateral sclerosis patient outcomes. Brain Sci. *9*.

Borgius, L., Restrepo, C.E., Leao, R.N., Saleh, N., and Kiehn, O. (2010). A transgenic mouse line for molecular genetic analysis of excitatory glutamatergic neurons. Mol. Cell. Neurosci. *45*, 245–257.

Borowska, J., Jones, C.T., Zhang, H., Blacklaws, J., Goulding, M., and Zhang, Y. (2013). Functional subpopulations of V3 interneurons in the mature mouse spinal cord. J. Neurosci. *33*.

Borowska, J., Jones, C.T., Deska-Gauthier, D., and Zhang, Y. (2015). V3 interneuron subpopulations in the mouse spinal cord undergo distinctive postnatal maturation processes. Neuroscience *295*, 221–228.

Boulting, G.L., Kiskinis, E., Croft, G.F., Amoroso, M.W., Oakley, D.H., Wainger, B.J., Williams, D.J., Kahler, D.J., Yamaki, M., Davidow, L., et al. (2011). A functionally characterized test set of human induced pluripotent stem cells. Nat. Biotechnol. *29*, 279–286.

Bourke, S.C., Tomlinson, M., Williams, T.L., Bullock, R.E., Shaw, P.J., and Gibson, G.J. (2006). Effects of non-invasive ventilation on survival and quality of life in patients with amyotrophic lateral sclerosis: a randomised controlled trial. Lancet Neurol. *5*, 140–147.

Boyden, E.S., Zhang, F., Bamberg, E., Nagel, G., and Deisseroth, K. (2005). Millisecond-timescale, genetically targeted optical control of neural activity. Nat. Neurosci. *8*, 1263–1268.

Brakeman, P.R., Lanahan, A.A., O'Brien, R., Roche, K., Barnes, C.A., Huganir, R.L., and Worley, P.F. (1997). Homer: a protein that selectively binds metabotropic glutamate receptors. Nature *386*, 284–288.

Brenner, D., and Weishaupt, J.H. (2019). Update on amyotrophic lateral sclerosis genetics. Curr. Opin. Neurol. *32*, 735–739.

Brenner, D., Yilmaz, R., Müller, K., Grehl, T., Petri, S., Meyer, T., Grosskreutz, J., Weydt, P., Ruf, W., Neuwirth, C., et al. (2018). Hot-spot KIF5A mutations cause familial ALS. Brain *141*, 688–697.

Briscoe, J., Sussel, L., Serup, P., Hartigan-O'Connor, D., Jessell, T.M., Rubenstein, J.L.R., and Ericson, J. (1999). Homeobox gene Nkx2.2 and specification of neuronal identity by graded Sonic hedgehog signalling. Nature *398*, 622–627.

Broadhead, M.J., and Miles, G.B. (2020). Bi-Directional Communication Between Neurons and Astrocytes Modulates Spinal Motor Circuits. Front. Cell. Neurosci. *14*.

Broadhead, M.J., Bonthron, C., Arcinas, L., Bez, S., Zhu, F., Goff, F., Nylk, J., Dholakia, K., Gunn-Moore, F., Grant, S.G.N., et al. (2020). Nanostructural diversity of synapses in the mammalian spinal cord. Sci. Rep. *10*.

Brown, C.R., Butts, J.C., McCreedy, D.A., and Sakiyama-Elbert, S.E. (2014). Generation of V2a interneurons from mouse embryonic stem cells. Stem Cells Dev. *23*, 1765–1776.

Brownstone, R.M., and Bui, T. V. (2010). Spinal interneurons providing input to the final common path during locomotion. Prog. Brain Res. *187*, 81–95.

Brownstone, R.M., and Lancelin, C. (2018). Escape from homeostasis: spinal microcircuits and progression of amyotrophic lateral sclerosis. J. Neurophysiol. *119*, 1782–1794.

Brozanski, B.S., Guthrie, R.D., Volk, E.A., and Cameron, W.E. (1989). Postnatal growth of genioglossal motoneurons. Pediatr. Pulmonol. *7*, 133–139.

Bruijn, L.I., Miller, T.M., and Cleveland, D.W. (2004). Unraveling the mechanisms involved in motor neuron degeneration in ALS. Annu. Rev. Neurosci. *27*, 723–749.

Brushart, T.M., Hoffman, P.N., Royall, R.M., Murinson, B.B., Witzel, C., and Gordon, T. (2002). Electrical stimulation promotes motoneuron regeneration without increasing its speed or conditioning the neuron. J. Neurosci. *22*, 6631–6638.

Bryson, J.B., Machado, C.B., Crossley, M., Stevenson, D., Bros-Facer, V., Burrone, J., Greensmith, L., and Lieberam, I. (2014). Optical control of muscle function by transplantation of stem cell-derived motor neurons in mice. Science *344*, 94–97.

Bryson, J.B., Machado, C.B., Lieberam, I., and Greensmith, L. (2016). Restoring motor function using optogenetics and neural engraftment. Curr. Opin. Biotechnol. *40*, 75–81.

Buntschu, S., Tscherter, A., Heidemann, M., and Streit, J. (2020). Critical components for spontaneous activity and rhythm generation in spinal cord circuits in culture. Front. Cell. Neurosci. *14*, 81.

Buosi, A.S., Matias, I., Araujo, A.P.B., Batista, C., and Gomes, F.C.A. (2018). Heterogeneity in synaptogenic profile of astrocytes from different brain regions. Mol. Neurobiol. *55*, 751–762.

Burke, R.E. (2006). Sir Charles Sherrington's The integrative action of the nervous system: a centenary appreciation. Brain *130*, 887–894.

Burrell, J.R., Kiernan, M.C., Vucic, S., and Hodges, J.R. (2011). Motor Neuron dysfunction in frontotemporal dementia. Brain *134*, 2582–2594.

Bushong, E.A., Martone, M.E., Jones, Y.Z., and Ellisman, M.H. (2002). Protoplasmic astrocytes in CA1 stratum radiatum occupy separate anatomical domains. J. Neurosci. *22*, 183–192.

Buzsáki, G. (2004). Large-scale recording of neuronal ensembles. Nat. Neurosci. *7*, 446–451.

Caldeira, V., Dougherty, K.J., Borgius, L., and Kiehn, O. (2017). Spinal Hb9::Cre-derived excitatory interneurons contribute to rhythm generation in the mouse. Sci. Rep. *7*, 41369.

Cambridge Electronic Design Ltd (1996). Signal Version 5 Manual.

Cameron, W.E., Averill, D.B., and Berger, A.J. (1985). Quantitative analysis of the dendrites of cat phrenic motoneurons stained intracellularly with horseradish peroxidase. J. Comp. Neurol. *231*, 91–101.

Cameron, W.E., Fang, H., Brozanski, B.S., and Guthrie, R.D. (1989). The postnatal growth of motoneurons at three levels of the cat neuraxis. Neurosci. Lett. *104*, 274–280.

Cameron, W.E., Brozanski, B.S., and Guthrie, R.D. (1990). Postnatal development of phrenic motoneurons in the cat. Dev. Brain Res. *51*, 142–145.

Canto-Bustos, M., Loeza-Alcocer, E., González-Ramírez, R., Gandini, M.A., Delgado-Lezama, R., and Felix, R. (2014). Functional expression of T-type Ca2+ channels in spinal motoneurons of the adult turtle. PLoS One *9*, e108187.

Carcagno, A.L., Di Bella, D.J., Goulding, M., Guillemot, F., and Lanuza, G.M. (2014). Neurogenin3 restricts serotonergic neuron differentiation to the hindbrain. J. Neurosci. *34*, 15223–15233.

Carrascal, L., Nieto-Gonzalez, J.L., Cameron, W.E., Torres, B., and Nunez-Abades, P.A. (2005). Changes during the postnatal development in physiological and anatomical characteristics of rat motoneurons studied in vitro. Brain Res. Rev. *49*, 377–387.

Cattin, A.-L., Burden, J.J., Van Emmenis, L., Mackenzie, F.E., Hoving, J.J.A., Garcia Calavia, N., Guo, Y., McLaughlin, M., Rosenberg, L.H., Quereda, V., et al. (2015). Macrophage-induced blood vessels guide Schwann cell-mediated regeneration of peripheral nerves. Cell *162*, 1127–1139.

Chai, N., Haney, M.S., Couthouis, J., Morgens, D.W., Benjamin, A., Wu, K., Ousey, J., Fang, S., Finer, S., Bassik, M.C., et al. (2020). Genome-wide synthetic lethal CRISPR screen identifies FIS1 as a genetic interactor of ALS-linked C9ORF72. Brain Res. *1728*, 146601.

Chan, K.M., Curran, M.W.T., and Gordon, T. (2016). The use of brief post-surgical low frequency electrical stimulation to enhance nerve regeneration in clinical practice. J. Physiol. *594*, 3553–3559.

Chen, T.-W., Wardill, T.J., Sun, Y., Pulver, S.R., Renninger, S.L., Baohan, A., Schreiter, E.R., Kerr, R.A., Orger, M.B., Jayaraman, V., et al. (2013). Ultrasensitive fluorescent proteins for imaging neuronal activity. Nature *499*, 295–300.

Chiang, C., Litingtung, Y., Lee, E., Young, K.E., Corden, J.L., Westphal, H., and Beachy, P.A. (1996). Cyclopia and defective axial patterning in mice lacking Sonic hedgehog gene function. Nature *383*, 407–413.

Chiò, A., Calvo, A., Moglia, C., Mazzini, L., Mora, G., and group*, P. study (2011). Phenotypic heterogeneity of amyotrophic lateral sclerosis: a population based study. J. Neurol. Neurosurg. Psychiatry *82*, 740–746.

Chiò, A., Logroscino, G., Traynor, B.J., Collins, J., Simeone, J.C., Goldstein, L.A., and White, L.A. (2013). Global epidemiology of amyotrophic lateral sclerosis: a systematic review of the published literature. Neuroepidemiology *41*, 118–130.

Chopek, J.W., Nascimento, F., Beato, M., Brownstone, R.M., and Zhang, Y. (2018). Sub-populations of spinal V3 interneurons form focal Modules of layered pre-motor microcircuits. Cell Rep. *25*, 146-156.e3.

Christopherson, K.S., Ullian, E.M., Stokes, C.C.A., Mullowney, C.E., Hell, J.W., Agah, A., Lawler, J., Mosher, D.F., Bornstein, P., and Barres, B.A. (2005). Thrombospondins are astrocyte-secreted proteins that promote CNS synaptogenesis. Cell *120*, 421–433.

Chung, W.-S., and Barres, B.A. (2012). The role of glial cells in synapse elimination. Curr. Opin. Neurobiol. *22*, 438–445.

Chung, W.-S., Clarke, L.E., Wang, G.X., Stafford, B.K., Sher, A., Chakraborty, C., Joung, J., Foo, L.C., Thompson, A., Chen, C., et al. (2013). Astrocytes mediate synapse elimination through MEGF10 and MERTK pathways. Nature *504*, 394–400.

Clarke, B.E., Taha, D.M., Tyzack, G.E., and Patani, R. (2020). Regionally encoded functional heterogeneity of astrocytes in health and disease: A perspective. Glia.

Clement, A.M., Nguyen, M.D., Roberts, E.A., Garcia, M.L., Boillée, S., Rule, M., McMahon, A.P., Doucette, W., Siwek, D., Ferrante, R.J., et al. (2003). Wild-type nonneuronal cells extend survival of SOD1 mutant motor neurons in ALS mice. Science (80-.). *302*, 113–117.

Connors, B.W. (2012). Tales of a dirty drug: carbenoxolone, gap junctions, and seizures. Epilepsy Curr. *12*, 66–68.

Cooper-Knock, J., Moll, T., Ramesh, T., Castelli, L., Beer, A., Robins, H., Fox, I., Niedermoser, I., Van Damme, P., Moisse, M., et al. (2019). Mutations in the glycosyltransferase domain of GLT8D1 are associated with familial amyotrophic lateral sclerosis. Cell Rep. *26*, 2298-2306.e5.

Corestem (2019). First licensed stem cell therapy for ALS.

Couratier, P., Sindou, P., Hugon, J., Couratier, P., Hugon, J., Vallat, J.M., and Dumas, M. (1993). Cell culture evidence for neuronal degeneration in amyotrophic lateral sclerosis being linked to glutamate AMPA/kainate receptors. Lancet *341*, 265–268.

Craig, A., Tran, Y., and Middleton, J. (2009). Psychological morbidity and spinal cord injury: a systematic review. Spinal Cord *47*, 108–114.

Craig, A.R., Hancock, K.M., and Dickson, H.G. (1994a). A longitudinal investigation into anxiety and depression in the first 2 years following a spinal cord injury. Spinal Cord *32*, 675–679.

Craig, A.R., Hancock, K.M., and Dickson, H.G. (1994b). Spinal cord injury: a search for determinants of depression two years after the event. Br. J. Clin. Psychol. *33 (Pt 2)*, 221–230.

Cui, W., Allen, N.D., Skynner, M., Gusterson, B., and Clark, A.J. (2001). Inducible ablation of astrocytes shows that these cells are required for neuronal survival in the adult brain. Glia *34*, 272–282.

Cullheim, S., Kellerth, J.-O., and Conradi, S. (1977). Evidence for direct synaptic interconnections between cat spinal α-motoneurons via the recurrent axon collaterals: A morphological study using intracellular injection of horseradish peroxidase. Brain Res. *132*, 1–10.

Cullheim, S., Fleshman, J.W., Glenn, L.L., and Burke, R.E. (1987). Membrane area and dendritic structure in type-identified triceps surae alpha motoneurons. J. Comp. Neurol. *255*, 68–81.

Dai, R., Stein, R.B., Andrews, B.J., James, K.B., and Wieler, M. (1996). Application of tilt sensors in functional electrical stimulation. IEEE Trans. Rehabil. Eng. *4*, 63–72.

Damiano, M., Starkov, A.A., Petri, S., Kipiani, K., Kiaei, M., Mattiazzi, M., Flint Beal, M., and Manfredi, G. (2006). Neural mitochondrial Ca^{2+} capacity impairment precedes the onset of motor symptoms in G93A Cu/Zn-superoxide dismutase mutant mice. J. Neurochem. *96*, 1349–1361.

Danner, S.M., Shevtsova, N.A., Frigon, A., and Rybak, I.A. (2017). Computational modeling of spinal circuits controlling limb coordination and gaits in quadrupeds. Elife *6*.

Deardorff, A.S., Romer, S.H., Deng, Z., Bullinger, K.L., Nardelli, P., Cope, T.C., and Fyffe, R.E.W. (2013). Expression of postsynaptic Ca2+-activated K+ (SK) channels at C-bouton synapses in mammalian lumbar α-motoneurons. J. Physiol. *591*, 875–897.

Deardorff, A.S., Romer, S.H., Sonner, P.M., and Fyffe, R.E.W. (2014). Swimming against the tide: investigations of the C-bouton synapse. Front. Neural Circuits *8*, 106.

Deda, H., Inci, M.C., Kürekçi, A.E., Sav, A., Kayihan, K., Ozgün, E., Ustünsoy, G.E., and Kocabay, S. (2009). Treatment of amyotrophic lateral sclerosis patients by autologous bone marrow-derived hematopoietic stem cell transplantation: a 1-year follow-up. Cytotherapy *11*, 18–25.

DeFreitas, M.F., Yoshida, C.K., Frazier, W.A., Mendrick, D.L., Kypta, R.M., and Reichard, L.F. (1995). Identification of integrin α3β1 as a neuronal thrombospondin receptor mediating neurite outgrowth. Neuron *15*, 333–343.

Deisseroth, K. (2015). Optogenetics: 10 years of microbial opsins in neuroscience. Nat. Neurosci. *18*, 1213–1225.

DeJesus-Hernandez, M., Mackenzie, I.R., Boeve, B.F., Boxer, A.L., Baker, M., Rutherford, N.J., Nicholson, A.M., Finch, N.A., Flynn, H., Adamson, J., et al. (2011). Expanded GGGGCC hexanucleotide repeat in noncoding region of C9ORF72 causes chromosome 9p-linked FTD and ALS. Neuron *72*, 245–256.

Dekkers, J., Becker, D.L., Cook, J.E., and Navarrete, R. (1994). Early postnatal changes in the somatodendritic morphology of ankle flexor motoneurons in the rat. Eur. J. Neurosci. *6*, 87–97.

Delaney, C.L., Brenner, M., and Messing, A. (1996). Conditional ablation of cerebellar astrocytes in postnatal transgenic mice. J. Neurosci. *16*, 6908–6918.

Deng, H.-X., Chen, W., Hong, S.-T., Boycott, K.M., Gorrie, G.H., Siddique, N., Yang, Y., Fecto,

F., Shi, Y., Zhai, H., et al. (2011). Mutations in UBQLN2 cause dominant X-linked juvenile and adult-onset ALS and ALS/dementia. Nature *477*, 211–215.

Denny-Brown, D., and Pennybacker, J.B. (1938). Fibrillation and fasciculation in voluntary muscle. Brain *61*, 311–312.

Deshpande, D.M., Kim, Y.-S., Martinez, T., Carmen, J., Dike, S., Shats, I., Rubin, L.L., Drummond, J., Krishnan, C., Hoke, A., et al. (2006). Recovery from paralysis in adult rats using embryonic stem cells. Ann. Neurol. *60*, 32–44.

DiPALS Writing Committee, DiPALS Study Group Collaborators, McDermott, C.J., Bradburn, M.J., Maguire, C., Cooper, C.L., Baird, W.O., Baxter, S.K., Bourke, S.C., Imam, I., et al. (2015). Safety and efficacy of diaphragm pacing in patients with respiratory insufficiency due to amyotrophic lateral sclerosis (DiPALS): a multicentre, open-label, randomised controlled trial. Lancet. Neurol. *14*, 883–892.

Djukic, B., Casper, K.B., Philpot, B.D., Chin, L.-S., and McCarthy, K.D. (2007). Conditional knock-out of Kir4.1 leads to glial membrane depolarization, inhibition of potassium and glutamate uptake, and enhanced short-term synaptic potentiation. J. Neurosci. *27*, 11354–11365.

Doble, A. (1996). The pharmacology and mechanism of action of riluzole. Neurology *47*, 233S-241S.

Donne, J. (1624). Meditation XVII. In Devotions Upon Emergent Occasions, (The Stationers' Company), pp. 31–32.

Donnelly, C.J., Zhang, P.-W., Pham, J.T., Haeusler, A.R., Heusler, A.R., Mistry, N.A., Vidensky, S., Daley, E.L., Poth, E.M., Hoover, B., et al. (2013). RNA toxicity from the ALS/FTD C9ORF72 expansion is mitigated by antisense intervention. Neuron *80*, 415–428.

Dorst, J., and Ludolph, A.C. (2019). Non-invasive ventilation in amyotrophic lateral sclerosis. Ther. Adv. Neurol. Disord. *12*, 1756286419857040.

Dorst, J., Dupuis, L., Petri, S., Kollewe, K., Abdulla, S., Wolf, J., Weber, M., Czell, D., Burkhardt, C., Hanisch, F., et al. (2015). Percutaneous endoscopic gastrostomy in amyotrophic lateral sclerosis: a prospective observational study. J. Neurol. *262*, 849–858.

Dougherty, K.J., and Ha, N.T. (2019). The rhythm section: an update on spinal interneurons setting the beat for mammalian locomotion. Curr. Opin. Physiol. *8*, 84–93.

Duma, C., Kopyov, O., Kopyov, A., Berman, M., Lander, E., Elam, M., Arata, M., Weiland, D., Cannell, R., Caraway, C., et al. (2019). Human intracerebroventricular (ICV) injection of autologous, non-engineered, adipose-derived stromal vascular fraction (ADSVF) for neurodegenerative disorders: results of a 3-year phase 1 study of 113 injections in 31 patients. Mol. Biol. Rep. *46*, 5257–5272.

East, E., Golding, J.P., and Phillips, J.B. (2009). A versatile 3D culture model facilitates monitoring of astrocytes undergoing reactive gliosis. J. Tissue Eng. Regen. Med. *3*, 634–646.

Eccles, J.C., Fatt, P., and Koketsu, K. (1954). Cholinergic and inhibitory synapses in a pathway from motor-axon collaterals to motoneurones. J. Physiol. *126*, 524–562.

Eccles, J.C., Eccles, R.M., and Magni, F. (1960). Monosynaptic excitatory action on motoneurones regenerated to antagonistic muscles. J. Physiol. *154*, 68–88.

Edaravone (MCI-186) ALS 16 study group (2017). A post-hoc subgroup analysis of outcomes in the first phase III clinical study of edaravone (MCI-186) in amyotrophic lateral sclerosis. Amyotroph. Lateral Scler. Front. Degener. *18*, 11–19.

Ederle, H., and Dormann, D. (2017). TDP-43 and FUS *en route* from the nucleus to the cytoplasm. FEBS Lett. *591*, 1489–1507.

Elden, A.C., Kim, H.-J., Hart, M.P., Chen-Plotkin, A.S., Johnson, B.S., Fang, X., Armakola, M., Geser, F., Greene, R., Lu, M.M., et al. (2010). Ataxin-2 intermediate-length polyglutamine expansions are associated with increased risk for ALS. Nature *466*, 1069–1075.

Enoka, R.M., and Duchateau, J. (2017). Rate Coding and the Control of Muscle Force. Cold Spring Harb. Perspect. Med. *7*.

Fecto, F., Yan, J., Vemula, S.P., Liu, E., Yang, Y., Chen, W., Zheng, J.G., Shi, Y., Siddique, N., Arrat, H., et al. (2011). SQSTM1 mutations in familial and sporadic amyotrophic lateral sclerosis. Arch. Neurol. *68*, 1440.

Feldman, E.L., Boulis, N.M., Hur, J., Johe, K., Rutkove, S.B., Federici, T., Polak, M., Bordeau, J., Sakowski, S.A., and Glass, J.D. (2014). Intraspinal neural stem cell transplantation in amyotrophic lateral sclerosis: Phase 1 trial outcomes. Ann. Neurol. *75*, 363–373.

Felix, L., and Zytnicki, D. (2015). Is hyperexcitability really guilty in amyotrophic lateral sclerosis? NEURAL Regen. Res. *10*.

Ferrari, R., Kapogiannis, D., Huey, E.D., and Momeni, P. (2011). FTD and ALS: a tale of two diseases. Curr. Alzheimer Res. *8*, 273–294.

Fogarty, M.J., Kanjhan, R., Bellingham, M.C., and Noakes, P.G. (2016). Glycinergic neurotransmission: a potent regulator of embryonic motor neuron dendritic morphology and synaptic plasticity. J. Neurosci. *36*, 80–87.

Forostyak, S., and Sykova, E. (2017). Neuroprotective potential of cell-based therapies in ALS: from bench to bedside. Front. Neurosci. *11*, 591.

Forostyak, S., Homola, A., Turnovcova, K., Svitil, P., Jendelova, P., and Sykova, E. (2014). Intrathecal delivery of mesenchymal stromal cells protects the structure of altered perineuronal nets in SOD1 rats and amends the course of ALS. Stem Cells *32*, 3163–3172.

Freischmidt, A., Wieland, T., Richter, B., Ruf, W., Schaeffer, V., Müller, K., Marroquin, N., Nordin, F., Hübers, A., Weydt, P., et al. (2015). Haploinsufficiency of TBK1 causes familial ALS and fronto-temporal dementia. Nat. Neurosci. *18*, 631–636.

Friese, A., Kaltschmidt, J.A., Ladle, D.R., Sigrist, M., Jessell, T.M., and Arber, S. (2009). Gamma and alpha motor neurons distinguished by expression of transcription factor Err3. Proc. Natl. Acad. Sci. U. S. A. *106*, 13588–13593.

Fukunishi, Y., Nagase, Y., Yoshida, A., Moritani, M., Honma, S., Hirose, Y., and Shigenaga, Y. (1999). Quantitative analysis of the dendritic architectures of cat hypoglossal motoneurons stained intracellularly with horseradish peroxidase. J. Comp. Neurol *405*, 345–358.

Gan, L.S., Ravid, E.N., Kowalczewski, J., Gauthier, M., Olson, J., Morhart, M., and Prochazka, A. (2011). First permanent human implant of the Stimulus Router System, a novel neuroprosthesis: preliminary testing of a polarity reversing stimulation technique. Conf. Proc. ... Annu. Int. Conf. IEEE Eng. Med. Biol. Soc. IEEE Eng. Med. Biol. Soc. Annu. Conf. *2011*, 3051–3054.

Gan, L.S., Ravid, E., Kowalczewski, J.A., Olson, J.L., Morhart, M., and Prochazka, A. (2012). First permanent implant of nerve stimulation leads activated by surface electrodes, enabling hand grasp and release: the stimulus router neuroprosthesis. Neurorehabil. Neural Repair *26*, 335–343.

Gao, B.-X., and Ziskind-Conhaim, L. (1998). Development of ionic currents underlying

changes in action potential waveforms in rat spinal motoneurons.

Garbuzova-Davis, S., Sanberg, C.D., Kuzmin-Nichols, N., Willing, A.E., Gemma, C., Bickford, P.C., Miller, C., Rossi, R., and Sanberg, P.R. (2008). Human umbilical cord blood treatment in a mouse model of ALS: optimization of cell dose. PLoS One *3*, e2494.

García, O., and Massieu, L. (2003). Glutamate uptake inhibitor L-trans-pyrrolidine 2,4-dicarboxylate becomes neurotoxic in the presence of subthreshold concentrations of mitochondrial toxin 3-nitropropionate: involvement of mitochondrial reducing activity and ATP production. J. Neurosci. Res. *74*, 956–966.

Gautam, M., Jara, J.H., Kocak, N., Rylaarsdam, L.E., Kim, K.D., Bigio, E.H., and Hande Özdinler, P. (2019). Mitochondria, ER, and nuclear membrane defects reveal early mechanisms for upper motor neuron vulnerability with respect to TDP-43 pathology. Acta Neuropathol. *137*, 47–69.

Gazula, V.-R., Roberts, M., Luzzio, C., Jawad, A.F., and Kalb, R.G. (2004). Effects of limb exercise after spinal cord injury on motor neuron dendrite structure. J. Comp. Neurol. *476*, 130–145.

Geijo-Barrientos, E., Pastore-Olmedo, C., De Mingo, P., Blanquer, M., Gómez Espuch, J., Iniesta, F., Iniesta, N.G., García-Hernández, A., Martín-Estefanía, C., Barrios, L., et al. (2020). Intramuscular injection of bone marrow stem cells in amyotrophic lateral sclerosis patients: a randomized clinical trial. Front. Neurosci. *14*, 195.

Gendron, T.F., Bieniek, K.F., Zhang, Y.-J., Jansen-West, K., Ash, P.E.A., Caulfield, T., Daughrity, L., Dunmore, J.H., Castanedes-Casey, M., Chew, J., et al. (2013). Antisense transcripts of the expanded C9ORF72 hexanucleotide repeat form nuclear RNA foci and undergo repeat-associated non-ATG translation in c9FTD/ALS. Acta Neuropathol. *126*, 829–844.

GenSight Biologics (2019). GenSight Biologics announces positive Data Safety Monitoring Board review and continuation of PIONEER Phase I/II clinical trial of GS030 combining gene therapy and Optogenetics for the treatment of Retinitis Pigmentosa.

Gezelius, H., Wallén-Mackenzie, Å., Enjin, A., Lagerström, M., and Kullander, K. (2006). Role of glutamate in locomotor rhythm generating neuronal circuitry. J. Physiol. *100*, 297–303.

Gibbs, K.L., Kalmar, B., Rhymes, E.R., Fellows, A.D., Ahmed, M., Whiting, P., Davies, C.H., Greensmith, L., and Schiavo, G. (2018). Inhibiting p38 MAPK alpha rescues axonal retrograde transport defects in a mouse model of ALS. Cell Death Dis. *9*, 596.

Gijselinck, I., Van Langenhove, T., van der Zee, J., Sleegers, K., Philtjens, S., Kleinberger, G., Janssens, J., Bettens, K., Van Cauwenberghe, C., Pereson, S., et al. (2012). A C9orf72 promoter repeat expansion in a Flanders-Belgian cohort with disorders of the frontotemporal lobar degeneration-amyotrophic lateral sclerosis spectrum: a gene identification study. Lancet Neurol. *11*, 54–65.

Gill, C., Phelan, J.P., Hatzipetros, T., Kidd, J.D., Tassinari, V.R., Levine, B., Wang, M.Z., Moreno, A., Thompson, K., Maier, M., et al. (2019). SOD1-positive aggregate accumulation in the CNS predicts slower disease progression and increased longevity in a mutant SOD1 mouse model of ALS. Sci. Rep. *9*, 6724.

Giordana, M.T., Ferrero, P., Grifoni, S., Pellerino, A., Naldi, A., and Montuschi, A. (2011). Dementia and cognitive impairment in amyotrophic lateral sclerosis: a review. Neurol. Sci. *32*, 9–16.

Gizzi, M., DiRocco, A., Sivak, M., and Cohen, B. (1992). Ocular motor function in motor neuron

disease. Neurology *42*, 1037–1046.

Glass, J., Hertzberg, V., Boulis, N., Riley, J., Federici, T., Polak, M., Bordeau, J., Fournier, C., Johe, K., Hazel, T., et al. (2016). Transplantation of spinal cord-derived neural stem cells for ALS: analysis of phase 1 and 2 trials. Neurology *87*.

Glass, J.D., Boulis, N.M., Johe, K., Rutkove, S.B., Federici, T., Polak, M., Kelly, C., and Feldman, E.L. (2012). Lumbar intraspinal injection of neural stem cells in patients with amyotrophic lateral sclerosis: results of a phase I trial in 12 patients. Stem Cells *30*, 1144–1151.

Golbs, A., Nimmervoll, B., Sun, J.-J., Sava, I.E., and Luhmann, H.J. (2011). Control of programmed cell death by distinct electrical activity patterns. Cereb. Cortex *21*, 1192–1202.

Gonzalez-Islas, C., and Wenner, P. (2006). Spontaneous network activity in the embryonic spinal cord regulates AMPAergic and GABAergic synaptic strength. Neuron *49*, 563–575.

Goodman, C.S., and Shatz, C.J. (1993). Developmental mechanisms that generate precise patterns of neuronal connectivity. Cell *72*, 77–98.

Gorassini, M., Eken, T., Bennett, D.J., Kiehn, O., and Hultborn, H. (2000). Activity of hindlimb motor units during locomotion in the conscious rat. J. Neurophysiol. *83*, 2002–2011.

Gordon, T. (2016). Electrical stimulation to enhance axon regeneration after peripheral nerve injuries in animal models and humans. Neurotherapeutics *13*, 295–310.

Gordon, P.H., Cheng, B., Katz, I.B., Pinto, M., Hays, A.P., Mitsumoto, H., and Rowland, L.P. (2006). The natural history of primary lateral sclerosis. Neurology *66*, 647–653.

Gordon, P.H., Delgadillo, D., Piquard, A., Bruneteau, G., Pradat, P.-F., Salachas, F., Payan, C., Meininger, V., and Lacomblez, L. (2011). The range and clinical impact of cognitive impairment in French patients with ALS: A cross-sectional study of neuropsychological test performance. Amyotroph. Lateral Scler. *12*, 372–378.

Gotoh, H., Ono, K., Nomura, T., Takebayashi, H., Harada, H., Nakamura, H., and Ikenaka, K. (2012). Nkx2.2+ progenitors generate somatic motoneurons in the chick spinal cord. PLoS One *7*, e51581.

Gould, T.W., Yonemura, S., Oppenheim, R.W., Ohmori, S., and Enomoto, H. (2008). The neurotrophic effects of glial cell line-derived neurotrophic factor on spinal motoneurons are restricted to fusimotor subtypes. J. Neurosci. *28*, 2131.

Gourine, A. V, Kasymov, V., Marina, N., Tang, F., Figueiredo, M.F., Lane, S., Teschemacher, A.G., Spyer, K.M., Deisseroth, K., and Kasparov, S. (2010). Astrocytes control breathing through pH-dependent release of ATP. Science *329*, 571–575.

Goutman, S.A., Brown, M.B., Glass, J.D., Boulis, N.M., Johe, K., Hazel, T., Cudkowicz, M., Atassi, N., Borges, L., Patil, P.G., et al. (2018). Long-term Phase 1/2 intraspinal stem cell transplantation outcomes in ALS. Ann. Clin. Transl. Neurol. *5*, 730–740.

Goutman, S.A., Savelieff, M.G., Sakowski, S.A., and Feldman, E.L. (2019). Stem cell treatments for amyotrophic lateral sclerosis: a critical overview of early phase trials. Expert Opin. Investig. Drugs *28*, 525–543.

Grad, L.I., Rouleau, G.A., Ravits, J., and Cashman, N.R. (2017). Clinical spectrum of Amyotrophic Lateral Sclerosis (ALS). Cold Spring Harb. Perspect. Med. *7*.

Granit, R., Pascoe, J.E., and Steg, G. (1957). The behaviour of tonic α and β motoneurones during stimulation of recurrent collaterals. J. Physiol. *138*, 381–400.

Greenway, M.J., Alexander, M.D., Ennis, S., Traynor, B.J., Corr, B., Frost, E., Green, A., and Hardiman, O. (2004). A novel candidate region for ALS on chromosome 14q11.2. Neurology *63*, 1936–1938.

Greenway, M.J., Andersen, P.M., Russ, C., Ennis, S., Cashman, S., Donaghy, C., Patterson, V., Swingler, R., Kieran, D., Prehn, J., et al. (2006). ANG mutations segregate with familial and “sporadic” amyotrophic lateral sclerosis. Nat. Genet. *38*, 411–413.

Grienberger, C., and Konnerth, A. (2012). Imaging Calcium in Neurons. Neuron *73*, 862–885.

Grieshammer, U., Lewandoski, M., Prevette, D., Oppenheim, R.W., and Martin, G.R. (1998). Muscle-specific cell ablation conditional upon cre-mediated DNA recombination in transgenic mice leads to massive spinal and cranial motoneuron loss. Dev. Biol. *197*, 234–247.

Guttenplan, K.A., Stafford, B.K., El-Danaf, R.N., Adler, D.I., Münch, A.E., Weigel, M.K., Huberman, A.D., and Liddelow, S.A. (2020). Neurotoxic reactive astrocytes drive neuronal death after retinal injury. Cell Rep. *31*, 107776.

Haase, G., Dessaud, E., Garcès, A., de Bovis, B., Birling, M.-C., Filippi, P., Schmalbruch, H., Arber, S., and DeLapeyrière, O. (2002). GDNF acts through PEA3 to regulate cell body positioning and muscle innervation of specific motor neuron pools. Neuron *35*, 893–905.

Haim, L. Ben, and Rowitch, D.H. (2016). Functional diversity of astrocytes in neural circuit regulation. Nat. Rev. Neurosci. *18*, 31–41.

Hamad, M.I.K., Krause, M., and Wahle, P. (2015). Improving AM ester calcium dye loading efficiency. J. Neurosci. Methods *240*, 48–60.

Han, X., and Boyden, E.S. (2007). Multiple-color optical activation, silencing, and desynchronization of neural activity, with single-spike temporal resolution. PLoS One *2*, e299.

Han, X., Qian, X., Bernstein, J.G., Zhou, H.-H., Franzesi, G.T., Stern, P., Bronson, R.T., Graybiel, A.M., Desimone, R., and Boyden, E.S. (2009). Millisecond-timescale optical control of neural dynamics in the nonhuman primate brain. Neuron *62*, 191–198.

Han, X., Chen, M., Wang, F., Windrem, M., Wang, S., Shanz, S., Xu, Q., Oberheim, N.A., Bekar, L., Betstadt, S., et al. (2013). Forebrain engraftment by human glial progenitor cells enhances synaptic plasticity and learning in adult mice. Cell Stem Cell *12*, 342–353.

Hancock, K.M., Craig, A.R., Dickson, H.G., Chang, E., and Martin, J. (1993). Anxiety and depression over the first year of spinal cord injury: a longitudinal study. Spinal Cord *31*, 349–357.

Hanson, M.G., and Landmesser, L.T. (2003). Characterization of the circuits that generate spontaneous episodes of activity in the early embryonic mouse spinal cord. J. Neurosci. *23*, 587–600.

Hanson, M.G., Milner, L.D., and Landmesser, L.T. (2008). Spontaneous rhythmic activity in early chick spinal cord influences distinct motor axon pathfinding decisions. Brain Res. Rev. *57*, 77–85.

Hayashi, M.K., Tang, C., Verpelli, C., Narayanan, R., Stearns, M.H., Xu, R.-M., Li, H., Sala, C., and Hayashi, Y. (2009). The postsynaptic density proteins Homer and Shank form a polymeric network structure. Cell *137*, 159–171.

Heads, T., Pollock, M., Robertson, A., Sutherland, W.H.E., and Allpress, S. (1991). Sensory nerve pathology in amyotrophic lateral sclerosis*.

Heck, N., Golbs, A., Riedemann, T., Sun, J.-J., Lessmann, V., and Luhmann, H.J. (2008).

Activity-dependent regulation of neuronal apoptosis in neonatal mouse cerebral cortex. Cereb. Cortex *18*, 1335–1349.

Henderson, C.E., Bloch-Gallego, E., and Camu, W. (1995). Purified embryonic motoneurons. In Nerve Cell Cultures: A Practical Approach, J. Cohen, and G. Wilkin, eds. (Oxford University, London), p.

Henneman, E. (1957). Relation between size of neurons and their susceptibility to discharge. Science (80-.). *126*, 1345–1347.

Herman, M.A., and Jahr, C.E. (2007). Extracellular glutamate concentration in hippocampal slice. J. Neurosci. *27*, 9736–9741.

Hertz, L., and Chen, Y. (2017). Integration between glycolysis and glutamate-glutamine cycle flux may explain preferential glycolytic increase during brain activation, requiring glutamate. Front. Integr. Neurosci. *11*, 18.

Herzog, E., Landry, M., Buhler, E., Bouali-Benazzouz, R., Legay, C., Henderson, C.E., Nagy, F., Dreyfus, P., Giros, B., and El Mestikawy, S. (2004). Expression of vesicular glutamate transporters, VGLUT1 and VGLUT2, in cholinergic spinal motoneurons. Eur. J. Neurosci. *20*, 1752–1760.

Herzog, E.L., Chai, L., and Krause, D.S. (2003). Plasticity of marrow-derived stem cells. Blood *102*, 3483–3493.

Hetz, C., Thielen, P., Matus, S., Nassif, M., Court, F., Kiffin, R., Martinez, G., Cuervo, A.M., Brown, R.H., and Glimcher, L.H. (2009). XBP-1 deficiency in the nervous system protects against amyotrophic lateral sclerosis by increasing autophagy. Genes Dev. *23*, 2294–2306.

Hill, E., Nagel, D., Parri, R., and Coleman, M. (2016). Stem cell-derived astrocytes: are they physiologically credible? J. Physiol. *594*, 6595–6606.

Hirano, A., Nakano, I., Kurland, L.T., Mulder, D.W., Holley, P.W., and Saccomando, G. (1984). Fine structural study of neurofibrillary changes in a family with amyotrophic lateral sclerosis. J. Neuropathol. Exp. Neurol. *43*, 471–480.

Hirose, T., Kimura, F., Tani, H., Ota, S., Tsukahara, A., Sano, E., Shigekiyo, T., Nakamura, Y., Kakiuchi, K., Motoki, M., et al. (2018). Clinical characteristics of long-term survival with noninvasive ventilation and factors affecting the transition to invasive ventilation in amyotrophic lateral sclerosis. Muscle Nerve *58*, 770–776.

Hoang, P.T., Chalif, J.I., Bikoff, J.B., Jessell, T.M., Mentis, G.Z., and Wichterle, H. (2018). Subtype diversification and synaptic specificity of stem cell-derived spinal interneurons. Neuron *100*, 135-149.e7.

Hochstim, C., Deneen, B., Lukaszewicz, A., Zhou, Q., and Anderson, D.J. (2008). Identification of positionally distinct astrocyte subtypes whose identities are specified by a homeodomain code. Cell *133*, 510–522.

Hockberger, P.E., Skimina, T.A., Centonze, V.E., Lavin, C., Chu, S., Dadras, S., Reddy, J.K., and White, J.G. (1999). Activation of flavin-containing oxidases underlies light-induced production of H2O2 in mammalian cells. Proc. Natl. Acad. Sci. U. S. A. *96*, 6255–6260.

Van Hoecke, A., Schoonaert, L., Lemmens, R., Timmers, M., Staats, K.A., Laird, A.S., Peeters, E., Philips, T., Goris, A., Dubois, B., et al. (2012). EPHA4 is a disease modifier of amyotrophic lateral sclerosis in animal models and in humans. Nat. Med. *18*, 1418–1422.

Hosoya, T., Takizawa, K., Nitta, K., and Hotta, Y. (1995). glial cells missing: a binary switch between neuronal and glial determination in Drosophila. Cell *82*, 1025–1036.

Hu, W., Li, Q., Li, B., Ma, K., Zhang, C., and Fu, X. (2020). Optogenetics sheds new light on tissue engineering and regenerative medicine. Biomaterials *227*, 119546.

Huebner, E.A., and Strittmatter, S.M. (2009). Axon regeneration in the peripheral and central nervous systems. Results Probl. Cell Differ. *48*, 339–351.

Hyung, S., Yoon Lee, B., Park, J.-C., Kim, J., Hur, E.-M., and Francis Suh, J.-K. (2015). Coculture of primary motor neurons and Schwann cells as a model for in vitro myelination. Sci. Rep. *5*, 15122.

Ibata, K., Sun, Q., and Turrigiano, G.G. (2008). Rapid synaptic scaling induced by changes in postsynaptic firing. Neuron *57*, 819–826.

Ichinose, T., and Miyata, Y. (1998). Recurrent excitation of motoneurons in the isolated spinal cord of newborn rats detected by whole-cell recording. Neurosci. Res. *31*, 179–187.

Ilieva, E. V., Ayala, V., Jove, M., Dalfo, E., Cacabelos, D., Povedano, M., Bellmunt, M.J., Ferrer, I., Pamplona, R., and Portero-Otin, M. (2007). Oxidative and endoplasmic reticulum stress interplay in sporadic amyotrophic lateral sclerosis. Brain *130*, 3111–3123.

Inglis, F.M., Furia, F., Zuckerman, K.E., Strittmatter, S.M., and Kalb, R.G. (1998). The role of nitric oxide and NMDA receptors in the development of motor neuron dendrites. J. Neurosci. *18*, 10493–10501.

Inglis, F.M., Crockett, R., Korada, S., Abraham, W.C., Hollmann, M., and Kalb, R.G. (2002). The AMPA receptor subunit GluR1 regulates dendritic architecture of motor neurons. J. Neurosci. *22*, 8042–8051.

Israel, M.A., Yuan, S.H., Bardy, C., Reyna, S.M., Mu, Y., Herrera, C., Hefferan, M.P., Van Gorp, S., Nazor, K.L., Boscolo, F.S., et al. (2012). Probing sporadic and familial Alzheimer's disease using induced pluripotent stem cells. Nature *482*, 216–220.

Jaiser, S.R., Mitra, D., Williams, T.L., and Baker, M.R. (2019). Mills' syndrome revisited. J. Neurol. *266*, 667–679.

Jarrar, W., Vauti, F., Arnold, H.-H., and Holz, A. (2015). Generation of a Nkx2.2Cre knock-in mouse line: Analysis of cell lineages in the central nervous system. Differentiation *89*, 70–76.

Jessell, T.M. (2000). Neuronal specification in the spinal cord: inductive signals and transcriptional codes. Nat. Rev. Genet. *1*, 20–29.

Johnson, J.O., Mandrioli, J., Benatar, M., Abramzon, Y., Van Deerlin, V.M., Trojanowski, J.Q., Gibbs, J.R., Brunetti, M., Gronka, S., Wuu, J., et al. (2010). Exome sequencing reveals VCP mutations as a cause of familial ALS. Neuron *68*, 857–864.

Johnson, J.O., Pioro, E.P., Boehringer, A., Chia, R., Feit, H., Renton, A.E., Pliner, H.A., Abramzon, Y., Marangi, G., Winborn, B.J., et al. (2014). Mutations in the Matrin 3 gene cause familial amyotrophic lateral sclerosis. Nat. Neurosci. *17*, 664–666.

Jones, C.L. (1979). The morphogenesis of the thigh of the mouse with special reference to tetrapod muscle homologies. J. Morphol. *162*, 275–309.

Jones, E. V, Bernardinelli, Y., Tse, Y.C., Chierzi, S., Wong, T.P., and Murai, K.K. (2011). Astrocytes control glutamate receptor levels at developing synapses through SPARC-beta-integrin interactions. J. Neurosci. *31*, 4154–4165.

Jose Sanz-Ezquerro, J., Pujades, C., Duester, G., Martin, B.L., Diez Del Corral, R., and Morales, A. V (2017). The multiple roles of FGF signaling in the developing spinal cord. Front. Cell Dev. Biol. | Www.Frontiersin.Org *1*, 58.

Jung, C., Higgins, C.M.J., and Xu, Z. (2002). Mitochondrial electron transport chain complex dysfunction in a transgenic mouse model for amyotrophic lateral sclerosis. J. Neurochem. *83*, 535–545.

Kabashi, E., Valdmanis, P.N., Dion, P., Spiegelman, D., McConkey, B.J., Velde, C. Vande, Bouchard, J.-P., Lacomblez, L., Pochigaeva, K., Salachas, F., et al. (2008). TARDBP mutations in individuals with sporadic and familial amyotrophic lateral sclerosis. Nat. Genet. *40*, 572–574.

Kalb, R., and Hockfield, S. (1990a). Induction of a neuronal proteoglycan by the NMDA receptor in the developing spinal cord. Science (80-.). *250*, 294–296.

Kalb, R.G., and Hockfield, S. (1990b). Large diameter primary afferent input is required for expression of the cat-301 proteoglycan on the surface of motor neurons. Neuroscience *34*, 391–401.

Kalb, R.G., and Hockfield, S. (1992). Activity-dependent development of spinal cord motor neurons. Brain Res. Brain Res. Rev. *17*, 283–289.

Kalb, R.G., Lidow, M.S., Halsted, M.J., and Hockfield, S. (1992). N-methyl-D-aspartate receptors are transiently expressed in the developing spinal cord ventral horn. Proc. Natl. Acad. Sci. U. S. A. *89*, 8502–8506.

Kaminski, H.J., Richmonds, C.R., Kusner, L.L., and Mitsumoto, H. (2002). Differential susceptibility of the ocular motor system to disease. Ann. N. Y. Acad. Sci. *956*, 42–54.

Kang, S.H., Li, Y., Fukaya, M., Lorenzini, I., Cleveland, D.W., Ostrow, L.W., Rothstein, J.D., and Bergles, D.E. (2013). Degeneration and impaired regeneration of gray matter oligodendrocytes in amyotrophic lateral sclerosis. Nat. Neurosci. *16*, 571–579.

Kanjhan, R., Fogarty, M.J., Noakes, P.G., and Bellingham, M.C. (2016). Developmental changes in the morphology of mouse hypoglossal motor neurons. Brain Struct. Funct. *221*, 3755–3786.

Kanning, K.C., Kaplan, A., and Henderson, C.E. (2010). Motor neuron diversity in development and disease. Annu. Rev. Neurosci. *33*, 409–440.

Karumbayaram, S., Kelly, T.K., Paucar, A.A., Roe, A.J.T., Umbach, J.A., Charles, A., Goldman, S.A., Kornblum, H.I., and Wiedau-Pazos, M. (2009). Human embryonic stem cell-derived motor neurons expressing SOD1 mutants exhibit typical signs of motor neuron degeneration linked to ALS. Dis. Model. Mech. *2*, 189–195.

Karussis, D.D., Karageorgiou, D.C., Vaknin-Dembinsky, D.A., Gowda-Kurkalli, D.B., Gomori, D.J.M., Kassis, M.I., Bulte, D.J.W.M., Petrou, D.P., Ben-Hur, D.T., Abramsky, D.O., et al. (2010). Safety and immunological effects of mesenchymal stem cell transplantation in patients with multiple sclerosis and amyotrophic lateral sclerosis. Arch. Neurol. *67*, 1187.

Kastanenka, K. V., and Landmesser, L.T. (2010). In-vivo activation of channelrhodopsin-2 reveals that normal patterns of spontaneous activity are required for motoneuron guidance and maintenance of guidance molecules. J. Neurosci. *30*, 10575–10585.

Kastanenka, K. V., and Landmesser, L.T. (2013). Optogenetic-mediated increases in in vivo spontaneous activity disrupt pool-specific but not dorsal-ventral motoneuron pathfinding. Proc. Natl. Acad. Sci. U. S. A. *110*, 17528–17533.

Kato, S., Shimoda, M., Watanabe, Y., Nakashima, K., Takahashi, K., and Ohama, E. (1996). Familial amyotrophic lateral sclerosis with a two base pair deletion in superoxide dismutase 1: gene multisystem degeneration with intracytoplasmic hyaline inclusions in astrocytes. J.

Neuropathol. Exp. Neurol. *55*, 1089–1101.

Kato, S., Sumi-Akamaru, H., Fujimura, H., Sakoda, S., Kato, M., Hirano, A., Takikawa, M., and Ohama, E. (2001). Copper chaperone for superoxide dismutase co-aggregates with superoxide dismutase 1 (SOD1) in neuronal Lewy body-like hyaline inclusions: an immunohistochemical study on familial amyotrophic lateral sclerosis with SOD1 gene mutation. Acta Neuropathol. *102*, 233–238.

Kayama, T., Suzuki, I., Odawara, A., Sasaki, T., and Ikegaya, Y. (2018). Temporally coordinated spiking activity of human induced pluripotent stem cell-derived neurons co-cultured with astrocytes. Biochem. Biophys. Res. Commun. *495*, 1028–1033.

Kelley, K.W., Ben Haim, L., Schirmer, L., Tyzack, G.E., Tolman, M., Miller, J.G., Tsai, H.-H., Chang, S.M., Molofsky, A. V, Yang, Y., et al. (2018). Kir4.1-dependent astrocyte-fast motor neuron interactions are required for peak strength. Neuron *98*, 306-319.e7.

Kikuchi, H., Almer, G., Yamashita, S., Guégan, C., Nagai, M., Xu, Z., Sosunov, A.A., McKhann, G.M., Przedborski, S., and Przedborski, S. (2006). Spinal cord endoplasmic reticulum stress associated with a microsomal accumulation of mutant superoxide dismutase-1 in an ALS model. Proc. Natl. Acad. Sci. U. S. A. *103*, 6025–6030.

Kim, H., Kim, H.Y., Choi, M.R., Hwang, S., Nam, K.-H., Kim, H.-C., Han, J.S., Kim, K.S., Yoon, H.S., and Kim, S.H. (2010). Dose-dependent efficacy of ALS-human mesenchymal stem cells transplantation into cisterna magna in SOD1-G93A ALS mice. Neurosci. Lett. *468*, 190–194.

Kim, H.J., Kim, N.C., Wang, Y.-D., Scarborough, E.A., Moore, J., Diaz, Z., MacLea, K.S., Freibaum, B., Li, S., Molliex, A., et al. (2013). Mutations in prion-like domains in hnRNPA2B1 and hnRNPA1 cause multisystem proteinopathy and ALS. Nature *495*, 467–473.

Kim, W.-K., Liu, X., Sandner, J., Pasmantier, M., Andrews, J., Rowland, L.P., and Mitsumoto, H. (2009). Study of 962 patients indicates progressive muscular atrophy is a form of ALS. Neurology *73*, 1686–1692.

King, A.E., Woodhouse, A., Kirkcaldie, M.T.K., and Vickers, J.C. (2016). Excitotoxicity in ALS: Overstimulation, or overreaction? Exp. Neurol. *275*, 162–171.

Kirkby, L.A., Sack, G.S., Firl, A., and Feller, M.B.B. (2013). A role for correlated spontaneous activity in the assembly of neural circuits. Neuron *80*, 1129–1144.

Kishore, S., and Fetcho, J.R. (2013). Homeostatic regulation of dendritic dynamics in a motor map in vivo. Nat. Commun. *4*, 2086.

Kleinlogel, S., Vogl, C., Jeschke, M., Neef, J., and Moser, T. (2020). Emerging approaches for restoration of hearing and vision. Physiol. Rev. physrev.00035.2019.

Kleopa, K.A., Sherman, M., Neal, B., Romano, G.J., and Heiman-Patterson, T. (1999). Bipap improves survival and rate of pulmonary function decline in patients with ALS. J. Neurol. Sci. *164*, 82–88.

Koester, J., and Siegelbaum, S.A. (2013). 8 Local Signaling: Passive Electrical Properties of the Neuron. In Principles of Neural Science, E.R. Kandel, J.H. Schwartz, T.M. Jessell, S. Siegelbaum, A.J. Hudspeth, and S. Mack, eds. (McGraw-Hill Education / Medical), pp. 140–149.

Kong, J., and Xu, Z. (1998). Massive mitochondrial degeneration in motor neurons triggers the onset of amyotrophic lateral sclerosis in mice expressing a mutant SOD1. J. Neurosci. *18*, 3241–3250.

Koutoumanou, E. (UCL G.O.S.I. of C.H., Wade, A. (UCL G.O.S.I. of C.H., and Lee, S. (UCL

G.O.S.I. of C.H. (2018). Introduction to dealing with missing data v5. UCL Cent. Appl. Stat. Courses 1–3.

Krutki, P., Hałuszka, A., Mrówczyński, W., Gardiner, P.F., and Celichowski, J. (2015). Adaptations of motoneuron properties to chronic compensatory muscle overload. J. Neurophysiol. *113*, 2769–2777.

Kucukdereli, H., Allen, N.J., Lee, A.T., Feng, A., Ozlu, M.I., Conatser, L.M., Chakraborty, C., Workman, G., Weaver, M., Sage, E.H., et al. (2011). Control of excitatory CNS synaptogenesis by astrocyte-secreted proteins Hevin and SPARC. Proc. Natl. Acad. Sci. U. S. A. *108*, E440-9.

Kullander, K., Butt, S.J.B., Lebret, J.M., Lundfald, L., Restrepo, C.E., Rydström, A., Klein, R., and Kiehn, O. (2003). Role of EphA4 and EphrinB3 in local neuronal circuits that control walking. Science (80-.). *299*, 1889–1892.

Kwiatkowski, T.J., Bosco, D.A., Leclerc, A.L., Tamrazian, E., Vanderburg, C.R., Russ, C., Davis, A., Gilchrist, J., Kasarskis, E.J., Munsat, T., et al. (2009). Mutations in the FUS/TLS gene on chromosome 16 cause familial amyotrophic lateral sclerosis. Science *323*, 1205–1208.

Lacomblez, L., Bensimon, G., Meininger, V., Leigh, P.., and Guillet, P. (1996). Dose-ranging study of riluzole in amyotrophic lateral sclerosis. Lancet *347*, 1425–1431.

Lagier-Tourenne, C., Baughn, M., Rigo, F., Sun, S., Liu, P., Li, H.-R., Jiang, J., Watt, A.T., Chun, S., Katz, M., et al. (2013). Targeted degradation of sense and antisense C9orf72 RNA foci as therapy for ALS and frontotemporal degeneration. Proc. Natl. Acad. Sci. U. S. A. *110*, E4530-9.

Lalancette-Hebert, M., Sharma, A., Lyashchenko, A.K., and Shneider, N.A. (2016). Gamma motor neurons survive and exacerbate alpha motor neuron degeneration in ALS. Proc. Natl. Acad. Sci. U. S. A. *113*, E8316–E8325.

Lamotte d'Incamps, B., Bhumbra, G.S., Foster, J.D., Beato, M., and Ascher, P. (2017). Segregation of glutamatergic and cholinergic transmission at the mixed motoneuron Renshaw cell synapse. Sci. Rep. *7*, 4037.

Lance-Jones, C. (1982). Motoneuron cell death in the developing lumbar spinal cord of the mouse. Dev. Brain Res. *4*, 473–479.

Lander, A.D., Fujii, D.K., and Reichardt, L.F. (1985). Laminin is associated with the "neurite outgrowth-promoting factors" found in conditioned media. Proc. Natl. Acad. Sci. U. S. A. *82*, 2183–2187.

Landgraf, M., Jeffrey, V., Fujioka, M., Jaynes, J.B., and Bate, M. (2003). Embryonic origins of a motor system: motor dendrites form a myotopic map in Drosophila. PLoS Biol. *1*, E41.

Landry, M., Bouali-Benazzouz, R., El Mestikawy, S., Ravassard, P., and Nagy, F. (2004). Expression of vesicular glutamate transporters in rat lumbar spinal cord, with a note on dorsal root ganglia. J. Comp. Neurol. *468*, 380–394.

Larkindale, J., Yang, W., Hogan, P.F., Simon, C.J., Zhang, Y., Jain, A., Habeeb-Louks, E.M., Kennedy, A., and Cwik, V.A. (2014). Cost of illness for neuromuscular diseases in the United States. Muscle Nerve *49*, 431–438.

Leigh, P.N., Anderton, B.H., Dodson, A., Gallo, J.M., Swash, M., and Power, D.M. (1988). Ubiquitin deposits in anterior horn cells in motor neurone disease. Neurosci. Lett. *93*, 197–203.

Lepore, A.C., Tolmie, C., O'Donnell, J., Wright, M.C., Dejea, C., Rauck, B., Hoke, A., Ignagni, A.R., Onders, R.P., and Maragakis, N.J. (2010). Peripheral hyperstimulation alters site of disease onset and course in SOD1 rats. Neurobiol. Dis. *39*, 252–264.

Leroy, F., Lamotte d'Incamps, B., Imhoff-Manuel, R.D., and Zytnicki, D. (2014). Early intrinsic hyperexcitability does not contribute to motoneuron degeneration in amyotrophic lateral sclerosis. Elife *3*.

Leroy, F., Lamotte d'Incamps, B., and Zytnicki, D. (2015). Potassium currents dynamically set the recruitment and firing properties of F-type motoneurons in neonatal mice. J. Neurophysiol. *114*, 1963–1973.

Leskelä, S., Huber, N., Rostalski, H., Natunen, T., Remes, A.M., Takalo, M., Hiltunen, M., and Haapasalo, A. (2019). C9orf72 proteins regulate autophagy and undergo autophagosomal or proteasomal degradation in a cell type-dependent manner. Cells *8*.

Li, H., and Harlow, M.L. (2014). Individual synaptic vesicles from the electroplaque of Torpedo californica, a classic cholinergic synapse, also contain transporters for glutamate and ATP. Physiol. Rep. *2*, e00206.

Li, K., Li, J., Zheng, J., and Qin, S. (2019). Reactive astrocytes in neurodegenerative diseases. Aging Dis. *10*, 664–675.

Li, W.-C., Soffe, S.R., Wolf, E., and Roberts, A. (2006). Persistent responses to brief stimuli: feedback excitation among brainstem neurons. J. Neurosci. *22*, 10580–10592.

Li, Y., Tzatzalos, E., Kwan, K.Y., Grumet, M., and Cai, L. (2016). Transcriptional regulation of Notch1 expression by Nkx6.1 in neural stem/progenitor cells during ventral spinal cord development. Sci. Rep. *6*, 38665.

Lin, J.Y., Knutsen, P.M., Muller, A., Kleinfeld, D., and Tsien, R.Y. (2013). ReaChR: a red-shifted variant of channelrhodopsin enables deep transcranial optogenetic excitation. Nat. Neurosci. *16*, 1499–1508.

Liu, J.-P., Laufer, E., and Jessell, T.M. (2001). Assigning the positional identity of spinal motor neurons: rostrocaudal patterning of Hox-c expression by FGFs, Gdf11, and retinoids.

Liu, Q., Shu, S., Wang, R.R., Liu, F., Cui, B., Guo, X.N., Lu, C.X., Li, X.G., Liu, M.S., Peng, B., et al. (2016). Whole-exome sequencing identifies a missense mutation in *hnRNPA1* in a family with flail arm ALS. Neurology *87*, 1763–1769.

Liu, T.T., Bannatyne, B.A., Jankowska, E., and Maxwell, D.J. (2009). Cholinergic terminals in the ventral horn of adult rat and cat: Evidence that glutamate is a cotransmitter at putative interneuron synapses but not at central synapses of motoneurons. Neuroscience *161*, 111–122.

Liu, Y., Grumbles, R.M., and Thomas, C.K. (2013). Electrical stimulation of embryonic neurons for 1 hour improves axon regeneration and the number of reinnervated muscles that function. J. Neuropathol. Exp. Neurol. *72*, 697–707.

Livet, J., Sigrist, M., Stroebel, S., De Paola, V., Price, S.R., Henderson, C.E., Jessell, T.M., and Arber, S. (2002). ETS gene Pea3 controls the central position and terminal arborization of specific motor neuron pools. Neuron *35*, 877–892.

Llewellyn, M.E., Thompson, K.R., Deisseroth, K., and Delp, S.L. (2010). Orderly recruitment of motor units under optical control in vivo. Nat. Med. *16*, 1161–1165.

Lobsiger, C.S., Boillee, S., McAlonis-Downes, M., Khan, A.M., Feltri, M.L., Yamanaka, K., and Cleveland, D.W. (2009). Schwann cells expressing dismutase active mutant SOD1

unexpectedly slow disease progression in ALS mice. Proc. Natl. Acad. Sci. U. S. A. *106*, 4465–4470.

Lock, J.T., Parker, I., and Smith, I.F. (2015). A comparison of fluorescent Ca2+ indicators for imaging local Ca2+ signals in cultured cells. Cell Calcium *58*, 638.

London, M., and Häusser, M. (2005). Dendritic computation. Annu. Rev. Neurosci. *28*, 503–532.

López-González, R., Kunckles, P., and Velasco, I. (2009). Transient recovery in a rat model of familial amyotrophic lateral sclerosis after transplantation of motor neurons derived from mouse embryonic stem cells. Cell Transplant. *18*, 1171–1181.

López-Murcia, F.J., Terni, B., and Llobet, A. (2015). SPARC triggers a cell-autonomous program of synapse elimination. Proc. Natl. Acad. Sci. U. S. A. *112*, 13366–13371.

Lulé, D., Ludolph, A.C., and Kübler, A. (2018). Psychological morbidity in amyotrophic lateral sclerosis: Depression, anxiety, hopelessness (Oxford University Press).

Lund, J.P., and Dellow, P.G. (1971). The influence of interactive stimuli on rhythmical masticatory movements in rabbits. Arch. Oral Biol. *16*, 215–223.

Luo, S., Xu, H., Zuo, Y., Liu, X., and All, A.H. (2020). A review of functional electrical stimulation treatment in spinal cord injury. NeuroMolecular Med. 1–17.

Lyons, M.R., and West, A.E. (2011). Mechanisms of specificity in neuronal activity-regulated gene transcription. Prog. Neurobiol. *94*, 259–295.

Machado, C.B., Pluchon, P., Harley, P., Rigby, M., Gonzalez Sabater, V., Stevenson, D.C., Hynes, S., Lowe, A., Burrone, J., Viasnoff, V., et al. (2019). In Vitro Modelling of Nerve-Muscle Connectivity in a Compartmentalised Tissue Culture Device. Adv. Biosyst. *3*.

Magown, P., Brownstone, R.M., and Rafuse, V.F. (2016). Tumor prevention facilitates delayed transplant of stem cell-derived motoneurons. Ann. Clin. Transl. Neurol. n/a-n/a.

Magown, P., Rafuse, V.F., and Brownstone, R.M. (2017). Microcircuit formation following transplantation of mouse embryonic stem cell-derived neurons in peripheral nerve. J. Neurophysiol. *117*, 1683–1689.

Maimon, B.E., Diaz, M., Revol, E.C.M., Schneider, A.M., Leaker, B., Varela, C.E., Srinivasan, S., Weber, M.B., and Herr, H.M. (2018). Optogenetic peripheral nerve immunogenicity. Sci. Rep. *8*, 14076.

Mannen, T. (2000). Neuropathological findings of Onuf's nucleus and its significance. Neuropathology *20*, 30–33.

Maravall, M., Mainen, Z.F., Sabatini, B.L., and Svoboda, K. (2000). Estimating intracellular calcium concentrations and buffering without wavelength ratioing. Biophys. J. *78*, 2655–2667.

Marchetti, C., Tabak, J., Chub, N., O'Donovan, M.J., and Rinzel, J. (2005). Modeling spontaneous activity in the developing spinal cord using activity-dependent variations of intracellular chloride. J. Neurosci. *25*, 3601–3612.

Martel, J., Esposti, S.D., Boulanger-Scemama, E., Galluppi, F., Vernadal, E., Gray, D., Taiel, M., Bloun, L., and Sahel, J.A. (2020). Optogenetics in the clinic: PIONEER, a phase 1/2a gene therapy program for non-syndromic retinitis pigmentosa. ARVO Annu. Meet. Abstr. Investig. Ophthalmol. Vis. Sci. *61*, 4491–4491.

Martin-Caraballo, M., and Greer, J.J. (1999). Electrophysiological properties of rat phrenic

motoneurons during perinatal development. J. Neurophysiol. *81*.

Martin, G.R., and Evans, M.J. (1975). Differentiation of clonal lines of teratocarcinoma cells: formation of embryoid bodies in vitro. Proc. Natl. Acad. Sci. U. S. A. *72*, 1441–1445.

Maruyama, H., Morino, H., Ito, H., Izumi, Y., Kato, H., Watanabe, Y., Kinoshita, Y., Kamada, M., Nodera, H., Suzuki, H., et al. (2010). Mutations of optineurin in amyotrophic lateral sclerosis. Nature *465*, 223–226.

Mason, S. (2017). Lactate shuttles in neuroenergetics—homeostasis, allostasis and beyond. Front. Neurosci. *11*, 43.

Mattiazzi, M., D'Aurelio, M., Gajewski, C.D., Martushova, K., Kiaei, M., Beal, M.F., and Manfredi, G. (2002). Mutated human SOD1 causes dysfunction of oxidative phosphorylation in mitochondria of transgenic mice. J. Biol. Chem. *277*, 29626–29633.

Mazzini, L., Mareschi, K., Ferrero, I., Vassallo, E., Oliveri, G., Boccaletti, R., Testa, L., Livigni, S., and Fagioli, F. (2006). Autologous mesenchymal stem cells: clinical applications in amyotrophic lateral sclerosis. Neurol. Res. *28*, 523–526.

Mazzini, L., Mareschi, K., Ferrero, I., Vassallo, E., Oliveri, G., Nasuelli, N., Oggioni, G.D., Testa, L., and Fagioli, F. (2008). Stem cell treatment in Amyotrophic Lateral Sclerosis. J. Neurol. Sci. *265*, 78–83.

Mazzini, L., Ferrero, I., Luparello, V., Rustichelli, D., Gunetti, M., Mareschi, K., Testa, L., Stecco, A., Tarletti, R., Miglioretti, M., et al. (2010). Mesenchymal stem cell transplantation in amyotrophic lateral sclerosis: a phase I clinical trial. Exp. Neurol. *223*.

Mazzini, L., Mareschi, K., Ferrero, I., Miglioretti, M., Stecco, A., Servo, S., Carriero, A., Monaco, F., and Fagioli, F. (2012). Mesenchymal stromal cell transplantation in amyotrophic lateral sclerosis: a long-term safety study. Cytotherapy *14*, 56–60.

Mazzini, L., Gelati, M., Profico, D.C., Sgaravizzi, G., Projetti Pensi, M., Muzi, G., Ricciolini, C., Rota Nodari, L., Carletti, S., Giorgi, C., et al. (2015). Human neural stem cell transplantation in ALS: initial results from a phase I trial. J. Transl. Med. *13*, 17.

Mazzini, L., Gelati, M., Profico, D.C., Sorarù, G., Ferrari, D., Copetti, M., Muzi, G., Ricciolini, C., Carletti, S., Giorgi, C., et al. (2019). Results from phase I clinical trial with intraspinal injection of neural stem cells in amyotrophic lateral sclerosis: a long-term outcome. Stem Cells Transl. Med. *8*, 887–897.

McCombe, P.A., and Henderson, R.D. (2010). Effects of gender in amyotrophic lateral sclerosis. Gend. Med. *7*, 557–570.

McCord, J.M., and Fridovich, I. (1969). Superoxide dismutase: an enzymic function for erythrocuprein (hemocuprein). J. Biol. Chem. *244*, 6049–6065.

McCreedy, D.A., Brown, C.R., Butts, J.C., Xu, H., Huettner, J.E., and Sakiyama-Elbert, S.E. (2014). A new method for generating high purity motoneurons from mouse embryonic stem cells. Biotechnol. Bioeng. *111*, 2041–2055.

McGann, J.C., Lioy, D.T., and Mandel, G. (2012). Astrocytes conspire with neurons during progression of neurological disease. Curr. Opin. Neurobiol. *22*, 850–858.

McLarnon, J.G. (1995). Potassium currents in motoneurones. Prog. Neurobiol. *47*, 513–531.

Mejzini, R., Flynn, L.L., Pitout, I.L., Fletcher, S., Wilton, S.D., and Akkari, P.A. (2019). ALS genetics, mechanisms, and therapeutics: where are we now? Front. Neurosci. *13*, 1310.

Mentis, G.Z., Alvarez, F.J., Bonnot, A., Richards, D.S., Gonzalez-Forero, D., Zerda, R., and O'Donovan, M.J. (2005). Noncholinergic excitatory actions of motoneurons in the neonatal mammalian spinal cord. Proc. Natl. Acad. Sci. *102*, 7344–7349.

Mezey, E., Chandross, K.J., Harta, G., Maki, R.A., and McKercher, S.R. (2000). Turning blood into brain: cells bearing neuronal antigens generated in vivo from bone marrow. Science (80-.). *290*, 1779–1782.

Miles, G., Dai, Y., and Brownstone, R. (2005). Mechanisms underlying the early phase of spike frequency adaptation in mouse spinal motoneurones. J. Physiol. *566*, 519–532.

Miles, G.B., Yohn, D.C., Wichterle, H., Jessell, T.M., Rafuse, V.F., and Brownstone, R.M. (2004). Functional properties of motoneurons derived from mouse embryonic stem cells. J. Neurosci. *24*.

Miller, R., Mitchell, J., Lyon, M., Moore, D., and Lyon, M. (2002). Riluzole for amyotrophic lateral sclerosis (ALS)/motor neuron disease (MND). In Cochrane Database of Systematic Reviews, R. Miller, ed. (Chichester, UK: John Wiley & Sons, Ltd), p.

Miller, R.G., Bouchard, J.P., Duquette, P., Eisen, A., Gelinas, D., Harati, Y., Munsat, T.L., Powe, L., Rothstein, J., Salzman, P., et al. (1996). Clinical trials of riluzole in patients with ALS. ALS/Riluzole Study Group-II. Neurology *47*, S86-90; discussion S90-2.

Milligan, C.E., Oppenheim, R.W., and Schwartz, L.M. (1994). Motoneurons deprived of trophic supportin vitro require new gene expression to undergo programmed cell death. J. Neurobiol. *25*, 1005–1016.

Mitsubishi Tanabe Pharma (2019). Six countries have approved edaravone for ALS treatment: NMPA approved Japan-originated ALS treatment Edaravone in China.

Miyashita, T., Shao, Y.R., Chung, J., Pourzia, O., and Feldman, D.E. (2013). Long-term channelrhodopsin-2 (ChR2) expression can induce abnormal axonal morphology and targeting in cerebral cortex. Front. Neural Circuits *7*, 8.

Mizielinska, S., Grönke, S., Niccoli, T., Ridler, C.E., Clayton, E.L., Devoy, A., Moens, T., Norona, F.E., Woollacott, I.O.C., Pietrzyk, J., et al. (2014). C9orf72 repeat expansions cause neurodegeneration in Drosophila through arginine-rich proteins. Science *345*, 1192–1194.

Molofsky, A. V, Kelley, K.W., Tsai, H.-H., Redmond, S.A., Chang, S.M., Madireddy, L., Chan, J.R., Baranzini, S.E., Ullian, E.M., and Rowitch, D.H. (2014). Astrocyte-encoded positional cues maintain sensorimotor circuit integrity. Nature *509*, 189–194.

Montague, K., Lowe, A.S., Uzquiano, A., Knüfer, A., Astick, M., Price, S.R., and Guthrie, S. (2017). The assembly of developing motor neurons depends on an interplay between spontaneous activity, type II cadherins and gap junctions. Development *144*, 830–836.

Montgomery, K.L., Yeh, A.J., Ho, J.S., Tsao, V., Mohan Iyer, S., Grosenick, L., Ferenczi, E.A., Tanabe, Y., Deisseroth, K., Delp, S.L., et al. (2015). Wirelessly powered, fully internal optogenetics for brain, spinal and peripheral circuits in mice. Nat. Methods *12*, 969–974.

Moore, N.J., Bhumbra, G.S., Foster, J.D., and Beato, M. (2015). Synaptic connectivity between Renshaw cells and motoneurons in the recurrent inhibitory circuit of the spinal cord.

Morel, L., Higashimori, H., Tolman, M., and Yang, Y. (2014). VGluT1+ neuronal glutamatergic signaling regulates postnatal developmental maturation of cortical protoplasmic astroglia. J. Neurosci. *34*, 10950–10962.

Mori, K., Weng, S.-M., Arzberger, T., May, S., Rentzsch, K., Kremmer, E., Schmid, B., Kretzschmar, H.A., Cruts, M., Van Broeckhoven, C., et al. (2013a). The C9orf72 GGGGCC

Repeat Is Translated into Aggregating Dipeptide-Repeat Proteins in FTLD/ALS. Science (80-.). *339*, 1335–1338.

Mori, K., Arzberger, T., Grässer, F.A., Gijselinck, I., May, S., Rentzsch, K., Weng, S.-M., Schludi, M.H., van der Zee, J., Cruts, M., et al. (2013b). Bidirectional transcripts of the expanded C9orf72 hexanucleotide repeat are translated into aggregating dipeptide repeat proteins. Acta Neuropathol. *126*, 881–893.

Morquette, P., Verdier, D., Kadala, A., Féthière, J., Philippe, A.G., Robitaille, R., and Kolta, A. (2015). An astrocyte-dependent mechanism for neuronal rhythmogenesis. Nat. Neurosci. *18*, 844–854.

Moviglia, G.A., Moviglia-Brandolino, M.T., Varela, G.S., Albanese, G., Piccone, S., Echegaray, G., Martinez, G., Blasseti, N., Farias, J., Farina, P., et al. (2012). Feasibility, safety, and preliminary proof of principles of autologous neural stem cell treatment combined with T-cell vaccination for ALS patients. Cell Transplant. *21 Suppl 1*, S57-63.

Mrówczyński, W., Krutki, P., Chakarov, V., and Celichowski, J. (2010). Doublet of action potentials evoked by intracellular injection of rectangular depolarization current into rat motoneurones. Exp. Brain Res. *205*, 95–102.

Mrówczyński, W., Celichowski, J., Raikova, R., and Krutki, P. (2015). Physiological consequences of doublet discharges on motoneuronal firing and motor unit force. Front. Cell. Neurosci. *9*, 81.

Mu, Y., Bennett, D. V., Rubinov, M., Narayan, S., Yang, C.-T., Tanimoto, M., Mensh, B.D., Looger, L.L., and Ahrens, M.B. (2019). Glia accumulate evidence that actions are futile and suppress unsuccessful behavior. Cell *178*, 27-43.e19.

Müller, C.M. (1990). Dark-rearing retards the maturation of astrocytes in restricted layers of cat visual cortex. Glia *3*, 487–494.

Myers, C.P., Lewcock, J.W., Hanson, M.G., Gosgnach, S., Aimone, J.B., Gage, F.H., Lee, K.-F., Landmesser, L.T., and Pfaff, S.L. (2005). Cholinergic input is required during embryonic development to mediate proper assembly of spinal locomotor circuits. Neuron *46*, 37–49.

Nabavi, S.M., Arab, L., Jarooghi, N., Bolurieh, T., Abbasi, F., Mardpour, S., Azimyian, V., Moeininia, F., Maroufizadeh, S., Sanjari, L., et al. (2019). Safety, feasibility of intravenous and intrathecal injection of autologous bone marrow derived mesenchymal stromal cells in patients with amyotrophic lateral sclerosis: an open label phase I clinical trial. Cell J. *20*, 592–598.

Nagai, M., Re, D.B., Nagata, T., Chalazonitis, A., Jessell, T.M., Wichterle, H., and Przedborski, S. (2007). Astrocytes expressing ALS-linked mutated SOD1 release factors selectively toxic to motor neurons. Nat. Neurosci. *10*, 615–622.

Nagel, G., Szellas, T., Huhn, W., Kateriya, S., Adeishvili, N., Berthold, P., Ollig, D., Hegemann, P., and Bamberg, E. (2003). Channelrhodopsin-2, a directly light-gated cation-selective membrane channel. Proc. Natl. Acad. Sci. U. S. A. *100*, 13940–13945.

Nakano-Kobayashi, A., Tai, Y., Kasri, N.N., and Aelst, L. Van (2014). The X-linked Mental Retardation Protein OPHN1 Interacts with Homer1b/c to Control Spine Endocytic Zone Positioning and Expression of Synaptic Potentiation. J. Neurosci. *34*, 8665–8671.

Nascimento, F., Spindler, L.R.B., and Miles, G.B. (2019). Balanced cholinergic modulation of spinal locomotor circuits via M2 and M3 muscarinic receptors. Sci. Rep. *9*, 14051.

NCT02556736, C. go. I. Phase I/IIa, open-label, dose-escalation study of safety and tolerability of intravitreal RST-001 in patients with advanced retinitis pigmentosa; 2015 December 4 [cited

2020 April 21];

NCT03326336, C. go. I. A phase 1/2a, open-label, non-randomized, dose-escalation study to evaluate the safety and tolerability of GS030 in subjects with retinitis pigmentosa; 2018 September 26 [cited 2020 April 21];

Neugebauer, K.M., Emmett, C.J., Venstrom, K.A., and Reichardt, L.F. (1991). Vitronectin and thrombospondin promote retinal neurite outgrowth: developmental regulation and role of integrins. Neuron *6*, 345–358.

Neumann, M., Sampathu, D.M., Kwong, L.K., Truax, A.C., Micsenyi, M.C., Chou, T.T., Bruce, J., Schuck, T., Grossman, M., Clark, C.M., et al. (2006). Ubiquitinated TDP-43 in frontotemporal lobar degeneration and amyotrophic lateral sclerosis. Science *314*, 130–133.

Nguyen, L., Montrasio, F., Pattamatta, A., Tusi, S.K., Bardhi, O., Meyer, K.D., Hayes, L., Nakamura, K., Banez-Coronel, M., Coyne, A., et al. (2019). Antibody therapy targeting RAN proteins rescues C9 ALS/FTD phenotypes in C9orf72 mouse model. Neuron.

Nicolas, A., Kenna, K.P., Renton, A.E., Ticozzi, N., Faghri, F., Chia, R., Dominov, J.A., Kenna, B.J., Nalls, M.A., Keagle, P., et al. (2018). Genome-wide analyses identify KIF5A as a novel ALS gene. Neuron *97*, 1268-1283.e6.

Niederreither, K., McCaffery, P., Dräger, U.C., Chambon, P., and Dollé, P. (1997). Restricted expression and retinoic acid-induced downregulation of the retinaldehyde dehydrogenase type 2 (RALDH-2) gene during mouse development. Mech. Dev. *62*, 67–78.

van Niekerk, E.A., Tuszynski, M.H., Lu, P., and Dulin, J.N. (2016). Molecular and cellular mechanisms of axonal regeneration after spinal cord injury. Mol. Cell. Proteomics *15*, 394–408.

Nimmervoll, B., White, R., Yang, J.-W., An, S., Henn, C., Sun, J.-J., and Luhmann, H.J. (2013). LPS-induced microglial secretion of TNFα increases activity-dependent neuronal apoptosis in the neonatal cerebral cortex. Cereb. Cortex *23*, 1742–1755.

Nishimaru, H., Restrepo, C.E., Ryge, J., Yanagawa, Y., and Kiehn, O. (2005). Mammalian motor neurons corelease glutamate and acetylcholine at central synapses. Proc. Natl. Acad. Sci. U. S. A. *102*, 5245–5249.

Nornes, H.O., and Carry, M. (1978). Neurogenesis in spinal cord of mouse: an autoradiographic analysis. Brain Res. *159*, 1–16.

Núñez-Abades, P.A., and Cameron, W.E. (1995). Morphology of developing rat genioglossal motoneurons studied in vitro: Relative changes in diameter and surface area of somata and dendrites. J. Comp. Neurol. *353*, 129–142.

Nüñez-Abades, P.A., He, F., Barrionuevo, G., and Cameron, W.E. (1994). Morphology of developing rat genioglossal motoneurons studied in vitro: Changes in length, branching pattern, and spatial distribution of dendrites. J. Comp. Neurol. *339*, 401–420.

O'donovan, M.J., Chub, N., and Wenner, P. (1998). Mechanisms of spontaneous activity in developing spinal networks. Dev. Neurobiol. *37*, 131–145.

O'Leary, T., and Wyllie, D.J.A. (2011). Neuronal homeostasis: Time for a change? J. Physiol. *589*, 4811–4826.

O'Shea, K.S., Liu, L.H., and Dixit, V.M. (1991). Thrombospondin and a 140 kd fragment promote adhesion and neurite outgrowth from embryonic central and peripheral neurons and from PC12 cells. Neuron *7*, 231–237.

Oberheim, N.A., Takano, T., Han, X., He, W., Lin, J.H.C., Wang, F., Xu, Q., Wyatt, J.D., Pilcher, W., Ojemann, J.G., et al. (2009). Uniquely hominid features of adult human astrocytes. J. Neurosci. *29*, 3276–3287.

Oberheim, N.A., Goldman, S.A., and Nedergaard, M. (2012). Heterogeneity of astrocytic form and function. Methods Mol. Biol. *814*, 23–45.

Oesterhelt, D., and Stoeckenius, W. (1971). Rhodopsin-like protein from the purple membrane of Halobacterium halobium. Nat. New Biol. *233*, 149–152.

Oh, K.-W., Moon, C., Kim, H.Y., Oh, S., Park, J., Lee, J.H., Chang, I.Y., Kim, K.S., and Kim, S.H. (2015). Phase I trial of repeated intrathecal autologous bone marrow-derived mesenchymal stromal cells in amyotrophic lateral sclerosis. Stem Cells Transl. Med. *4*, 590.

Oh, K.-W., Noh, M.-Y., Kwon, M.-S., Kim, H.Y., Oh, S.-I., Park, J., Kim, H.-J., Ki, C.-S., and Kim, S.H. (2018). Repeated intrathecal mesenchymal stem cells for amyotrophic lateral sclerosis. Ann. Neurol. *84*, 361–373.

Okuno, D., Asaumi, M., and Muneyuki, E. (1999). Chloride concentration dependency of the electrogenic activity of halorhodopsin. Biochemistry *38*.

Oliveira, A.L.R., Hydling, F., Olsson, E., Shi, T., Edwards, R.H., Fujiyama, F., Kaneko, T., Hökfelt, T., Cullheim, S., and Meister, B. (2003). Cellular localization of three vesicular glutamate transporter mRNAs and proteins in rat spinal cord and dorsal root ganglia. Synapse *50*, 117–129.

Olsen, M.L., Campbell, S.L., and Sontheimer, H. (2007). Differential distribution of Kir4.1 in spinal cord astrocytes suggests regional differences in K+ homeostasis. J. Neurophysiol. *98*, 786–793.

Oppenheim, R.W. (1991). Cell Death During Development of the Nervous System. Annu. Rev. Neurosci. *14*, 453–501.

Oppenheim, R.W., Houenou, L.J., Johnson, J.E., Lin, L.-F.H., Li, L., Lo, A.C., Newsome, A.L., Prevette, D.M., and Wang, S. (1995). Developing motor neurons rescued from programmed and axotomy-induced cell death by GDNF. Nature *373*, 344–346.

Oskarsson, B., Gendron, T.F., and Staff, N.P. (2018). Amyotrophic Lateral Sclerosis: an update for 2018. Mayo Clin. Proc. *93*, 1617–1628.

Osterhout, D.J., Frazier, W.A., and Higgins, D. (1992). Thrombospondin promotes process outgrowth in neurons from the peripheral and central nervous systems. Dev. Biol. *150*, 256–265.

Pansarasa, O., Bordoni, M., Diamanti, L., Sproviero, D., Gagliardi, S., and Cereda, C. (2018). SOD1 in Amyotrophic Lateral Sclerosis: “Ambivalent” Behavior Connected to the Disease. Int. J. Mol. Sci. *19*.

Park, S., Koppes, R.A., Froriep, U.P., Jia, X., Achyuta, A.K.H., McLaughlin, B.L., and Anikeeva, P. (2015). Optogenetic control of nerve growth. Sci. Rep. *5*, 9669.

Peckham, P.H., and Knutson, J.S. (2005). Functional electrical stimulation for neuromuscular applications. Annu. Rev. Biomed. Eng. *7*, 327–360.

Peljto, M., Dasen, J.S., Mazzoni, E.O., Jessell, T.M., and Wichterle, H. (2010). Functional diversity of ESC-derived motor neuron subtypes revealed through intraspinal transplantation. Cell Stem Cell *7*, 355–366.

Peron, S., Chen, T.-W., and Svoboda, K. (2015). Comprehensive imaging of cortical networks.

Curr. Opin. Neurobiol. *32*, 115–123.

Personius, K., Chang, Q., Bittman, K., Panzer, J., and Balice-Gordon, R. (2001). Gap junctional communication among motor and other neurons shapes patterns of neural activity and synaptic connectivity during development. Cell Commun. Adhes. *8*, 329–333.

Personius, K.E., Chang, Q., Mentis, G.Z., O'Donovan, M.J., and Balice-Gordon, R.J. (2007). Reduced gap junctional coupling leads to uncorrelated motor neuron firing and precocious neuromuscular synapse elimination. Proc. Natl. Acad. Sci. U. S. A. *104*, 11808–11813.

Personius, K.E., Slusher, B.S., and Udin, S.B. (2016). Neuromuscular NMDA receptors modulate developmental synapse elimination. J. Neurosci. *36*, 8783–8789.

Peters, O.M., Ghasemi, M., Brown, R.H., and Jr. (2015). Emerging mechanisms of molecular pathology in ALS. J. Clin. Invest. *125*, 1767–1779.

Petros, T.J., Tyson, J.A., and Anderson, S.A. (2011). Pluripotent stem cells for the study of CNS development. Front. Mol. Neurosci. *4*, 30.

Petrou, P., Gothelf, Y., Argov, Z., Gotkine, M., Levy, Y.S., Kassis, I., Vaknin-Dembinsky, A., Ben-Hur, T., Offen, D., Abramsky, O., et al. (2016). Safety and Clinical Effects of Mesenchymal Stem Cells Secreting Neurotrophic Factor Transplantation in Patients With Amyotrophic Lateral Sclerosis: Results of Phase 1/2 and 2a Clinical Trials. JAMA Neurol. *73*, 337–344.

Petrov, D., Mansfield, C., Moussy, A., and Hermine, O. (2017). ALS clinical trials review: 20 years of failure. Are we any closer to registering a new treatment? Front. Aging Neurosci. *9*, 68.

Pfrieger, F.W., and Barres, B.A. (1997). Synaptic efficacy enhanced by glial cells in vitro. Science (80-.). *277*, 1684–1687.

Post, M.W.M., and van Leeuwen, C.M.C. (2012). Psychosocial issues in spinal cord injury: a review. Spinal Cord *50*, 382–389.

Prabhakar, S., Marwaha, N., Lal, V., Sharma, R.R., Rajan, R., and Khandelwal, N. (2012). Autologous bone marrow-derived stem cells in amyotrophic lateral sclerosis: a pilot study. Neurol. India *60*, 465–469.

Pringle, C.E., Hudson, A.J., Munoz, D.G., Kiernan, J.A., Brown, W.F., and Ebers, G.C. (1992). Primary lateral sclerosis: clinical features, neuropathology and diagnostic criteria.

Prochazka, A., Gauthier, M., Wieler, M., and Kenwell, Z. (1997). The bionic glove: An electrical stimulator garment that provides controlled grasp and hand opening in quadriplegia. Arch. Phys. Med. Rehabil. *78*, 608–614.

Procko, C., and Shaham, S. (2010). Assisted morphogenesis: glial control of dendrite shapes. Curr. Opin. Cell Biol. *22*, 560–565.

Proctor, E.A., Fee, L., Tao, Y., Redler, R.L., Fay, J.M., Zhang, Y., Lv, Z., Mercer, I.P., Deshmukh, M., Lyubchenko, Y.L., et al. (2016). Nonnative SOD1 trimer is toxic to motor neurons in a model of amyotrophic lateral sclerosis. Proc. Natl. Acad. Sci. U. S. A. *113*, 614–619.

Puls, I., Jonnakuty, C., LaMonte, B.H., Holzbaur, E.L.F., Tokito, M., Mann, E., Floeter, M.K., Bidus, K., Drayna, D., Oh, S.J., et al. (2003). Mutant dynactin in motor neuron disease. Nat. Genet. *33*, 455–456.

Pun, S., Santos, A.F., Saxena, S., Xu, L., and Caroni, P. (2006). Selective vulnerability and pruning of phasic motoneuron axons in motoneuron disease alleviated by CNTF. Nat.

Neurosci. *9*, 408–419.

Purves, D., Johnson, D.A., and Hume, R.I. (1981). Regulation of synaptic connections in the rabbit ciliary ganglion. In Ciba Foundation Symposium, pp. 232–251.

Raaphorst, J., de Visser, M., Linssen, W.H.J.P., de Haan, R.J., and Schmand, B. (2010). The cognitive profile of amyotrophic lateral sclerosis: A meta-analysis. Amyotroph. Lateral Scler. *11*, 27–37.

Ramesh, N., and Pandey, U.B. (2017). Autophagy dysregulation in ALS: when protein aggregates get out of hand. Front. Mol. Neurosci. *10*.

Ravits, J., Appel, S., Baloh, R.H., Barohn, R., Brooks, B.R., Elman, L., Floeter, M.K., Henderson, C., Lomen-Hoerth, C., Macklis, J.D., et al. (2013). Deciphering amyotrophic lateral sclerosis: what phenotype, neuropathology and genetics are telling us about pathogenesis. Amyotroph. Lateral Scler. Frontotemporal Degener. *14 Suppl 1*, 5–18.

Rekling, J.C., Funk, G.D., Bayliss, D.A., Dong, X.-W., and Feldman, J.L. (2000). Synaptic control of motoneuronal excitability. Physiol. Rev. *80*, 767–852.

Renshaw, B. (1946). Central effects of centripetal impulses in axons of spinal ventral roots. J. Neurophysiol. *9*, 191–204.

Renton, A.E., Majounie, E., Waite, A., Simón-Sánchez, J., Rollinson, S., Gibbs, J.R., Schymick, J.C., Laaksovirta, H., van Swieten, J.C., Myllykangas, L., et al. (2011). A hexanucleotide repeat expansion in C9ORF72 is the cause of chromosome 9p21-linked ALS-FTD. Neuron *72*, 257–268.

RetroSense-Therapeutics (2016). RetroSense Therapeutics doses first patient in phase 1/2 clinical trial for lead compound RST-001. Eyewire News.

Richards, D.S., Griffith, R.W., Romer, S.H., and Alvarez, F.J. (2014). Motor axon synapses on Renshaw cells contain higher levels of aspartate than glutamate. PLoS One *9*, e97240.

Richter, C., and Bruegmann, T. (2019). No light without the dark: Perspectives and hindrances for translation of cardiac optogenetics. Prog. Biophys. Mol. Biol.

Riley, J., Federici, T., Polak, M., Kelly, C., Glass, J., Raore, B., Taub, J., Kesner, V., Feldman, E.L., and Boulis, N.M. (2012). Intraspinal stem cell transplantation in amyotrophic lateral sclerosis: a phase I safety trial, technical note, and lumbar safety outcomes. Neurosurgery *71*, 405–416; discussion 416.

Riley, J., Glass, J., Feldman, E.L., Polak, M., Bordeau, J., Federici, T., Johe, K., and Boulis, N.M. (2014). Intraspinal stem cell transplantation in amyotrophic lateral sclerosis: a phase I trial, cervical microinjection, and final surgical safety outcomes. Neurosurgery *74*, 77–87.

Ringholz, G.M., Appel, S.H., Bradshaw, M., Cooke, N.A., Mosnik, D.M., and Schulz, P.E. (2005). Prevalence and patterns of cognitive impairment in sporadic ALS. Neurology *65*, 586–590.

Robinson, R.B., and Siegelbaum, S.A. (2003). Hyperpolarization-activated cation currents: from molecules to physiological function. Annu. Rev. Physiol. *65*, 453–480.

Ron, D., and Walter, P. (2007). Signal integration in the endoplasmic reticulum unfolded protein response. Nat. Rev. Mol. Cell Biol. *8*, 519–529.

Rosato-Siri, M.D., Zoccolan, D., Furlan, F., and Ballerini, L. (2004). Interneurone bursts are spontaneously associated with muscle contractions only during early phases of mouse spinal network development: a study in organotypic cultures. Eur. J. Neurosci. *20*, 2697–2710.

Rosen, D.R., Siddique, T., Patterson, D., Figlewicz, D.A., Sapp, P., Hentati, A., Donaldson, D., Goto, J., O'Regan, J.P., Deng, H.-X., et al. (1993). Mutations in Cu/Zn superoxide dismutase gene are associated with familial amyotrophic lateral sclerosis. Nature *362*, 59–62.

Rothstein, J.D. (2017). Edaravone: a new drug approved for ALS. Cell *171*.

Rothstein, J.D., Tsai, G., Kuncl, R.W., Clawson, L., Cornblath, D.R., Drachman, D.B., Pestronk, A., Stauch, B.L., and Coyle, J.T. (1990). Abnormal excitatory amino acid metabolism in amyotrophic lateral sclerosis. Ann. Neurol. *28*, 18–25.

Rothstein, J.D., Martin, L.J., and Kuncl, R.W. (1992). Decreased glutamate transport by the brain and spinal cord in amyotrophic lateral sclerosis. N. Engl. J. Med. *326*, 1464–1468.

Rothstein, J.D., Dykes-Hoberg, M., Pardo, C.A., Bristol, L.A., Jin, L., Kuncl, R.W., Kanai, Y., Hediger, M.A., Wang, Y., Schielke, J.P., et al. (1996). Knockout of glutamate transporters reveals a major role for astroglial transport in excitotoxicity and clearance of glutamate. Neuron *16*, 675–686.

Rousso, D.L., Gaber, Z.B., Wellik, D., Morrisey, E.E., and Novitch, B.G. (2008). Coordinated actions of the Forkhead Protein Foxp1 and Hox proteins in the columnar organization of spinal motor neurons. Neuron *59*, 226–240.

Rowland, L.P. (2010). Progressive muscular atrophy and other lower motor neuron syndromes of adults. Muscle Nerve *41*, 161–165.

Rybak, I.A., Dougherty, K.J., and Shevtsova, N.A. (2015). Organization of the mammalian locomotor CPG: review of computational model and circuit architectures based on genetically identified spinal interneurons. ENeuro *2*.

Sabatier, M.J., Redmon, N., Schwartz, G., and English, A.W. (2008). Treadmill training promotes axon regeneration in injured peripheral nerves. Exp. Neurol. *211*, 489–493.

Sancho, J., Martínez, D., Bures, E., Díaz, J.L., Ponz, A., and Servera, E. (2018). Bulbar impairment score and survival of stable amyotrophic lateral sclerosis patients after noninvasive ventilation initiation. ERJ Open Res. *4*.

Santiago Ramón y Cajal (1906). Nobel Lecture: The structure and connexions of neurons.

Sareen, D., O'Rourke, J.G., Meera, P., Muhammad, A.K.M.G., Grant, S., Simpkinson, M., Bell, S., Carmona, S., Ornelas, L., Sahabian, A., et al. (2013). Targeting RNA foci in iPSC-derived motor neurons from ALS patients with a C9ORF72 repeat expansion. Sci. Transl. Med. *5*, 208ra149.

Sasaki, S., and Iwata, M. (1999). Ultrastructural change of synapses of Betz cells in patients with amyotrophic lateral sclerosis. Neurosci. Lett. *268*, 29–32.

Schafer, D.P., Lehrman, E.K., Kautzman, A.G., Koyama, R., Mardinly, A.R., Yamasaki, R., Ransohoff, R.M., Greenberg, M.E., Barres, B.A., and Stevens, B. (2012). Microglia sculpt postnatal neural circuits in an activity and complement-dependent manner. Neuron *74*, 691–705.

Scheuss, V., Yasuda, R., Sobczyk, A., and Svoboda, K. (2006). Nonlinear [Ca2+] signaling in dendrites and spines caused by activity-dependent depression of Ca2+ extrusion. J. Neurosci. *26*, 8183–8194.

Schousboe, A., Scafidi, S., Bak, L.K., Waagepetersen, H.S., and McKenna, M.C. (2014). Glutamate metabolism in the brain focusing on astrocytes. Adv. Neurobiol. *11*, 13–30.

Schrøder, H.D., and Reske-Nielsen, E. Preservation of the nucleus X-pelvic floor motosystem

in amyotrophic lateral sclerosis. Clin. Neuropathol. *3*, 210–216.

Selvaraj, B.T., Livesey, M.R., Zhao, C., Gregory, J.M., James, O.T., Cleary, E.M., Chouhan, A.K., Gane, A.B., Perkins, E.M., Dando, O., et al. (2018). C9ORF72 repeat expansion causes vulnerability of motor neurons to Ca2+-permeable AMPA receptor-mediated excitotoxicity. Nat. Commun. *9*.

Sendtner, M., Pei, G., Beck, M., Schweizer, U., and Wiese, S. (2000). Developmental motoneuron cell death and neurotrophic factors. Cell Tissue Res. *301*, 71–84.

Sherrington, C. (1906). The integrative action of the nervous system (London: Yale University Press).

Shneider, N.A., Brown, M.N., Smith, C.A., Pickel, J., and Alvarez, F.J. (2009). Gamma motor neurons express distinct genetic markers at birth and require muscle spindle-derived GDNF for postnatal survival. Neural Dev. *4*, 42.

Smith, C.C., and Brownstone, R.M. (2020). Spinal motoneuron firing properties mature from rostral to caudal during postnatal development of the mouse. J. Physiol.

Smith, B.N., Newhouse, S., Shatunov, A., Vance, C., Topp, S., Johnson, L., Miller, J., Lee, Y., Troakes, C., Scott, K.M., et al. (2013). The C9ORF72 expansion mutation is a common cause of ALS+/-FTD in Europe and has a single founder. Eur. J. Hum. Genet. *21*, 102–108.

Smith, B.N., Ticozzi, N., Fallini, C., Gkazi, A.S., Topp, S., Kenna, K.P., Scotter, E.L., Kost, J., Keagle, P., Miller, J.W., et al. (2014). Exome-wide rare variant analysis identifies TUBA4A mutations associated with familial ALS. Neuron *84*, 324–331.

Smith, B.N., Topp, S.D., Fallini, C., Shibata, H., Chen, H.-J., Troakes, C., King, A., Ticozzi, N., Kenna, K.P., Soragia-Gkazi, A., et al. (2017a). Mutations in the vesicular trafficking protein annexin A11 are associated with amyotrophic lateral sclerosis. Sci. Transl. Med. *9*.

Smith, C.C., Paton, J.F.R., Chakrabarty, S., and Ichiyama, R.M. (2017b). Descending systems direct development of key spinal motor circuits. J. Neurosci. *37*, 6372.

Sobuś, A., Baumert, B., Litwińska, Z., Gołąb-Janowska, M., Stępniewski, J., Kotowski, M., Pius-Sadowska, E., Kawa, M.P., Gródecka-Szwajkiewicz, D., Peregud-Pogorzelski, J., et al. (2018). Safety and feasibility of Lin- cells administration to ALS patients: a novel view on humoral factors and miRNA profiles. Int. J. Mol. Sci. *19*.

Solomon, D.A., Mitchell, J.C., Salcher-Konrad, M.-T., Vance, C.A., and Mizielinska, S. (2019). Review: Modelling the pathology and behaviour of frontotemporal dementia. Neuropathol. Appl. Neurobiol. *45*, 58–80.

Soundararajan, P., Miles, G.B., Rubin, L.L., Brownstone, R.M., and Rafuse, V.F. (2006). Motoneurons derived from embryonic stem cells express transcription factors and develop phenotypes characteristic of medial motor column neurons. J. Neurosci. *26*, 3256–3268.

Spitzer, N.C., and Lamborghini, J.E. (1976). The development of the action potential mechanism of amphibian neurons isolated in culture (calcium current/sodium current/birthdates/Rohon-Beard cells/Xenopus laevis).

Spitzer, N.C., Vincent, A., and Lautermilch, N.J. (2000a). Differentiation of electrical excitability in motoneurons. Brain Res. Bull. *53*, 547–552.

Spitzer, N.C., Lautermilch, N.J., Smith, R.D., and Gomez, T.M. (2000b). Coding of neuronal differentiation by calcium transients. BioEssays *22*, 811–817.

Sreedharan, J., Blair, I.P., Tripathi, V.B., Hu, X., Vance, C., Rogelj, B., Ackerley, S., Durnall,

J.C., Williams, K.L., Buratti, E., et al. (2008). TDP-43 mutations in familial and sporadic amyotrophic lateral sclerosis. Science (80-.). *319*, 1668–1672.

Staff, N.P., Madigan, N.N., Morris, J., Jentoft, M., Sorenson, E.J., Butler, G., Gastineau, D., Dietz, A., and Windebank, A.J. (2016). Safety of intrathecal autologous adipose-derived mesenchymal stromal cells in patients with ALS. Neurology *87*, 2230–2234.

Stellwagen, D., and Malenka, R.C. (2006). Synaptic scaling mediated by glial TNF-α. Nature *440*, 1054–1059.

Stellwagen, D., Beattie, E.C., Seo, J.Y., and Malenka, R.C. (2005). Differential regulation of AMPA receptor and GABA receptor trafficking by Tumor Necrosis Factor-alpha. J. Neurosci. *25*, 3219–3228.

Sternfeld, M.J., Hinckley, C.A., Moore, N.J., Pankratz, M.T., Hilde, K.L., Driscoll, S.P., Hayashi, M., Amin, N.D., Bonanomi, D., Gifford, W.D., et al. (2017). Speed and segmentation control mechanisms characterized in rhythmically-active circuits created from spinal neurons produced from genetically-tagged embryonic stem cells. Elife *6*, e21540.

Stifani, N. (2014). Motor neurons and the generation of spinal motor neuron diversity. Front. Cell. Neurosci. *8*, 293.

Su, C.-K., Mellen, N.M., and Feldman, J.L. (1997). Intrinsic and extrinsic factors affecting phrenic motoneuronal excitability in neonatal rats.

Syková, E., Rychmach, P., Drahorádová, I., Konrádová, Š., Růžičková, K., Voříšek, I., Forostyak, S., Homola, A., and Bojar, M. (2017). Transplantation of mesenchymal stromal cells in patients with amyotrophic lateral sclerosis: results of phase I/IIa clinical trial. Cell Transplant. *26*, 647–658.

Tadesse, T., Gearing, M., Senitzer, D., Saxe, D., Brat, D.J., Bray, R., Gebel, H., Hill, C., Boulis, N., Riley, J., et al. (2014). Analysis of graft survival in a trial of stem cell transplant in ALS. Ann. Clin. Transl. Neurol. *1*, 900–908.

Taga, A., Dastgheyb, R., Habela, C., Joseph, J., Richard, J., Gross, S.K., Lauria, G., Lee, G., Haughey, N., and Maragakis, N.J. (2019). Role of human-induced pluripotent stem cell-derived spinal cord astrocytes in the functional maturation of motor neurons in a multielectrode array system. Stem Cells Transl. Med. *8*, 1272.

Takazawa, T., Croft, G.F., Amoroso, M.W., Studer, L., Wichterle, H., and MacDermott, A.B. (2012). Maturation of spinal motor neurons derived from human embryonic stem cells. PLoS One *7*, e40154.

Takeda, T., Kitagawa, K., and Arai, K. (2020). Phenotypic variability and its pathological basis in amyotrophic lateral sclerosis. Neuropathology *40*, 40–56.

Takei, K., Watanabe, K., Yuki, S., Akimoto, M., Sakata, T., and Palumbo, J. (2017). Edaravone and its clinical development for amyotrophic lateral sclerosis. Amyotroph. Lateral Scler. Front. Degener. *18*, 5–10.

Talman, P., Forbes, A., and Mathers, S. (2009). Clinical phenotypes and natural progression for motor neuron disease: Analysis from an Australian database clinical phenotypes and natural progression for motor neuron disease. Amyotroph. Lateral Scler. *10*, 79–84.

Talman, P., Duong, T., Vucic, S., Mathers, S., Venkatesh, S., Henderson, R., Rowe, D., Schultz, D., Edis, R., Needham, M., et al. (2016). Identification and outcomes of clinical phenotypes in amyotrophic lateral sclerosis/motor neuron disease: Australian National Motor Neuron Disease observational cohort. BMJ Open *6*, e012054.

Tanaka, M., Sakata, T., Palumbo, J., and Akimoto, M. (2016). A 24-Week, phase III, double-blind, parallel-group study of Edaravone (MCI-186) for treatment of Amyotrophic Lateral Sclerosis (ALS). Neurology *86*.

Taylor, A.R., Gifondorwa, D.J., Newbern, J.M., Robinson, M.B., Strupe, J.L., Prevette, D., Oppenheim, R.W., and Milligan, C.E. (2007). Astrocyte and muscle-derived secreted factors differentially regulate motoneuron survival.

Taylor, J.P., Brown, R.H., Cleveland, D.W., and Cleveland, D.W. (2016). Decoding ALS: from genes to mechanism. Nature *539*, 197–206.

Teng, Y.D., Benn, S.C., Kalkanis, S.N., Shefner, J.M., Onario, R.C., Cheng, B., Lachyankar, M.B., Marconi, M., Li, J., Yu, D., et al. (2012). Multimodal actions of neural stem cells in a mouse model of ALS: a meta-analysis. Sci. Transl. Med. *4*, 165ra164.

Teyssou, E., Takeda, T., Lebon, V., Boillée, S., Doukouré, B., Bataillon, G., Sazdovitch, V., Cazeneuve, C., Meininger, V., LeGuern, E., et al. (2013). Mutations in SQSTM1 encoding p62 in amyotrophic lateral sclerosis: genetics and neuropathology. Acta Neuropathol. *125*, 511–522.

Toma, J.S., Shettar, B.C., Chipman, P.H., Pinto, D.M., Borowska, J.P., Ichida, J.K., Fawcett, J.P., Zhang, Y., Eggan, K., and Rafuse, V.F. (2015). Motoneurons derived from induced pluripotent stem cells develop mature phenotypes typical of endogenous spinal motoneurons. J. Neurosci. *35*, 1291–1306.

Tropel, P., Platet, N., Platel, J.-C., Noël, D., Albrieux, M., Benabid, A.-L., and Berger, F. (2006). Functional neuronal differentiation of bone marrow-derived mesenchymal stem cells. Stem Cells *24*, 2868–2876.

Tsai, H.-H., Li, H., Fuentealba, L.C., Molofsky, A. V, Taveira-Marques, R., Zhuang, H., Tenney, A., Murnen, A.T., Fancy, S.P.J., Merkle, F., et al. (2012). Regional astrocyte allocation regulates CNS synaptogenesis and repair. Science *337*, 358–362.

Tsuzuki, S., Yoshida, S., Yamamoto, T., and Oka, H. (1995). Developmental changes in the electrophysiological properties of neonatal rat oculomotor neurons studied in vitro. Neurosci. Res. *23*, 389–397.

Tu, J.C., Xiao, B., Yuan, J.P., Lanahan, A.A., Leoffert, K., Li, M., Linden, D.J., and Worley, P.F. (1998). Homer binds a novel proline-rich motif and links group 1 metabotropic glutamate receptors with IP3 receptors. Neuron *21*, 717–726.

Turner, B.J., and Talbot, K. (2008). Transgenics, toxicity and therapeutics in rodent models of mutant SOD1-mediated familial ALS. Prog. Neurobiol. *85*, 94–134.

Tzingounis, A. V., and Wadiche, J.I. (2007). Glutamate transporters: confining runaway excitation by shaping synaptic transmission. Nat. Rev. Neurosci. *8*, 935–947.

Ulfhake, B., and Cullheim, S. (1988). Postnatal development of cat hind limb motoneurons. III: Changes in size of motoneurons supplying the triceps surae muscle. J. Comp. Neurol. *278*, 103–120.

Ulfhake, B., and Kellerth, J.-O. (1981). A quantitative light microscopic study of the dendrites of cat spinal α-motoneurons after intracellular staining with horseradish peroxidase. J. Comp. Neurol. *202*, 571–583.

Ulfhake, B., and Kellerth, J.-O. (1983). A Quantitative morphological study of HRP-labelled cat α-motoneurones supplying different hindlimb muscles. Brain Res. *264*, 1–19.

Ullian, E.., Harris, B.., Wu, A., Chan, J.., and Barres, B.. (2004a). Schwann cells and

astrocytes induce synapse formation by spinal motor neurons in culture. Mol. Cell. Neurosci. *25*, 241–251.

Ullian, E.M., Sapperstein, S.K., Christopherson, K.S., and Barres, B.A. (2001). Control of synapse number by glia. Science (80-.). *291*, 657–661.

Ullian, E.M., Christopherson, K.S., and Barres, B.A. (2004b). Role for glia in synaptogenesis. Glia *47*, 209–216.

Vance, C., Rogelj, B., Hortobágyi, T., De Vos, K.J., Nishimura, A.L., Sreedharan, J., Hu, X., Smith, B., Ruddy, D., Wright, P., et al. (2009). Mutations in FUS, an RNA processing protein, cause familial amyotrophic lateral sclerosis type 6. Science *323*, 1208–1211.

Vann, K.T., and Xiong, Z.-G. (2016). Optogenetics for neurodegenerative diseases. Int. J. Physiol. Pathophysiol. Pharmacol. *8*, 1.

Viana, F., Bayliss, D.A., and Berger, A.J. (1994). Postnatal changes in rat hypoglossal motoneuron membrane properties. Neuroscience *59*, 131–148.

Vinay, L., Brocard, F., and Clarac, F. (2000a). Differential maturation of motoneurons innervating ankle flexor and extensor muscles in the neonatal rat. Eur. J. Neurosci. *12*, 4562–4566.

Vinay, L., Brocard, F., Pflieger, J.-F., Simeoni-Alias, J., and Clarac, F. (2000b). Perinatal development of lumbar motoneurons and their inputs in the rat. Brain Res. Bull. *53*, 635–647.

Visser, J., van den Berg-Vos, R.M., Franssen, H., van den Berg, L.H., Wokke, J.H., Vianney de Jong, J.M., Holman, R., de Haan, R.J., and de Visser, M. (2007). Disease course and prognostic factors of progressive muscular atrophy. Arch. Neurol. *64*, 522.

Vrieseling, E., and Arber, S. (2006). Target-induced transcriptional control of dendritic patterning and connectivity in motor neurons by the ETS gene Pea3. Cell *127*, 1439–1452.

Wagner, F.B., Mignardot, J.-B., Le Goff-Mignardot, C.G., Demesmaeker, R., Komi, S., Capogrosso, M., Rowald, A., Seáñez, I., Caban, M., Pirondini, E., et al. (2018). Targeted neurotechnology restores walking in humans with spinal cord injury. Nature *563*, 65–71.

Walker, M.C., and Kullmann, D.M. (2019). Optogenetic and chemogenetic therapies for epilepsy. Neuropharmacology 107751.

Wallén-Mackenzie, A., Gezelius, H., Thoby-Brisson, M., Nygård, A., Enjin, A., Fujiyama, F., Fortin, G., and Kullander, K. (2006). Vesicular glutamate transporter 2 is required for central respiratory rhythm generation but not for locomotor central pattern generation. J. Neurosci. *26*, 12294–12307.

Walton, K., and Fulton, B.P. (1986). Ionic mechanisms underlying the firing properties of rat neonatal motoneurons studied in vitro. Neuroscience *19*, 669–683.

Wang, I.-F., Tsai, K.-J., and Shen, C.-K.J. (2013). Autophagy activation ameliorates neuronal pathogenesis of FTLD-U mice: a new light for treatment of TARDBP/TDP-43 proteinopathies. Autophagy *9*, 239–240.

Wang, J., Guo, C., Liu, S., Qi, H., Yin, Y., Liang, R., Sun, M.-Z., and Greenaway, F.T. (2014). Annexin A11 in disease. Clin. Chim. Acta *431*, 164–168.

Ward, P.J., Jones, L.N., Mulligan, A., Goolsby, W., Wilhelm, J.C., and English, A.W. (2016). Optically-Induced Neuronal Activity Is Sufficient to Promote Functional Motor Axon Regeneration In Vivo. PLoS One *11*, e0154243.

Warp, E., Agarwal, G., Wyart, C., Friedmann, D., Oldfield, C.S., Conner, A., Del Bene, F., Arrenberg, A.B., Baier, H., and Isacoff, E.Y. (2012). Emergence of patterned activity in the developing zebrafish spinal cord. Curr. Biol. *22*, 93–102.

Wei, Z., Lin, B.-J., Chen, T.-W., Daie, K., Svoboda, K., and Druckmann, S. (2020). A comparison of neuronal population dynamics measured with calcium imaging and electrophysiology. PLOS Comput. Biol. *16*, e1008198.

Wen, X., Tan, W., Westergard, T., Krishnamurthy, K., Markandaiah, S.S., Shi, Y., Lin, S., Shneider, N.A., Monaghan, J., Pandey, U.B., et al. (2014). Antisense proline-arginine RAN dipeptides linked to C9ORF72-ALS/FTD form toxic nuclear aggregates that initiate in vitro and in vivo neuronal death. Neuron *84*, 1213–1225.

Wentz, C.T., Bernstein, J.G., Monahan, P., Guerra, A., Rodriguez, A., and Boyden, E.S. (2011). A wirelessly powered and controlled device for optical neural control of freely-behaving animals. J. Neural Eng. *8*, 046021.

Wichterle, H., Lieberam, I., Porter, J.A., and Jessell, T.M. (2002). Directed differentiation of embryonic stem cells into motor neurons. Cell *110*, 385–397.

Wijesekera, L.C., Mathers, S., Talman, P., Galtrey, C., Parkinson, M.H., Ganesalingam, J., Willey, E., Ampong, M.A., Ellis, C.M., Shaw, C.E., et al. (2009). Natural history and clinical features of the flail arm and flail leg ALS variants. Neurology *72*, 1087–1094.

Williams, P.A., Bellinger, D.L., and Wilson, C.G. (2019). Changes in the morphology of hypoglossal motor neurons in the brainstem of developing rats. Anat. Rec. *302*, 869–892.

Wilson, L., and Maden, M. (2005). The mechanisms of dorsoventral patterning in the vertebrate neural tube. Dev. Biol. *282*, 1–13.

Wilson, C.M., Grace, G.M., Munoz, D.G., He, B.P., and Strong, M.J. (2001). Cognitive impairment in sporadic ALS: a pathologic continuum underlying a multisystem disorder. Neurology *57*, 651–657.

Wilson, J.M., Rempel, J., and Brownstone, R.M. (2004). Postnatal development of cholinergic synapses on mouse spinal motoneurons. J. Comp. Neurol. *474*, 13–23.

Wilson, J.M., Hartley, R., Maxwell, D.J., Todd, A.J., Lieberam, I., Kaltschmidt, J.A., Yoshida, Y., Jessell, T.M., and Brownstone, R.M. (2005). Conditional rhythmicity of ventral spinal interneurons defined by expression of the Hb9 homeodomain protein. J. Neurosci. *25*, 5710–5719.

Wilson, J.M., Dombeck, D.A., Díaz-Ríos, M., Harris-Warrick, R.M., and Brownstone, R.M. (2007). Two-photon calcium imaging of network activity in XFP-expressing neurons in the mouse. J. Neurophysiol. *97*.

Witzemann, V. (2006). Development of the neuromuscular junction. Cell Tissue Res. *326*, 263–271.

Writing Group, K., Edaravone (MCI-186) ALS 19 Study Group, M., Tsuji, S., Itoyama, Y., Sobue, G., Togo, M., Hamada, C., Tanaka, M., Akimoto, M., Nakamura, K., et al. (2017). Safety and efficacy of edaravone in well defined patients with amyotrophic lateral sclerosis: a randomised, double-blind, placebo-controlled trial. Lancet. Neurol. *16*, 505–512.

Wu, C.-H., Fallini, C., Ticozzi, N., Keagle, P.J., Sapp, P.C., Piotrowska, K., Lowe, P., Koppers, M., McKenna-Yasek, D., Baron, D.M., et al. (2012). Mutations in the profilin 1 gene cause familial amyotrophic lateral sclerosis. Nature *488*, 499–503.

Wu, Q., Wang, Q., Li, Z., Li, X., Zang, J., Wang, Z., Xu, C., Gong, Y., Cheng, J., Li, H., et al.

(2018). Human menstrual blood-derived stem cells promote functional recovery in a rat spinal cord hemisection model. Cell Death Dis. *9*, 882.

Xiao, B., Tu, J.C., Petralia, R.S., Yuan, J.P., Doan, A., Breder, C.D., Ruggiero, A., Lanahan, A.A., Wenthold, R.J., and Worley, P.F. (1998). Homer regulates the association of group 1 metabotropic glutamate receptors with multivalent complexes of Homer-related, synaptic proteins. Neuron *21*, 707–716.

Xiao, Y., Tian, W., and López-Schier, H. (2015). Optogenetic stimulation of neuronal repair. Curr. Biol. *25*, R1068–R1069.

Xie, H., and Ziskind-Conhaim, L. (1995). Blocking Ca*+-Dependent Synaptic Release Delays Motoneuron Differentiation in the Rat Spinal Cord.

Xie, Y., Zhou, B., Lin, M.-Y., and Sheng, Z.-H. (2015). Progressive endolysosomal deficits impair autophagic clearance beginning at early asymptomatic stages in fALS mice. Autophagy *11*, 1934–1936.

Xu, H., and Sakiyama-Elbert, S.E. (2015). Directed differentiation of V3 interneurons from mouse embryonic stem cells. Stem Cells Dev. *24*, 2723–2732.

Xu, H., Iyer, N., Huettner, J.E., and Sakiyama-Elbert, S.E. (2015). A puromycin selectable cell line for the enrichment of mouse embryonic stem cell-derived V3 interneurons. Stem Cell Res. Ther. *6*, 220.

Xu, X., Mee, T., and Jia, X. (2020). New era of optogenetics: from the central to peripheral nervous system. Crit. Rev. Biochem. Mol. Biol. *55*, 1–16.

Xu, Y.-F., Gendron, T.F., Zhang, Y.-J., Lin, W.-L., D'Alton, S., Sheng, H., Casey, M.C., Tong, J., Knight, J., Yu, X., et al. (2010). Wild-type human TDP-43 expression causes TDP-43 phosphorylation, mitochondrial aggregation, motor deficits, and early mortality in transgenic mice. J. Neurosci. *30*, 10851–10859.

Yamanaka, K., and Komine, O. (2018). The multi-dimensional roles of astrocytes in ALS. Neurosci. Res. *126*, 31–38.

Yamanaka, K., Chun, S.J., Boillee, S., Fujimori-Tonou, N., Yamashita, H., Gutmann, D.H., Takahashi, R., Misawa, H., and Cleveland, D.W. (2008). Astrocytes as determinants of disease progression in inherited amyotrophic lateral sclerosis. Nat. Neurosci. *11*, 251–253.

Yohn, D.C., Miles, G.B., Rafuse, V.F., and Brownstone, R.M. (2008). Transplanted mouse embryonic stem cell-derived motoneurons form functional motor units and reduce muscle atrophy. J. Neurosci.

Yuste, R., and Denk, W. (1995). Dendritic spines as basic functional units of neuronal integration. Nature *375*, 682–684.

Yvert, B., Branchereau, P., and Meyrand, P. (2004). Multiple spontaneous rhythmic activity patterns generated by the embryonic mouse spinal cord occur within a specific developmental time window. J. Neurophysiol. *91*.

Zemelman, B. V, Lee, G.A., Ng, M., and Miesenböck, G. (2002). Selective photostimulation of genetically chARGed neurons. Neuron *33*, 15–22.

Zhang, F., Wang, L.-P., Brauner, M., Liewald, J.F., Kay, K., Watzke, N., Wood, P.G., Bamberg, E., Nagel, G., Gottschalk, A., et al. (2007). Multimodal fast optical interrogation of neural circuitry. Nature *446*, 633–639.

Zhang, F., Vierock, J., Yizhar, O., Fenno, L.E., Tsunoda, S., Kianianmomeni, A., Prigge, M.,

Berndt, A., Cushman, J., Polle, J., et al. (2011). The microbial opsin family of optogenetic tools. Cell *147*, 1446–1457.

Zhang, H.-M., Robinson, N., Gómez-Curet, I., Wang, W., and Harrington, M.A. (2009). Neuronal and network activity in networks of cultured spinal motor neurons. Neuroreport *20*, 849–854.

Zhang, L., Schessl, J., Werner, M., Bonnemann, C., Xiong, G., Mojsilovic-Petrovic, J., Zhou, W., Cohen, A., Seeburg, P., Misawa, H., et al. (2008a). Role of GluR1 in activity-dependent motor system development. J. Neurosci. *28*, 9953–9968.

Zhang, Y., Narayan, S., Geiman, E., Lanuza, G.M., Velasquez, T., Shanks, B., Akay, T., Dyck, J., Pearson, K., Gosgnach, S., et al. (2008b). V3 spinal neurons establish a robust and balanced locomotor rhythm during walking. Neuron *60*, 84–96.

Zhao, C., Devlin, A., Chouhan, A.K., Selvaraj, B.T., Stavrou, M., Burr, K., Brivio, V., He, X., Mehta, A.R., Story, D., et al. (2019). Mutant *C9orf72* human iPSC-derived astrocytes cause non-cell autonomous motor neuron pathophysiology. Glia glia.23761.

Zhou, X., Ren, J., Brown, E., Schneider, D., Caraballo-Lopez, Y., and Galligan, J.J. (2002). Pharmacological properties of nicotinic acetylcholine receptors expressed by guinea pig small intestinal myenteric neurons. J. Pharmacol. Exp. Ther. *302*, 889–897.

Zhu, C., Beck, M. V, Griffith, J.D., Deshmukh, M., and Dokholyan, N. V (2018). Large SOD1 aggregates, unlike trimeric SOD1, do not impact cell viability in a model of amyotrophic lateral sclerosis. Proc. Natl. Acad. Sci. U. S. A. *115*, 4661–4665.

Zou, J.-L., Liu, S., Sun, J.-H., Yang, W.-H., Xu, Y.-W., Rao, Z.-L., Jiang, B., Zhu, Q.-T., Liu, X.-L., Wu, J.-L., et al. (2018). Peripheral nerve-derived matrix hydrogel promotes remyelination and inhibits synapse formation. Adv. Funct. Mater. *28*, 1705739.

Zu, T., Gibbens, B., Doty, N.S., Gomes-Pereira, M., Huguet, A., Stone, M.D., Margolis, J., Peterson, M., Markowski, T.W., Ingram, M.A.C., et al. (2011). Non-ATG-initiated translation directed by microsatellite expansions. Proc. Natl. Acad. Sci. U. S. A. *108*, 260–265.

Gene Detail :: Allen Brain Atlas: Developing Mouse Brain: Lim1/Lhx1.

9 Appendix

9.1 R code for the calculation of df/f0 from calcium imaging data

#This R code describes the process of calculating df/f0 from the raw intensity signal of calcium recordings generated by experiments described in Chapter 6.

 # Call raw data file

data2 = read.csv(file.choose())

Calculate df_f0

 # Subtracting the Background signal from the recordings.

n <- ncol(data2) #Find the number of columns in the dataset

subtract_background <- data2[2:n] - data2$Background

 # This subtracts the Background signal from all columns and puts it in a new matrix. The Background signal is recorded from a part of the field of view not containing a neuron. Manual designation of an ROI as 'Background' in the raw data is necessary.

Calculating $(f_t - f_0) / f_0$

Identify baseline section

 # Find number of columns in subtract_background:

c <- ncol(subtract_background)

 # If the beginning of the trace can be used as baseline, create a new matrix containing the first few values in each recording:

f0_values <- head(subtract_background[1:c])

 # If the trace begins in the middle of a burst then the beginning of the trace is not considered representative of baseline signal and a part of the trace (in this case, datapoint 811) where there is no activity is manually identified.

d <- c+811

f0_values <- subtract_background[811:d, 1:c]

 # Create a matrix for f_0 (the mean of a few values at baseline). Warning, each column heading becomes a row name:

f0 <- colMeans(f0_values)

 # Make new table with f_0 means in first row:

subtractbackground <- rbind(means = f0, subtract_background)

Subtract baseline

 # Calculate the difference (delta f) between f_0 means and the signal (f_t) by subtracting the f_0 means in the first row from the whole table (according to columns). At this point, the data becomes a matrix instead of a data frame. This row is for troubleshooting purposes.

deltaf <- apply(subtractbackground, 2, function(x) x - x[1])

 # Use the f_0 means in the first row which represent f_0 to calculate f_t - f_0 / f_0.

deltaf_f0x <- apply(subtractbackground, 2, function(x) (x - x[1]) / x [1])

 # Remove the extra row where the means used to be. This includes the final df/f0 values.

deltaf_f0 = deltaf_f0x[-1,]

 # Add the Timestamp column onto the front of the new matrix.

deltaf_f0t <- cbind(Timestamp = data2$Timestamp, deltaf_f0)

 # Convert back to a data frame, which is necessary to be able to use some of the functions below

df_f0x <- as.data.frame(deltaf_f0t, row.names = NULL,optional = NULL, make.names = TRUE, stringsAsFactors = default.stringsAsFactors())

 # Delete the Background column, which now contains missing values.

df_f0 = subset(df_f0x, select = -c(Background))

Decide if bleaching occurred universally based on plots of the traces. Bleaching was defined as a sustained decrease in calcium fluorescence over a long timescale. However, the same code was used to remove a sustained increase in calcium fluorescence.

 # If only a subset of neurons show bleaching then remove bleaching neurons. Will need to check these neurons are not firing. If they are, do something else.

df_f0b = subset(df_f0, select = -c(MN_1)

 # If bleaching occurred and was present in every neuron, then decide whether to correct universal bleaching (bleaching = 1) or not (bleaching = 0). In the example below, universal bleaching was corrected by subtracting the signal of a manually selected reference neuron in column 4 (r). To be selected as a reference neuron, a neuron needs to show bleaching similar to the rest of the dataset and be silent (have no calcium bursts).

bleaching = 1

r = 4

if (bleaching == 1) {

df_f0b = df_f0 - df_f0[,r]

df_f0b <- df_f0b[, ! apply(df_f0b , 2 , function(x) all(x==0))]

}

 # df_f0b was the final dataset used in further data processing and burst activity analysis in R and Spinalcore.